SHH SIGNALLING AND THE DYNAMIC PATTERNING OF THE VERTEBRATE NEURAL TUBE

Ana Catarina Esteves Ribeiro

October, 2011

Division of Developmental Neurobiology
MRC National Institute for Medical Research
Mill Hill, London

Department of Cell and Developmental Biology
University College London

Thesis submitted to University College London for the degree of Doctor of Philosophy

Declaration of Authenticity

I, Ana Catarina Esteves Ribeiro, confirm that the work presented in this thesis is my own. Where information has been derived from other sources, I confirm that this has been indicated in the thesis.

Ana Ribeiro

July, 2011

ABSTRACT

The formation of the central nervous system depends on the patterned generation of different neuronal and glial cell types during embryogenesis. In ventral regions of the neural tube, the graded activity of the secreted molecule Sonic Hedgehog (Shh) controls the position along the dorsoventral axis at which different neuronal subtypes differentiate. Here, using chick and mouse embryos, we systematically and quantitatively documented the spatial and temporal expression patterns of the transcription factors that delineate the progenitor domains of these neurons. We investigated the coordination of the patterning activity of Shh with tissue growth and cell differentiation and discovered a high degree of conservation in pattern formation between mouse and chick. In addition, quantification of the levels of Shh protein in vivo and downstream signalling activity using a mouse reporter of Gli activity confirmed the non-linear relation between ligand concentration, levels of intracellular signalling and expression of the target genes in vivo. These data support a model in which progenitor cells respond to the cumulative amount of Gli activity.

To advance our understanding of how cells transduce the Shh signal we investigated the vertebrate orthologs of Costal2, a component of the Hedgehog pathway in Drosophila. Using a gain of function assays in chick we confirmed that one of the orthologs, the kinesin Kif7, is a negative regulator of the Shh signalling pathway, acting downstream of Smoothened. The inhibitory activity of Kif7 required only the N-terminal region containing the motor domain. By contrast, the kinesin Kif27, which appears equally similar to Costal2 as Kif7, was unable to inhibit Shh signalling. These data provided evidence that Kif7 was a novel component of the vertebrate Hh signalling and revealed a greater conservation between the Drosophila and vertebrate system than previous views suggested.

ACKNOWLEDGEMENTS

I would first like to thank my supervisor James Briscoe for all the help and support during my PhD. For always being available for questions and discussions and for the continuous incentive. His passion for science continuously amazed me, and, during the writing of this thesis, so did his patience. I am also very grateful to Anna Kicheva for all the help in the analysis of my data and for opening my mind to new ideas and new ways to approach the data. This work would also not have been accomplished without the help and inspiration of Eric Dessaud, who introduced me to most of the lab tools I needed for my work, and always with a smile. I would also like to give a special thanks to my benchmate Vanessa Ribes, for always being able to lift the mood in the lab and for all the invaluable help and incentive for my work. I must also thank present and past members of the Briscoe lab, for all the cooperation and advices, and for making this such a cool lab to work in.

This PhD would have been considerably harder without the company of my London "family", Emilie, Valentina, Arnaud, Nicole, Hendrik and little Ella. Thank you for always being ready to hear my complaints and to drown them with a few beers. My time in London would not have the same without you. Finally, I would like to thank my actual family, my parents and my sister Inês. Without your confidence and encouragement I would not have made it this far.

TABLE OF CONTENTS

LIST OF FIGURES

LIST OF TABLES

ABBREVIATIONS

AP	Anteroposterior
AB	Apico-Basal
Bcd	Bicoid
bHLH	basic Helix-Loop-Helix
BMP	Bone Morphogenetic Protein
BSA	Bovine Serum Albumin
CNS	Central Nervous System
Cos2	Costal2
Ci	Cubitus interruptus
Dpp	Decapentaplegic
DIG	Digoxigenin
Dhh	Desert Hedgehog
Dl	Dorsal
DV	Dorsoventral
E	Embryonic day
EDTA	Ethylenediaminetetraacetic acid
FGF	Fibroblast Growth Factor
FP	Floor Plate
Fu	Fused
GBS	Gli Binding Site
GFP	Green Fluorescent Protein
GRN	Gene Regulatory Network
Hh	Hedgehog
HH	Hamburger & Hamilton stage
hpe	hours post electroporation
hpf	hours post fertilization
hps	hours post initiation of somitogenesis
Ihh	Indian Hedgehog
LB	Luria-Bertani Broth

MN	Motor Neurons
p	progenitor
PB	Phosphate Buffer
PBS	Phosphate Buffer Saline
PD	Proximodistal
PFA	Paraformaldehyde
PKA	Protein Kinase A
Ptc	Patched
Ptch1	Patched1
RA	Retinoic Acid
RC	Rostrocaudal
ROI	Region of interest
RT	Room Temperature
Smo	Smoothened
Shh	Sonic Hedgehog
SSC	Salt Sodium Citrate
Sufu	Suppressor of Fused
TGF-ß	Transforming Growth Factor-ß
TRIS	Tris[hydroxymethyl]aminomethane
V	Interneuron class subtype

CHAPTER 1 – INTRODUCTION

1.1 Morphogens and tissue patterning

1.1.1 Introduction to morphogens

Fundamental to embryonic development is the transformation of a naïve field of cells into a reproducible pattern of tissues and organs, comprising highly organized arrays of specialized cell types. This process often involves signalling molecules that instruct and organize fields of cells by providing positional information that defines the identity of the cells within the field. These signals can function locally and involve interactions between neighboring cells, or act on cells positioned at a distance from the signal source. The long-range signals are known as morphogens.

The idea that the position of a cell in the embryo determined its identity was introduced by Hans Driesch at the end of the 19th century. Driesch demonstrated that sea urchin embryos could develop into normal larvae even after removal of parts of the body, leading him to conclude that a coordinate system specified cell position and thus determined its fate (reviewed in Wolpert, 1996). The possibility that pattern formation could be controlled by a gradient was later proposed by Thomas Hunt Morgan, based on his work on regeneration. Morgan's studies stated how a gradient could provide polarity in a tissue and how cells could be patterned in response to different thresholds (reviewed in Wolpert, 1996). The idea of gradients was explored by Boveri and Hörstadius to explain the patterning of the sea urchin embryo (reviewed in Wolpert, 1996). These and other works contributed to the understanding of pattern formation, but the mechanisms of how gradient could be set, maintained or how they could generate pattern remained elusive (reviewed in Wolpert, 1996).

In 1952 A. M. Turing proposed that tissue pattern can arise from the reaction and diffusion of chemical substances, which he termed morphogens (Turing, 1952). This model was later expanded to include the idea that morphogens are released from localized sources. In 1969 Lewis Wolpert formalized the concept of positional

information, which proposes that cells have their spatial position specified according to a coordinate system and translate such positional information into specific cell behaviors, enabling an organized pattern to arise (Wolpert, 1969). Wolpert's ''French Flag" model states that a morphogen signal subdivided a tissue into domains of different gene expression: a blue stripe, a white stripe and a red stripe. The size of the tissue over which the morphogen acts is quite small, around 50 cells long, leading Francis Crick to propose that morphogens are diffusible molecules, whose concentration specifies position (Crick, 1970). Hence, in the current formulation of the model, the morphogen is secreted from a localized source and spreads through the tissue to establish a gradient of activity. Cells respond to this signal expressing different target genes at distinct concentration thresholds, that is, at different distances to the source (Wolpert, 1996). Since this model was first proposed, several molecules have been identified that act as morphogens to pattern a wide variety of organs and species (reviewed in Wolpert, 2011).

The first definite demonstration of a morphogen gradient was provided with the identification and visualization of Bicoid (Bcd), which establishes anteroposterior (AP) polarity in the Drosophila embryo (Driever and Nüsslein-Volhard, 1988a, 1988b). The Bicoid gradient arises from an anteriorly localized source of *bicoid* mRNA in the syncytial embryo (Ephrussi and St Johnston, 2004). The homeodomain transcription factor encoded by this mRNA moves from its site of production and accumulates in nuclei during each interphase, where it binds to its target sites. Bicoid induces the expression of different target genes, termed "gap genes", in a concentration-dependent manner, leading to their expression in distinct spatial domains along the AP axis (Driever et al., 1989a; Driever and Nüsslein-Volhard, 1989; St Johnston and Nüsslein-Volhard, 1992; Struhl et al., 1989). The pattern of gap gene expression is subsequently refined through the cross-regulatory interactions between the gap genes themselves, which also function as transcription factors (Rivera-Pomar and Jäckle, 1996).

Since the identification of Bicoid, other molecules with morphogen action were identified in Drosophila. Dorsal (Dl) patterns the dorsoventral (DV) axis of the Drosohila embryo (Roth et al., 1989). Decapentaplegic (Dpp) regulates the patterning of the dorsal ectoderm in the early embryo and controls the patterning of the AP axis of the wing imaginal disc (Ferguson and Anderson, 1992; Podos and Ferguson, 1999).

In vertebrate systems, examples of molecules with morphogen activity include Activin (a member of the transforming growth factor-β (TGF-β) family), which controls the patterning of the mesoderm (Green and Smith, 1990), Retinoic Acid (RA) and Fibroblast Growth Factors (FGFs) specify the proximodistal (PD) axis of the vertebrate limb (Niswander et al., 1993; Summerbell and Harvey, 1983; Tickle et al., 1982) and Shh patterns the AP axis of the limb (Riddle et al., 1993) and the DV axis of the neural tube (Ericson et al., 1997; Marti et al., 1995; Roelink et al., 1995).

The extensive study of the processes underlying pattern formation has shown that morphogen gradients are one of the main mechanisms used by signalling molecules to provide positional information to a naïve tissue. This has led to the current definition of a morphogen as a ligand with two distinguishing features: it acts on cells at a distance from its source; and it induces differential gene expression in a concentration-dependent manner. To understand how morphogens drive patterning it is important to know how gradients are formed and how they are interpreted by cell. These mechanisms are discussed in the following section.

1.1.2 Morphogen gradient formation and interpretation

1.1.2.1 Measurement of morphogen gradients

The nested expression of target genes and the spatial shifts in their expression domains following changes in the level of the signal have been used to show the existence of morphogens. Changes in Bicoid concentration along its gradient result in shifts in the expression domains of the target gap genes and alter the fate of cells (Driever et al., 1989a; Driever and Nüsslein-Volhard, 1989; Rivera-Pomar and Jäckle, 1996; St Johnston and Nüsslein-Volhard, 1992; Struhl et al., 1989). In addition, changes of target gene expression domain are useful to infer properties of the morphogen gradient (Wartlick et al., 2009). For example, differences in the response of low- and high-threshold genes to altered morphogen distribution may help understand which features of the gradient are important for its distribution.

To demonstrate the graded profile of a molecule it is crucial to directly visualize its distribution. A morphogen gradient can be visualized using antibody staining and/or GFP fusion proteins. To be able to quantify the distribution of the morphogen, the imaging conditions must ensure that the fluorescence intensity is linearly proportional to concentration (Wartlick et al., 2009). Downstream of the ligand itself, activity gradients can be monitored by measuring downstream intracellular responses.

The quantification of different morphogens in Drosophila, such as Bicoid in the syncytial embryo and Dpp and Wingless in the wing imaginal disc, has shown that these morphogens form gradients with a slope that is well approximated with an exponential shape (Houchmandzadeh et al, 2002; Kicheva et al., 2007). This is consistent with the idea that gradients form by diffusion. Thus, exponential decay functions ($c=c_0e^{(-x/\lambda)}$) can be used to fit the measured morphogen profile and infer characteristic features of the gradient. The shape of exponential gradients depends on two parameters: the amplitude c0, which corresponds to the concentration of the morphogen at the source boundary; and the decay length λ, which provides a measure of the steepness of the slope - the distance over which the gradient decays. The two parameters can be used to model the spread of a morphogen across the field (reviewed in Barkai and Shilo, 2009; Wartlick et al., 2009). This procedure has shown that the Bicoid gradient in the Drosophila embryo, with a decay length of 100µm, is larger than the Dpp and Wingless gradients in the wing imaginal disc, with decay lengths of 20µm and 6µm, respectively (Houchmandzadeh et al, 2002; Kicheva et al., 2007). The decay length of the gradient depends on the diffusion (D) and degradation (β) rates ($\lambda=\sqrt{D/\beta}$) (Wartlick et al., 2009).

The estimation of the properties of the morphogen gradients based on the exponential approximation is useful to understand how the gradients are formed. Moreover, gradients that are formed through different molecular or cellular mechanisms can have similar shapes. For example, Bicoid and Dpp both show an exponential profile, but the Bicoid gradient is formed through diffusion in the cytoplasm and nuclear membranes, whereas Dpp transport requires transcytosis (Gregor et al., 2007; Kicheva et al., 2007). Therefore it is difficult to determine the underlying mechanism from the shape of the gradient. Mathematical and numerical analysis can be useful in developing hypothesis concerning the mechanisms that are acting during the formation of the gradient. The gradient can be modeled to predict

the dynamics of the formation of a gradient when a specific mechanism is assumed. This prediction can be then compared with experimental data (Ibañez and Belmonte, 2008). Another approach to infer the mechanisms of gradient formation is to obtain the parameters that characterize this process (the rates of production, transport and degradation) by measuring its dynamics. This can be performed by in vivo imaging in conditions in which the gradient is perturbed. These parameters can then be introduced in the model to test and infer new parameters. This approach has been used to characterize the kinetics of the Dpp and Wingless gradients in the Drosophila wing disc (Kicheva et al., 2007).

1.1.2.2 Morphogen gradient formation

The formation of a morphogen gradient is a dynamic process, influenced by the kinetics of morphogen production, transport and degradation. These processes, which determine the shape of the gradient, are presumably tightly controlled to ensure the reproducibility between embryos (Barkai and Shilo, 2009). When production, diffusion and degradation are equilibrated (i.e. the shape of gradient appears constant over time), the gradient is said to have reached a steady-state (Wartlick et al., 2009). However, in certain developmental processes that occur rapidly, such as the Bicoid-dependent patterning of the syncytium, cell fate may be specified before reaching steady state (Bergmann et al., 2007; Bergmann et al., 2008). This may also be the case in growing tissues, in which the gradient is continuously changing either because the amount of morphogen produced is changing or the size of the field of cells changes. These conditions might be particularly relevant to Shh in the neural tube (Chamberlain et al., 2008).

The source of the morphogen is sometimes assumed to be a homogeneous domain, with an unchanging rate of production in space and time (Ibañez and Belmonte, 2008). However, in a developing tissue this may not be true. Changes in the production rate may be observed in a dynamic gradient, before it reaches steady-state. The production rate may also vary as a result of biological noise, thus influencing the robustness of the gradient. Perturbations in the production rate have distinct effects on the specification of different target genes depending on the

underlying model of gradient formation and particularly on the type of degradation (Barkai and Shilo, 2009).

The spreading of the morphogen across the tissue can be achieved by simple diffusion (intracellular or extracellular) or by active mechanisms that facilitate ligand transport, such as endocytosis or transport through gap junctions. At the same time, cell division and growth can dilute and transport molecules over space. Several of these transport mechanisms may be involved in the formation of a single gradient (Ibañez and Belmonte, 2008). The Bicoid gradient has been proposed to rely on diffusion as a transport mechanism. However, different measurements of the Bicoid diffusion rate have yielded contradicting values (Gregor et al., 2005; 2007). In addition, these values are unable to account for the formation of the Bicoid gradient in the required developmental period. Several hypothesis have been proposed to explain these data: pre-steady-state decoding of the gradient (Bergmann et al., 2007; Bergmann et al., 2008); different diffusion rates over space and time (Gregor et al., 2007); and active transport mechanisms that yield faster diffusion (Gregor et al., 2007). The Dpp gradient is formed by transcytosis in the Drosophila wing imaginal disk (Kicheva et al., 2007).

The formation of a gradient is facilitated by morphogen degradation. Crick's early model described gradient formation as a diffusing morphogen produced by a localized source and destroyed in a "sink" cell at a distance (Crick, 1970). However, gradient formation does not require a localized sink and many morphogen are degraded everywhere in the target tissue or are not degraded at all (Wartlick et al., 2009).

The degradation can be linear, forming exponential steady-state gradients. The Bicoid gradient in the embryo and the Dpp and Wingless gradients in the wing imaginal disc have been analyzed using a model of effective diffusion and linear degradation (Gregor et al., 2007; Kicheva et al., 2007). In a morphogen gradient formed by linear degradation, a single decay length controls both the spread of the morphogen and the sensitivity of patterning to changes in the morphogen production rate (Barkai and Shilo, 2009). Thus, a smaller decay length will lower the sensitivity of the system, but will also limit the range of the gradient.

Other models of gradient formation include examples of non-linear degradation, such as "self-enhanced" degradation (Eldar et al., 2003). In these models feedback mechanisms result in a rate of morphogen degradation that changes across

the tissue - for example, morphogen signalling enhances its own degradation. The result is that morphogen gradients can not be characterized by a single decay length. These mechanisms have been proposed to increase the robustness of the gradient without compromising the gradient range (Barkai and Shilo, 2009). When morphogen signalling enhances its own degradation the gradient decays rapidly close to the source (where levels of signalling are high), and decays slower at a distance from the source (where morphogen levels are lower) (Barkai and Shilo, 2009). Mathematically this type of gradients are better approximated by power-law functions. This type of model has been used to describe the dynamics of the Hh gradient (Eldar et al., 2003) and the Retinoid Acid (RA) gradient (White et al., 2007). In the Drosophila wing disc Hh upregulates its receptor Patched (Ptc), which in turn restricts the spread of the ligand (Chen and Struhl, 1996), most likely by causing its internalization and degradation (Eldar et al., 2003). Similarly, in the zebrafish embryo RA forms a posterior-to-anterior gradient in the anterior neural tube, and RA signalling induces the expression of RA-degrading enzyme Cyp26a1 (White et al, 2007).

1.1.2.3 Gradient interpretation

The function of a gradient is to specify position by regulating the expression of target genes and ultimately define cell identity. To understand how graded positional cues control cell fate specification it is important to understand how cells interpret concentration-dependent information.

Most morphogens integrate signal transduction pathways that ultimately regulate the activity of transcriptional effectors. The differential activity of the transcriptional effectors in cells exposed to distinct levels of ligand determines the differential induction of target gene expression, and thus the identity of the cells. According to the conventional model of morphogen interpretation the signal transduction between the morphogen and the transcriptional effectors is linear, and therefore the level of ligand generate equivalent levels of transcriptional effector (reviewed in Ashe and Briscoe, 2006). Hence, a graded ligand is directly converted into graded transcriptional activity, which differentially regulates target gene expression. This model of morphogen interpretation appears to apply to some

morphogens, such as Activin, which seems to be linearly transduced into nuclear Smad2 concentration in *Xenopus* (Shimizu and Gurdon, 1999). However, increasing evidence indicate that morphogen signal transduction is not always linear and the graded information (or signal) that is interpreted varies depending on the morphogen (reviewed in Ibañez and Belmonte, 2008). Thus, cells may respond to the steady-state amount of morphogen around a cell or the amount of morphogen in a transient dynamic state (Bergmann et al., 2007; Casali and Struhl, 2004; Dyson and Gurdon, 1998). The graded signal that is interpreted may also be the slope of the gradient, instead of levels of morphogen (Rogulja and Irvine, 2005). Moreover, an increasing number of studies proposes that morphogen levels are integrated over time, and the duration of signalling is also important for morphogen interpretation, and not just the levels of signal.

The key role of time in morphogen interpretation was first introduced by Pages and Kerridge, in a model termed "sequential cell context" (Pages and Kerridge, 2000). This model proposed that the response of target cells to ongoing morphogen signalling changes over time. Thus, initially morphogen signalling activates an early set of genes. The products of these genes act synergistically with signalling to allow the expression of a distinct set of genes at later times. This model was used by Pages and Kerridge as an alternative to explain AP patterning of the Drosophila wing disc by Dpp and mesoderm induction by activin in Xenopus (Pages and Kerridge, 2000).

Further evidence of the importance of the duration of signalling for tissue patterning comes from studies in the determination of digit identity by Shh in vertebrates (Ahn and Joyner, 2004; Harfe et al., 2004; Scherz et al., 2007; Yang et al., 1997). These studies proposed a model in which precursors exposed to high levels of Shh for increasingly longer periods of time acquire progressively more posterior digit identities. In this case, the signal that is interpreted is be the total amount of morphogen cells were exposed to over time (Ahn and Joyner, 2004; Harfe et al., 2004).

Shh interpretation in the vertebrate neural tube is also dependent on time. Recent studies in the patterning of the ventral neural tube have shown that the levels of morphogen are transduced into graded periods of signalling, which that are then interpreted (Dessaud et al., 2007; Dessaud et al., 2010; discussed below).

The graded information provided by the morphogen, whether it is in the form of different levels or duration of signal, is converted into levels of gene expression that determine cell identity. Different strategies can account for differential gene regulation by graded signals and some morphogen pathways may use a combination of mechanisms to control gene expression (reviewed in Ashe and Briscoe, 2006).

The differential expression of target genes may result from different sensitivities to the morphogen signal. For instance, different target genes can have morphogen-effector binding sites with different affinities: targets with low affinity respond only to high levels of signalling whereas targets with high affinity are induced by low levels of signalling. Such a mechanism has been described for the Dorsal (Dl) gradient in the Drosophila embryo. Dl regulates DV patterning and gastrulation through the concentration-dependent activation and repression of target genes (Stathopoulos and Levine, 2004).

Although binding-site affinity can account for some of the differential responses to graded morphogens, in general affinities alone are insufficient to generate the full range of transcriptional responses. In many cases, the activation of target genes requires the input of additional transcription factors other than the morphogen effector. This is the case in the regulation of different Bicoid target genes. The pattern of expression of the target gene *hunchback* is determined solely by the affinity of its Bicoid binding-sites (Driever et al., 1989b; Struhl et al., 1989), whereas the enhancers of other Bicoid target genes are also bound by other transcription factors, such as Hunchback, Caudal and/or Krüppel (Ochoa-Espinosa et al., 2005).

The downstream interactions between responding genes may also contribute to the regulation and refinement of the expression patterns of target genes. These strategies may include feed-forward loops and cross repression. In feed-forward loop mechanisms a signal initially activates a set of genes, which act together with the signal to regulate the expression of a second set of genes. This mechanism is reminiscent of the "sequential cell context" model proposed by Pages and Kerridge (Pages and Kerridge, 2000). Repressive interactions between morphogen target genes can also contribute to the interpretation of the signal. Cross-repressive interactions have been shown to be important in the Shh-dependent specification of different neuronal identities in the vertebrate neural tube (Briscoe et al., 2000; discussed below).

1.1.3 Morphogens and growth

The patterning of cells by morphogens often occurs in growing tissues. Therefore it is important to coordinate the processes that regulate cell proliferation and cell specification to ensure that development proceeds correctly. Although the study of morphogens has been focused on their role in cell specification, there is increasing evidence that morphogens also act as mitogenic/survival factors in developing tissues. Thus, cell specification and proliferation may be regulated and coordinated by the same signals (reviewed in Schwank and Basler, 2010; Ulloa and Briscoe, 2007).

The identification of morphogens as patterning agents and growth factors raises the question of whether specification and proliferation respond in a similar manner to morphogen gradients. Morphogen gradients specify cell fates by regulating gene expression in a concentration-dependent manner. Therefore, the response of cells within the tissue varies according to their position (i.e. the distance to the morphogen source). If proliferation also responds positively to morphogen gradients in a concentration-dependent manner, proliferation rates would be expected to change as function of the distance to the source, such that proliferation levels are higher close to the source and lower at wider distances. However, studies on organ growth suggest that morphogens drive uniform proliferation despite their graded distribution. For example, Shh and FGFs establish in a graded manner the pattern of the Anteroposterior (AP) and Proximodistal (PD) axes in the vertebrate limb bud. In addition these morphogens also control cell proliferation and expansion of the limb bud, but unlike patterning, proliferation occurs uniformly across the target field (Ten Berge et al., 2008; Towers et al., 2008; Zhu et al., 2008). Similarly, cells in the Drosophila wing imaginal disc proliferate uniformly, at the same time their AP and DV fates are being patterned by Dpp and Wingless, respectively (Milan et al., 1996; Martin-Castellanos and Edgar, 2002; Schwank et al., 2008).

Several models have been proposed to explain how a gradient can generate uniform proliferation, although most of these models have not been demonstrated experimentally (reviewed in Schwank and Basler, 2010).

The “memory models” propose that the morphogen acts on proliferation in a sequential manner. The initial activity of the morphogen desensitizes target cells in a way that cells exposed to higher levels of morphogen are less sensitive to the

mitogenic activity of the morphogen than cells exposed to lower levels of morphogen (reviewed in Schwank and Basler, 2010). The degree of desensitization endows the cells with a memory of the levels of morphogen they were exposed, which determines the response of the cells at later times in development. Because the mitogenic sensitivity of cells is continuously adjusted to the different concentrations of morphogen, the proliferation becomes uniform across the field of cells. Importantly, cells show different sensitivities only for the mitogenic action of the morphogen, but not for the patterning response. A prediction of this model is that proliferation is not uniform in the very early phase of morphogen activity.

A second group of models, the "threshold models" propose that proliferation is induced in an all-or-none response if the levels of morphogen are above a certain threshold (reviewed in Schwank and Basler, 2010). However, if uniform proliferation is achieved through a morphogen threshold, changes in the level of morphogen would not be expected to influence the rate of proliferation, as long as the levels were maintained above the threshold. This is not the case in the growth of the Drosophila wing discs driven by Dpp or the growth of the vertebrate neural tube controlled by Shh (Burke and Basler, 1996; Capdevilla and Guerrero, 1994; Cayuso et al., 2006). In these organs, ectopic uniform activation of the morphogens leads to overgrowth of the tissues.

Another class of models comprises the "gradient models", in which proliferation depends on the slope of the morphogen gradient (Gelbart, 1989; Lawrence and Struhl, 1996; reviewed in Schwank and Basler, 2010). In this model the proliferation of cells is not determined by the absolute level of morphogen, but rather the relative differences in levels as perceived by neighbouring cells. When the differences between the levels in adjacent cells are sufficiently high, that is, when the gradient is sufficiently steep, cells proliferate. This mechanism has been proposed to act during the Dpp-dependent growth regulation of the Drosophila wing disc (Day and Lawrence, 2000; Rogulja and Irvine, 2005). A related but distinct gradient model is that instead of a spatial gradient, cells use a temporal gradient. In this model cells continue to proliferate while they experience an increasing amount of signal over time (Wartlick et al., 2011).

Finally, the "multiple growth parameter models" assume that growth is regulated by a morphogen in combination with other growth modulator, which might also be morphogens (reviewed in Schwank and Basler, 2010). The combination

of the input of the different factors ensures uniform proliferation. This could be achieved by the use of opposing gradients and could apply to the regulation of growth in the vertebrate neural tube. In the neural tube, Shh and BMPs/Wnts form opposing gradients along the DV axis, and evidence suggests that these factors control cell survival and proliferation, as well as patterning the tissues (Cayuso et al., 2006; Ille et al., 2007; Jeong and McMahon, 2005; Megason and McMahon, 2002; Zechner et al., 2003). It is possible that the reciprocal action of the opposing gradient results in uniform proliferation and the DV axis of the neural tube.

The contribution of these different mechanisms to the regulation of growth by morphogen will likely vary depending on the morphogen and the organ it acts on. Regardless of the mechanism used, the coordination between patterning and growth through the action of a morphogen could contribute to a higher degree of precision and robustness of patterning.

Given the relationship between patterning and growth it is important to understand how patterns adapt to changes in size, i.e., how patterns "scale". Scaling mechanisms are important for different aspects of organ development. Organs can show differences in absolute size as a result of embryo-to-embryo variability, but have similar proportions. For example, Drosophila larvae that are starved stop growing and have reduced dimensions in adults compared to individuals cultured on rich food. Despite the differences in size, the proportions of the patterns of the starved animals are normal (Beadle et al., 1938; reviewed in Schwank and Basler, 2010). A scaling mechanism must also be in action as organs grow over the course of development, to ensure that the proportions of pattern are maintained over time. Moreover, scaling is also observed in closely related species with different sizes (Gregor et al., 2005).

In principle, different mechanisms could account for the adaptation of patterns to size (reviewed in Schwank and Basler, 2010). Scaling could be achieved by adjusting the amplitude of the morphogen gradient to the size of the tissue. Alternatively, cells could adapt their response to the morphogen to compensate for the change in tissue size. Another possibility is that the expression patterns of the target genes are established early in development, when the fields of cells are similar in size, and subsequently maintained in proportion by uniform expansion of the tissue. Which of these mechanisms are used and in what tissues in currently unclear.

The study of the mode of action of morphogens has provided invaluable insight into the mechanisms that govern the formation of a wide range of tissues and organs, in many different organisms. In the vertebrate neural tube morphogens have been shown to play a crucial role in the establishment and organization of several neuronal cell types. In the following sections I present the mechanisms involved in the patterning of the neural tube, highlighting the role of the morphogen Shh.

1.2 Formation and patterning of the neural tube

1.2.1 Specification and organization of the spinal cord

Over a hundred years ago Santiago Ramón y Cajal laid the ground for modern neuroscience with the idea that neurons serve as the functional signalling units in the nervous system and that neurons establish precise connections to one another (Ramon y Cajal, 1906; reviewed in Albright et al., 2001). To operate properly, the different neuronal subtypes must be specified at precise positions and at the correct time during development. The Central Nervous System (CNS) derives from the dorsal epiblast of the vertebrate gastrula (reviewed in Beddington and Robertson, 1999). The neural fate is induced in medial cells in the ectodermal layer by a combination of signals that emanate from the underlying mesoderm (reviewed in Stern, 2001). The induced neural plate undergoes a series of morphogenetic movements that result in the shaping, bending and, finally, closure of the neural plate, forming the neural tube (reviewed in Colas and Schoenwolf, 2001). The developmental potential of neural tube cells is progressively restricted by local environment signals. After neural progenitor cells acquire their identity, they begin to generate post-mitotic neurons with specific functional properties. The distinct neuronal subtypes will then establish the correct connections to assemble functional neuronal circuits (reviewed in Tanabe and Jessell, 1996).

The early stages of neural patterning, controlled by a set of inductive signals, result in the regionalization of the neural tube along both the rostrocaudal (RC; also referred as anteroposterior (AP) in early stages) and dorsoventral (DV). The RC

patterning establishes the main subdivisions of the CNS: the forebrain, the midbrain, the hindbrain and the spinal cord. The first formed part of the neural plate is rostral (forebrain) in character and more caudal regions (midbrain, hindbrain, spinal cord) are laid down as the organizer regresses posteriorly (Hensen's node in chick, the node in mouse). As the neural plate extends posteriorly, DV patterning is simultaneously taking place, resulting in the generation of different neuronal subtypes and neural structures at specific dorsoventral positions of the neural tube (reviewed in Wilson and Maden, 2005).

Understanding how early patterning is regulated is a key issue in developmental neuroscience. Important advances in this field have been achieved through the study of spinal cord development. This region of the CNS is particularly amenable to experimental manipulation and has been extensively used to study cell fate specification. Spinal cord neurons have two main functions, which are to a large extent spatially segregated: neurons generated in the dorsal region relay sensory information to the brain, whereas ventrally located interneurons and motor neurons (MN) integrate proprioceptive input (position-movement sensation of the parts of the body) and coordinate motor output (reviewed in Jessell, 2000). Dorsal neurons are subdivided into 6 groups (dI1-6), while ventral interneurons and motor neurons are divided into 5 groups (V3-V0 and MNs). The spatially segregated neuronal subtypes derive from defined progenitor cells that are generated at defined DV positions of the neural tube (reviewed in Jessell, 2000).

The following section reviews the signalling systems that drive patterning along the RC and DV axes, focusing mainly on the specification of ventral cells fates.

1.2.2 Signals involved in the patterning of the spinal cord

In vertebrates, the neural plate forms in response to organizer-derived neural-inducing signals, which are thought to include Fibroblast Growth Factors (FGFs), and secreted inhibitors that counteract the epidermis-inducing activity of Bone Morphogenetic Proteins (BMPs) (reviewed in Wilson and Edlund, 2001). The caudal most region of the neural plate generates the spinal cord. Soon after neural induction the prospective spinal cord cells acquire a caudal neural fate by means of a series of extrinsic signal. These signals, which emerge from the primitive streak/marginal zone

in early stages and paraxial or lateral mesodermal populations later on, include members of the FGFs, Retinoic Acid (RA), BMPs and Wnts (Blumberg et al., 1997; Lamb and Harland, 1995; McGrew et al., 1995; Muhr et al., 1999; Nordstrom et al., 2002; Storey et al., 1998). FGFs maintain the neural plate cells in an undifferentiated state by repressing neurogenesis (Diez del Corral et al., 2002). As cells leave the precursor zone, exposure to somite-derived RA attenuates FGF signalling, allowing the progression of neuronal patterning (Diez del Corral et al., 2003).

The signalling events involved in the rostrocaudal patterning of the neural tube are still poorly understood. The RC axis of the spinal cord can be roughly divided into five domains based on the position and projection of the cell types contained in each region: cervical, brachial, thoracic, lumbar and sacral domain (reviewed in Wilson and Maden, 2005). Most of the neuronal subtypes specified along the DV spinal cord are uniformly generated along the entire RC axis, suggesting a minimal contribution of RC signalling to the establishment of subtype identity. The exception to the apparent uniformity in neuronal subtype identity is the formation of different subtypes of motor neurons at different RC levels (reviewed in Jessell, 2000). The subtype identity of motor neurons is defined by their position, axon trajectory and pattern of muscle innervation, and motor neurons with similar axon trajectories are grouped in motor columns (Landmesser, 2001). The specification of motor column identity has been attributed to members of the Hox-c and Hox-d gene clusters, which are expressed at the appropriate RC levels of the spinal cord (reviewed in Dasen and Jessel, 2009).

Dorsoventral patterning generates a range of neuronal subtypes, including floor plate cells, motor neurons, ventral interneurons, dorsal interneurons and roof plate cells. The DV polarity of the neural tube is controlled by the combined effects of various extracellular signals, but the main effectors are the opposing gradients of Shh ventrally and BMPs and Wnts dorsally.

Dorsal neuronal subtype specification requires the activity of members of the TGF-β family, notably BMPs, which are released by the ectoderm overlying the neural tube and, later on, the roof plate (Liem et al., 1997). Members of the Wnt family originating from the roof plate have also been proposed to be required for the formation of certain dorsal subtypes (Muroyama et al., 2002).

The patterning of the ventral spinal cord is triggered by signals emanating from the notochord, a rod of axial mesodermal cells underlying the neural tube, and subsequently by floor plate cells (Placzek, 1995). The main signalling activities of the notochord and floor plate are mediated by the secreted protein Shh (Chang et al., 1994; Echelard et al., 1993; Krauss et al., 1993; Riddle et al., 1993; Roelink et al., 1994). Loss-of-function experiments, in which Shh signalling was blocked either biochemically or genetically, demonstrated that Shh is required for the generation of most ventral neuronal subtypes (Chiang et al., 1996; Ericson et al., 1996). In addition, ectopic expression of Shh in vitro or in vivo appears to be sufficient to induce ventral cell fates (Ericson et al., 1996; Marti et al., 1995; Roelink et al., 1995). The generation of certain groups of intermediate interneurons (V0 and V1) do not require Shh signalling, even though Shh is able to induce these cell types in vitro (Pierani et al., 1999). Instead, V0 and V1 interneurons depend on RA signalling for their specification (Pierani et al., 1999; Wilson et al., 2004).

As well as demonstrating the role of Shh in the specification of different classes of neurons, these studies also provided insight into the mechanism of action of Shh. Gain-of-function experiments in vitro showed that progressive two- to threefold changes in Shh concentration generated five distinct classes of ventral neurons from progenitor cells (Ericson et al., 1997; Roelink et al., 1995). Moreover, the concentration of Shh required to induce a particular neuronal subtype in vitro reflected the distance from the midline at which the neuronal subtype was generated in vivo (Ericson et al., 1997). Neurons generated at progressively more ventral positions required correspondingly higher levels of Shh to be induced. These findings, showing that Shh induces distinct cell types in a concentration-dependent manner, provided initial evidence that Shh acts as a morphogen.

Further evidence of the morphogen activity of Shh derived from studies showing the direct long-range activity of Shh signalling in vivo. Visualization of the Shh protein in neural tissue revealed the presence of the ligand at considerable distance from the source (Chamberlain et al., 2008; Gritli-Linde et al., 2001). The signalling activity of Shh, as reported by the direct target of the pathway Ptch, was also widely spread in the neural tube (Marigo and Tabin, 1996). Moreover, the ectopic activation of Shh signalling, using a constitutively active form of Smo, induced ventral cell fates cell-autonomously (Hynes et al., 2000). By contrast, the inhibition of Shh signalling, either by elimination of a key component of the pathway (Wijgerde et

al., 2002), or by the ectopic expression of a dominant inhibitor of the pathway (Briscoe et al., 2001), caused cell-autonomous ventral-to-dorsal identity switches. Together, these studies demonstrated that Shh acts as a morphogen to provide positional information to the ventral neural tube.

The verification that a gradient of Shh signalling activity directs the differentiation of ventral neuronal subtypes raised the question of how neural progenitor cells interpret graded Shh signals. Several studies suggest that Shh specifies ventral cell fates by regulating the expression of a set of homeodomain (HD) and basic Helix-Loop-Helix (bHLH) transcription factors (Figure 1.1).

The transcription factors are sub-divided into two classes, based on their mode of regulation by Shh (Figure 1.1B). Class I genes appear to be constitutively expressed in the neural tube and their expression is repressed by Shh. Conversely, the expression of Class II genes is dependent on Shh (Briscoe et al., 1999; Briscoe et al., 2000; Ericson et al., 1997; Muhr et al., 2001; Novitch et al., 2001; Pierani et al., 1999; Vallstedt et al., 2001). The differential transcriptional response of these genes to graded Shh signalling establishes distinct dorsal and ventral limits of expression for each factor. However, the response to Shh signalling is not sufficient to explain the discrete domains of expression. The defined delimitation of the expression domains is achieved through cross-repressive interactions between complementary pairs of Class I and Class II proteins that share a boundary of gene expression. For example, the Class I factor Pax6 and the Class II factor Nkx2.2 have adjacent and mutually exclusive expression domains. Ectopic expression of of Pax6 downregulates the expression of Nkx2.2, whereas the genetic removal of Pax6 results in the dorsal expansion of the Nkx2.2 domain (Briscoe et al., 2000; Ericson et al., 1997). Conversely, the induction of Nkx2.2 in the Pax6 domain results in the repression of Pax6 expression (Briscoe et al., 2000). Similar relationships have been observed between other pairs of Class I and Class II proteins and also between pairs of Class II proteins (Briscoe et al., 2000; Dessaud et al., 2008; Novitch et al., 2001; Sander et al., 2000; Vallstedt et al., 2001). These cross-repressive interactions help establish the dorsoventral patterns of expression of the Class I and Class II proteins, and, furthermore, ensure that the boundaries between progenitor domains are sharply delineated.

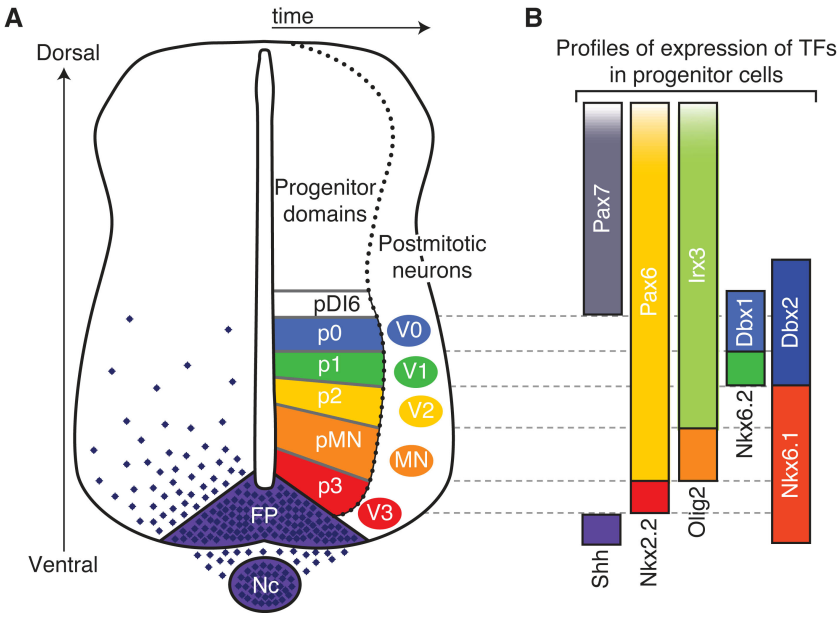

Figure 1.1 Ventral neural tube patterning by Shh.

(**A**) Schematic of the vertebrate neural tube, where Shh (purple dots) secreted from, the Notochord (Nc) and Floor Plate (FP) forms a ventral to dorsal gradient. Positional differences in the concentration of Shh determine the spatial organization of five distinct progenitor (p) domains p3, pMN, p2, p1 and p0, which generate ventral interneuron subtypes V0-V3 and Motor Neurons (MN). Shh controls the positional identity of these progenitor domains by regulating the expression of a set of transcription factors (**B**). Shh signalling represses the expression of Pax7, Pax6 and Irx3 (Class I genes) and activates the expression of Nkx2.2, Olig2, Nkx6.1, Nkx6.2, Dbx1 and Dbx2 (Class II genes). The differential response of each gene to the gradient of Shh determines the position of its expression boundaries. In addition, cross-repressive interactions between adjacent pairs of transcription factors further refines their boundaries of expression. The combinatorial expression of these transcription factors in each progenitor domain specifies the identity of the domain (B). [Figure adapted from Ribes and Briscoe, 2009].

The combinatorial expression of Class I and Class II transcription factors defines the identity of neural progenitor cells, which later generate post-mitotic neuronal subtypes (Briscoe et al., 2000). This combinatorial code divides the ventral neural tube into five distinct progenitor domains: p0, p1, p2, pMN and p3 (Figure 1.1A). Each progenitor domain occupies a distinct DV position and will generate spatially segregated neuronal subtypes: V0, V1, V2, MN and V3 (Briscoe et al., 2000; Sander et al., 2000; Vallstedt et al., 2001).

The regulation of the expression of Class I and Class II transcription factors by Shh requires that different concentrations of signal are converted into different levels and durations of intracellular signalling activity, that ultimately define the transcriptional response of the cell. Therefore, to understand how cells interpret the graded Shh it is crucial to understand the molecular processes involved in the intracellular signal transduction. In the following section I introduce the Hh signalling pathway and afterwards I explore the mechanisms employed by cells to interpret a gradient of Shh signal, focused on the vertebrate neural tube.

1.3 Hedgehog (Hh) signalling pathway

The Hh signal transduction pathway is an evolutionarily conserved signalling cascade that is required for the proper patterning of several developing tissues (reviewed in Huangfu and Anderson, 2006; Varjosalo and Taipale, 2008; Wilson and Chuang, 2010). In all bilaterians, secreted Hh binds to the receptor Patched (Ptc), relieving the inhibition of Ptc on Smoothened (Smo), and active Smo relays the signal to the transcriptional effectors of the pathway, Ci/Gli. Here, I review the current understanding of the molecular mechanisms underlying Hh intracellular signalling and I will particularly focus on apparent differences between Drosophila and vertebrates.

1.3.1 Hh signalling in Drosophila

The Hh gene was first discovered in *Drosophila melanogaster* (Nüsslein-Volhard and Wieschaus, 1980) and much of the current knowledge of Hh signalling has emerged from the study of this pathway in the fruit fly.

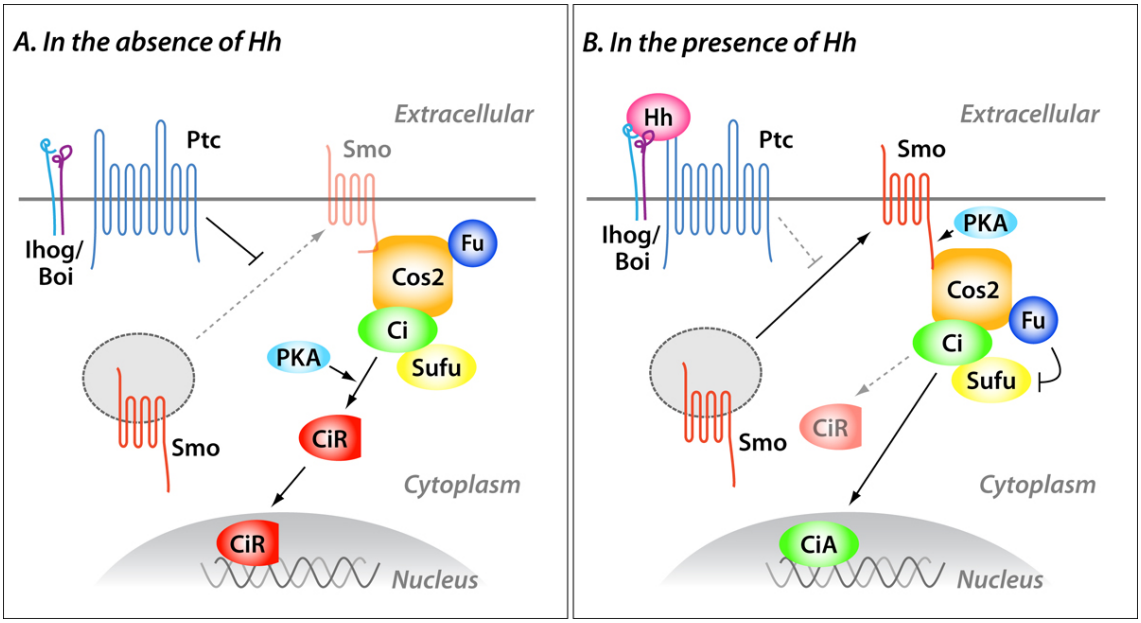

Figure 1.2 The Hedgehog pathway in Drosophila.

The Hedgehog (Hh) signal transduction in the absence (**A**) and presence of ligand (**B**). In the absence of Hh, Patched (Ptc) prevents the activation of Smoothened (Smo) and its accumulation at the cell surface (Nakano et al., 2004) (A). In Smo-inactive cells Costal2 (Cos2) facilitates the interaction between Cubitus interruptus (Ci) and Protein Kinase A (PKA), enabling Ci phosphorylation (Zhang et al., 2005). PKA-mediated phosphorylation primes Ci for the phosphorylation by CKI and GSK3 and subsequent recognition by the E3 ubiquitin ligase Slimb, which targets Ci to the proteasome (Smelkinson et al., 2007). In the proteasome Ci is proteolytically processed to generate a Ci Repressor form (CiR). CiR translocates to the nucleus, where it represses the expression of Hh target genes (Aza-Blanc et al., 1997). Cos2 further regulates Ci activity by retaining full-length Ci in the cytoplasm, together with Sufu (Wang et al., 2000; Wang and Jiang, 2004) (A). In cells exposed to Hh, the receptor Ptc binds to the ligand, facilitated by the co-receptors Ihog and Boi (Lum et al., 2003a; Yao et al., 2006; Zheng et al., 2010) (B). Hh-bound Ptc is internalized, allowing Smo to accumulate at the plasma membrane (Denef et al., 2000). The mechanism underlying Ptc-dependent regulation of Smo activity is not well understood. Smo activation is associated with the PKA- and CKI-dependent hyperphosphorylation and ensuing conformational change, and the plasma membrane localization (Jia et al., 2004; Zhao et al., 2007) (B). In Hh-stimulated cells, phosphorylation of Cos2 by Fused (Fu) promotes the dissociation of Cos2 from Smo and allows Smo phosphorylation (Liu et al., 2007) (B). Subsequently, Cos2 binds to the C-terminal region of Smo (Jia et al., 2003) and possibly disrupts Ci and PKA/CKI/GSK3 interaction, thus impairing Ci processing. In addition, Fu antagonizes Sufu activity, enabling the translocation of full-length Ci to the nucleus, where it act as a transcriptional activator (CiA) of Hh target gene expression (Lum et al., 2003b) (B).

1.3.1.1 Establishment of the Hh gradient: production and spread

The Hh family members act on varying developmental contexts either as short-range inducers or as long-range morphogens. Therefore, the secretion and propagation of the Hh signals must be tightly controlled to ensure the formation of appropriate activity gradients (for reviews see Ingham and McMahon, 2001; Jia and Jiang, 2006; Torroja et al., 2005).

Hh is produced as a ~45KDa precursor that undergoes a series of processing steps in the secretory pathway, before being released from the secreting cell. The maturation of the precursor molecule is initiated with the cleavage of the signal sequence. After the removal of the signal sequence, the Hh protein undergoes an additional cleavage event followed by the addition of a molecule of cholesterol. This reaction is catalyzed by the C-terminal half of the precursor Hh and results in the formation of a biologically active protein, HhN (Bumcrot et al., 1995; Lee et al., 1994; Porter et al. 1996; Tabata and Kornberg, 1994). The cholesterol modification results in the association of Hh to the membrane, facilitating the final processing step of palmitoylation (Chamoun et al., 2001). The addition of the fatty acid palmitate to the N-terminus of HhN is catalyzed by the acyltransferase skinny hedgehog (ski) (Amanai and Jiang, 2001; Chamoun et al., 2001; Lee and Treisman, 2001; Micchelli et al., 2002), resulting in the final, fully functional form of Hh.

Although the lipid-modified form of Hh is associated to the plasma membrane, it still forms a signalling gradient. In this regard, the release and the spread of Hh relies on specific molecular and cellular mechanisms, albeit that these mechanisms are not yet well understood. The secretion of the lipid-modified Hh from the producing cell requires the activity of the 12-span transmembrane protein, Dispatched (Disp) (Burke et al., 1999). Biochemical studies have also shown that Hh monomers can form multimeric complexes, which hide the hydrophobic regions, making the complex soluble and diffusible (Zeng et al., 2001; Chen et al., 2004a). Consistent with these data, the formation of multimers in vivo has been linked to the assembly of large punctate structures present in active Hh gradients (Gallet et al., 2006).

The movement of Hh through the tissues is also facilitated by extracellular factors. A group of these factors comprises the heparan sulfate proteoglycans (HSPGs). Loss of the heparan sulfate synthesizing enzymes, such as tout-velu (ttv),

brother of tout-velu (botv) and sister of tout-velu (sotv), impairs Hh distribution throughout the extracellular matrix and its signalling activity (Bellaiche et al., 1998; Bornemann et al., 2004; Han et al., 2004a). In addition, the glypicans Dally and Dally-like, core proteins of the HSPGs, also affect Hh signalling by facilitating the binding of Hh to the cell surface (Han et al., 2004b; Lum et al., 2003a).

The Hh receptor Ptc also plays an important role in the shaping of the gradient. Ptc expression is upregulated in response to the signal, sequestering the ligand and thereby limiting its spread (Chen and Struhl, 1996; Tabata and Kornberg, 1994; Torroja et al., 2004). The increased Ptc expression in response to activated Hh signalling has also been proposed to incorporate a negative feedback mechanism that results in the progressive adaptation of signalling activity in cells exposed to ongoing signals, in the mammalian neural tube (Dessaud et al., 2007; see section 1.4.2) Another regulator of Hh spreading as been described in Drosophila, the product of a secreted protein encoded by the gene shifted that interacts with Hh (Glise et al., 2005; Gorfinkiel et al., 2005).

1.3.1.2 Reception of Hh: Ptc and Smo

In responding cells, the 12-pass transmembrane protein Patched (Ptc) is implicated in the reception of extracellular Hh. Although studies in mammals suggest that Ptc interacts directly with Hh (Fuse et al., 1999; Marigo et al., 1996a; Stone et al., 1996), in Drosophila no direct interaction of Hh with Ptc has been demonstrated (Zheng et al., 2010). The association of Hh with Ptc is facilitated by the transmembrane proteins Interference hedgehog (Ihog) and Brother of Interference hedgehog (Boi), which bind to Hh and appear to function as coreceptors for Hh (Lum et al., 2003a; Yao et al., 2006; Zheng et al., 2010). In the absence of signal Ptc represses the activity of another transmembrane protein, the G-coupled-protein receptor Smoothened (Smo) (Taipale et al., 2002) (Figure 1.2 A). The binding of Hh to Ptc releases the inhibition of Smo, and this switch in the activation state of the pathway appears to be correlated with changes in the subcellular localization of Ptc and reciprocal changes in the localization of Smo (Denef et al., 2000; Zhu et al., 2003; Nakano et al., 2004; Zhao et al., 2007) (Figure 1.2 B). In the absence of Hh, Ptc localizes in the plasma membrane and internal vesicles and prevents the movement of Smo

from intracellular vesicles to the plasma membrane. Ptc has been proposed to keep Smo in an unphosphorylated state, promoting its destabilization and clearance from the cell surface via endocytosis (Jia et al., 2004; Nakano et al., 2004; Zhang et al., 2004). The binding of Hh to Ptc causes Ptc to be internalized from the plasma membrane, allowing Smo to be phosphorylated and accumulate in the plasma membrane (Denef et al.,2000).

The molecular mechanism by which Ptc regulates the activity of Smo is still poorly understood, but the available evidence suggest that this process does not involve a direct interaction between Ptc and Smo (Zhu et al., 2003). In fact, the repression of Smo is non-stoichiometric, with one molecule of Ptc inhibiting approximately 50 molecules of Smo (Taipale et al., 2002). The sequence similarity of Ptc to the members of the resistance-nodulation cell division (RND) superfamily of permeases and transporters has led to the proposal that Ptc mediates the transmembrane movement of small molecules that agonize or antagonize Smo (Taipale et al., 2002). In support of this hypothesis, in vertebrates Smo activity can be modulated by sterol-related small molecules, such as cyclopamine and jervine (Chen et al., 2002). However, these small molecules have no affect on the Drosophila Hh pathway, suggesting different modes of regulation of Smo in flies and vertebrates (Chen et al., 2002; Chen et al., 2001; Taipale et al., 2000).

The phosphorylation of Smo and cell-surface accumulation are coupled with the activation of the pathway (Figure 1.2 B). The C-terminal tail of Smo contains a set of sites for phosphorylation by protein kinase A (PKA) and casein kinase I (CKI), and becomes hyperphosphorylated upon exposure to Hh (Jia et al., 2004; Zhang et al., 2004). Mutations that mimic gain or loss of phosphorylation have shown that the levels of Smo cell-surface accumulation and activity correlate with its levels of phosphorylation (Jia et al., 2004). The activation of Smo has been proposed to involve a conformational switch of the protein, which also relies on its phosphorylation state. The cytoplasmic tail of Smo contains multiple Arg clusters that maintain Smo in an inactive conformation in the absence of ligand and may promote endocytosis and degradation. Hh-induced phosphorylation of this domain triggers a conformational change, which may allow the interaction with other transducers of the pathway (Zhao et al., 2007).

1.3.1.3 Hh signal transduction: Hh signalling complex in the absence and presence of ligand

Downstream of Smo, a cytosolic signalling complex is involved in relaying the signal to the nucleus. This complex, which includes the kinesin-like protein Costal2 (Cos2), the kinase Fused (Fu), the PEST domain protein Suppressor of Fused (Sufu) and the transcription factor Cubitus Interruptus (Ci), regulates the subcellular localization and processing of Ci in response to the extracellular levels of Hh (reviewed in Wilson and Chuang, 2010). At the core of the signalling complex is the atypical kinesin Cos2 that, depending on the Hh state of the cell, physically binds to different components of the pathway and promotes their interaction. Thus, Cos2 has been suggested to be important both for the positive and negative regulation of Hh signalling.

Cos2 predicted structure is similar to the structure of members of the kinesin family (Robbin et al., 1997; Sisson et al., 1997). Kinesins are motor proteins, frequently assembled in dimers, that use ATP hydrolysis to move along microtubules (Hirokawa et al., 2009). Kinesins are composed of a N-terminal motor domain, which binds to microtubules and ATP, and a stalk and C-tail domains, which are involved in dimerization and/or binding to cargos, adaptors or scaffold proteins (Hirokawa et al., 2009).

A Cos2-containing complex has been shown to bind to two regions of Smo C-tail important for Smo activity, a membrane proximal region (651-686) (Lum et al., 2003b) and a C-terminal region (818-1035) (Jia et al., 2003). In the absence of ligand Cos2 and Fu form a stable complex with Smo, possibly through the membrane proximal region. The Cos2-Smo interaction has been proposed to prevent Smo phosphorylation, a step required for its activation (Liu et al., 2007). When Hh is absent Cos2 also facilitates the processing of full-length Ci155 (155 kD), presumably by bringing it in contact with the kinases PKA, CKI and GSK3 (Smelkinson et al., 2007; Zhang et al., 2005) (Figure 1.2 A). The sequential phosphorylation of Ci targets it for ubiquitination by E3 ubiquitin ligase Slimb and posterior proteasome-mediated cleavage. The truncated form Ci75 (75 kD) can then dissociate from the complex and translocate to the nucleus where it acts as a transcriptional repressor of Hh target genes (Aza-Blanc et al., 1997). The ability of Cos2 to promote Ci processing requires its motor activity, although it is not clear whether motor activity is important for Ci

phosphorylation or subsequent targeting for degradation (Farzan et al., 2008). Ci activity is further restricted in inactive cells by the Cos2/Sufu-dependent tethering of full-length Ci to the cytoplasm, preventing its translocation into the nucleus (Wang et al., 2000; Wang and Jiang, 2004) (Figure 1.2 A).

Upon Hh stimulation Fu-dependent phosphorylation of Cos2 on Ser572 promotes its dissociation from Smo, allowing Smo phosphorylation (Liu et al., 2007). The activation of Smo, accompanied by a conformational change, might expose other Cos2-interacting regions in the C-terminal domain allowing its association with Cos2-Fu. The binding of Smo to Cos2 could obstruct the binding of the kinases PKA, CKI and GSK3 and subsequent processing of Ci155 (Figure 1.2 B). Additionally, the destabilization of the signalling complex following Cos2 phosphorylation might result in the release of Ci from the inhibitory complex (Ruel et al., 2007). Fu further promotes pathway activation by antagonizing Sufu function, allowing unprocessed Ci to enter the nucleus and transcriptionally activate target genes (Lum et al., 2003b).

Thus, Drosophila Hh signal transduction displays a complex behavior and a dynamic biochemical composition depending on the state of pathway activation. Although the precise mechanisms underlying the Hh signal transduction are still under scrutiny, remarkable progress has been achieved in the recent years. The knowledge of the pathway in Drosophila has provided valuable insight to the understanding of Hh signalling in higher vertebrates.

1.3.2 Hh signalling in vertebrates

Although the core components of the Hh pathway are conserved between Drosophila and vertebrates, aspects of the signal transduction mechanism appear to have evolved differently in these organisms (reviewed in Huangfu and Anderson, 2006; Varjosalo and Taipale, 2008; Wilson and Chuang, 2010) (Figure 1.3). In addition, there are multiple vertebrate orthologs of some of the components, such as Hh, Ptc and Ci.

In mouse and chick there are three Hh homologues: Sonic Hedgehog, Indian Hedgehog (Ihh) and Desert Hedgehog (Dhh) (Echelard *et al.*, 1993). These genes have specific expression patterns and roles. Shh and Ihh are implicated in neural

development, whereas Dhh regulates spermatogenesis (Ingham and McMahon et al., 2001). Two Ptc homologues have been identified in vertebrates, Ptch1 and Ptch2. Loss of function studies suggest that Ptch1 is the main receptor for Shh during embryonic development (Goodrich *et al.*, 1997). Downstream of Ptch1, a single homolog of Smo mediates all vertebrate signalling (Akiyama *et al.*, 1997). Ci function is distributed between three Gli proteins, Gli1, Gli2, Gli3 (Bai et al., 2004; Hui et al., 1994; Marigo et al., 1996b; Motoyama et al., 2003; Ruppert et al., 1988). Gli1 and Gli2 act primarily as activators, while Gli3 acts primarily as a repressor but also appears to have potential as an activator.

The role of primary cilia in vertebrate Hh signal transduction is also a distinguishing feature of the vertebrate pathway (for reviews see Eggenschwiler and Anderson, 2007; Goetz and Anderson, 2009) (Figure 1.3). In mammals several components of the pathway have been shown to localize in the primary cilium, including Ptch1, Smo, Gli1, Gli2, Gli3 and Sufu (Chen et al., 2009; Corbit et al., 2005; Haycraft et al., 2005; Rohatgi et al., 2007). In addition, the disruption of cilia assembly or function results in Hh-related phenotypes in mouse (Huangfu and Anderson, 2005; Huangfu et al., 2003; Liu et al., 2005; May et al., 2005), chick (*talpid*^{3} mutant; Yin et al., 2009) and zebrafish (Huang and Schier, 2009). Conversely, loss of cilia function in Drosophila has no effect on Hh signalling (Avidor-Reiss et al., 2004; Han et al., 2003; Sarpal et al., 2003). Indeed, flies only display cilia in sensory neurons and spermatozoa. Until recently the involvement of cilia in the Hh pathway was proposed to be a newly acquired function, characteristic of the vertebrate lineage. However, a new study has found a link between Hh signalling and cilia function in planarians (Rink et al., 2009). This finding points to an ancestral connection between cilia and Hh signalling and its subsequent loss in specific groups, such as the Drosophila lineage.

The following section presents the current knowledge of the Shh signal transduction, highlighting the differences in the pathway between flies and vertebrates.

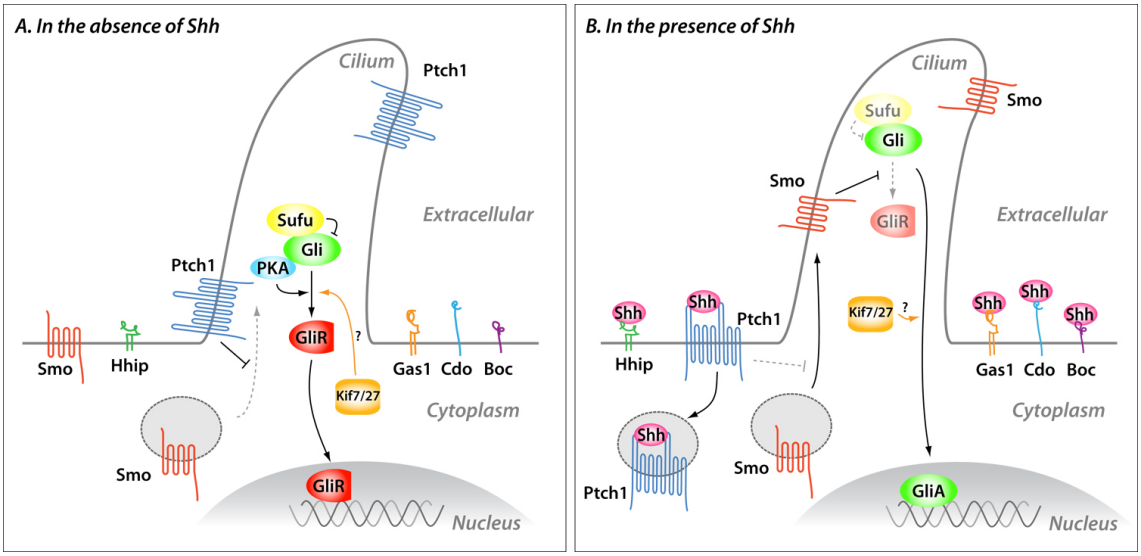

Figure 1.3 The Hedgehog pathway in vertebrates.

The Sonic Hedgehog (Shh) signal transduction in the absence (**A**) and presence of ligand (**B**). In the absence of Shh Patched1 (Ptch1) represses the activity of Smoothened (Smo), possibly by acting as a transporter of small modulators of Smo activity (Bijlsma et al., 2006; Corcoran and Scott, 2006; Dwyer et al., 2007) (A). The enrichment of Ptch1 in cilia may also block the entry of Smo into cilia (Rohatgi et al., 2007). When Smo is inactive full-length Gli proteins are phosphorylated by the kinases PKA, CKI and GSK3, followed by β-TrCP-mediated ubiquitination and subsequent targeting to the proteasome (Pan et al., 2006). In the proteasome, Gli proteins are either degraded (mostly Gli2) or proteolytically processed into repressor forms (GliR; mostly Gli3). PKA-mediated phosphorylation also inhibits the formation of Gli activators (GliA) by blocking full-length Gli SUMOylation (Cox et al., 2010). The levels of Gli proteins in the absence of Shh are further regulated by SPOP-mediated proteolysis, which results in the complete degradation of Gli proteins (Zhang et al., 2006b; Zhang et al., 2009). Sufu counteracts SPOP activity, preventing the degradation of Gli proteins (Chen et al., 2009). In addition, Sufu restricts Gli transcriptional activity by retaining full-length Gli proteins in the cytoplasm (Chen et al., 2009; Humke et al., 2010; Svard et al., 2006) (A). By contrast, GliR forms are able to translocate to the nucleus and repress Shh target gene expression (Persson et al., 2002) (A). In Shh-stimulated cell, Shh-bound Ptch1 exits the cilium and is internalized (Incardona et al., 2002). Shh also binds other transmembrane proteins, including Hhip, which acts as a negative regulator of the pathway (Jeong and McMahon, 2005), and Gas1, Cdo and Boc, which enhance pathway activation (Allen et al., 2007; Martinelli and Fan, 2007; Tenzen et al., 2006; Yao et al., 2006; Zhang et al., 2006a). The removal of Ptch1 from cilia allows Smo to translocate from lateral membranes and intracellular pools and enter the cilium (Milenkovic et al., 2009; Wang et al., 2009) (B). The accumulation of Smo in cilia is followed by the movement of Gli proteins and Sufu to the tip

of cilia (Haycraft et al., 2005; Tukachinsky et al., 2010) (B). The translocation of Gli proteins to the tip of cilia possibly inhibits their processing and/or degradation. In addition, the transport of Gli-Sufu complexes to the tip of cilia results in the dissociation of the complex, allowing full-length Gli proteins to translocate to the nucleus (Tukachinsky et al., 2010). Full-length Gli proteins likely undergo additional post-translational modifications that enhance their transcriptional activity, such as SUMOylation (Cox et al., 2010). Fully active Gli proteins present in the nucleus activate the expression of Shh target genes (Barnfield et al., 2005; Merchant et al., 2004; Pan et al., 2006). The present study aims to address the role of the Cos2 homologs Kif7 and Kif27 in the negative and/or positive branches of the Shh transduction pathway.

1.3.2.1 Establishment of the Shh gradient: production and spread

Like Drosophila Hh, biologically active Shh is auto-catalytically cleaved, cholesterol modified at the C-end and palmitoylated at the N-end (reviewed in Dessaud et al., 2008). The lipid modifications of Shh are required for the formation of a soluble multimeric protein complex that are active at long-range (Chen et al., 2004, Zeng et al., 2001). The release of fully lipidated Shh from producing cells depends on the transmembrane protein Dispatched1 (Disp1) (Caspary et al., 2002; Kawakami et al., 2002; Ma et al., 2002).

The spread of Shh in the target tissue is influenced by components of the extracellular matrix, including HSPGs, and transmembrane proteins, such as Ptch1, Hhip1, Gas1, Cdo and Boc (reviewed in Dessaud et al., 2008). HSPGs have been suggested to bind extracellular Shh and restrict its diffusion (Rubin et al., 2002). Ptch1, the Shh receptor, and Hhip1 both bind and sequester Shh protein, cell-autonomously inhibiting the pathway (Briscoe et al., 2001; Incardona et al., 2002; Jeong and McMahon, 2005). In addition, the sequestration of the ligand decreases its availability at greater distances from the source (Chamberlain et al., 2008; Chuang et al., 2003; Chuang and McMahon, 1999; Goodrich et al., 1997; Jeong and McMahon, 2005). The expression of Ptch1 and Hhip1 is also transcriptionally induced by Shh signalling, resulting in a negative feedback mechanism that modulates the activity and spread of the signal and possibly helps to increase the robustness of the gradient (Jeong and McMahon, 2005; Eldar, et al., 2003). Another class of transmembrane

proteins, which include Gas1, Cdo and Boc, also bind and sequester Shh, but act cell-autonomously to promote Shh signalling (Allen et al., 2007; Martinelli and Fan, 2007; Tenzen et al., 2006; Yao et al., 2006; Zhang et al., 2006a). These molecules could enhance Shh signalling by acting as co-receptors with Ptch1 and sensitizing cells to low levels of ligand. The expression of this class of proteins is generally inhibited by Shh signalling, suggesting a model in which the sequestration of Shh enhances signalling when cells are exposed to low levels of ligand and inhibits signalling when Shh levels are high (reviewed in Dessaud et al., 2008; Ribes and Briscoe, 2010).

1.3.2.2 Reception of Shh: Ptch and Smo

The core steps of signal reception are conserved between Drosophila and vertebrates. In the absence of ligand Ptch1 represses the activity of Smo (reviewed in Dessaud et al., 2008; Ingham and McMahon, 2001). When bound to Shh, Ptch1 relieves its inhibition of Smo, allowing Smo to transduce the signal intracellularly. However, some observations have suggested that the mechanisms of regulation of Smo activity have diverged during evolution. In mammals, the trafficking of Smo in and Ptch1 out of the primary cilia is associated the activation of the pathway (Corbit et al., 2005; Rohatgi et al., 2007; Wang et al., 2009). In addition, the activity of vertebrate Smo is inhibited or activated directly by several sterol-like molecules (Bijlsma et al., 2006; Corcoran and Scott, 2006; Dwyer et al., 2007), whereas Drosophila Smo appears to be insensitive to these small-molecule modulators (Chen et al., 2002; Taipale et al., 2000). Moreover, the structure of the C-terminus of Smo has significantly diverged between the two lineages (Huangfu and Anderson, 2006).

The C-terminal tail of vertebrate Smo is considerably shorter and lacks several PKA and CKI phosphorylation sites required for the activation of the pathway in Drosophila (Huangfu and Anderson, 2006). Nevertheless, vertebrate Smo is phosphorylated by the kinase GRK2 upon ligand binding (Chen et al., 2004b) and it is possible that other kinases are involved in Smo activation (Varjosalo et al., 2008). In addition, mSmo undergoes a conformational change in response to Shh, a process that may rely on a stretch of Arg/Lys residues in the cytoplasmic tail (Zhao et al., 2007), hinting at a mechanism of regulation of Smo analogous to Drosophila.

Taken together these findings show that in both organisms the activation of Smo is also accompanied by the re-localization to specific structures. But, whereas Drosophila Smo accumulates at the cell surface, mammalian Smo localizes to cilia. In the absence of Shh, Ptch1 is enriched in the primary cilium; after binding to Shh, Ptch1 is removed from the cilium (Rohatgi et al., 2007) (Figure 1.3 A,B). Concomitantly, Smo translocates to the cilium either from lateral regions of the plasma membrane or from intracellular stores (Milenkovic et al., 2009; Wang et al., 2009). The movement of Smo to the primary cilium appears to be necessary to but not sufficient to activate the pathway, as Smo also accumulates in the cilium when cells are treated with the antagonist cyclopamine that blocks the pathway (Rohatgi et al., 2009; Wang et al., 2009; Wilson et al., 2009a). A recent study proposes that Smo can adopt multiple conformations, with different levels of activity (Wilson et al., 2009a). Both inactive and active conformations allow Smo to move into cilia, but may target Smo to different regions of the primary cilium. The specific location of Smo on the primary cilium may allow the interaction with specific components of the Hh cascade and differentially regulate the signal transduction.

1.3.2.3 Shh signal transduction: divergence of the vertebrate homologs (Sufu, Fu, Cos2)

In addition to the differences in the cell biology of signal transduction, several studies of the intracellular signalling mechanism in vertebrates have suggested that components have functionally diverged from their Drosophila counterparts. These include Fu and Sufu.

In Drosophila the serine/threonine kinase Fu is required for the response to high levels of Hh (Alves et al., 1998; Therond et al., 1999). Zebrafish Fu is also involved in the positive regulation of Hh signalling (Wolff et al., 2003) and has been shown to have a role in the biogenesis of motile cilia (Wilson et al., 2009b). By contrast, loss of Fu in mice has no effect on Hh signalling, instead causing Hh-independent defects on motile cilia assembly (Chen et al., 2005; Merchant et al., 2005; Wilson et al., 2009b).

While mammalian Fu has lost its function in Hh signalling, Sufu has acquired an increased, and crucial, influence on the pathway. Drosophila Sufu appears to be involved in the control of Ci stability and nuclear accumulation (Méthot and Basler,

2000; Wang et al., 2000). However, the inhibitory function of Sufu has only a modest effect on the pathway, as Sufu-null flies are viable and fertile and only show a phenotype when Fu is also mutated (Preat et al.,1992). By contrast, the knockdown of Sufu in zebrafish results in a Hh-related phenotype in muscle specification (Wolff et al., 2003). Though mild, the zebrafish phenotype points to a more important role for vertebrate Sufu in Hh regulation. Indeed, the targeted mutation of Sufu in mice has an even more dramatic effect on the pathway, causing a strong upregulation of the Hh pathway and early embryonic lethality (Cooper et al., 2005; Svärd et al., 2006). The mechanisms by which Sufu controls vertebrate Hh signalling are still not well understood. Similar to fly Sufu, mouse Sufu appears to be involved in the regulation of Gli protein levels and their trafficking into the nucleus (Chen et al., 2009; Humke et al., 2010; Svärd et al., 2006). Like other components of the pathway, Sufu also localizes to cilia, but the ciliary localization is dispensable for the regulation of the Gli protein levels by Sufu (Chen et al., 2009; Jia et al., 2009). Sufu has been proposed to antagonize SPOP, thus preventing degradation of full-length Gli2 and Gli3 (Chen et al., 2009). This Sufu-SPOP circuit appears to be conserved from Drosophila, since Sufu protects Ci from degradation promoted by the fly homolog of SPOP, Hib (Zhang et al., 2006b). Conversely, Gli1 is unaffected by SPOP-promoted degradation, and its expression is upregulated in Sufu mutants, suggesting that Gli1 may be the main contributor to the Sufu phenotype (Chen et al., 2009; Svärd et al., 2006). The activation of the pathway in the absence of Sufu could also result from the loss of Gli repressors and/or the gain of Gli activators (Humke et al., 2010).

Several studies have addressed the functional divergence of a core component of the Drosophila signalling complex, the atypical kinesin Costal2. Sequence analysis of vertebrate genomes identified 2 putative orthologs of Costal2: Kif7 in zebrafish (Tay et al., 2005) and Kif7 and Kif27 in mouse (Katoh and Katoh, 2004a; Katoh and Katoh, 2004b).

In zebrafish the kinesin-related protein zKif7 shows significant sequence homology to Cos2, which extends beyond the motor domain. The function of Cos2 also appears to be at least partially conserved, as the loss of zKif7 results in the ectopic activation of the pathway in two Hh-responding regions, the somites and the ventral neural tube (Tay et al., 2005). In the myotome several muscle fibre types differentiate in response to distinct levels of Hh. The injection of zKif7 morpholinos

induced the upregulation of ptc1 in muscle precursor cells and consequent increase in the number of Hh-dependent muscle fibre types. The lateral floor-plate cells, a ventral neural tube cell type that requires Hh signalling, are also expanded in Kif7 morphants. Moreover, Kif7 is able to form a complex with Gli1, hinting at a possible involvement of zKif7 in Gli processing and activation, as described in Drosophila.

At the time when this work was initiated the role of the Cos2 orthologs in amniotes had only been tested in one study, which used mammalian cells lines (Varjosalo et al., 2006). In this work no connection was found between either Kif7 or Kif27 and Hh signalling. This led the authors to conclude that Cos2-like function had been lost in higher vertebrates. This study described the inability of Kif7 and Kif27 cargo domains to associate with mSmo and, accordingly, the putative Cos2 binding regions were found to be dispensable in mSmo for the induction of Gli activity. Consistent with these results, the expression of Drosophila Cos2 had no effect on wild type mSmo activity, while the replacement of the mouse Smo C-terminal tail with the corresponding fly sequence rendered it sensitive to Drosophila Cos2. The manipulation of the mouse proteins Kif7 and Kif27 in cultured cells also had negligible impact in Hh signalling. The gain and loss-of function of Kif7 and Kif27, alone or in combination, had no effect in the induction of Gli transcriptional activity. Furthermore, the exogenous expression of Kif7 or Kif27 was unable to restrict the sub-cellular localization of Gli2 and Gli3-GFP fusion proteins. The apparent divergence of Cos2 function in mammalian cells was suggested to be linked with the vertebrate specific involvement of primary cilia in Hh signalling, with this structure taking on the scaffolding role performed by Cos2 in Drosophila. However, considering the dual role of Cos2 both in the positive and negative regulation of the pathway, it is possible that cell-based assays were not sufficiently sensitive to assess Cos2-like function. Subsequently, work in the chick neural tube, described here, and loss-of-function studies in mouse demonstrated a role of Kif7 in Hh signalling in higher vertebrates (see Section 2).

1.3.3 Ci/Gli regulation

In all species, the activation of the signalling cascade in response to Hh culminates in an alteration of the balance between activator and repressor forms of

Ci/Gli proteins (Ruiz i Altaba et al., 2007). However, while in Drosophila Ci provides all the repressor and activator functions, in vertebrates these functions are partitioned among the three Gli proteins. The vertebrate Gli repressor activity is largely derived from Gli3, while Gli activator function mainly depends on Gli2. Like Ci, Gli2 and Gli3 contain both the repressor and the activator domains and can be proteolytically processed (Dai *et al.*, 1999; Sasaki *et al.*, 1999). Gli1 is a transcriptional target of Hh signalling and acts only as an activator to reinforce GliA activity. Gli1 contains the zinc finger DNA binding and activator domains, but lacks a repressor domain (Dai *et al.*, 1999; Sasaki *et al.*, 1999).

In the absence of ligand, Ci/Gli2/Gli3 are phosphorylated by PKA, CKI and GSK3, recognized by Slimb/β-TrCP and subsequently targeted for proteasome dependent processing or degradation (Bhatia et al., 2006; Jia et al., 2002; Jia et al., 2005; Pan et al., 2006; Price and Kalderon, 2002; Wang and Li, 2006). In addition, Ci/Gli proteins contain degradation motifs recognized by Hib/SPOP, a BTB-containing protein that acts as a substrate recognition subunit for the Cul3-E3 ubiquitin ligase. The Cul3-E3-mediated ubiquitinylation caused the complete degradation of Ci/Gli2/Gli3 (Zhang et al., 2006b; Zhang et al., 2009). The presence of Hh prevents the phosphorylation or ubiquitinylation of Ci/Gli and leads to nuclear accumulation of full-length activator forms of the proteins.

In vertebrates Gli processing events, as well as activation of the pathway, appear to be associated with cilia localization. Mutations in intraflagellar transport (IFT) subunits and other factors required for primary ciliogenesis result in impaired Gli3 processing (Huangfu and Anderson, 2005; Liu et al., 2005; May et al., 2005). Recent studies indicate that PKA, which is present at the base of cilia (Barzi et al., 2010), promotes the removal of Gli2 and Gli3 from cilia (Tukachinsky et al., 2010; Wen et al., 2010; Zeng et al., 2010). In the presence of Hh PKA is inhibited, permitting full-length Gli proteins to accumulate in cilia. In addition, upon Hh stimulation Gli-Sufu complexes are recruited to cilia, possibly resulting in their dissociation, allowing Gli to enter the nucleus (Tukachinsky et al., 2010; Zeng et al., 2010). Full-length Glis likely require additional modifications to become fully active, at present not well understood. One such modification is proposed to be the Pias1-dependent SUMOylation of full-length Gli2 and Gli3, which appears to enhance Gli transcriptional activity (Cox et al., 2010). PKA-mediated phosphorylation of Gli proteins appears to inhibit the addition of SUMO groups (Cox et al., 2010).

1.4 Interpretation of graded Shh signalling

1.4.1 Graded Gli activity mediates graded Shh signalling

In vertebrates all three Gli genes are expressed in the neural tube and together control the expression of Shh target genes (Hui et al., 1994; Lee et al., 1997; Ruiz i Altaba, 1998; reviewed in Jacob and Briscoe, 2003). Gli1 is expressed in the ventral neural tube and its expression depends on Shh signalling (Bai et al., 2002). Since Gli1 mutant mice lack any developmental defects (Bai and Joyner, 2001; Park et al., 2000), it has been proposed that Gli1 does not mediate the initial response of cells to Shh and this function depends on Gli2 instead (Bai et al., 2002). Both Gli2 and Gli3 are expressed in neural tissue even in the absence of Shh signalling (Hui et al., 1994; Lee et al., 1997). As development progresses Gli2 is expressed uniformly in the neural tube, with the exception of the floor plate, and Gli3 becomes restricted to dorsal and intermediate neural tube (Lee et al., 1997).

In regions of the neural tube where Shh levels are low the repressor form of Gli3 is expected to dominate, resulting in the transcriptional inhibition of target genes (reviewed in Ribes and Briscoe, 2009). Consistent with this prediction, Gli3 mutant mice show a dorsal expansion of intermediate markers of the neural tube (Persson et al., 2002). These defects are rescued by an allele of Gli3 that encodes only the transcriptional repressor domain, establishing the crucial role of Gli3 repressor function in defining the dorsal extent of Shh target genes in the neural tube (Persson et al., 2002).

In cells exposed to Shh the levels of Gli3R are reduced (reviewed in Ribes and Briscoe, 2009). Accordingly, the loss of MNs and certain classes of interneurons in Shh mutant mice is partially rescued by the concomitant removal of Gli3 (Litingtung and Chiang, 2000; Persson et al., 2002). The depletion of all three Gli proteins (Bai et al., 2004; Lei et al., 2004) or the removal of both Smo and Gli3 (Wijgerde et al., 2002) yields similar phenotypes. These data indicate that Shh acts by counteracting the repressive function of Gli3 to specify p1, p2 and pMN cell identities. However, although several ventral cell fates can develop in the absence of Gli function, the organization of these progenitor identities is disrupted, with altered numbers of cells and intermingled positions (Bai et al., 2004; Lei et al., 2004; Wijgerde et al., 2002).

Thus, the correct patterning of the neural tube requires an input from the Shh gradient and balanced Gli protein activities.

The specification of the most ventral identities, the p3 and FP domains, requires not just the removal of Gli repressor activity but also Gli activator function (reviewed in Ribes and Briscoe, 2009). In the ventral-most region of the neural tube, exposed to high levels of Shh, Gli2 degradation is inhibited and the full-length Gli2 accumulates (Pan et al., 2006). At the same time, Gli1 expression is induced and Gli3 is repressed (Dai et al., 1999; Lee et al., 1997; Marigo et al., 1996b; Ruiz i Altaba 1998). In addition, the activity of full-length Gli1 and Gli2 appears to be further enhanced by Shh-mediated post-translational modifications (Barnfield et al., 2005; Cox et al., 2010; Merchant et al., 2004; Pan et al., 2006). Hence, the differential regulation of the levels and activity of Gli proteins in response to Shh results in an overall increase in GliA activity. The requirement for Gli2 function for the response to the highest levels of Shh is supported by the analysis of embryos lacking Gli2 function, which lose the floor plate and have a reduced number of p3 cells (Ding et al., 1998; Matise et al., 1998; Park et al., 2000). These defects can be rescued by genetic replacement of Gli1 into the Gli2 locus, suggesting that only the activator function is required for normal patterning of the neural tube (Bai and Joyner, 2001).

Together, these studies suggest that the interpretation of the Shh gradient in the neural tube was mediated by the differential activity of the transcriptional effectors of the pathway - Gli proteins: increasingly higher Shh concentrations progressively inhibit Gli repressor activity and generate increasing amounts of Gli activator (reviewed in Jacob and Briscoe, 2003). Consistent with this model, gain-of-function experiments have shown that different levels of Gli activity are sufficient to induce, cell autonomously, the full range of Shh-dependent neuronal identities (Lei et al., 2004; Stamataki et al., 2005). These data suggest that the sum of the activity of individual Gli proteins in a cell determines its transcriptional response to Shh signalling.

1.4.2 Temporal integration of graded Shh signalling

In addition to the level of Gli activity, the duration of Gli activity also appears to play a crucial role in the interpretation of the Shh gradient. Increasing times of

exposure to Shh signalling induce increasingly more ventral identities (Dessaud et al., 2007; Stamataki et al., 2005). These works suggested a more complex model of morphogen interpretation than Wolpert's "French Flag" model, which relies solely on concentration thresholds.

In the neural tube the p3 domain is located ventrally to the pMN domain, and these domains are defined by the expression of the transcription factors Nkx2.2 and Olig2 respectively (Briscoe et al., 1999; Novitch et al., 2001). High levels of Gli activity are sufficient to induce Nkx2.2 expression, whereas medium levels of Gli activity generate Olig2 cells in an equivalent period, 24-48 hours post electroporation (hpe) (Stamataki et al., 2005). However, after longer periods of incubation (72hpe), medium levels of Gli activity elicit Nkx2.2 expression, indicating that, together with the strength of signalling, the duration of signalling is critical in the specification of cell identity.

Similarly, in ex vivo assays, cells exposed to a constant concentration of Shh (4nM) upregulate first Olig2 and Nkx2.2 is expressed later (Dessaud et al., 2007). This result is consistent with the sequential induction of Nkx2.2 and Olig2 expression in vivo. In the neural tube Olig2 is induced first in cells in the ventral midline (Jeong and McMahon, 2005; Stamataki et al., 2005). As Olig2 expression gradually expands dorsally, cells in the ventral midline start to express Nkx2.2 and downregulate Olig2. Nkx2.2 expression then also expands dorsally and progressively downregulates Olig2. The dorsal expansion of Nkx2.2 expression is more restricted than Olig2 expression, thus resulting in two non-overlapping domains. Hence, Nkx2.2 expression can be induced both by higher concentrations and longer periods of Shh exposure.

The measurement of the levels of Gli activity in explants using a reporter shows that the concentration of ligand determines the duration of signalling (Dessaud et al., 2007; Dessaud et al., 2010). Concentrations of Shh below 1nM, which specify more dorsal identities (p0-p2), result in proportional levels of Gli activity (Dessaud et al., 2010). Short exposures to Olig2- or Nkx2.2-inducing concentrations (>1nM) generate saturating levels of Gli activity. After a period of time the level of Gli activity decreases both with high and low concentrations of Shh, due to the adaptation of cells to ongoing signalling (Dessaud et al., 2007; Dessaud et al., 2010). The rate of this decline depends of the the concentration of Shh: in cells exposed high levels of Shh Gli activity takes longer to return to basal levels than in cells exposed to low levels of

Shh. This model, termed "temporal adaptation", is based on the progressive decrease in the sensitivity of cells to ongoing Shh signalling (Dessaud et al., 2007) (Figure 1.4). At early times cells are highly sensitive to Shh and low concentrations of ligand are sufficient to activate the highest levels of signalling. With increasing time, cells become progressively desensitized to Shh and higher concentrations of signal are required to sustain high levels of intracellular signalling. Thus, the concentration of Shh a cell is exposed to determines the level and duration of intracellular signalling that ultimately define its positional identity. High levels and durations of signalling are required for the more ventral domains, pMN and p3 (Dessaud et al., 2007). Intermediate domains (p0-p2) are induced by lower concentrations of Shh, but the duration of signalling is also important for the specification of the neuronal subtypes (Dessaud et al., 2010). In addition, cells require that signalling levels are maintained above basal levels for an extended period of time, reverting to antecedent identities if the signalling levels fall below a threshold (Dessaud et al., 2010). Hence, the duration of signalling is important not only for the establishment but also for the refinement and maintenance of positional identity.

These data propose a model of neural tube patterning in which the positional identity of progenitors is determined in a dynamic manner by the levels and duration - the "time integral" - of signalling (Dessaud et al., 2010).

The adaptation to the continuous exposure to Shh can be explained, at least in part, by the upregulation of Ptch1 (Figure 1.4). The Shh receptor Ptch1 is both a Shh-target gene and a negative regulator of the pathway (Goodrich et al., 1996; Goodrich et al., 1997; Jeong and McMahon, 2005; Marigo and Tabin, 1996). Increasing levels of Shh result in the accumulation of Ptch1. Consequently, increasing concentrations of Shh are required to block the inhibitory activity of Ptch1 and sustain high levels of intracellular signalling. As a result, the levels of Shh are not linearly converted into levels of intracellular signalling, but into proportional periods of signalling. Consistent with this, when Ptch1 upregulation is inhibited ex vivo, lower concentrations of Shh are required to induce the expression of ventral genes (Dessaud et al., 2007). Thus, the negative feedback mechanisms involving the Shh-dependent induction of Ptch1, and possibly other ligand binding inhibitors, is important not only for the shaping of the gradient itself but also for the gradual adaptation of cells of ongoing signalling. These data are in contrast with the

conventional view of morphogens, which states that the establishment of the morphogen gradient is independent of the interpretation of positional information (Jaeger and Reinitz, 2006; Wolpert, 1969).

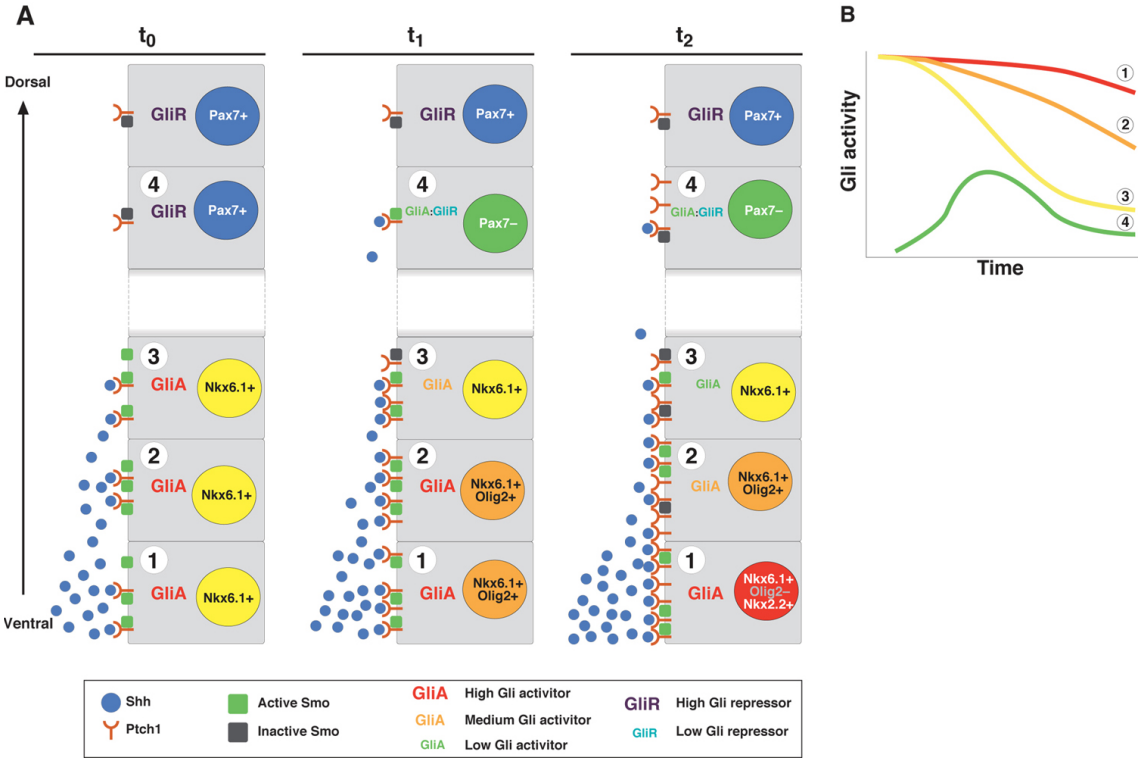

Figure 1.4 A "temporal adaptation" model for interpreting graded Shh signalling.
(**A**) The progressive specification of ventral neural progenitor domains is established by a dynamic gradient of Shh signalling. At early time points (t_0) the receptor Ptch1 (brown) is expressed at low levels, which are rapidly saturated by Shh molecules (blue). As a result, even low concentrations of Shh (cell 3, t_0)are able to activate the pathway (Active Smo - green) and generate high levels of Gli activity (GliA - red). The activation of the pathway induces the up-regulation of Ptch1 (and possibly other negative regulators of the pathway), resulting in increased levels of Ptch1 at later time points (t_1). Due to the increased number of Ptch1 molecules, higher concentrations of Shh are required to sustain high levels of Gli activity (cell 2, t_1). In cells exposed to levels of Shh that are insufficient to occupy all receptors (cell 3, t_1), the level of Gli activity declines (GliA - orange). The desensitization of cells to ongoing Shh signalling continues over time (t_2), resulting in the progressive decline in Gli activity (GliA - green) in cells at a distance from the source (cell 3, t_2). Hence, cells at different positions from the ligand source (cels 1-4) experience different levels and durations of Gli activity, and consequently exhibit distinct profiles of gene expression. For example, the sequential

induction of Nkx2.2 and Olig2 expression is at least partially explained by the duration of Shh signalling: cells exposed to high levels of Shh for short periods of time express Olig2 (cell 1-2, t_1), but after more prolonged periods of high Shh signalling Nkx2.2 expression is induced and Olig2 expression is repressed (cell 1, t_2). (**B**) As a result of the gradual adaptation of cells to ongoing Shh signalling, cells at different positions of the neural tube (cells 1-4 in A), and thus exposed to different Shh concentrations, exhibit distinct temporal profiles of Gli activity. [Figure adapted from Dessaud et al., 2008].

1.4.3 The gene regulatory network of the ventral neural tube

The accurate interpretation of the Shh gradient depends not only on the transcriptional response of cells to Shh signalling, but also on further interactions between the Shh target genes. Gli proteins appear to directly regulate the expression of transcription factors that incorporate the gene regulatory network (GRN) operating in the neural tube. The expression of Class I transcription factors is repressed by Shh signalling and the expression of Class II transcription factors requires Shh signalling. In addition, some of these factors function as transcriptional repressors and regulate the expression of other members of the GRN (Muhr, 2001). The cross-regulatory interactions between pairs of transcription factors downstream of Shh-Gli signalling have a key role in the correct spatial organization of the neural cell fates (Bailey et al., 2006; Briscoe et al., 2000).

The dynamic patterning of the neural tube GRN proteins might also be partly explained by their repressive activities (reviewed in Dessaud et al., 2008). The delay in the expression of some Shh target genes in the neural tube could depend on a mechanism in which the early response of cells to the morphogen influences its subsequent response, in line with the "sequential cell context" model proposed by Pages and Kerridge (Pages and Kerridge, 2000). An early period of Gli activity would result in the transcriptional inhibition of a target gene with repressive activity, for example a Class I gene. The removal of this repressive factor would allow the reciprocal Class II gene to respond to later periods of Gli activity. Hence, the positional identity of a neural progenitor cell might be dynamically established

through the combined action of the morphogen gradient and the transcriptional state of the gene regulatory network in the responding cell (Dessaud et al., 2010).

1.5 Aims

The patterning of the ventral neural tube is a dynamic process that depends on the action of the morphogen Shh. The interpretation of the Shh gradient in the neural tube appears to differ from conventional models of morphogen interpretation in that the positional information is provided by both levels and durations of Shh signalling. However, the mechanisms of morphogen interpretation have only been examined in in vitro studies. We hypothesized that in vivo the levels of Shh are also not sufficient to define the position of target gene boundaries in the neural tube and cells continuously respond and adapt to the levels of Shh over time.

To acquire a better understanding of the dynamics of the vertebrate neural tube in vivo I undertook a quantitative approach to systematically characterize the spatial and temporal expression patterns of the transcription factors that delineate the neural progenitor domains in chick and mouse. This quantitative analysis also included the spatial and temporal dynamics of the Shh gradient and a reporter for Shh intracellular signalling. Based on this analysis I tested the relationship between the signal, intracellular response and pattern in vivo. This approach also allowed me to address how patterning and growth are coordinated during the development of the neural tube. In addition I compared the conservation of pattern formation between two different species, chick and mouse.

This study also aimed to address the mechanism of Shh signalling, in particular whether there was more evolutionary conservation in the signal transduction pathway than had been proposed by Varjosalo et al. (Varjosalo et al., 2006). We hypothesized that Costal2 function is involved in the transduction of the Shh signalling pathway in vertebrates.

To this end I assessed the activity of Costal2 and vertebrate orthologs of Costal2 , Kif7 and Kif27, in the neural tube.

CHAPTER 2 - MATERIAL AND METHODS

2.1 Embryo manipulation

2.1.1 Embryo collection and staging

Chick embryos were obtained from fertilised eggs incubated at 38ºC for timed periods. The harvested embryos were dissected in cold PBS to remove surrounding tissues and staged. Embryos with less than 42 somites were staged according to the somite number (Table 1). For later time points, when new somites are no longer being formed, the staging was based on Hamburger & Hamilton (HH; Hamburger and Hamilton, 1951). To facilitate embryo comparisons, the stage of the embryos was transformed into "effective developmental time" (hours post fertilisation - hpf) by assuming that the first pair of somites is formed 23h after fertilisation (Hamburger and Hamilton, 1951) and that one pair of somites is added every 90 minutes of incubation (Palmeirim et al., 1997) (see Table 1). For the comparison with mouse stages, chick embryos were staged in hours post initiation of somitogenesis (hps), which excludes the initial 23h period of development (Table 1).

Mouse embryos were obtained from timed matings of wild-type Parkes mice or transgenic *Tg(GBS-GFP)* reporter mice (generated by Vanessa Ribes). Embryos were dissected from the uterus and isolated from the placenta and extra-embryonic tissues. The day of the vaginal plug discovery was considered as embryonic day E0.5. Mouse embryos from E8.0 to E9.5 were staged according to the number of somites, and converted to developmental time assuming that a pair of somites is formed every two hours (Bessho et al., 2001; Hirata et al., 2002)(Table 2). The time converted from the number of somites was expressed as hours post initiation of somitogenesis (hps). Embryos older than E9.5 were staged according to the number of days post-plug discovery.

Table 1. Nomenclature for chick embryo staging

Developmental time (hpf)	Developmental time (hps)	HH stage	Number of somites
23	15	7	1
38-40	15-16.5	10	10-11
41-44	18-21	11	12-14
45-49	22.5-25.5	12	15-17
50-53	27-30	13	18-20
54-59	31.5-36	14	21-24
60-62	37.5-39	15	25-26
63-65	40.5-42	16	27-28
66-71	43.5-48	17	29-32
72-77	49.5-54	18	33-36
78-82	55.5-58.5	19	37-39
83-87	60-64.5	20	40-43
96	73	22	NA
120	97	25	NA
144	121	28	NA
168	145	30	NA

Table 2. Nomenclature for mouse embryo staging

Developmental time (hps)	Embryonic day	Number of somites
2	E7.25	1
8	E7.5	4
20	E8	10
40	E8.5	20
50	E9	25
60	E9.5	30
70	E10	35
80	E10.5	40
90	E11	45
100	E11.5	NA

2.1.2 Embryo processing

The harvested embryos were dissected in cold PBS to remove surrounding tissues and transferred to a 4% paraformaldehyde (PFA)/0.12M Phosphate Buffer (PB) solution, on ice. The fixation time varied from 45 to 90min, depending on the size of the embryos. After fixation the embryos were thoroughly washed in cold PBS and placed in a 15% sucrose/0.12M PB solution at 4^{o}C until equilibrated. The samples were then incubated in a 7.5% gelatin/15% sucrose/0.12M PB solution, warmed to 42^{o}C. When the embryos were equilibrated in the gelatin solution they were transferred to a plastic mould and positioned in an orientation suitable for sectioning. After solidification of the gelatin the block was frozen in an isopentane solution at -40^{o}C and stored at -80^{o}C. The frozen gelatin blocks containing the embryos were cut into 14 μm-thick sections using a cryostat and arranged in slides. The embryos were sectioned along the transverse plane.

2.2 Immunohistochemistry

The slides with the cryo-sections were washed in PBS warmed to 42ºC (4 x 5min) to remove the gelatine, followed by a wash in PBT (PBS/0.1% Triton X-100). The samples were blocked in a PBS/0.1% Triton X-100/1% BSA solution for 1h. After blocking the slides were incubated with the primary antibodies (Table 3) diluted in blocking solution and placed overnight in a humidified chamber at 4ºC. The following day the sections were washed in PBT (5 x 5min) and incubated for 2h in the dark at room temperature (RT) with the secondary antibody diluted in blocking solution according to the manufacturer's specifications (Jackson ImmunoResearch Labs; conjugated to FITC, Cy3 or Cy5). After incubation the slides were washed in PBT (3 x 5min) and PBS (2 x 5min), mounted with ProLong Gold antifade Dapi (Invitrogen) and protected with coverslips.

Table 3. Primary antibodies used for immunohistochemistry

Antibody	Species	Dilution	Origin
Arx	Rabbit	1:1000	Gift from Dr. Chelly J.
Acetylated α-tubulin	Mouse	1:3000	Sigma
Flag	Rabbit	1:10000	Sigma
Foxa2 (HNF3ß)	Mouse	1:25	Hybridoma Bank (4C7)
γ-tubulin	Mouse	1:5000	Sigma (T6557)
GFP	Sheep	1:1000	Sigma
GFP	Rabbit	1:1000	Invitrogen, Molecular Probes (A11122)
Myc	Mouse	1:5000	Sigma
Nkx2.2	Mouse	1:50	Hybridoma Bank (74.5A5)
Nkx2.2	Rabbit	1:800	Gift from Dr. Kutejova E.

Antibody	Species	Dilution	Origin
Olig2	Guinea Pig	1:6000	Gift from Dr. Novitch B.
Olig2	Rabbit	1:2000	Millipore (AB9610)
Olig2	Goat	1:1000	R&D systems (AF2418)
Pax6	Mouse	1:20	Hybridoma Bank
Pax7	Mouse	1:20	Hybridoma Bank
Ptch1	Rabbit	1:500	Gift from Dr. Argraves W. S. (Morales et al., 2009)
Shh	Mouse	1:20	Hybridoma Bank (5E1)

2.3 Fluorescent in situ hybridisation

2.3.1 Synthesis of riboprobes for in situ hybridisation

Plasmid DNA was linearised using the appropriate enzyme for 2h and gel purified using Gel Band Purification Kit (GE Healthcare) according the manufacturer's instructions. The linearised DNA was used as a template for in vitro RNA transcription: 1µg linearised DNA, 1X DIG-RNA labelling mix (Roche), 1X Transcription Buffer (Roche), 60 Units RNase inhibitor (Roche) and 40 units RNA polymerase (T3, T7 or SP6; Roche) in a total volume of 50µl were incubated at 37°C for 2h. 20U of DNase I (Roche) were added to remove template DNA and the reaction was stopped with 2µl of 0.5M EDTA pH8.0. RNA probes were purified through a G-50 column (Amersham Biosciences). The approximate concentration of the probes was estimated by gel electrophoresis and diluted appropriately for the subsequent hybridisation (1:100 to 1:400).

2.3.2 Fluorescent in situ hybridisation on cryostat sections

Frozen cryostat sections were defrosted 30 minutes at RT. The riboprobe was diluted in hybridisation buffer (Table 4) and denatured at 70ºC for 5 minutes. The sections were covered with the hybridisation buffer, protected with a coverslip and incubated at 70ºC overnight in a humidified chamber (chamber solution: 50% Formamide/1X SSC). The following day the slides were washed 15 minutes at 65ºC in washing buffer (50% Formamide/2X SSC/0.1% Tween-20) to remove coverslips. After an additional wash in washing buffer for 30 minutes at 65ºC, the slides were washed in 50% Formamide/0.2X SSC/0.1% Tween-20 at 65ºC (2 x 30 minutes). Slides were then transferred to TNT (0.1M Tris pH7.5/0.15M NaCl/0.1% Tween-20) (3 x 5 minutes at RT). Sections were blocked in 0.5% heat inactivated sheep serum/TNT for 30 minutes at RT. The blocking solution was replaced with the antibody solution (1:2000 Anti-DIG-POD in 0.5% heat inactivated sheep serum/TNT) and the slides were incubated overnight at 4ºC in a humidified chamber. The following day the slides were washed in TNT at RT (3 x 5 minutes). The detection of the signal was performed using the Tyramide Signal Amplification System (PerkinElmer). The fluorophore tyramide working solution was added to the slides (250µl), followed by an incubation for 4 to 6 minutes in the dark at RT. The reaction was stopped with TNT (4 x 5 minutes at RT). After a wash with PBS, the slides were mounted with ProLong Gold antifade Dapi (Invitrogen) and protected with coverslips.

Table 4. Solutions for in situ hybridisation

Solution	Formulation
Hybridisation Buffer	1X SALT, 50% Formamide, 10% Dextran sulphate, 1mg/ml Yeast RNA, 1X Denhardt's
10X SALT	0.19M NaCl, 10mM Tris pH7.2, 5mM Phosphate Buffer pH6.8 (7.8g $NaH_2PO_4.2H_2O$/7.1g Na_2HPO_4 per 1L), 5mM EDTA

2.4 Preparation of plasmid DNA

2.4.1 Transformation of competent bacteria

Plasmid DNA (pCAGGS expression vector with or without inserted cDNA) was transformed into chemically competent DH5-α E.coli bacteria. Up to 50ng of DNA was added to a 50µl aliquot of competent bacteria thawed on ice. The mixture was gently mixed and incubated on ice for 20 min, followed by heat shock at 42°C for 2 min and cooled on ice for 5 min. 800µl of LB medium (Luria-Bertani Broth; 10g/l Tryptone, 5g/l Yeast Extract, 10g/l NaCl, pH 7.0) was added to the mixture and incubated at 37°C for 30 min, while shaking. The bacteria were spun down and resuspended in 200µl of LB medium. The bacteria were plated on LB agar plates (LB broth + 15g/l agar) containing a selective antibiotic (0.1mg/ml ampicillin, 50µg/ml kanamycin) and incubated at 37°C overnight.

2.4.2 Plasmid DNA purification

For large scale DNA preparation, the bacterial colonies were grown in 500ml of LB medium with the appropriate antibiotic, incubated overnight at 37°C shaking. The bacterial culture was processed using the HiSpeed Plasmid Maxi Kit (Qiagen), according to manufacturers' guidelines.

2.4.3 DNA quantification

Plasmid DNA concentration was determined by measuring the absorbance at 260nm using a ND-1000 NanoDrop® (LabTech) spectrophotometer. An absorbance of 1 unit at this intensity corresponds to 50µg/ml of double stranded DNA. The A_{260}/A_{280} ratio provided an estimate of the purity of the DNA, with a ratio of 1.8 being indicative of a pure preparation.

2.5 Chick in ovo electroporation

Eggs containing HH st10-12 chick embryos (approximately 45h of incubation) were windowed and the lumen of the neural tube of the embryo injected with plasmid DNA. The plasmid DNA was diluted in TE to a concentration of 1.5µg/µl DNA and labelled with Fast Green (diluted to 0.2%; Sigma). Embryos were electroporated by placing electrodes on either side of the neural tube and delivering five 50ms pulses of 33V using a BTX electroporator. The transfected embryos were returned in the incubator to continue developing for 24 to 48h. After the specified incubation time the embryos were harvested, fixed and processed for immunohistochemistry.

2.6 Measurement of Gli transcriptional activity using a luciferase reporter assay

SmoM2, Kif7 or pCAGGS as a control were electroporated in chick embryos together with GBS-Luc, a firefly luciferase reporter construct containing eight repeats of the Gli binding sequence (Sasaki *et al*., 1999) and a Renilla-luciferase reporter carrying the CMV immediate early enhancer promoter (Promega) for normalisation. After incubation for the specified times, the transfected embryos were homogenised in Passive Lysis Buffer using a douncer on ice. The measurement of firefly and Renilla luciferase activities was performed using the Dual Luciferase Reporter Assay System (Promega).

2.7 Embryo culture experiments

Mouse embryos with 6 to 8 somites were explanted from the uterus of timed pregnant females and dissected with intact yolk sacs in pre-warmed Tyrode solution at 37°C. Embryos were cultured for 12h or 24 h in culture medium (50% heat inactivated rat serum, 50% Tyrode solution; 3 to 6 embryos per tube). Cyclopamine (Sigma) was dissolved in Ethanol and used at a concentration of 10 µM. Purmorphamine (Calbiochem) was dissolved in DMSO and used at a concentration of 5-10µM. Cultures were performed in a water-saturated roller-tube incubator at 37°C,

5% CO_2 and 5% O_2. After culture, embryos were fixed and processed for immunohistochemistry. Gene expression and the activity of the *Tg(GBS-GFP)* were always compared between embryos processed in the same culture experiment in appropriate control conditions.

2.8 Image acquisition

The images of immunostained sections were acquired using a Leica SP2 or SP5 confocal microscope with Leica software. Each fluorescence-labelled marker was detected in a single channel, with a maximum of 4 channels available. The gain of the microscope was set to obtain a minimal number of saturated pixels and the offset was adjusted to have pixels outside of the embryo equal to zero. For each marker similar settings were used for all developmental stages. Each section was scanned in three optical planes within an 1µm interval along the z axis, producing three grayscale images per channel. The three optical sections for each channel were averaged using ImageJ to create the final images. The output images were used for the quantification of the expression patterns of neural progenitors along the DV axis of the spinal cord. The grayscale images were converted to colour images using Adobe Photoshop.

2.9 Quantification of gene expression patterns

To systematically quantify the expression domains of the proteins studied we used a method based on the Plot Profile tool incorporated into the image processing software ImageJ. This tool measures the intensity profile along a region of interest (ROI) within an image. The output data contain the widthwise average intensity levels for every pixel along the length of the ROI. To measure the intensity profiles in the neural tube images, we defined a region of interest that encompassed the total DV length of the neural tube and had a width of approximately two cells (*ca*. 15µm) (Figure 2.1 A). For each section both sides of the neural tube were measured. The DV extent of the neural tube was defined using the Dapi channel to identify the most ventral cells (floor plate) and the most dorsal cells (roof plate). Along the medial-

lateral axis the ROIs were placed adjacent to the lumen walls on both sides of the neural tube. The width of the measurement region was set narrower than the width of the neural tube to avoid measuring unequal boundaries. In later stages some domain boundaries are not perpendicular to the lumen walls, this could introduce positional errors. The background levels for each marker were measured in regions of the embryo where the marker is not expressed. The background levels were then subtracted from the raw intensity levels.

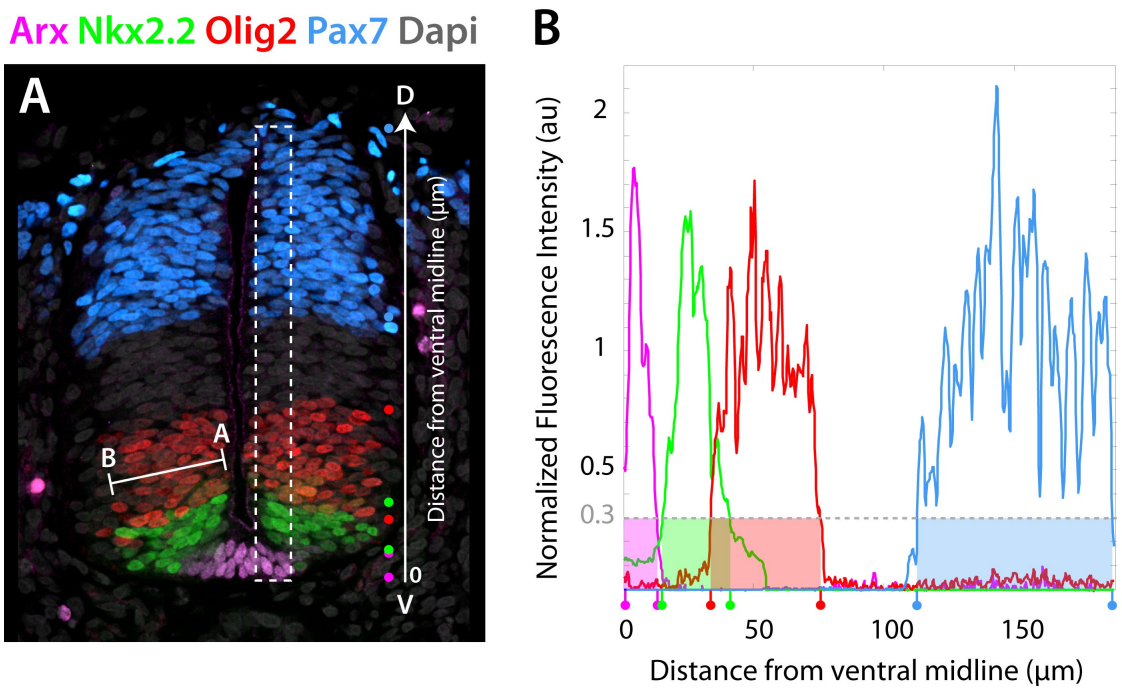

Figure 2.1 Quantification of the expression domain boundaries.
(**A**) Immunohistochemistry showing the expression patterns of the transcription factors Arx (Floor Plate - pink), Nkx2.2 (p3 - green); Olig2 (pMN - red) and Pax7 (dI1-6 - blue) at HH stage 18. The rectangle (white dashed line) identifies the region of the neural tube used to quantify the gene expression patterns. The rectangle was placed adjacent to the lumen and from the base of the floor plate (0µm) to the top of the roof plate. The apico-basal (AB) distance was measured by placing a line in the middle of the domain, perpendicular to the lumen. (**B**) Expression levels of the labelled transcription factors in the rectangle region, presented as fluorescence intensity normalized to the average intensity in arbitrary units (au), as a function of the distance from the ventral midline. The position of the boundary for each transcription factor was defined as the position where the normalized fluorescence intensity falls bellow 0.3 (colored dots identify these positions on the x axis).

After acquiring the background-subtracted intensity profiles the data for the progenitor markers were analysed to obtain the positions of the domain boundaries (Figure 2.1 B). The boundaries were defined using the following criteria: the intensity values were normalised to the average intensity within the domain; the average intensity of the domain was calculated from the average of all the intensity values above two times the background levels; the boundary position was defined as the DV point were the normalised intensity crossed the threshold 30% of the average intensity. The threshold value of 0.3 closely reflected the edge of the expression domain as identified by visual inspection of the images.

To measure the apico-basal (AB) size of the domains we used ImageJ to measure the distance from the lumen to the basal border, in a line placed at half the DV size of the domain (Figure 2.1 A).

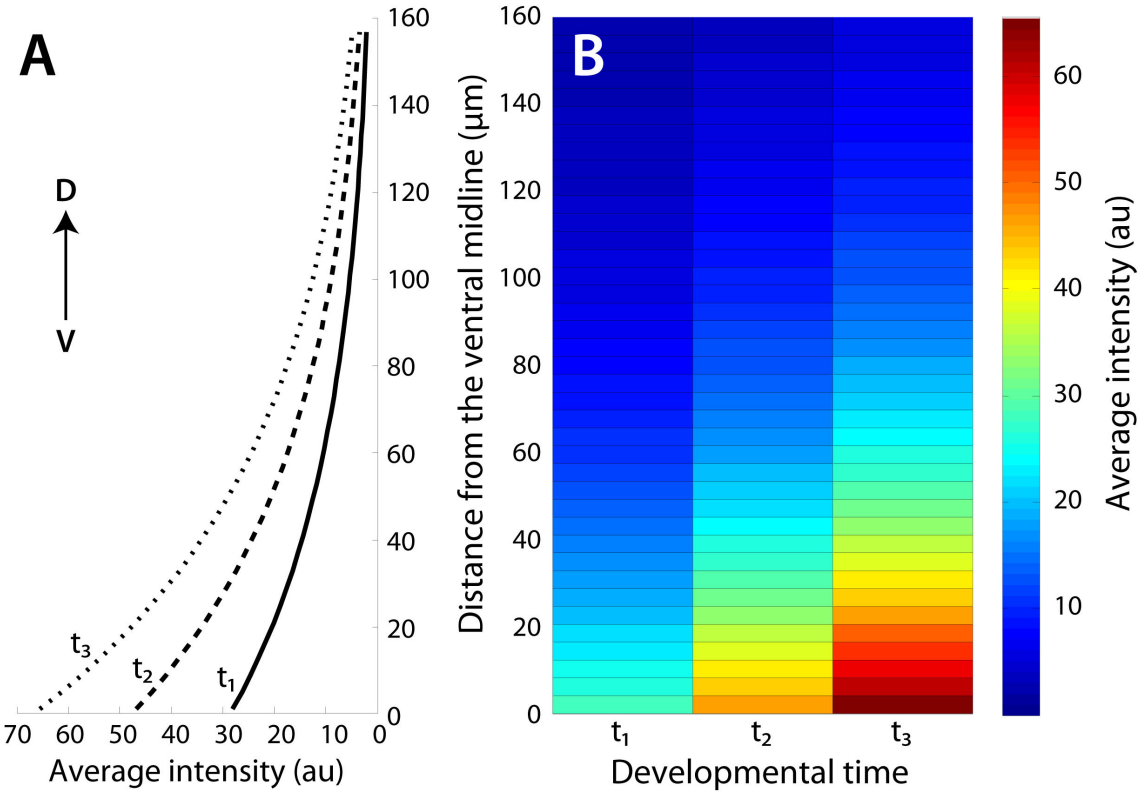

Figure 2.2 Visualization of graded profiles of expression.

(**A**) Schematics of the graded distribution of hypothetical protein at three different developmental stages (t_1, t_2 and t_3). The average intensity of the molecule in arbitrary units (au) is expressed as a function of the distance from the ventral midline in µm (0 µm corresponds to the most ventral position). (**B**) Heat map depicting the average intensity at

different positions from the ventral midline, at three developmental stages (t_1, t_2 and t_3). Each rectangle corresponds to a bin of 4 μm in which intensity was measured, and the color bin the bin reflects the value of the average intensity, from red (highest) to blue (lowest). The color bar shows the color range and corresponding intensity values (in au).

To visualise the distribution of graded proteins, such as Shh, Ptch1 and the Shh signalling reporter *Tg(GBS-GFP)*, we made use of the pcolor plotting tool available in MATLAB (MathWorks, Natick, MA). This tool provides a colour-coded plot, in which the highest values are presented in red, and the lowest in blue. The fluorescence intensity levels of the immunostained proteins were quantified in a small region adjacent to the lumen of the neural tube using ImageJ, as described in Figure 2.1A. For these plots, the average fluorescence intensity of each protein was measured in 4μm (or 1% of the neural tube) bins, placed at increasing distances from the ventral midline (Figure 2.2 A,B). This type of plot allows the comparison of the spatial distribution and levels of expression of the proteins of interest between different developmental stages.

SECTION I

CHAPTER 3 - QUANTITATIVE ANALYSIS OF NEURAL TUBE PATTERNING

Dorsoventral patterning of the developing neural tube establishes the functional organization of the vertebrate spinal cord. The spatial distribution of the neural progenitor domains is directed by opposing signals: the graded activity of Sonic Hedgehog (Shh) specifies the ventral domains, whereas BMP and Wnt signalling appear to provide positional information in the dorsal neural tube (reviewed in Jessell, 2000). Cell identity in the ventral neural tube is established progressively (Briscoe et al., 2000; Dessaud et al., 2007; Ericson et al., 1997). In particular, it has been shown that both the concentration of Shh and duration of Shh signalling are important for determining distinct cell fates (Dessaud et al., 2007; Ericson et al., 1997; Jeong and McMahon, 2005). However, to date most studies have utilised either gain- and loss-of-function approaches to assay the effects at defined developmental time points (Stamataki et al., 2005) or have been largely based on ex vivo culture of neural explants (Dessaud et al., 2007). Thus, while there is evidence that ventral patterning changes in time (Jeong and McMahon, 2005; Stamataki et al., 2005), the temporal dynamics of Shh target gene activation in vivo and the precision of patterning have not been documented in detail. This raises the question, how the Shh gradient regulates the temporal dynamics of ventral patterning in vivo (reviewed in Kutejova et al., 2009).

According to conventional models of tissue patterning, based on the influential theoretical work of Wolpert (1969), morphogens form stable long-range gradients across a developing tissue. Cells at different distances to the morphogen source read the morphogen concentration and respond by activating the expression of transcription factors that establish the progenitor identities. In this model, cells respond directly to morphogen levels, by activating target gene expression at distinct concentration thresholds. However, this model does not take into account the dynamics of the patterning process. The progressive nature of pattern formation is exemplified in the neural tube by the expression of Olig2 and Nkx2.2. Olig2, which ultimately defines the motor neuron producing pMN domain of progenitors, is initially expressed in ventral midline cells and, as time progresses, expands to more dorsal positions. The more ventral cells then down-regulate Olig2 expression and activate Nkx2.2 expression, which later is the definite marker of the p3 progenitor (Chamberlain et al., 2008; Jeong and McMahon, 2005; Stamataki et al., 2005). These

changes in gene expression patterns are accompanied by an increase in the amplitude and range of the Shh gradient (Chamberlain et al., 2008). As a consequence, the time and concentration of Shh that cells, at a particular DV position, are exposed to is dynamic. Moreover, additional complexity arises from the fact that this process occurs in a growing tissue, in which proliferation contributes to the elaboration of the patterning and is likely to influence the distribution of the morphogen over time. Thus, the mechanism of cell interpretation of the positional information provided by a dynamic gradient is likely to be a complex process.

Here, we attempt to dissect part of this complexity by carefully characterising the temporal dynamics of dorsoventral patterning, how they are coordinated with the growth of the neural tube and how they correlate with temporal changes in the Shh gradient.

3.1 Characterisation of gene expression patterns of progenitor markers Arx, Nkx2.2, Olig2 and Pax7 during development

I set out to systematically and quantitatively document the spatial and temporal expression patterns of key transcription factors over the course of approximately 5 days of development. The chosen transcription factors identify four distinct regions of the neural tube: Arx labels the floor plate cells (Ribes et al., 2010); Nkx2.2 is expressed in the p3 domain (Briscoe et al., 1999), which gives rise to V3 interneurons; Olig2 is expressed in progenitors of motor neurons (pMN) (Novitch et al., 2001); Pax7 marks the dorsal region (Ericson et al., 1996), comprising the progenitor domains that give rise to the dorsal interneurons, dI1-6. In addition, the intermediate region between the dorsal boundary of Olig2 and the ventral boundary of Pax7 delineates the DV extent of the p0-p2 domains, which generate V0-V2 interneurons. I initiated the analysis in embryos at the stage corresponding to the onset of induction of Nkx2.2 in anterior regions of the prospective spinal cord - this is Hamilton and Hamburger (HH) stage 12. The measurements of the expression patterns in the different stages were performed in equivalent anteroposterior (AP) levels of the neural tube, adjacent to somite 15 (Figure 3.1) (see Materials and Methods for details on the quantification method). The developmental stage of the embryos was expressed as hours post fertilisation (hpf; see Table 1 in Chapter 2).

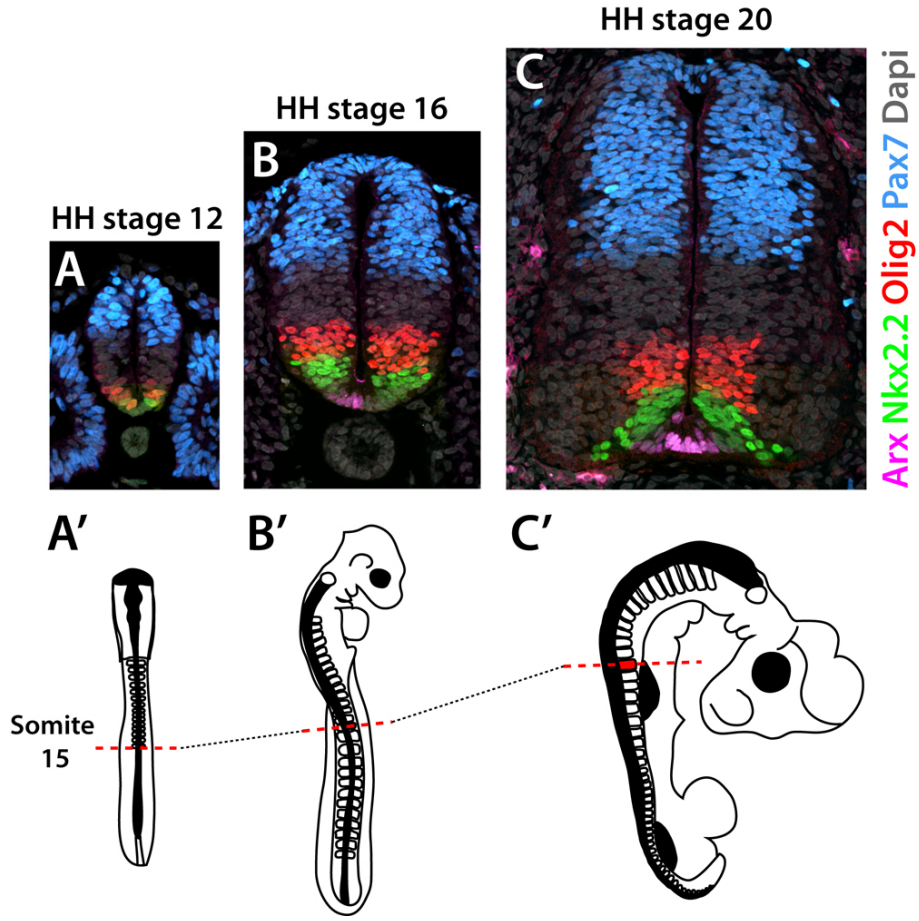

Figure 3.1 Neural tube patterning at distinct developmental stages.
(**A-C**) Immunohistochemistry showing the expression patterns of the transcription factors Arx (Floor Plate - pink), Nkx2.2 (p3 - green); Olig2 (pMN - red) and Pax7 (dI1-6 - blue) at three developmental stages: (A) HH stage 12 (47hpf); (B) HH stage 16 (64hpf); (C) HH stage 20 (85hpf). The expression patterns of these transcription factors were imaged and quantified at the somite 15 level of the neural tube (in the anteroposterior axis) for all developmental stages analyzed (A′, B′, C′).

The average expression patterns of the progenitor markers over time are illustrated in Figure 3.3. Representative images of different stages are shown in Figure 3.2. The data reveal the growth of the neural tube with a continuous increase in the DV length of the neural tube as the embryos developed (Figure 3.3 A). This increase in DV size appeared to be approximately linear with time. One possibility that could account for this linearity is that many progenitors will be differentiating to post-mitotic cells that migrate to the mantle layer, or dividing asymmetrically to generate

one progenitor daughter cell that remains in the ventricular zone, and one mantle layer post-mitotic cell (Wilcock et al., 2007). Another possibility is that growth occurs exponentially, via symmetric self-renewing divisions, however with a cell cycle rate that increases over time, such that the overall change in size in the time period I have analysed appears linear. Alternatively, the growth of the neural tube may remain linear in the DV dimension but grow exponentially in volume.

As anticipated, as the neural tube grows the positions of the domain borders also shift with respect to the DV axis and the size of the progenitor domains changes over time (Figure 3.3 A,C). Replotting the data relative to the total neural tube size to account for the growth of the neural tube revealed that the changes in the positions and sizes of the domains were not proportional to the changes in the total size of the neural tube. Thus, the progenitor domains do not scale in proportion with neural tube growth (Figure 3.3 B,D). Instead, we observed that, during specific developmental periods, some domains grew while others decreased or maintained their relative size. For example, between 64 and 96h of development the size of the Pax7 domain increased at a higher rate than predicted by the average growth of the neural tube, while the Olig2 domain grew less than the average and the p0-p2 region maintained an average growth (Figure 3.3 D).

This observation raised the question of how the elaboration of the size and position of the different progenitor domains was controlled. In the neural tube, changes in the size and the position of progenitor domains are defined by the balance between proliferation, differentiation and changes in gene expression - morphogen-dependent cell fate specification (apoptosis is negligible in the neural tube; Cayuso et al., 2006). A higher rate of proliferation or signal-induced cell-fate change would result in the increased expansion of a progenitor domain when compared to other domains. Conversely, a domain with a higher rate of differentiation would become proportionally smaller, as post-mitotic cells exit the ventricular zone. The combination of these effects in each domain determines the effective changes in size and position. The input of each factor may vary depending on the progenitor identity and on the developmental stage. To begin to dissect the regulatory events underlying the formation of the different progenitor domains the data were subdivided into three phases: early (45-64hpf), intermediate (64-120hpf) and late (120-168hpf).

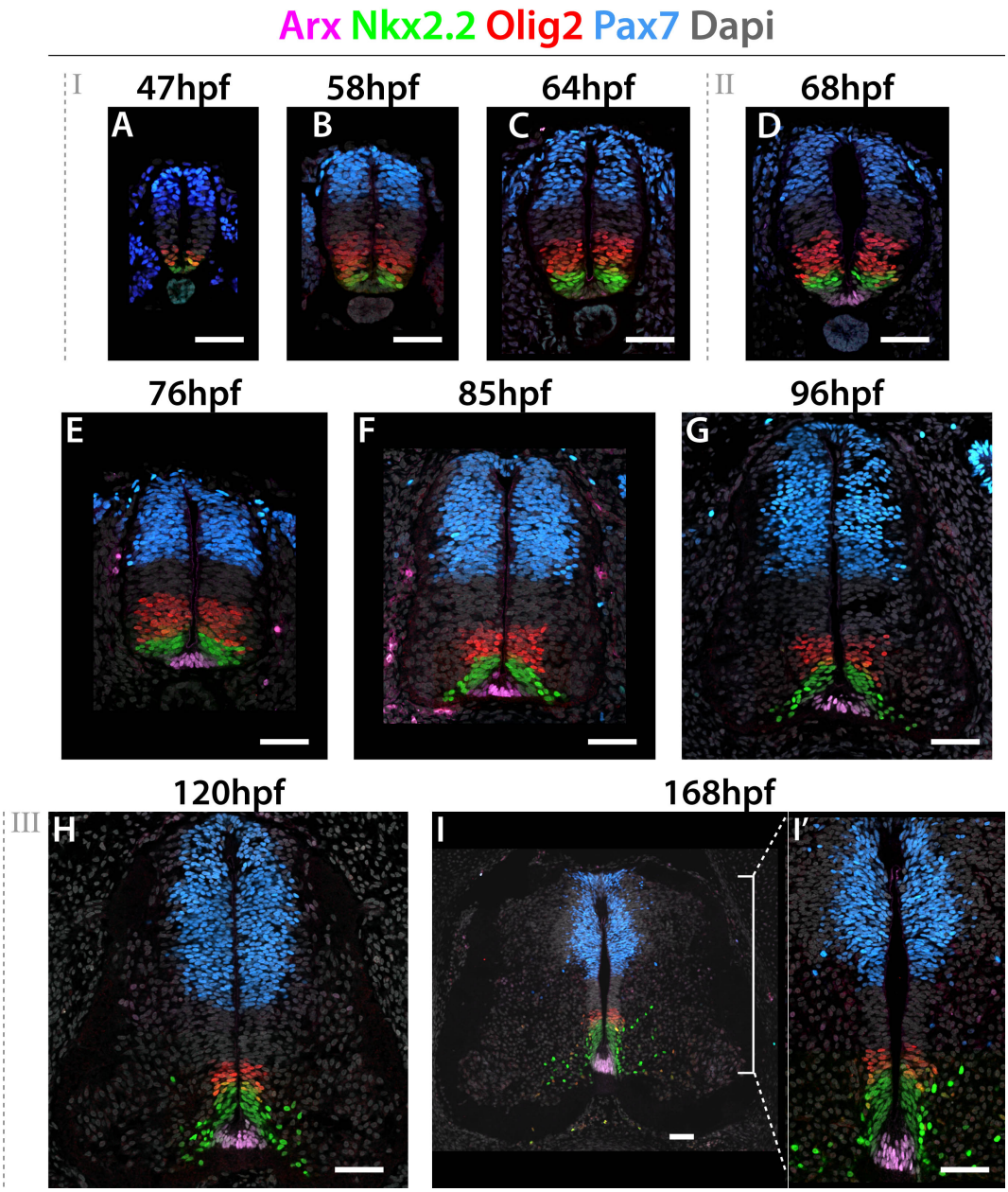

Figure 3.2 Dynamic patterning of the chick neural tube.

(**A-I'**) Immunohistochemistry showing the expression patterns of the transcription factors Arx (floor plate marker - pink), Nkx2.2 (p3 marker - green), Olig2 (pMN marker - red) and Pax7 (dorsal domain marker - blue) in transverse sections of the neural tube in embryos at the indicated stages in hours post fertilization (hpf) (in HH stages, 47hpf: HH stage 12 (A); 58hpf: HH stage 14 (B); 64hpf: HH stage 16 (C); 68hpf: HH stage 17 (D); 76hpf: HH stage 18 (E); 85hpf: HH stage 20 (F); 96hpf: HH stage 22 (G); 120hpf: HH stage 25 (H); 168hpf: HH stage 30 (I,I'). (**I'**) Higher magnification image of the region highlighted in I (white brackets). Dashed lines separate the patterning phases: I (early), II (intermediate) and III (late). Scale bars: 50 µm.

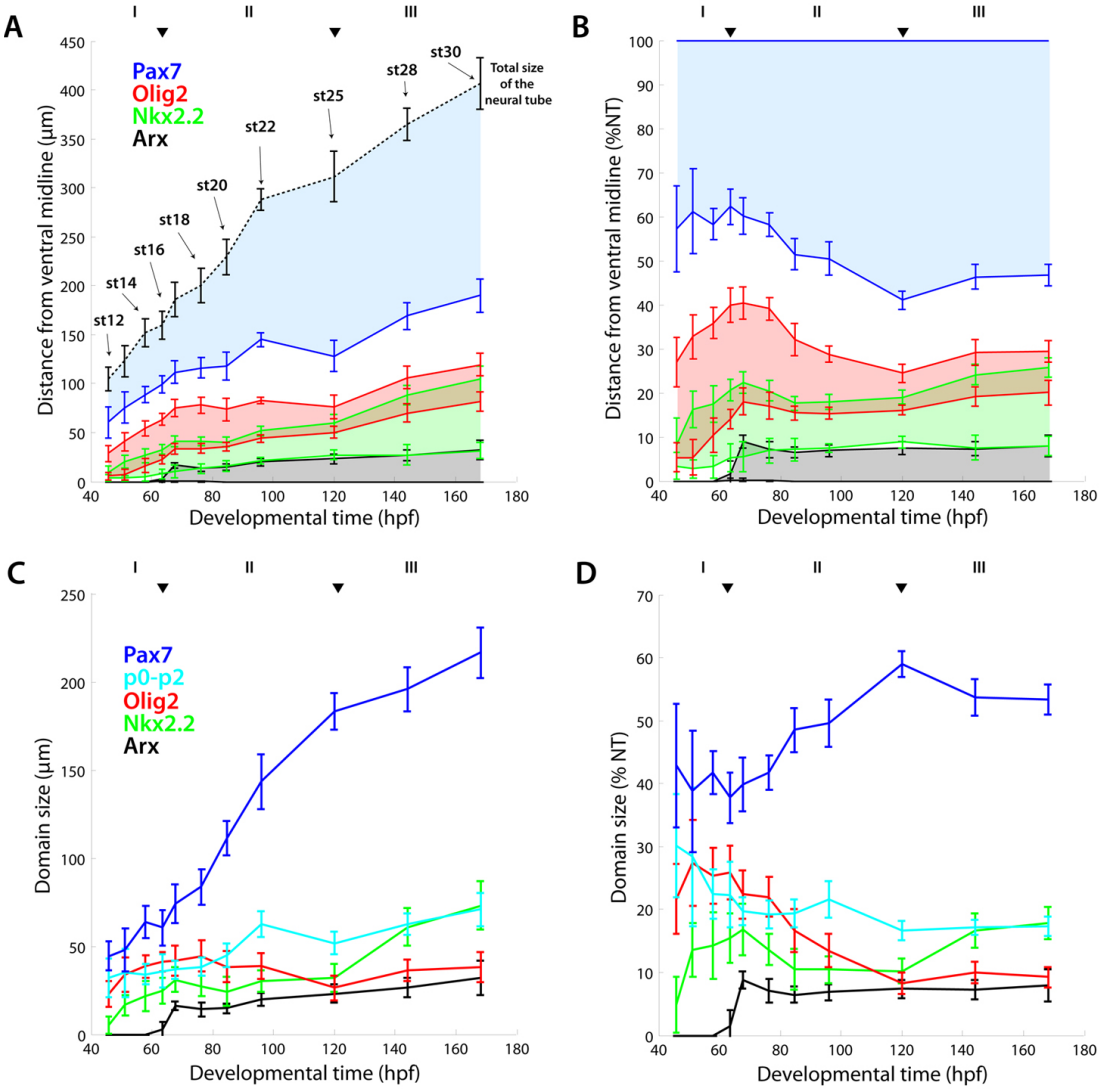

Figure 3.3 Spatial and temporal changes in the expression patterns of Arx, Nkx2.2, Olig2 and Pax7 in the chick neural tube during development.

(**A**) Quantification of the position of the boundaries of expression of the transcription factors Arx (floor plate marker - black), Nkx2.2 (p3 marker - green), Olig2 (pMN marker - red) and Pax7 (dorsal domain marker - blue) in the neural tube of chick embryos staged from 45 hours post fertilization (hpf; HH stage 12) to 168hpf (HH stage 30). The boundary positions (mean ± s.d; n≥3 embryos/stage) are expressed as the distance from the ventral midline in µm, along the dorsoventral (DV) axis of the neural tube. (**B**) Boundary positions of the progenitor domains in (A) expressed as the distance from the ventral midline relative to the total size of the neural tube (percentage of the neural tube size (%NT)). (**C**) Quantification of the size (µm) of the progenitor domains marked by the expression of the transcription factors Arx (floor plate - black), Nkx2.2 (p3 domain - green), Olig2 (pMN domain - red), Pax7 (dorsal domain - blue) and the region delimited by the dorsal boundary of the Olig2 domain and the ventral

boundary of the Pax7 domain, encompassing the p0-p2 domains (cyan) (mean ± s.d; n≥3 embryos/stage). (**D**) Absolute sizes of progenitor domains in (C) converted to sizes relative to the total size of the neural tube (% NT). Arrow heads (▼) mark the transition between patterning phases: I (early - 45 to 64hpf), II (intermediate - 64 to 120hpf) and III (late - 120 to 168hpf).

In the early period of pattern formation (45hpf to 64hpf) each of the progenitor domains gradually increased in absolute size, with the exception of the intermediate region, which maintained a constant size (Figure 3.3 A I, C I). The analysis of the domain sizes normalized to the total size of the neural tube revealed that the change in DV size was not uniform along the DV axis (Figure 3.3 B I, D I). The domains of Nkx2.2 and Olig2 expression increased in relative size, whereas the p0-p2 region decreased and the Pax7 domain remained proportionally constant in size. These data indicate that in this early phase the expression of the genes that mark the ventral domains of the neural tube expand to occupy a larger proportion of the neural tube and this is at the expense of the region that will contain the p0-p2 domains.

The observed differences in the rate at which the gene expression patterns changed raised the hypothesis that these differences emerged from differences in the proliferation or differentiation rates of each domain. To determine if the progenitor cells in distinct domains divide at different rates, the mitotic index was quantified along the neural tube (experiment performed by Anna Kicheva). The mitotic index is defined as the fraction of progenitor cells that are in mitosis. Using Dapi-stained sections of the neural tube, the condensed mitotic figures were identified and their position was determined along the DV axis. The mitotic index for each progenitor domain over time is presented in Figure 3.4. These data show that all domains have similar mitotic indexes. This was true for all the developmental stages analysed, even though the fraction of dividing cells progressively decreased over time. These results suggest that the proliferation rate does not vary according to the progenitor identity.

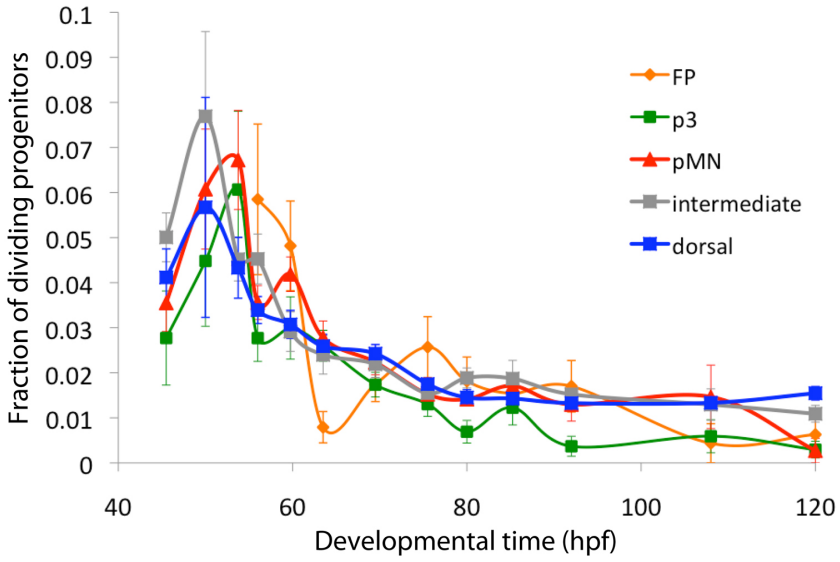

Figure 3.4 Mitotic index is constant along the dorsoventral axis of the neural tube.
Fraction of dividing progenitors (mitotic index), identified as the number of mitotic figures (with condensed Dapi staining) relative to the total number of progenitor cells within each domain (mean ± s.d; n≥3 embryos/stage). The identity of progenitor cells was determined using the expression of the transcription factors Arx (floor plate - FP), Nkx2.2 (p3 domain), Olig2 (pMN domain), Pax7 (dorsal domain) and the intermediate region between the Olig2 and Pax7 domain (p0-p2 domains). The mitotic index is similar in all progenitor domains for each developmental stage analyzed. From 50hpf (hour post fertilization) the mitotic index decreased over time, but remained similar between the different progenitor domains positioned along the dorsoventral axis of the neural tube. Experiment performed by Anna Kicheva.

The changes in the DV size of the progenitor domains could also be associated with complementing changes in the apico-basal (AB) size of the domains. For example, the ventral domains might display larger sizes than dorsal domains in the DV axis, but smaller sizes in the AB. To examine whether AB differences could account for the the differences in the DV proportions of the domains, we measured the width of each domain, at the different developmental stages (Figure 3.5). This quantification showed that the AB size is similar in all progenitor domains at the early patterning phase (I). This result indicates that the changes in the size of the domains cannot be explained by differences in AB size.

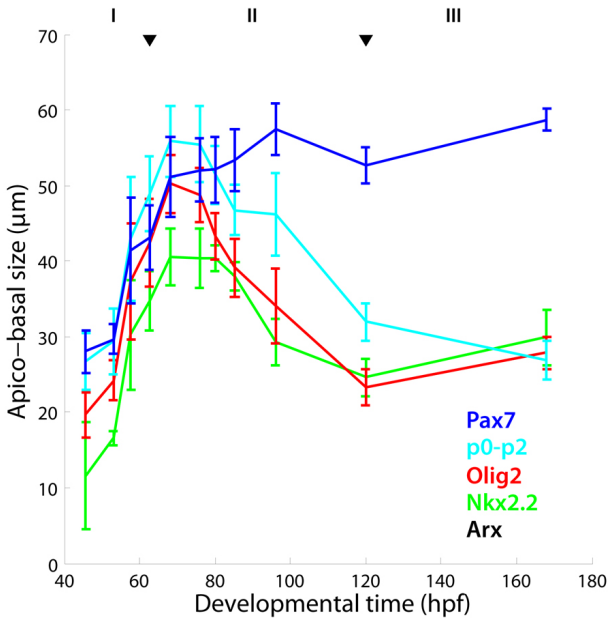

Figure 3.5 Dynamics of the apico-basal size of progenitor domains.
Quantification of the width of the expression domains of Arx (floor plate marker - black), Nkx2.2 (p3 marker - green), Olig2 (pMN marker - red), Pax7 (dorsal domain marker - blue) the intermediate region between the Olig2 and Pax7 domain (p0-p2 domains - cyan) as a function of developmental time (hours post fertilization - hpf). The apico-basal size was measured in the middle of the domain, in each side of the neural tube (mean ± s.d; n≥3 embryos/stage). Arrow heads (▼) mark the transition between patterning phases: I (early - 45 to 64hpf), II (intermediate - 64 to 120hpf) and III (late - 120 to 168hpf).

Another possibility is that the differentiation rates are different. However, the quantification of the number of post-mitotic neurons generated over time suggests that differentiation is minimal at these early stages (Anna Kicheva, personal communication). Therefore, other mechanisms must be involved in promoting the expansion of the p3 and pMN domains at the expense of the intermediate region. This process is likely to result from cell fate changes induced by the activity of Shh, which progressively induces increasingly more ventral fates. This hypothesis is explored in section 3.2.

Following this early phase in which the size of the ventral domains changed substantially, an intermediate phase ensued that was characterised by the increase in

size of the Pax7 domain (64-120hpf). The p0-p2 region displayed a more subtle, but progressive increase in size. Conversely, the p3 and pMN domains exhibited constant boundary positions, and therefore, constant sizes (Figure 3.3 A II,C II).

The beginning of the intermediate phase coincided with the initiation of the expression of the floor plate marker Arx. At the time of induction of Arx (58-64hpf) the ventral boundary of Nkx2.2 shifted dorsally, reflecting the exclusion of Nkx2.2 from the floor plate (Ribes et al., 2010). The floor plate region remained proportionally stable in size, as did the ventral limit of Nkx2.2, complementary to the floor plate boundary (Figure 3.3 B II). Conversely, the dorsal border of Nkx2.2 displayed a ventral shift in relative position, resulting in the observed decrease in size (Figure 3.3 B II, D II). The reduction in the size of the domain during this period coincides with the onset of the generation of V3 interneuron (Briscoe et al. 1999; A. Kicheva, personal communication). Similarly, the ventral boundary of Olig2 closely followed the dorsal border of Nkx2.2, while the dorsal boundary acquired progressively more ventral positions over time, resulting in a proportionally smaller domain (Figure 3.3 A II, B II). The period of the decrease in the relative size of the Olig2 domain tightly coincides with the peak of motor neuron differentiation (60-120hpf/ HH stage 15 to 22; Ericson et al., 1992; A. Kicheva, personal communication). Together with the published and unpublished data on the onset of neural differentiation, these results suggest that the dynamics of the Nkx2.2 and Olig2 domains during the intermediate phase result mainly from increased differentiation rates and a halt in the dorsal expansion in the induction of these genes.

In contrast to the Nkx2.2 and Olig2 domains, the Pax7 domain expanded. This increase in relative size did not appear to result from increased proliferation rates, as indicated by the mitotic index data (Figure 3.4). However, the lower rate of differentiation of cells in this domain, compared to p3 and pMN progenitors (A. Kicheva, personal communication) could explain the differences in the rate of expansion between the domains. From 64hpf onwards the changes in the ventral limit of Pax7 paralleled those of the dorsal border of the Olig2 domain (Figure 3.3 A II, B II). Consequently, the proportions of the intermediate region remained approximately constant during this period (Figure 3.3 C II). Together, the data suggest that the ratio between proliferation, cell-fate changes and differentiation in some or all of the domains has changed between phase 1 and phase 2 and this appears to

account for the observed changes in domain sizes.

To examine whether differences in the differentiation rate also affected the AB axis, we analysed the width of the progenitor domains (Figure 3.5). The measurement of the AB size showed that in the intermediate phase (II) the width of the ventral domains (p3, pMN and p2-p0) progressively decreased, whereas the width of the dorsal domain (marked by Pax7) remained constant. This result is consistent with the higher fraction of differentiating cells in the ventral half of the neural tube than in the dorsal half (A. Kicheva, personal communication).

In the last phase (120-168hpf) all domains maintained similar proportions over time. The stable proportions of the domains suggest that the ratio between proliferation and differentiation rates is similar in the different domains. Noticeably from 150h, the Nkx2.2 domain displayed an accentuated dorsal expansion, as the dorsal border of Nkx2.2 shifted into the Olig2 domain. The visual inspection of the images confirmed that a fraction of the Olig2^{+} cells also expressed Nkx2.2 (Figure 3.2 I'). The late emergence of Nkx2.2/Olig2 co-expressing cells was likely associated with the initiation of gliogenesis and the onset of oligodendrocytes generation (Zhou et al., 2001).

In summary, the characterisation of the dynamics of the progenitor domains uncovered a changing ratio between proliferation, morphogen-induced cell fate changes and differentiation during pattern formation. In the early phase of patterning the sizes of the domains do not scale with neural tube size, suggesting differences in the elaboration of the different domains. However, the quantification of the fraction of mitotic cells shows similar rates of division along the DV axis, independent of progenitor identity. In addition, the number of differentiating cells is very low in the initial developmental stages analysed (45-64hpf) (A. Kicheva, personal communication). As proliferation and differentiation differences cannot account for the changes in the sizes of the different domains during this phase, these changes are likely to result from changes in gene expression. The ventral region of the neural tube is still being actively patterned at these early times, and more ventral cell fates (Nkx2.2 and Olig2) are progressively induced at the expense of more intermediate and dorsal cell fates. As a result, the size of the p3 and pMN domains increases

proportionally faster than the p0-p2 and dorsal region. The contribution of cell-fate changes to the progressive ventralization of the neural tube has been previously demonstrated in lineage tracing studies. For example, p3 cells have previously expressed Olig2 (Dessaud et al., 2007), and pMN cells have previously expressed Dbx1 (Dessaud et al., 2010). The transition point between the early and the intermediate phases coincided with the induction of Arx and, importantly, the onset of motor neuron differentiation. Together, these events shape the dynamics of patterning during this phase.

With the induction of Arx, Nkx2.2 is excluded from the floor plate. In addition, post-mitotic V3 interneurons start to be generated. As a result, the size of the p3 domain remains constant, even though progenitor cells are still proliferating. Similarly, a large fraction of pMN cells differentiate into post-mitotic motor neurons, which migrate out of the progenitor domain. Unlike proliferation, differentiation rates appear to vary depending on the identity of the progenitor cells. The fraction of differentiating cells appears to be smaller in the Pax7 domain (A. Kicheva, personal communication). As a consequence, the Pax7 domain becomes proportionally larger, whereas the Nkx2.2 and Olig2 domains contract and the region comprising the p0-p2 domains remained constant in relative size. The differences between domains were even more obvious when the width of the domains was measured, showing the sharp reduction in the AB size of the ventral domains, in contrast to the uniform AB size of the dorsal region. These observations are consistent with a scenario in which there are DV differences in the rate of differentiation, such that during this phase progenitors in the Pax7 domain have a lower probability to differentiate, the p0-p2 have intermediate rates of differentiation and the pMN and p3 progenitors differentiate at the highest rate. Alternatively, it is possible that cell fate changes occur during this phase, in which ventral cell would acquire progressively more dorsal identities. More detailed lineage tracing data and differentiation rate measurements during this phase would be required to discriminate between the different possibilities. In the last stages analysed (120-168hpf) all the domains exhibited stable proportions over time, reflecting similar ratios between proliferation and differentiation along the DV axis. Only the dorsal border of the Nkx2.2 domain showed an exceptional dorsal shift in this late phase. The detection of Nkx2.2/Olig2 co-expressing cell possibly reflects a new period of induction of Nkx2.2 expression, associated to the onset of gliogenesis.

3.2 Dynamics of the Shh gradient

The dynamic changes in the expression of Nkx2.2 and Olig2 during the early stages of development raised the possibility that ventral cells are responding to a continuously changing signal. This hypothesis led us to examine the temporal changes in the Shh distribution and how these changes correlate with the dynamic expression of the target genes Nkx2.2 and Olig2.

To describe the temporal changes of the Shh gradient we measured the Shh profiles in embryos in developmental stages that span the period of active patterning of the target genes Nkx2.2 and Olig2 (47hpf to 85hpf; HH stages 12 to 20). The visualisation of the Shh distribution using an anti-Shh antibody showed a strong signal in the notochord and floor plate, the Shh production sites (Figure 3.6 A). In addition, protein detected with the antibody exhibited a graded distribution along the ventral to dorsal axis, both in the lumen and within the neuroepithelium.

The quantification of the Shh signal was consistent with the qualitative description of the Shh distribution (Figure 3.6 A,B). The highest intensity levels were detected in the Shh-producing floor plate region. Dorsally to the floor plate the Shh intensity levels gradually decreased. The distribution of the Shh protein from the ventral border of the Nkx2.2 domain was well fitted by an exponential decay function $C(x)=C_0.e^{-x/\lambda}$, where x (μm) is the distance from the floor plate boundary, C_0 is the gradient amplitude measured in units of fluorescence intensity (arbitrary units: au), and λ is the decay length (μm). The amplitude corresponds to the concentration of Shh at the source boundary and the decay length λ provides a measure of the distance over which the gradient decays, which determines the spread of the morphogen across the field (Barkai and Shilo, 2009; Wartlick et al., 2009). For this HH stage 18 embryo, C_0=100.4 au and λ =19.9 μm (r^2=0.9308) (Figure 3.6 B). The exponential form of the gradient is consistent with the previously published distribution of Shh in embryos, visualised using genetically engineered mice expressing Shh-GFP (Chamberlain et al., 2008) and with theoretical considerations of gradient formation by diffusion mechanisms (Wartlick et al., 2009).

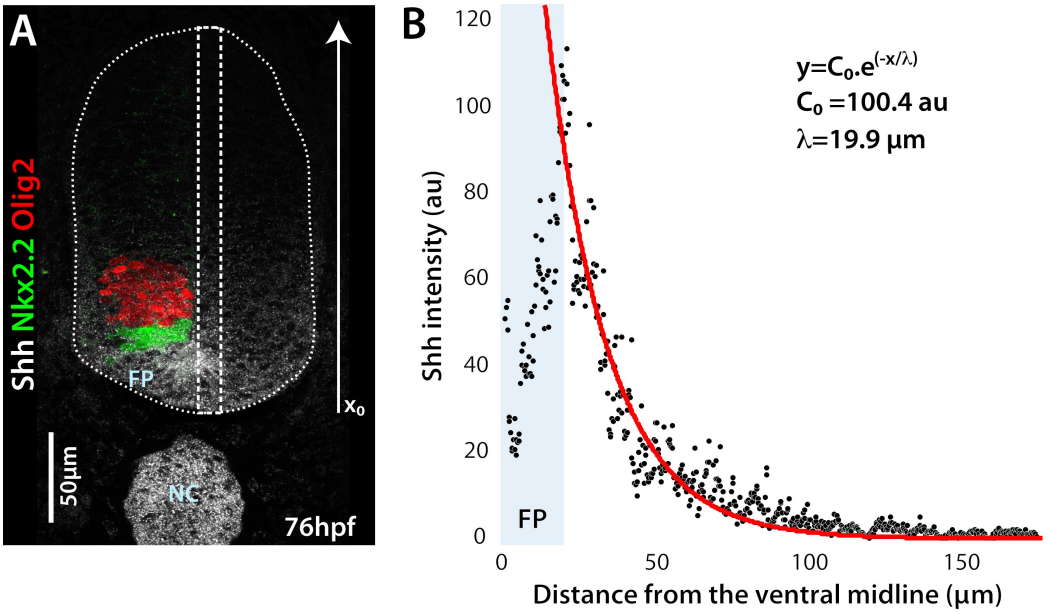

Figure 3.6 Shh protein displays an exponential distribution from the source boundary in the neural tube.

(**A**) Image of a transverse section of the neural tube of a 76hpf chick embryo (HH stage 18), immunostained for Shh protein (white) and for the Shh targets Nkx2.2 (green) and Olig2 (red). Shh protein is secreted from the notochord (NC) and the floor plate (FP), the morphogen sources, and spreads across the neural field from ventral to dorsal positions. (**B**) Quantification of Shh protein distribution along the dorsoventral (DV) axis of the neural tube. The intensity of the Shh signal was measured in a selected region (white dashed rectangle in A) located adjacent to the lumen along the DV axis, from the ventral midline (x_0 in A) to the roof plate. (B). The distribution of Shh from the floor plate boundary (floor plate region highlighted in blue) is well fitted by the exponential decay function $y=C_0.e^{(-x/\lambda)}$, in which x (µm) is the distance from the floor plate boundary, C_0 is the gradient amplitude (fluorescence intensity in arbitrary units: au), and λ is the decay length (µm). Scale bar: 50 µm.

The average Shh profiles at the different developmental stages are presented in Figure 3.8, with representative images of Shh-stained neural tubes shown in Figure 3.7. At the first stage analysed (approximately 47hpf; HH stage 12) the Shh signal was very low and the protein was only detected in the ventral midline (Figure 3.7 A, A', Figure 3.8 A). The Shh gradient progressively increased in intensity and range from 47 to 64hpf (HH stage 12 to 16) (Figure 3.7 A-C, A'-C', Figure 3.8 A). The high levels of Shh

persisted for the remaining developmental stages analysed (76hpf and 85hpf; HH stage 18 and 20) (Figure 3.7 D, E, D′, E′, Figure 3.8 A). A closer analysis of the average Shh profiles over time revealed that after the initial increase in amplitude, the shape of the gradient remained stable from 64hpf to 85hpf (Figure 3.8 B). However, the position of the peak intensity of Shh, corresponding to the Nkx2.2/floor plate boundary, gradually shifted dorsally. This shift reflected an increase in the size of the source of Shh.

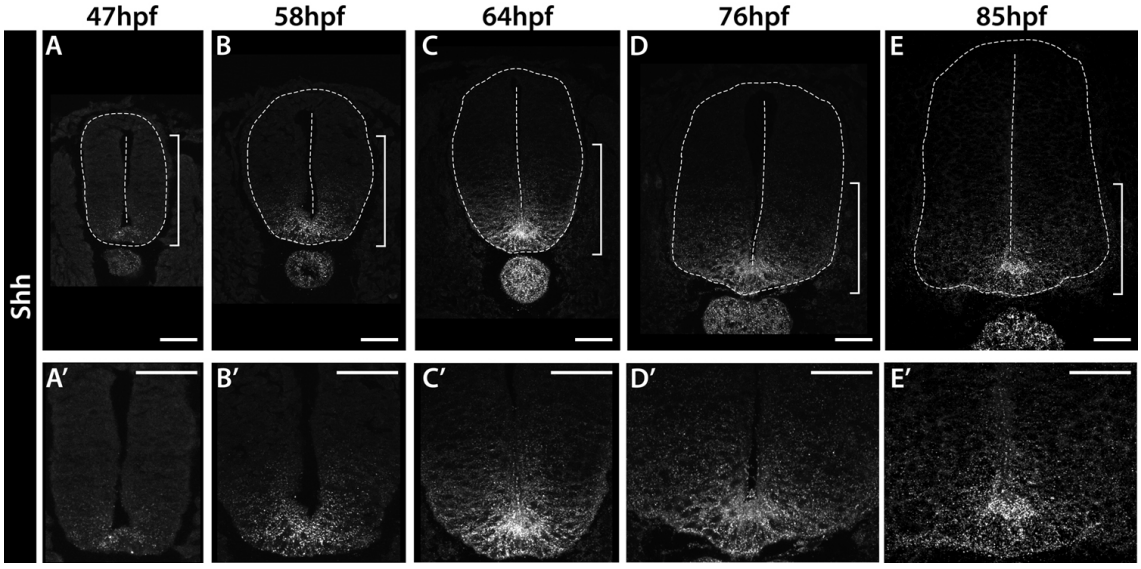

Figure 3.7 Temporal changes in Shh distribution in the chick neural tube.
(**A-E**) Immunohistochemistry showing the expression of Shh in transverse sections of the neural tube in embryos at the indicated stages in hours post fertilization (hpf) (in HH stages, A: HH stage 12; B: HH stage 14; C: HH stage 16; D: HH stage 18; E: HH stage 20). (**A′-E′**) High magnification images of the regions highlighted in A-E (white brackets). Scale bars: 50 µm.

The characteristics of the gradient were analysed in more detail by fitting exponential curves to the data using a curve fitting algorithm (MATLAB). This procedure resulted in curves with a good approximation to the gradient (average r^2=0.81 for 47hpf and above 0.90 for older stages). The parameters of the exponential curves, amplitude C_0 and decay length λ, were estimated from the individual Shh profiles, measured from the ventral boundary of Nkx2.2 (source boundary). In addition, to assess the accuracy of the estimated amplitude the value of the peak Shh

intensity was also measured in each image. The values of the estimated amplitude and decay length and the measured peak intensity were then averaged between embryos in the same developmental stage (Figure 3.8 C-E). As observed in the average Shh profiles, the Shh levels at the source boundary increased during the initial stages of development (47 to 64hpf) and remained constant in the older stages analysed (64 to 85hpf) (Figure 3.8 C). Similar dynamics were obtained with both the peak Shh intensities and the C_0 estimated from the exponential fits (compare red line with black line in Figure 3.8 C). The initial increase in Shh concentration at the source boundary is likely to result from the induction of Shh expression in ventral midline cells and then increase in the size of the source. However, the floor plate continues to expand in later stages, whereas the levels of Shh at the boundary remain constant. Therefore other mechanisms must be involved in regulating Shh concentration. Changes in the production rate of source cells may explain the changes in Shh levels, but we are unable to test this hypothesis at present. It is also possible that Shh-induced up-regulation of Ptch1 results in increased internalization and degradation of the ligand close to the source, thus limiting the increase in Shh concentration (non-linear morphogen degradation; Eldar et al., 2003).

The parameter estimation also revealed that the decay length of the Shh gradient remained mostly constant over time, with a value of approximately 20 μm (5 cell diameters) (Figure 3.8 D). Only the earliest stage transition showed a modest increase in λ, but not statistically significant ($p=0.076$). A decay length of ~20μm means that the concentration of Shh decreases by approximately one third every 5 to 6 cell diameters and by 64hpf there is approximately one order of magnitude difference between the concentration of Shh at the boundary of the floor plate and the dorsal limit of Olig2 expression. The unvarying decay length suggested that the gradient was not adjusting to the growth of the target field. Indeed, the calculation of the decay length normalised to the size of the tube revealed that, as embryos developed, λ gradually become proportionally smaller (Figure 3.8 E). Further understanding the dynamics of the decay length, and the underlying mechanisms, will require the characterisation of the diffusion and degradation rates, which is currently unavailable.

The characterisation of the Shh distribution confirmed the exponential decay of the Shh gradient and is consistent with the previously described Shh

quantification (Chamberlain et al., 2008). Moreover, the amplitude of the gradient increased during the period of induction of the ventral target genes. This result is consistent with the hypothesis that the dynamic patterning of the ventral neural tube results, at least in part, from temporal changes in the morphogen gradient.

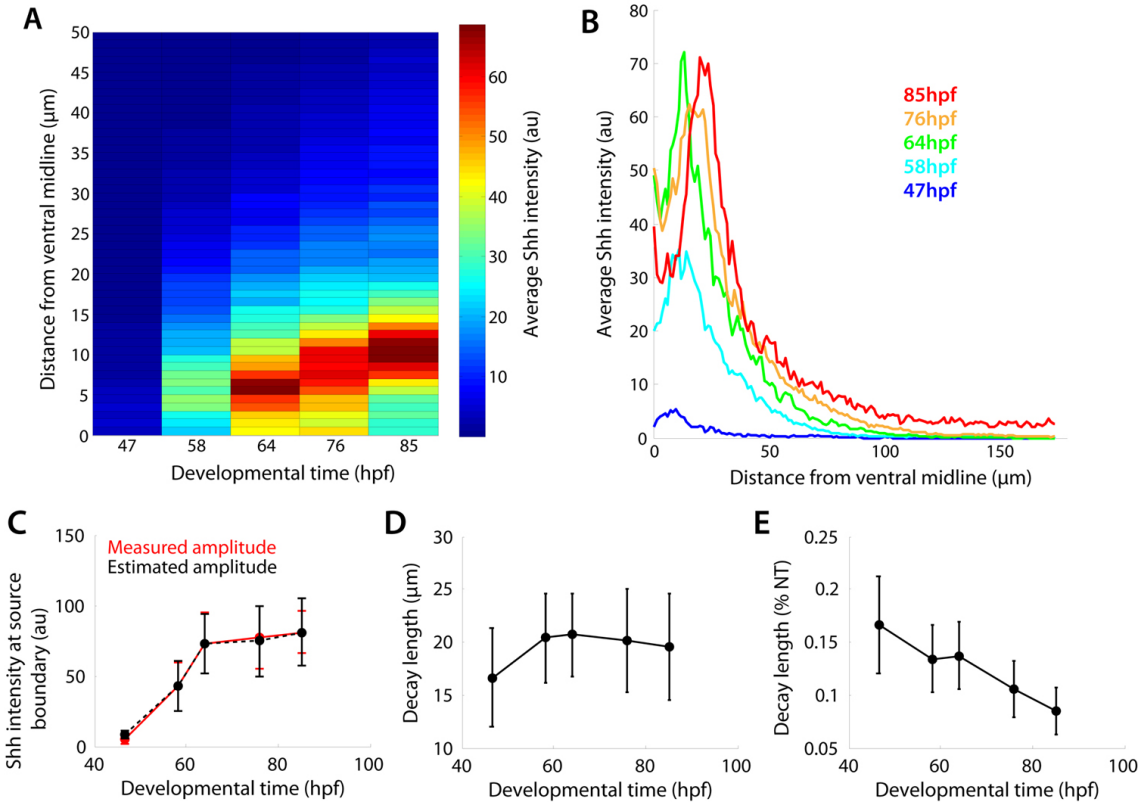

Figure 3.8 Characterization of the Shh gradient in the chick neural tube.

(**A, B**) Quantification of the Shh intensity levels as a function of the distance from the ventral midline (µm) at the indicated developmental stages in hours post fertilization (hpf) (in HH stages, 47hpf: HH stage 12; 58hpf: HH stage 14; 64hpf: HH stage 16; 76hpf: HH stage 18; 85hpf: HH stage 20). (**A**) Heat map depicting the average Shh fluorescence intensity (arbitrary units (au)) in 4µm bins along the dorsoventral axis of the neural tube of chick embryos at the indicated stages (n≥3 embryos/stage). (**B**) Average Shh fluorescence intensity profiles (arbitrary units (au)) as a function of the distance from the ventral midline (µm) at the indicated stages. Both plots show the gradual increase in intensity levels and range of the Shh gradient in initial stages of development (45 to 64hpf) followed by a period of constant levels until 85hpf (A,B). (**C**) Quantification of the Shh fluorescence intensity at the position of the source boundary (red line; mean ± s.d in arbitrary units (au)) and amplitude of the

gradient estimated from the exponential curve fits (black line; mean ± s.d in arbitrary units (au)) in embryos at the indicated stages. These quantifications show that the peak of Shh intensity increases until 64hpf and stabilizes afterwards. (**D**) Decay length of the Shh gradient (mean ± s.d in μm) estimated from exponential functions fitted to the Shh profiles in embryos at the indicated stages. The absolute decay length of the Shh gradient remains constant as the amplitude of the gradient changes. (**E**) Decay length of the Shh gradient (mean ± s.d in percentage of the neural tube size (%NT)) estimated from exponential functions fitted to the Shh profiles normalized to the total size of the neural tube in embryos at the indicated stages. The normalized decay length of the Shh gradient decreases over time, which suggests that the gradient is not adjusting to the growth of the neural tube.

To confirm that the changing profiles of the Shh protein accompanied the progressive establishment of the Nkx2.2 and Olig2 domains we compared the average intensity levels of Shh along the DV axis to the position of the boundaries of the progenitor markers (Figure 3.9 A, B). At the earliest stage analysed (47hpf; HH stage 12), when Nkx2.2 was starting to be induced, the levels of Shh were barely detectable. From 58 to 64hpf (HH stage 14 to 16), as the boundary positions of the boundaries of Nkx2.2 and Olig2 expression moved dorsally, the Shh gradient also increased in amplitude and range. The parallel changes are consistent with the idea that the changes in the expression of the target genes in these early stages are due to the response of cells to the evolving morphogen gradient. Importantly, at each stage Nkx2.2 expression was associated with the highest levels of Shh, while the Olig2 domain was located in the region of intermediate to low Shh concentrations. This is consistent with the different levels of signal required for the induction of these genes. At the later stages analysed (64 to 85hpf; HH stage 16 to 20), the shape of the Shh gradient (determined by the amplitude and decay length) remained stable. However, the source boundary moved dorsally as the FP expanded (see above), resulting in a dorsal shift in the gradient. Coincidently, the boundary positions of the target genes also shifted dorsally, but the sizes of the Nkx2.2 and Olig2 domains remained constant.

The similar dynamics between Shh and its target genes prompted us to investigate how the Shh concentration behaved at the position of the target gene

boundaries. A simple model of morphogen interpretation would predict that, target gene induction would always occur at the same morphogen concentration. Thus, in an increasing gradient, specific morphogen thresholds would be associated with progressively more dorsal positions, and therefore establish the limits of expression of target gene at progressively more dorsal positions. To determine the relation between Shh concentration and boundary position we measured the intensity levels of the Shh protein at the location of the boundaries (Figure 3.9 C). These data showed that the levels of Shh at each boundary changed over time (Figure 3.9 D). The extent of these changes was more striking in earlier stages, in which the level of Shh at the boundaries of Nkx2.2 and Olig2 increased with time (47 to 64hpf). At later times, the ventral limit of Nkx2.2, corresponding to the source boundary, had stable levels of Shh, in agreement with the stability in the gradient amplitude measurements. By contrast, the boundary between Nkx2.2 and Olig2 displayed decreasing levels of Shh. The dorsal boundary of Olig2 maintained overall low levels of Shh, but with a subtle increase over time. However, it should be noted that the Shh levels at this boundary are close to the limit of detection, thus more susceptible to quantification errors.

Together, these results suggest that the boundary positions of the target genes are not associated with constant Shh thresholds. The initial increase in Shh levels at the boundaries is consistent with the hypothesis that ventrally located cells, when exposed to increasingly higher levels of Shh, become less responsive to the ligand due to feedback inhibition mechanisms and therefore the threshold for the expression of the target genes increases (Dessaud et al., 2007). The subsequent decrease in Shh levels at the Nkx2.2/Olig2 boundary is likely to result from the fact that, while the Shh gradient remains stable, the neural tube continues to grow. Consequently, the range of the gradient decreases, as suggested also by the size-normalised measurements of the Shh distribution (Figure 3.8 B). The observed decrease in Shh levels at the boundary also raised the question of whether after induction target gene expression requires similar amounts of signal for its maintenance. Although continued Shh signalling has been shown to be required for the maintenance of ventral gene expression (Dessaud et al., 2010), it is unclear what level of signalling needs to be maintained.

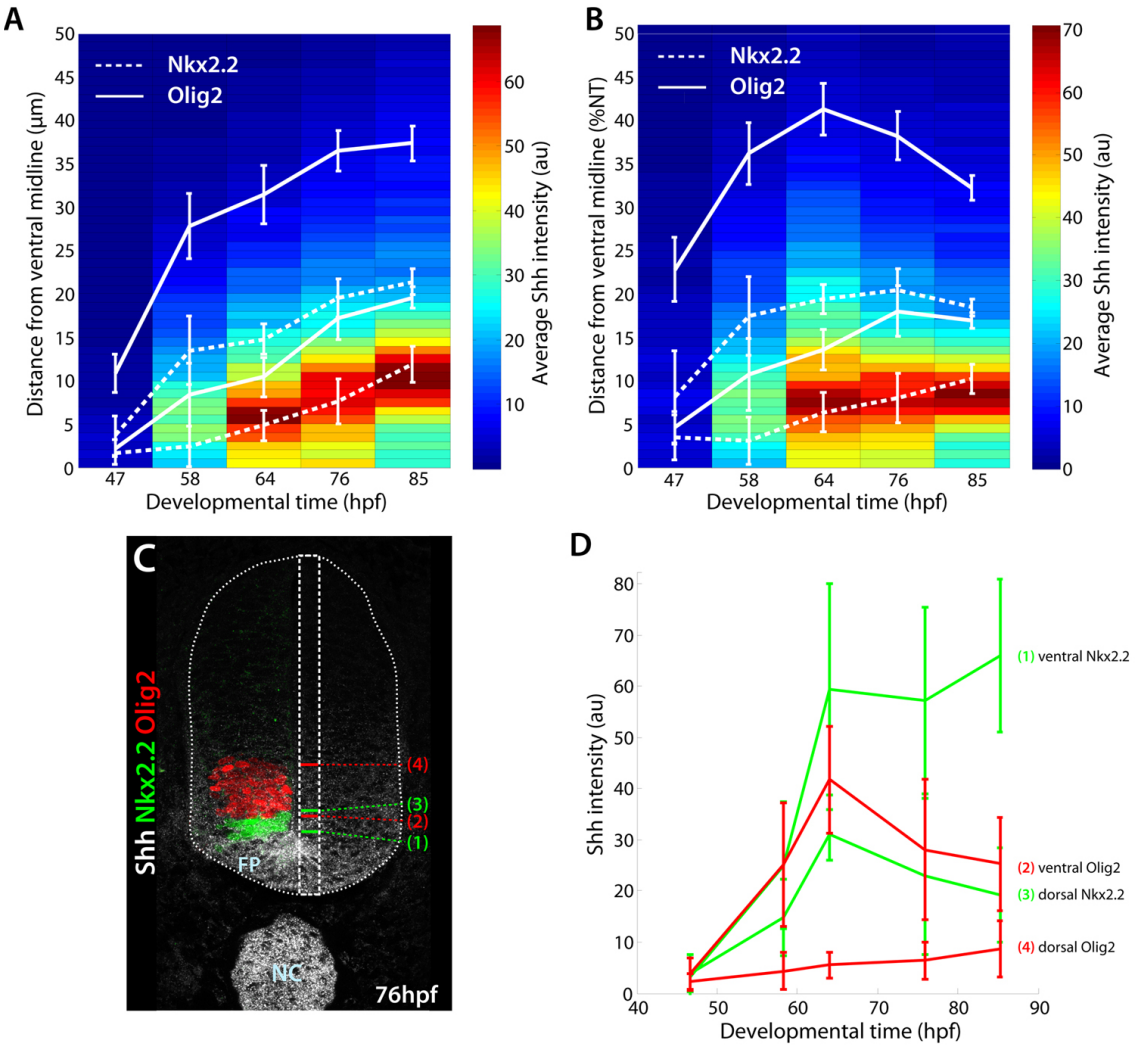

Figure 3.9 Shh intensity does not correlate with the position of the target gene boundaries.

(**A**) Heat map representing the average Shh fluorescence intensity (arbitrary units (au)) along the dorsoventral axis of the neural tube of chick embryos at the indicated stages, as well as the position of the boundaries of the target genes Nkx2.2 (dashed white line) and Olig2 (full white line), expressed as the distance from the ventral midline in µm (mean ± s.d; n≥3 embryos/stage). The increase in the levels and range of the Shh gradient is paralleled by the location of the boundaries of Nkx2.2 and Olig2 at increasingly more dorsal positions. The dorsal boundary of Nkx2.2 is generally located more dorsally than the ventral boundary of Olig2, suggesting an overlap between the two domains. This overlap can depend on different factors: cells coexpressing Nkx2.2 and Olig2, intermixed Nkx2.2 and Olig2 cells and differences in the position of the boundaries between different embryos in the same developmental stage. (**B**) Heat map of the average Shh fluorescence intensity (arbitrary units (au)) as a function of the distance from the ventral midline normalized to the total size of the

neural tube (percentage of the neural tube size (%NT)). The relative positions of the boundaries of the target genes Nkx2.2 (dashed white line) and Olig2 (full white line) are also depicted (percentage of the neural tube size (%NT)). From 64hpf the relative range of the Shh gradient decreases as the size of the neural tube increases. The Nkx2.2 domain is consistently associated with higher levels of Shh than the Olig2 domain. (**C**) Image of a transverse section of the neural tube of a 76hpf chick embryo, immunostained for Shh protein (white) and for the Shh targets Nkx2.2 (green) and Olig2 (red) (NC - notochord; FP - floor plate). The Shh fluorescence intensity was measured at the position of the ventral (1) and dorsal (3) boundaries of Nkx2.2 and the ventral (2) and dorsal (4) boundaries of Olig2. (**D**) Quantification of the Shh fluorescence intensity at the position of the boundaries of the Nkx2.2 and Olig2 domains (1-4) (mean ± s.d in arbitrary units (au); n≥3 embryos/stage). The positions of the Shh target gene boundaries of expression are not associated with particular concentrations of Shh.

In summary, the quantification of Shh distribution in the developing neural tube allowed us to verify the temporal changes in the Shh gradient, with increasing amplitude in the early patterning stages. The increase in the Shh levels is likely to result from an increase in the number of producing cells. At later times, the levels of Shh at the source boundary stabilised, despite the continued increase in the size of the source. Changes in the production, degradation and diffusion rates of the morphogen may also contribute to the changes in the amplitude and spread of the morphogen during development. In fact, the expression of several factors that bind to Shh and modulate its spread is regulated by Shh itself, such as Ptch1, Hhip1, Cdo, Boc and Gas1 (Allen et al. 2007; Chuang et al. 2003; Goodrich et al. 1996; Goodrich et al. 1997; Jeong and McMahon 2005; Marigo and Tabin 1996; Martinelli and Fan 2007; Tenzen et al. 2006; Yao et al. 2006; Zhang et al. 2006). The quantification of the parameters that determine the shape of morphogen, production, degradation and diffusion, will help understand the dynamics of gradient formation.

The gradual accumulation of Shh correlated with the progressive induction of Nkx2.2 and Olig2. Importantly, this increasing accumulation of Shh matched the requirement for increasing concentrations of Shh to specify progressively more ventral cell fates, as shown by in vitro studies (Ericson et al., 1997). However, the actual quantification of the Shh levels at the target gene boundaries revealed that, as

development proceeded, the boundaries were not always positioned at the same Shh concentration threshold. This result suggests that the dynamic activation of target genes in neural progenitor cells does not result from a direct, linear interpretation of the graded Shh concentrations. This finding is not unexpected, as ex vivo the signal transduction is also not linearly proportional to Shh concentration (Dessaud et al., 2007). The non-linearity of Shh signalling allows the morphogen concentration to control not only the level of intracellular signalling activity, but also the duration. Therefore, to understand the dynamics of target gene expression, it is important to characterise the temporal changes in signal transduction.

To investigate the dynamics of signal transduction an in vivo reporter of intracellular Shh signalling is required. Such a reporter was recently generated: a transgenic reporter mouse in which GFP expression is regulated by Gli binding sites (*Tg(GBS-GFP)*; generated by Vanessa Ribes). However, before quantifying Gli activity it was necessary to verify that the dynamics of patterning are similar between species.

The next chapter addresses the conservation of the pattern formation process between chick and mouse. In addition, the temporal changes in the Shh gradient are also characterised in mouse. The following chapter focuses on the temporal dynamics of signalling activity.

CHAPTER 4 - COMPARATIVE ANALYSIS OF NEURAL TUBE PATTERNING IN MOUSE AND CHICK

4.1 Characterisation of gene expression patterns of progenitor markers Nkx2.2, Olig2 and Pax7 in mouse

To define the dynamics of neural tube patterning in mouse embryos over an equivalent developmental window to that used in chick we quantified the expression patterns of Nkx2.2, Olig2 and Pax7 in mouse embryos spanning a period of approximately four days: E8 to E11 (Figure 4.1). Due to limitations of the anti-Pax7 antibody it was only possible to detect Pax7 expression in mouse from the 18-somite stage (36hps) onwards. The earliest stage analysed, the six-somite stage (12hps), corresponded to the stage when Nkx2.2 expression was first detected in neural tissue (Figure 4.1 A).

The average positions of the domain boundaries in mouse are presented in Figure 4.2, compared side-by-side with the chick expression profiles. An initial inspection of the temporal dynamics of expression of Nkx2.2, Olig2 and Pax7 transcription factors showed a clear similarity between mouse and chick. However, this qualitative inspection also exposed the difficulties posed by the comparison of different species. In particular, it raised the question of how to define equivalent stages - a ”registration” problem. The expression patterns were plotted as a function of the developmental time, converted from the number of somites (1.5h/somite in chick, 2h/somite in mouse; see Materials and Methods). Note that the developmental time in chick included the period antecedent to the initiation of somite formation (approximately 23h), whereas in mouse time was counted from the start of somitogenesis. In both species the time of induction of Nkx2.2 expression was used as the first measured stage (15 somites in chick and 6 somites in mouse). However, patterning may occur at a different pace in different species, that is, the developmental time required for the expression boundary of a gene to reach its final position may be different, if, for example, the proliferation and differentiation rates vary. In this case, additional adjustments to the temporal profiles may be necessary in order to compare mouse and chick data. The problem of the definition of equivalent stages is also relevant for the comparison of the sizes of the domains and the neural tube.

To begin to address the differences between the two organisms, the mouse data was first analysed independently of the chick data. This analysis sought to characterise the dynamics of gene expression based on the patterning phases previously defined in chick. After identifying the defining events, the mouse and chick data were then directly compared.

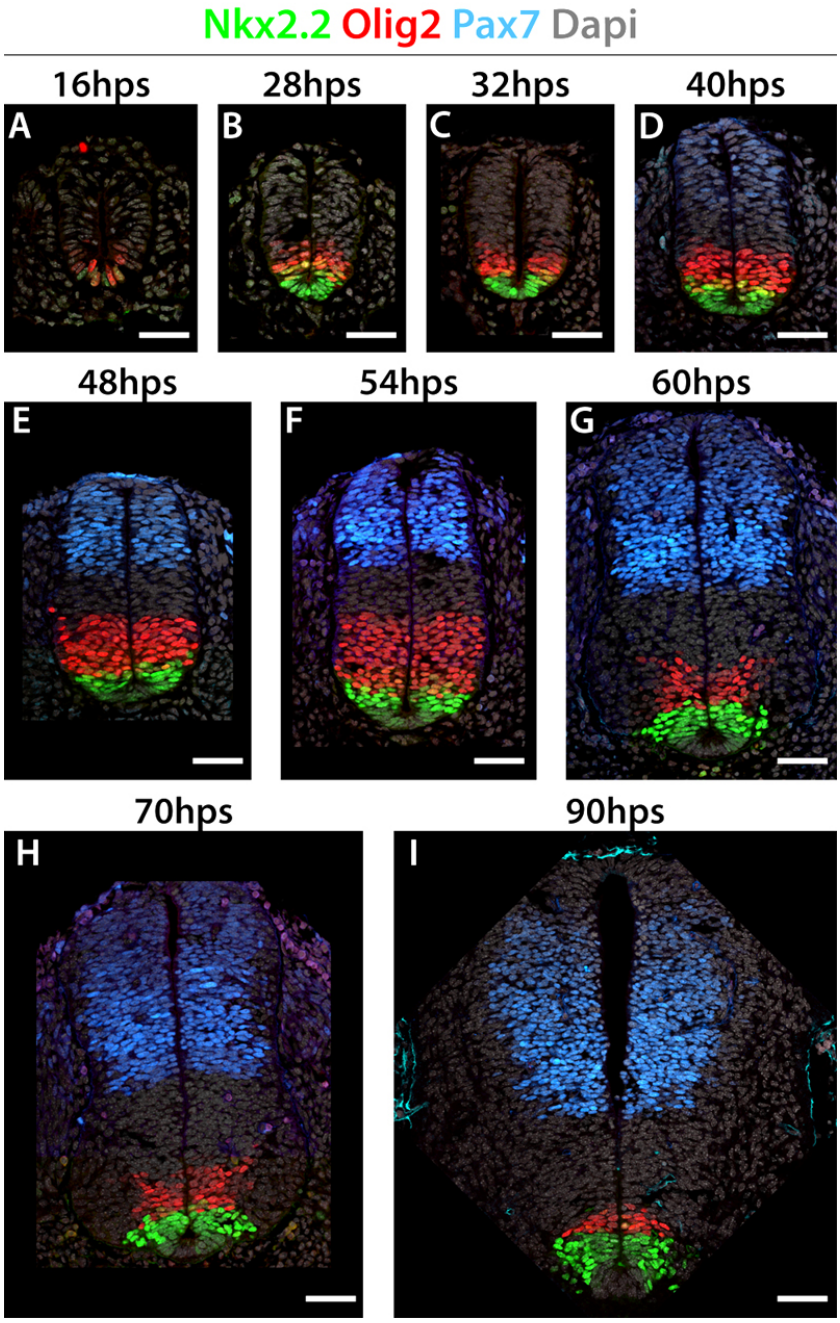

Figure 4.1 Dynamic patterning of the mouse neural tube.

(**A-I**) Immunohistochemistry showing the expression patterns of the transcription factors Nkx2.2 (p3 marker - green), Olig2 (pMN marker - red) and Pax7 (dorsal domain marker - blue)

in transverse sections of the neural tube at the level of somite 10 in embryos at the indicated stages in hours post initiation of somitogenesis (hps). Scale bars: 50 µm.

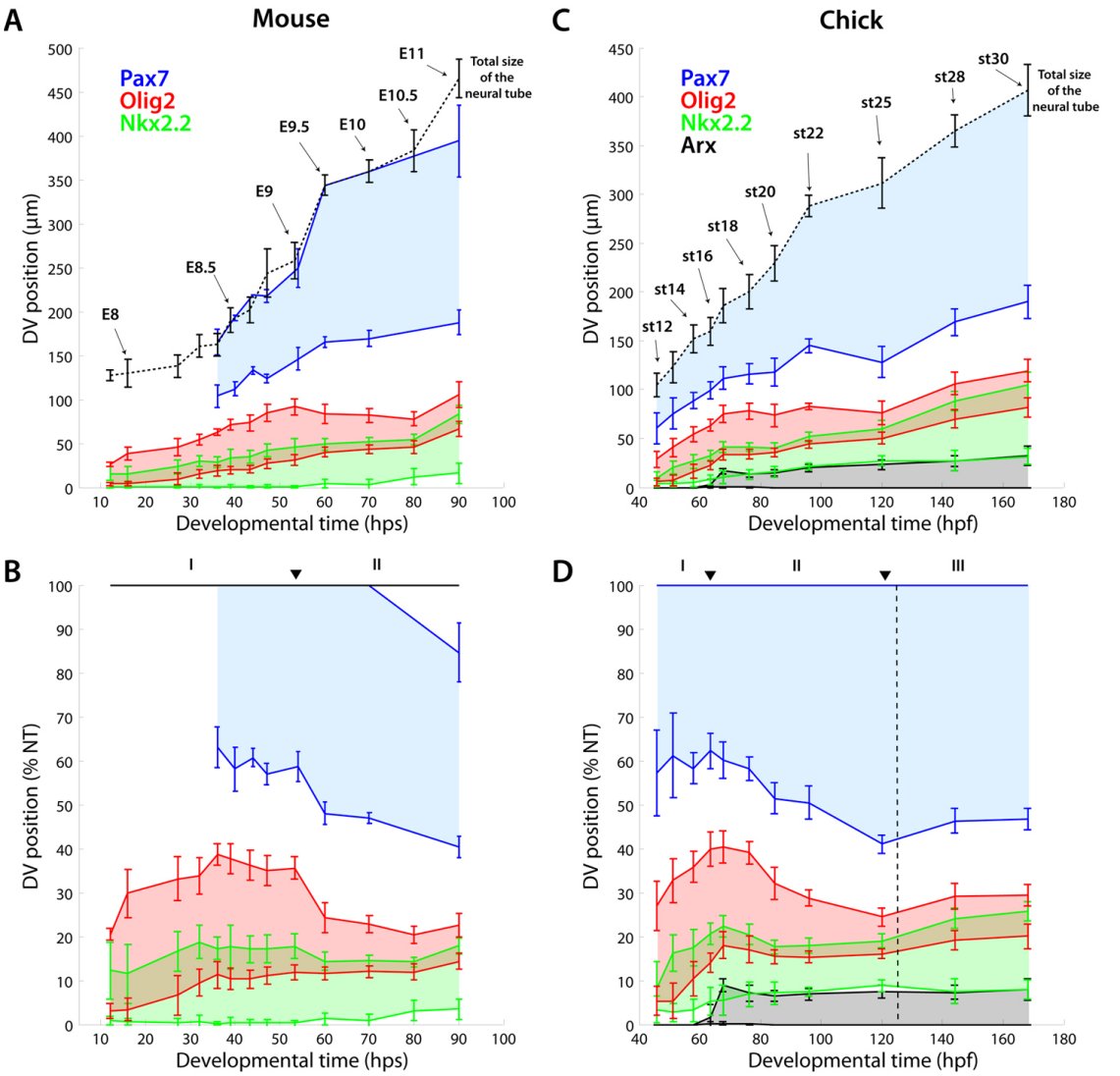

Figure 4.2 Dynamics of neural tube patterning in mouse and chick.

(**A**) Quantification of the position of the boundaries of expression of the transcription factors Nkx2.2 (p3 marker - green), Olig2 (pMN marker - red) and Pax7 (dorsal domain marker - blue) in the neural tube of mouse embryos staged from 12 hours post initiation of somitogenesis (hps) to 90hps. The boundary positions (mean ± s.d; n≥3 embryos/stage) are expressed as the distance from the ventral midline in µm, along the dorsoventral (DV) axis of the neural tube. The total size of the neural tube is indicated (black dashed line). The Embryonic day (E) staging nomenclature is indicated for some stages. (**B**) Boundary positions of the mouse progenitor domains in (A) expressed as the distance from the ventral midline relative to the total size of the neural tube (percentage of the neural tube size (%NT)). Arrow head (▼) marks

the transition between patterning phases: I (early - 12 to 54hps) and II (intermediate - 54 to 90hps).(**C**) Quantification of the position of the boundaries of expression of the transcription factors Arx (floor plate marker - black), Nkx2.2 (p3 marker - green), Olig2 (pMN marker - red) and Pax7 (dorsal domain marker - blue) in the neural tube of chick embryos staged from 45 hours post fertilization (hpf) to 168hpf. The boundary positions (mean ± s.d; n≥3 embryos/stage) are expressed as the distance from the ventral midline in μm. The Hamburger & Hamilton staging nomenclature is also indicated (st). (**D**) Boundary positions of the chick progenitor domains in (C) expressed as the distance from the ventral midline relative to the total size of the neural tube (percentage of the neural tube size (%NT)). Arrow heads (▼) mark the transition between patterning phases: I (early - 45 to 64hpf), II (intermediate - 64 to 120hpf) and III (late - 120 to 168hpf). The mouse data set covers a narrower period of development than the chick data set. The following analysis include only patterning phases I and II (region left to the dashed line in D).

The quantification of the neural tube size showed that, as in chick, the mouse neural tube continuously increased along the DV axis as development proceeded (Figure 4.2 A). The profile of neural tube growth in mouse was equally well-fitted by linear and exponential growth functions (r^2=0.92). Additional stages will be needed to distinguish between the two types of growth.

The growth of the neural tube was accompanied by changes in the position and size of the progenitor domains. The nature of these changes allowed us to identify the distinct patterning phases. The early patterning phase in chick was characterised by the induction of Nkx2.2 and Olig2 expression at progressively more dorsal positions, which resulted in the expansion of the domains at the expense of the intermediate region. Although the size of the p0-p2 region could not be determined in the early stages of mouse development, due to the inability to detect Pax7, the quantification of Nkx2.2 and Olig2 expression showed an initial period in which the dorsal limit of expression of these markers shifted to increasingly more dorsal positions, both in absolute and, importantly, relative distances (Figure 4.2 A,B). Hence, the size of the p3 and pMN domains increased at a higher rate than the average growth of the neural tube (Figure 4.3 B). This period of induction occurred approximately from 12hps to 32hps of development (6- to 16-somite stages).

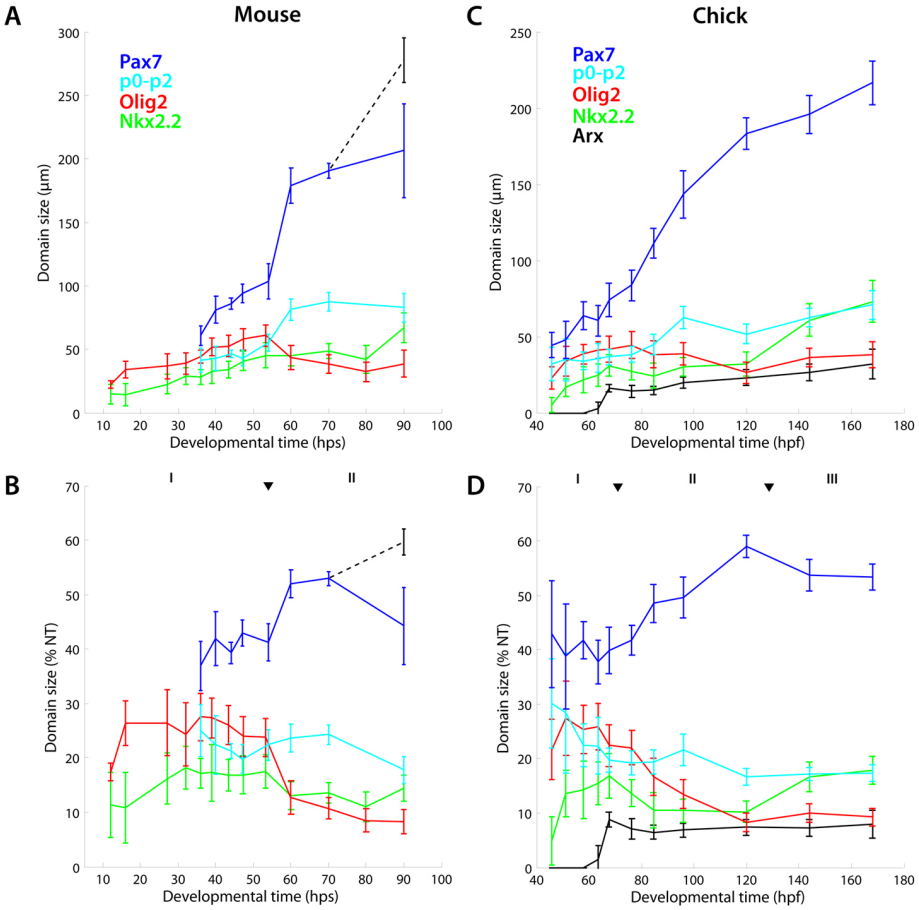

Figure 4.3 Dynamics of the size of progenitor domains in mouse and chick.

(**A**) Quantification of the size (µm) of the progenitor domains marked by the expression of the transcription factors Nkx2.2 (p3 domain - green), Olig2 (pMN domain - red), Pax7 (dorsal domain - blue; at stage 90hps the size of the dorsal domain is indicated as a black dashed line) and the region delimited by the dorsal boundary of the Olig2 domain and the ventral boundary of the Pax7 domain, encompassing the p0-p2 domains (cyan) in mouse embryos (mean ± s.d; n≥3 embryos/stage). (**B**) Absolute sizes of mouse progenitor domains in (A) converted to sizes relative to the total size of the neural tube (% NT). Arrow head (▼) marks the transition between patterning phases: I (early - 12 to 54hps) and II (intermediate - 54 to 90hps). (**C**) Quantification of the absolute size (µm) of the progenitor domains marked by the expression of the transcription factors Arx (floor plate - black), Nkx2.2 (p3 domain - green), Olig2 (pMN domain - red), Pax7 (dorsal domain - blue) and the p0-p2 region (cyan) in chick embryos (mean ± s.d; n≥3 embryos/stage). (**D**) Absolute sizes of chick progenitor domains in (C) converted to sizes relative to the total size of the neural tube (% NT). Arrow heads (▼) mark the transition between patterning phases: I (early - 45 to 64hpf), II (intermediate - 64 to 120hpf) and III (late - 120 to 168hpf).

In chick the phase of "active patterning" was followed by a period in which neuronal differentiation was initiated. During this period the dynamics of the progenitor domains were determined mainly by the generation and migration of post-mitotic cells, namely motor neurons and, to a lesser extent, V3 interneurons. In mouse the period of induction was followed by a period of stable growth of all the domains along the DV axis, from 36hps to 54hps of development (18- to 27-somite stages) (Figure 4.2 B). The transition to the differentiation period appeared to occur at 54hps. A marked decrease both in absolute and relative size of the Olig2 domain was observed from 54hps to 80hps (27- to 40-somite stages). This period coincided with the described period of motor neuron generation in mouse, from E9 to E10.5 (Arber et al., 1999; Nornes and Carry, 1978). The Nkx2.2 domain showed a more modest decrease in relative size. During this period Nkx2.2 expression started to be excluded from the ventral-most region. However, the shift in the position of the ventral limit of Nkx2.2 expression was less pronounced than in chick. Although Arx expression was not measured in mouse, recent data have shown that Arx induction in the mouse neural tube occurs at developmental day E9.5 (Ribes et al., 2010), which matches the time of the dorsal shift of Nkx2.2 ventral boundary (60hps) (Figure 4.2 A). In addition, post-mitotic V3 interneurons start to differentiate at E10.5 (approximately 80hps) (Briscoe et al., 1999).

From the chick data a third phase in the elaboration of pattern could be identified, in which each of the progenitor domains exhibited a period of proportional growth along the DV axis. This observation suggested a similar ratio between differentiation and proliferation in all domains. The examination of the mouse dynamics of gene expression failed to reveal an equivalent period. In the later stages analysed in mouse, Nkx2.2 expression expanded, the Olig2 domain remained constant and the Pax7 and intermediate regions contracted, when compared to the average growth of the neural tube (Figure 4.2 B, 4.3 B). These results suggest that the developmental stages measured in mouse cover a narrower range of developmental processes. This analysis also revealed an interesting difference between mouse and chick: from 80hps of mouse development the expression of Pax7 started to be down-regulated from the dorsal-most region of the neural tube (Figure 4.1 I). This down-regulation likely explained the observation that Pax7 expression failed to accompany the overall growth of the neural tube.

The comparative characterisation of the expression patterns of Nkx2.2, Olig2 and Pax7 revealed that the general shape of the DV patterns over time closely resembled the chick neural tube. Nevertheless, mouse-specific features were observed, such as the persistence of Nkx2.2 expression close to the ventral midline, and the late down-regulation of Pax7 in the dorsal tip of the neural tube. This analysis helped identify the events that define the transition points between patterning phases. For the subsequent comparison between the two species the following defining events were taken into account: the time of induction of Nkx2.2, which corresponds the first measured point; the time and extent of the exclusion on Nkx2.2 from the floor plate; the time of the peak generation of motor neurons. In addition, the late period of chick development (approximately 120hpf to 168hpf) was not included in the comparative analysis, as an equivalent period was not measured in mouse.

4.2 Comparison of the expression patterns of Nkx2.2, Olig2 and Pax7 between mouse and chick

The direct comparison of expression patterns in different organisms is likely to reveal differences in the sizes and positions of the expression domains. These differences may result from global differences in the size of the neural tube, domain-specific differences in size and differences in the temporal dynamics of pattern elaboration. Differences in neural tube size will result in a general DV displacement of the domains in absolute distance, but the expression patterns will scale between the two species when normalised to the neural tube size. In the case of domain-specific size differences, no scaling should be observed when domain sizes are normalized to the total size of the neural tube. Finally, the formation of the patterns may occur at different speeds, that is, particular developmental periods, defined by particular events, may appear contracted or expanded in time when compared to a different species. Therefore, it is important to also compare the shape of the temporal profile of each boundary between the two species. All these possibilities were taken into account when determining whether the expression patterns of neural progenitor markers were comparable between chick and mouse.

The mouse and chick DV patterns were first compared using absolute time in hours, where the zero time point was set as the beginning of somitogenesis. We call this "developmental time" and express it as units of hours post initiation of somitogenesis (hps). In practice, to derive the developmental time we did not measure absolute time, but the number of somites of each embryo. We then converted the number of somites into hps, by using the published measurements of the periodicity of somite generation in mouse and chick, i.e. it takes 1.5h in chick and 2h in mouse for the formation of a single pair of somites (see Material and Methods; Palmeirim et al., 1997; Bessho et al., 2001; Hirata et al., 2002). However, to directly compare the developmental times in the two species, the conversion of somites to hours in chick was done without including the pre-somitogenesis period (note that the values of the chick developmental times in the following data were shifted 23h from the values presented in the previous chapter).

The direct comparison of developmental times resulted in a good correlation between the position of the Nkx2.2 and Olig2 domain, with the exception of the ventral limit of Nkx2.2 (Figure 4.4 A). However, registering the two data sets in this way resulted in a discrepancy in the size of the neural tube and in the position of the ventral boundary of Pax7. By contrast, normalising boundary positions to the size of the neural tube resulted in the scaling of the Pax7 boundary position between the two species, whereas the Nkx2.2 and Olig2 domains displayed considerably different relative positions in chick and mouse (Figure 4.4 B). This could indicate that the dorsal and ventral halves of the neural tube scale in size, however, individual dorsal and ventral subpopulations do not. One possible explanation for this could be that functionally it might be important to maintain a particular ratio between sensory (dorsal) neurons and motor (ventral) neuronal types, however, species-specific differences would arise from altering the sizes of specific subpopulations.

On a closer examination, however, the data revealed that besides the poor scaling of the ventral subdomains, particular "events" characteristic of spinal cord patterning during these stages occurred at different times in mouse and chick. For instance, the time of induction of Arx in chick (40hps/HH stage 16) and the time of induction of Arx in mouse (50 to 60hps/E9.5; Ribes et al., 2010) were dissimilar. In addition, this method of registering the developmental age of each species placed the stage of induction of Nkx2.2 at different developmental times. These differences between mouse and chick argue that using time post-somitogenesis may not be the

best method to compare the two species. It could be that patterning in the two species is more similar than revealed by this analysis, but occurs with a delay in one species relative to the other. This could be, for example, because Shh signalling is initiated at different developmental times in the two species. Given the gap between the time of induction of Nkx2.2 (approximately 11h), we sought to determine if adjusting the temporal profiles to this time point would provide better scaling.

Adjusting the two sets of expression patterns relative to one another so that the time of Nkx2.2 induction was the same in both species resulted in similar neural tube sizes in chick and mouse, during the early stages of development (Figure 4.4 C). In later stages, the mouse neural tube exhibited a greater increase in size in mouse than chick. As with the previous mode of registration, the Pax7 domain scaled, whereas the ventral domains Nkx2.2 and Olig2 showed differences in relative position (Figure 4.4 D). Even though the Nkx2.2 and Olig2 domains did not scale perfectly, the adjustment of the time of induction of Nkx2.2 resulted in a better overall adjustment of the temporal profiles of these domains between the two species (Figure 4.4 B,D). This analysis suggests that, after Nkx2.2 is induced, the patterning events in chick and mouse have similar temporal dynamics. However, the delayed time of Nkx2.2 induction in chick suggests that the patterning events prior to Nkx2.2 induction may be different in the two species. One possibility is that the early dynamics of the Shh gradient also differ between chick and mouse, but at these stages the levels of Shh are below the threshold where they can be reliably measured.

Although the adjustment of the temporal profiles revealed the similar dynamics between species, some differences were still noticeable in the patterning of the Nkx2.2 and Olig2 domains. The ventral boundary of Nkx2.2 showed a gradual dorsal shift in chick, whereas this boundary in mouse remained close to the ventral midline for a longer period of time (Figure 4.4 B,D). The earlier exclusion of Nkx2.2 from the floor plate region in chick is consistent with the earlier time of induction of Arx in chick (40hps / 29hps in the mouse axis) than in mouse (60hps). The ventral boundary of the chick Olig2 domain was also positioned more dorsally than the mouse domain (Figure 4.4 B,D). In addition, the peak of motor neuron generation occurred later in mouse (54-60hps) than in chick (53-62hps / 42-51hps in the mouse axis). These differences were examined in more detail to assess their effect on the temporal dynamics of the progenitor domains.

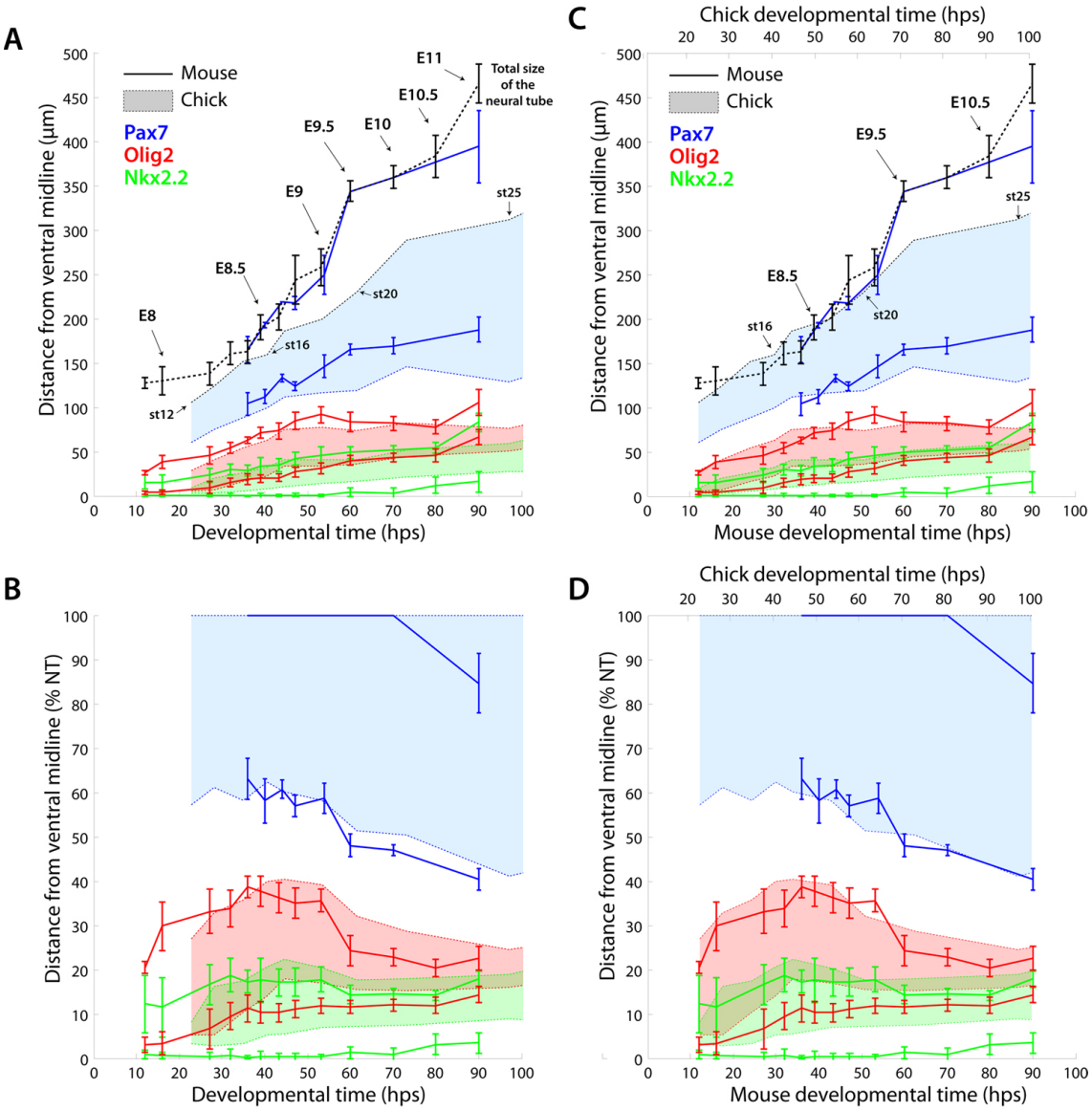

Figure 4.4 Registration of the mouse and chick data sets using developmental time.

(**A**) Juxtaposition of the mouse and chick expression patterns of Nkx2.2 (p3 marker - green), Olig2 (pMN marker - red) and Pax7 (dorsal domain marker - blue) expressed as the distance from the ventral midline in µm. The boundary positions in mouse (lines with error bars - mean ± s.d; n≥3 embryos/stage) and in chick (borders of filled areas - mean; n≥3 embryos/stage) are plotted as a function of developmental time (hours post initiation of somitogenesis - hps; see Tables 1 and 2 in Materials and Methods). The total size of the neural tube is indicated (black dashed line). The mouse Embryonic day (E) and chick Hamburger & Hamilton (st) staging nomenclatures are indicated for some stages. (**B**) Boundary positions of the progenitor domains in (A) expressed as the distance from the ventral midline relative to the total size of the neural tube (percentage of the neural tube size (%NT)). (**C**) Juxtaposition of the mouse and chick data sets shown in (A), adjusted to the time of induction of Nkx2.2

(12hps in mouse and 24hps in chick). The mouse and chick data sets are plotted with different scales (mouse scale on the bottom x-axis and the chick scale on the top x-axis). (**D**) Boundary positions of the progenitor domains in (C) expressed as the distance from the ventral midline relative to the total size of the neural tube (percentage of the neural tube size (%NT)). Using the time of induction of Nkx2.2 as the starting point (B,D) resulted in a better registration of the mouse and chick data sets than using just developmental time (A,B).

To investigate the effect of the floor plate we plotted the expression patterns from the ventral boundary of Nkx2.2 expression, instead of using the ventral midline (Figure 4.5). At initial stages (until approximately 40hps), in which the size of the neural tube is similar in chick and mouse, the positions of the boundaries of Nkx2.2 and Olig2 were very similar in mouse and chick, when plotted from the ventral limit of Nkx2.2 (Figure 4.5 A). The normalisation of the positions of the domains to the distance between the floor plate boundary and the roof plate generated scaled expression patterns for Nkx2.2 and Olig2 between mouse and chick in these early stages (Figure 4.5 B).

At later stages (after 40hps/20-somite stage in the mouse axis), the positions of the boundaries were dorsally shifted in mouse compared to chick (Figure 4.5 A,B). During this period, the size of the mouse neural tube from the floor plate boundary was also consistently larger than the chick neural tube. This suggested that the differences in the positions of the domains resulted from differences in neural tube size. Indeed, when plotted as relative size from the floor plate boundary the DV patterns showed similar proportions in the two species, for most of the expression boundaries analysed (Figure 4.5 B). This result suggests that differences in the size of the floor plate, defined by the down-regulation of Nkx2.2 expression and induction of Arx (Ribes et al., 2010), influence the relative position of more dorsal boundaries. These differences derive at least in part from the later time of induction of Arx in mouse, in relation to the time of induction of Nkx2.2 (~20h).

Although the adjustment of the expression patterns to the floor plate boundary resulted in very similar temporal profiles of expression between chick and mouse, the relative positions of the dorsal boundaries of Nkx2.2 and Olig2 diverged at the 54hps time point (in the mouse axis; Figure 4.5 A). This time point corresponds

to the onset of motor neuron differentiation, which occurs earlier in chick. Due to the different timing of the peak of motor neuron differentiation between chick and mouse, the temporal profile of the progenitor domains in early stages appeared more stretched in mouse. This observation raised the possibility that the conversion of the number of somites to hours may not be the most appropriate method to compare the two species. Rather, the dynamics of the patterns may be better adjusted temporally if the expression patterns are plotted as a function of the number of somites. To determine if this is the case we compared the temporal profiles of the Nkx2.2, Olig2 and Pax7 domains expressed as number of somites and adjusted to the stage of Nkx2.2 induction (Figure 4.5 C,D). Strikingly, this mode of registration resulted in more similar patterning dynamics, particularly in early stages. In the initial developmental stages (until the 20-somite stage in the mouse axis) the size of the neural tube was similar between chick and mouse, as were the absolute positions of the dorsal boundaries of Nkx2.2 and Olig2 (15- to 30-somite stages in chick and 6- to 20-somite stages in mouse) (Figure 4.5 C). In later stages, the increase in the size of the neural tube, and the dorsal shift of the domain boundaries, were more pronounced in mouse than chick (Figure 4.5 C). The comparison of the expression patterns normalised to the neural tube size and plotted as a function of the number of somites showed a better adjustment of the temporal profiles of the domains in the early patterning phase, compared to the expression patterns plotted as a function of the developmental time (Figure 4.5 B,D). As the chick temporal profiles became more stretched compared to mouse, the period of the peak differentiation of motor neurons was better adjusted between the two species (approximately 27- to 30-somites stages in the mouse axis) (Figure 4.5 D). One possible explanation for the better registration using somite number could be that the patterning of the neural tube is coordinated with somite formation, and timing differences between species affect both processes. However, in later stages (60hps/ 30-somite stage in the mouse axis) the relative positions of the domains were more similar when the two data sets were registered using developmental time than with somite number, particularly the dorsal boundary of Olig2 (Figure 4.5 B,D). Thus, although the temporal profiles of the progenitor markers are similar between chick and mouse, the exact dynamics varies depending on the mode of registration.

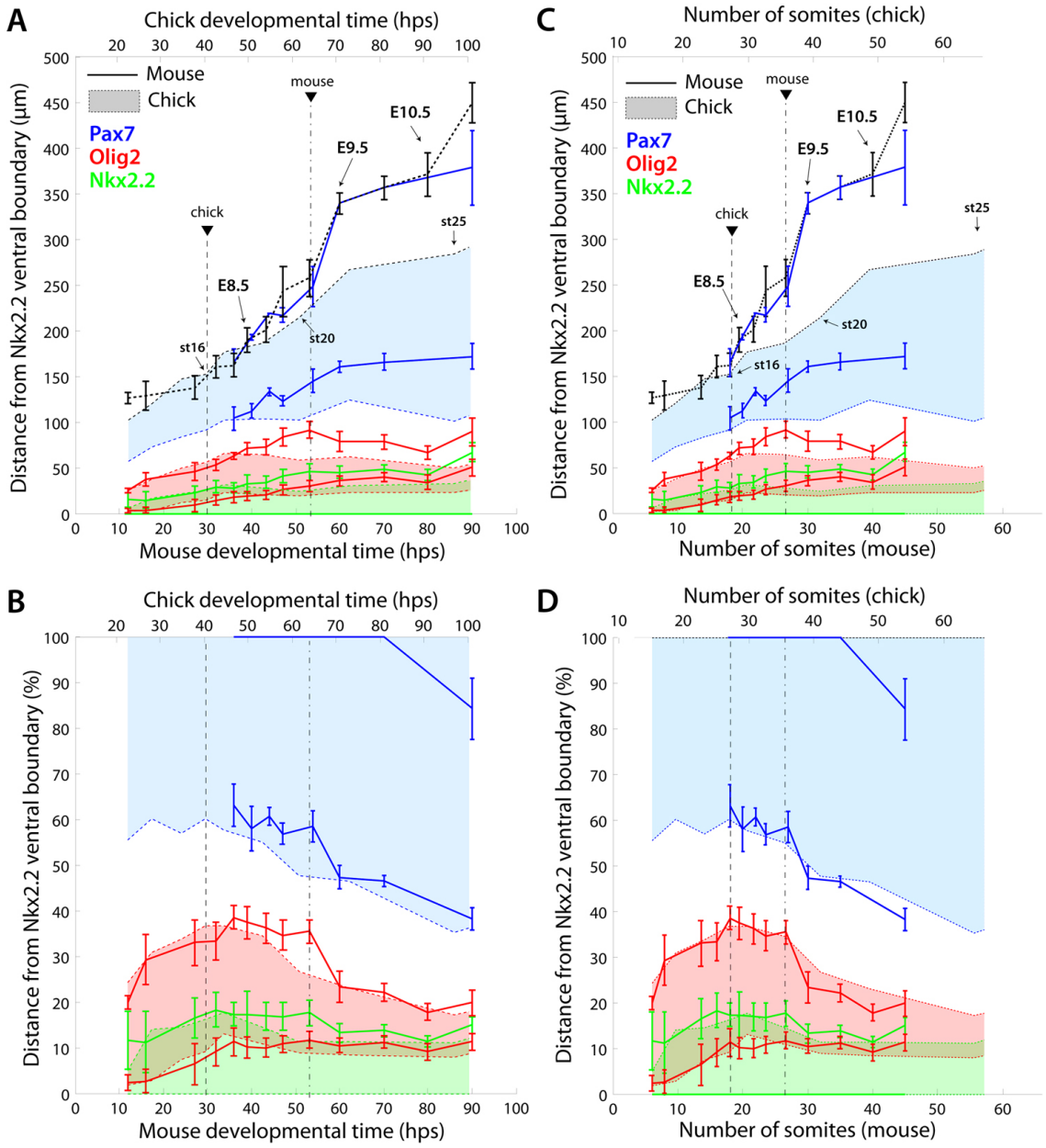

Figure 4.5 Registration of the mouse and chick data sets adjusted to the ventral boundary of Nkx2.2.

(**A**) Juxtaposition of the mouse and chick expression patterns of Nkx2.2 (p3 marker - green), Olig2 (pMN marker - red) and Pax7 (dorsal domain marker - blue) expressed as the distance from the ventral boundary of Nkx2.2 (µm). The boundary positions in mouse (lines with error bars - mean ± s.d; n≥3 embryos/stage) and in chick (borders of filled areas - mean; n≥3 embryos/stage) are plotted as a function of developmental time (hours post initiation of somitogenesis - hps) and adjusted to the time of induction of Nkx2.2. The mouse and chick data sets are plotted with different scales (mouse scale on the bottom x-axis and the chick scale on the top x-axis). The total size of the neural tube is indicated (black dashed line). The mouse Embryonic day (E) and chick Hamburger & Hamilton (st) staging nomenclatures are

indicated for some stages. (**B**) Boundary positions of the progenitor domains in (A) expressed as the distance from the ventral boundary of Nkx2.2 relative to the total size of the neural tube (percentage of the neural tube size (%NT)). Using the ventral boundary of Nkx2.2 as x_0 resulted in a better registration of the chick and mouse data sets than using the ventral midline. (**C**) Juxtaposition of the mouse and chick data sets shown in (A), plotted as a function of the number of somites. (**D**) Boundary positions of the progenitor domains in (C) expressed as the distance from the ventral boundary of Nkx2.2 relative to the total size of the neural tube (percentage of the neural tube size (%NT)). Arrow heads (▼) mark the transition between patterning phases I and II in chick (dashed line) and mouse (dash-dotted line). Using developmental time resulted in a better registration of patterning phase II, whereas using number of somites resulted in a better registration of patterning phase I.

To determine if there were differences in the final size of the domains between the two species, the size of the domains were directly compared using both modes of registration. The comparison of the absolute size of the Nkx2.2 domain revealed similar dimensions between mouse and chick in early stages, both as a function of developmental times and number of somites (Figure 4.6 A, Figure 4.7 A), with the exception of the first stage. By 44hps/22-somite stage the size of the mouse domain markedly increased in comparison to chick. This difference appeared to derive in part from differences in the overall size of the neural tube, as the normalisation of the sizes reduced the difference between the species at later stages (Figure 4.6 E, Figure 4.7 E). Nevertheless, there were still some differences in the size of the Nkx2.2 domain, with a larger domain in the mouse neural tube. However, as this domain is small and the measurements are noisy, the differences between mouse and chick may not be significantly different.

The Pax7 domain and the p0-p2 region showed similar dynamics, with comparable absolute domain sizes in early stages, followed by a marked increase in the size of the domains in mouse from 54hps/27-somite stage onwards (Figure 4.6 C,D, Figure 4.7 C,D). After normalization, these domains presented similar proportions throughout development (Figure 4.6 G,H, Figure 4.7 G,H). Exceptionally, the size of the mouse Pax7 domain in the last stage analysed (90hps/45-somite stage) was proportionally smaller that the chick domain at an equivalent stage. This result

was likely explained by the downregulation of mouse Pax7 from the dorsal-most region of neural tube, which did not occur in chick. However, the size of the region of the neural tube dorsal to the Pax7 ventral boundary showed good scaling between the two data sets in this last stage, when registered according to developmental times (Figure 4.6 H). By contrast, the size of the dorsal region plotted as a function of the number of somites was different between mouse and chick (Figure 4.7 H).

The analysis of the Olig2 domain displayed different dynamics from the other progenitor domains. In mouse the period of induction of Olig2 expression resulted in a larger pMN domain than in chick (Figure 4.6 B, Figure 4.7 B). In both species, the period of expansion of Olig2 was followed by a period of reduction of size. This decrease, reflecting the increased generation and migration of MN, occurred more rapidly in mouse. However, the timing of the peak MN generation differed depending on the mode of registration of the two data sets. Expressed as a function of developmental time, the peak of MN differentiation occurred later in mouse: 54hps in mouse compared to ~40hps in chick (in the mouse axis) (Figure 4.6 B). Following this differentiation peak the size of the domain scaled between chick and mouse (Figure 4.6 F). Conversely, the registration of the chick and mouse data according to the number of somites resulted in coincident times of maximal MN differentiation (Figure 4.7 B). However, in later time points the size of the mouse Olig2 domain was proportionally smaller than the chick domain (Figure 4.7 F). Although the registration of the two data sets using developmental time resulted in the scaling of the Olig2 domains in later stages, we cannot exclude the possibility that the registration using somite numbers is more accurate and the mouse Olig2 domain has smaller proportions than the chick domain. To determine if the Olig2 domain scales between species after the period of motor neuron differentiation it will be necessary to accurately identify the stage of the end of MN differentiation in mouse and compare the size of the Olig2 to the equivalent stage in chick.

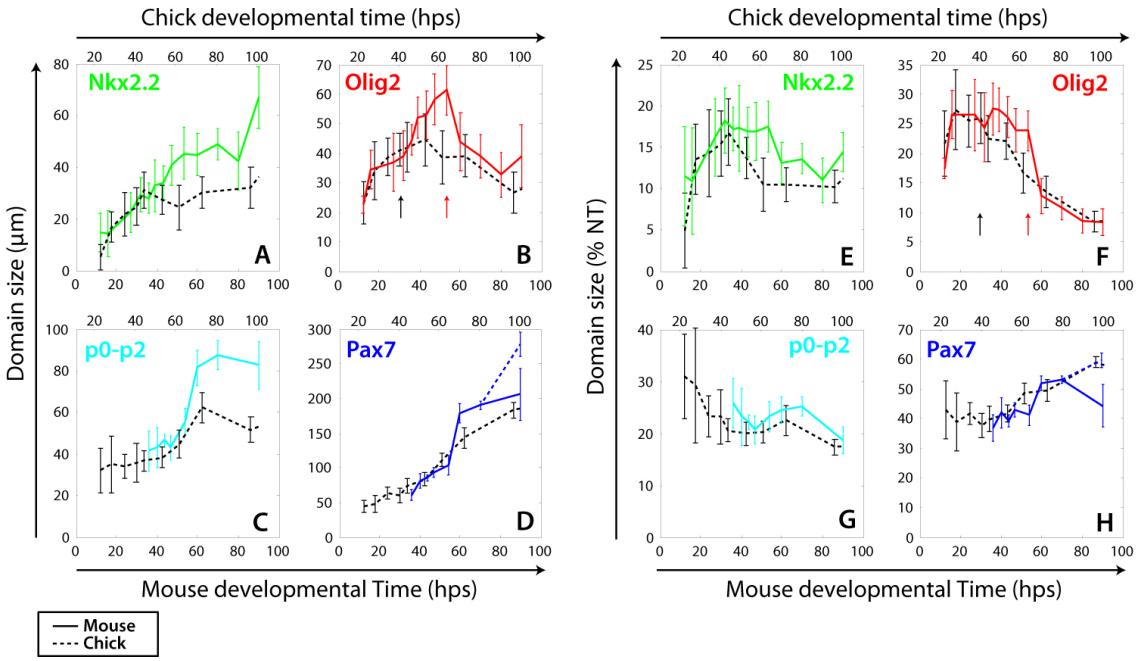

Figure 4.6 Comparison of progenitor domain sizes in mouse and chick using developmental time.

(**A-D**) Quantification of the absolute size (µm) of the progenitor domains marked by the expression of the transcription factors Nkx2.2 (A), Olig2 (B), the p0-p2 region (C) and Pax7 (D; dorsal domain - blue; at stage 90hps the size of the dorsal domain is indicated as a blue dashed line) in mouse (color full line) and chick (black dashed line) embryos (mean ± s.d; n≥3 embryos/stage). The domain sizes are plotted as a function of developmental time (hours post initiation of somitogenesis - hps) and adjusted to the time of induction of Nkx2.2. The mouse and chick data sets are plotted with different scales (mouse scale on the bottom x-axis and the chick scale on the top x-axis). (**E-H**) Absolute sizes of progenitor domains in (A-D) converted to sizes relative to the total size of the neural tube (% NT). Arrows in (B, F) indicate the onset of motor neuron generation in mouse (red) and chick (black). When registered using developmental time, the sizes of the domains in the last stage analyzed scaled between chick and mouse (E-H). However, in intermediate stages the proportions of the Nkx2.2 and Olig2 domains differed between the two species (E, F).

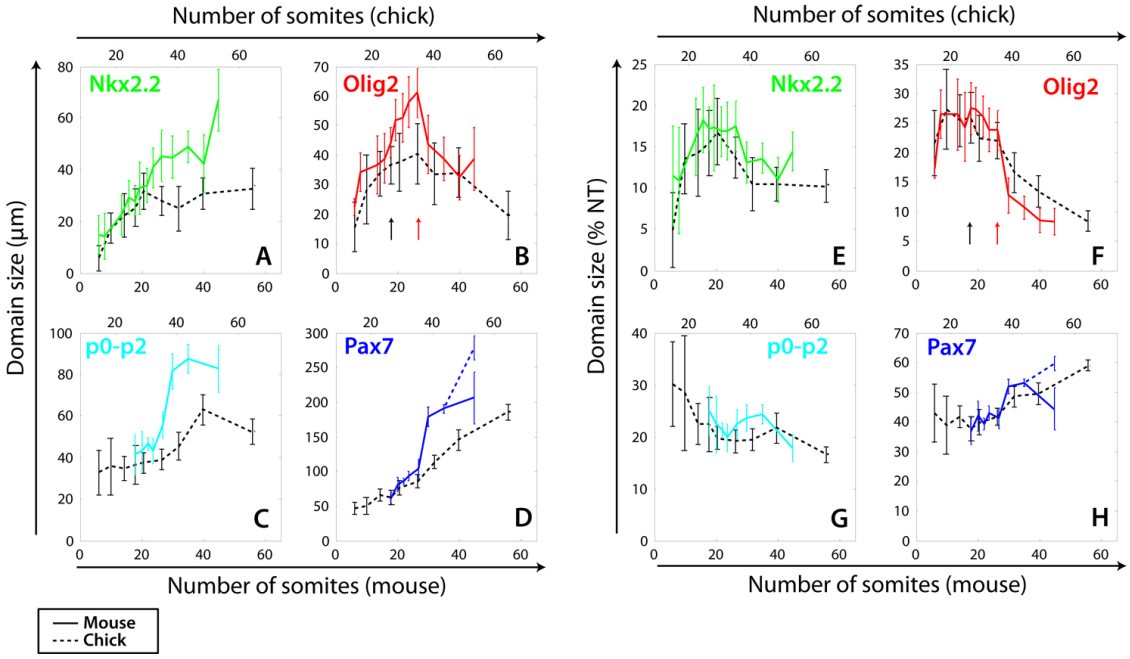

Figure 4.7 Comparison of progenitor domain sizes in mouse and chick using number of somites.

(**A-D**) Quantification of the absolute size (µm) of the progenitor domains marked by the expression of the transcription factors Nkx2.2 (A), Olig2 (B), the p0-p2 region (C) and Pax7 (D; dorsal domain - blue; at stage 90hps the size of the dorsal domain is indicated as a blue dashed line) in mouse (color full line) and chick (black dashed line) embryos (mean ± s.d; n≥3 embryos/stage). The domain sizes are plotted as a function of the number of somites and adjusted to the time of induction of Nkx2.2. The mouse and chick data sets are plotted with different scales (mouse scale on the bottom x-axis and the chick scale on the top x-axis). (**E-H**) Absolute sizes of progenitor domains in (A-D) converted to sizes relative to the total size of the neural tube (% NT). Arrows in (B, F) indicate the onset of motor neuron generation in mouse (red) and chick (black). The registration of the mouse and chick data sets using number of somites resulted in similar relative sizes of the progenitor domains in the initial patterning phase, but the domains did not scale in later stages (E-H).

The comparison of the expression patterns of the progenitor markers Nkx2.2, Olig2 and Pax7 in chick and mouse shows that in early developmental stages the size of the neural tube and the positions of the boundaries are similar between the two organisms. The registration of the two data sets using the number of somites adjusted to the time of induction of Nkx2.2 provides a better scaling of the positions of the boundaries than the registration with developmental times, in these early stages. In later stages the size of the Nkx2.2, p0-p2 and Pax7 domains increase at a higher rate in mouse than in chick, but proportionally to the overall size of the neural tube. The Olig2 domain shows an increased absolute size in mouse prior to the onset of differentiation, but similar absolute sizes in mouse and chick after the peak differentiation period. This suggests that the rate of differentiation during this period is higher in mouse to achieve this effect - a hypothesis that would be interesting to test. In these later stages the size of the Olig2 domain in chick and mouse scaled in developmental times, but not in somite numbers. Further tests will be necessary to enable us to choose the best mode of registration. For instance, a more detailed analysis of the periodicity of somite formation in chick and mouse, and how it changes over time, will help achieve a better registration of the two data sets. In addition, the inclusion of later time points to the mouse data set will likely facilitate the comparison of the patterning dynamics between the two species.

Nevertheless, the comparison of the current data sets shows the remarkable similarity in the dynamics of gene expression between chick and mouse, particularly during early patterning, which prompted us to investigate the dynamics of the Shh distribution in mouse.

4.3 Dynamics of the Shh gradient in mouse

The visualisation of the Shh protein showed a graded DV distribution, with increasing levels as development proceeded (Figure 4.8). At 12hps to 16hps stages Shh levels were very low and restricted to the ventral midline. For this reason, Shh distribution was not measured in these early stages. The mouse stages used for this quantification covered a wider period of development than the chick Shh measurements (28-90hps in mouse vs 24-63hps in chick). The comparison of the Shh

gradients between mouse and chick was performed using hour post-initiation of somitogenesis (hps).

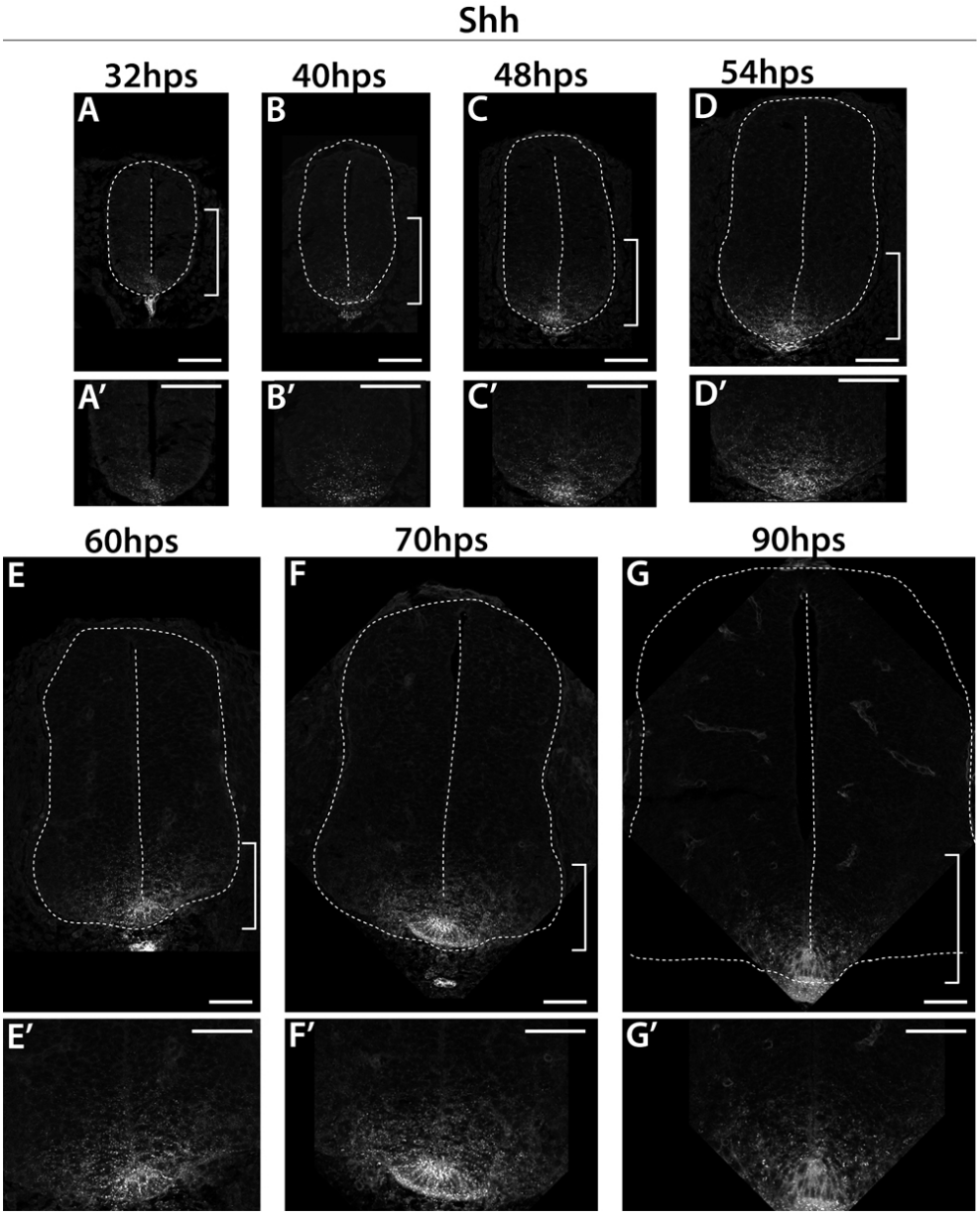

Figure 4.8 Temporal changes in Shh distribution in the mouse neural tube.

(**A-G**) Visualization of Shh distribution in neural tube sections of embryos at the indicated stages in hours post initiation of somitogenesis (hps) using immunohistochemistry. (**A′-G′**) High magnification images of the regions highlighted in A-E (white brackets). The Shh gradient shows a gradual increase in amplitude and spread in the neural tube until 70hps (A-F′), and subsequently declines (G,G′). Scale bars: 50 μm.

The quantification of the Shh distribution over time showed the progressive increase in the levels of Shh, from 28hps to 60hps (E9.5) (Figure 4.9 A,B). From 60hps to 70hps the levels of Shh remained stable and again decreased from 70hps to 90hps. The initial accumulation, followed by a stabilisation of Shh levels was consistent with the observed Shh dynamics in chick. Although Shh distribution was not measured in later chick stages, the inspection of images of HH stage 25 chick embryos stained with Shh suggested that the late decrease in Shh levels also occurred in chick (data not shown).

The shape of the Shh profiles was well approximated by an exponential decay function (Figure 4.9 B). Hence, to characterise the dynamics of the Shh gradient, and compare it between species, we fitted exponential decay functions to the data and extracted the parameters that determine the gradient shape: amplitude and decay length. The gradient amplitude in mouse showed a minor increase up to ~50hps, followed by a rapid three-fold increase (Figure 4.9 C). By contrast, the chick gradient amplitude showed a more rapid increase at early developmental stages (~30hps in the chick axis). These measurements suggest that the initial dynamics of the Shh gradient is different in the two species. However, it is possible that the Shh dynamics is similar between chick and mouse, but the number of early stages analysed in chick is insufficient to capture this similarity. The chick gradient reached its highest levels ~30hps earlier than the mouse gradient. Note that for this comparison we used Nkx2.2 induction as the zero time point; if we use absolute time post somitogenesis the time difference between the peak amplitude levels in the two species would be even larger.

The different dynamics in the establishment of the Shh gradient between the two species correlated well with the timing of induction of Arx: in chick 40hps / HH stage 16 (Figure 4.2B), and in mouse ~60hps / E9.5 (Ribes et al., 2010). Arx is a relatively late marker for cells that have acquired a definite floor plate identity, which simultaneously express Shh (Ribes et al., 2010). Hence, the increase in amplitude could be a direct consequence of floor plate specification and the enhancement of Shh secretion by floor plate cells. However, the small size of the mouse floor plate at this stage suggested that the number of Shh producing cells was not increasing extensively. It is possible that the transition to a definite floor plate identity results in

a higher Shh production rate of floor plate cells - a hypothesis that would be interesting to test in the future. After reaching the maximum level, the amplitude values remained constant until 70hps, and subsequently decreased.

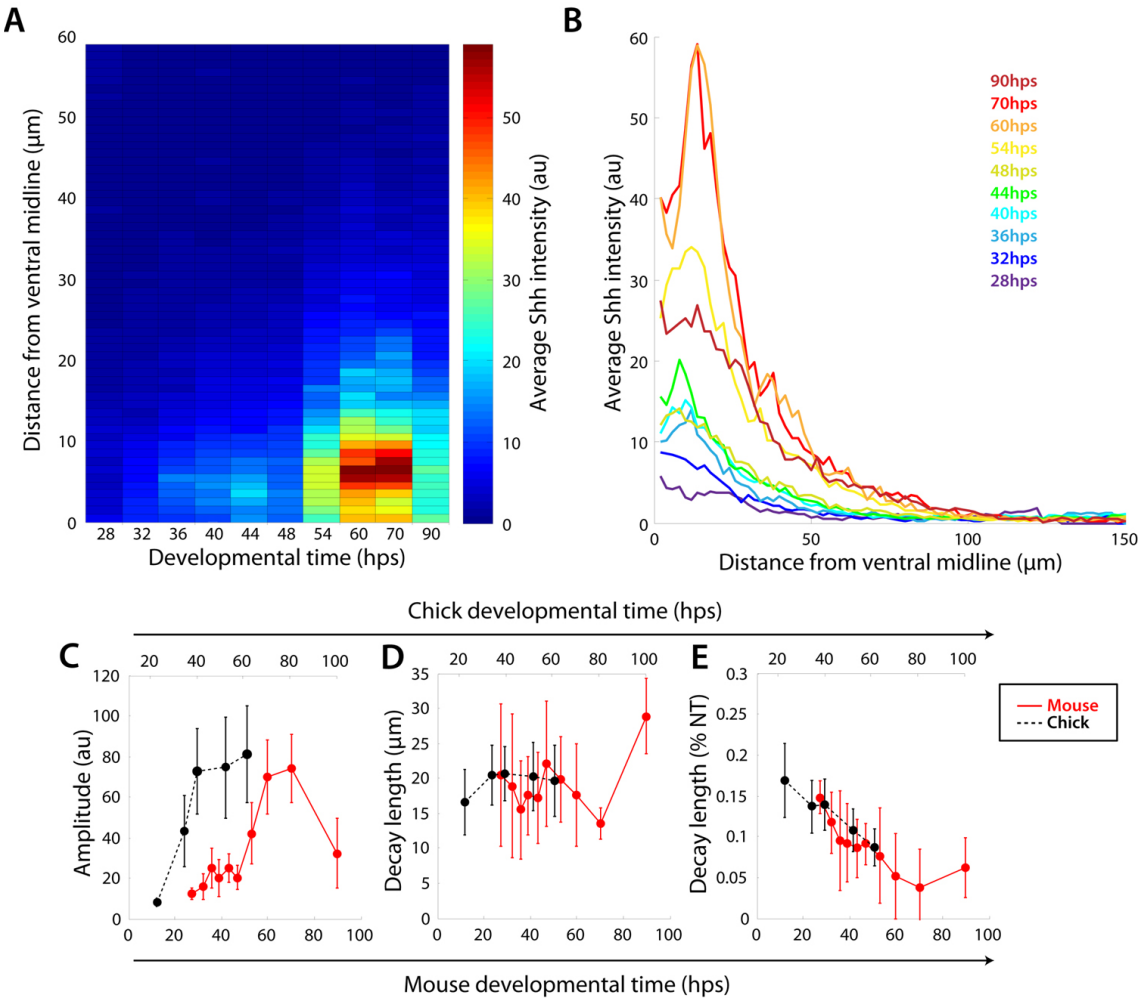

Figure 4.9 Characterization of the Shh gradient in the mouse neural tube.

(**A, B**) Quantification of the Shh intensity levels as a function of the distance from the ventral midline (µm) at the indicated developmental stages in hours post initiation of somitogenesis (hps). (**A**) Heat map depicting the average Shh fluorescence intensity (arbitrary units (au)) in 4µm bins along the dorsoventral axis of the neural tube of mouse embryos at the indicated stages (n≥3 embryos/stage). (**B**) Average Shh fluorescence intensity profiles (arbitrary units (au)) as a function of the distance from the ventral midline (µm) at the indicated stages. The quantification of Shh distribution shows the gradual increase in intensity levels and range of the Shh gradient in initial stages of development followed by a decline at the last stage analyzed (A,B). (**C**) Quantification of the amplitude of the gradient estimated from the

exponential curve fits in mouse (red line; mean ± s.d in arbitrary units (au)) and chick (black dashed line; mean ± s.d in arbitrary units (au)) embryos at the indicated stages. The mouse and chick data are plotted with different scales, adjusted to the time of Nkx2.2 induction (mouse scale on the bottom x-axis and the chick scale on the top x-axis). The chick gradient reaches the peak amplitude at an earlier time point than the mouse gradient. At the last mouse stage the amplitude of the gradient declines. (**D**) Decay length of the Shh gradient (mean ± s.d in μm) estimated from exponential functions fitted to the Shh profiles in mouse (red line) and chick (black dashed line) embryos at the indicated stages. The absolute decay length of the Shh gradient is similar between mouse and chick and remains constant as the amplitude of the gradient changes. In last mouse stage the decay length increases. (**E**) Decay length of the Shh gradient (mean ± s.d in percentage of the neural tube size (%NT)) estimated from exponential functions fitted to the Shh profiles normalized to the total size of the neural tube in mouse (red line) and chick (black dashed line) embryos at the indicated stages. In both species the normalized decay length of the Shh gradient decreases over time (with the exception of the last mouse stage), which suggests that the gradient is not adjusting to the growth of the neural tube.

The estimation of the decay length of the mouse Shh gradient showed that this parameter was in the same range as the chick decay length, approximately 20μm, although the mouse values displayed a higher variability (Figure 4.9 D). Like in chick, the decay length values normalised to the size of the neural tube decreased over time, suggesting that the gradient does not scale with tissue size (Figure 4.9 E). It is worth noting that the relative decay lengths in mouse and chick followed almost exactly the same dynamics in the two species. In other words, even though the neural tube size was different in mouse and chick at a particular time point, the gradient decay length was the same percent of the size. A possible explanation for this observation would be a difference in cell size between mouse and chick. Alternatively, this dynamics could be actively regulated by tuning the diffusion and degradation rates of the ligand. The decay length of the Shh profile in the last mouse stage analysed suggested a slower decay of the morphogen along the tissue. This increase in the decay length may be indicative of a change in the diffusion and/or degradation rates.

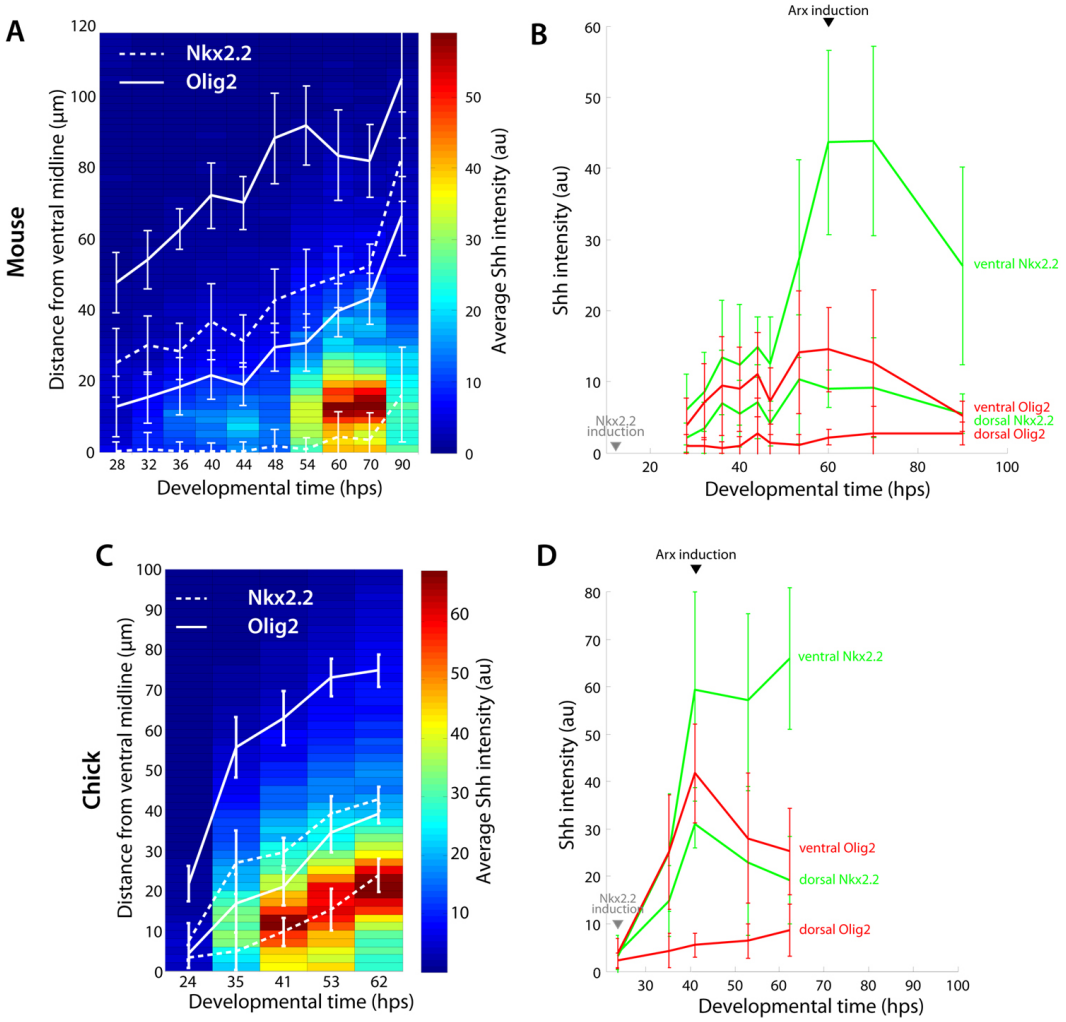

Figure 4.10 The position of the target gene boundaries is not associated with fixed Shh threshold in the mouse neural tube.

(**A,C**) Heat map representing the average Shh fluorescence intensity (arbitrary units (au)) along the dorsoventral axis of the neural tube of mouse (A) and chick (C) embryos at the indicated stages (hours post initiation of somitogenesis - hps). The position of the boundaries of the target genes Nkx2.2 (dashed white line) and Olig2 (full white line) are also shown, expressed as the distance from the ventral midline in µm (mean ± s.d; n≥3 embryos/stage). In both species the progressive induction of Nkx2.2 and Olig2 expression at increasingly more dorsal positions mirrors the increase in levels and range of the Shh gradient. (**B,D**) Quantification of the Shh fluorescence intensity at the position of the boundaries of the Nkx2.2 and Olig2 domains (mean ± s.d in arbitrary units (au); n≥3 embryos/stage) in mouse (B) and chick (D) embryos, plotted as a function of developmental time (hps). In mouse, as in chick, the concentration of Shh at the position of the boundaries of expression of Shh target genes changes over time.

To determine how the temporal changes of the Shh gradient in mouse correlated with the dynamic expression of its target genes we compared the DV distribution of Shh with the boundary positions of Nkx2.2 and Olig2 (Figure 4.10 A). The time period over which the Shh gradient expanded correlated very closely with the time period over which the boundaries of the Olig2 and Nkx2.2 domains shifted dorsally. In chick, the gradient expanded up to ~40hps chick time (~30hps mouse time) and the domain boundaries were positioned at gradually more dorsal positions (Figure 4.10 A). After this time point, the absolute positions of the Nkx2.2 and Olig2 boundaries remained constant or slightly decreased (Figure 4.10 A). In mouse both the gradient and the boundary positions expanded up to ~50hps mouse time and subsequently remained constant or decreased. Thus, the dynamics of the boundary positions correlated well with the expansion of the gradient in both species, and occurred with a ~30h delay in mouse compared to chick. This observation is consistent with the known role of Shh in the specification of the p3 and pMN domains.

Although the Nkx2.2-expressing region was consistently associated with higher Shh levels than the Olig2 domain, the concentration of Shh at specific boundaries changed as development proceeded (Figure 4.10 A,B). These results are in agreement with the data obtained in chick (Figure 4.10 C,D), which propose that the levels of ligand are not linearly transduced into levels of transcriptional activation. Noticeably, the temporal changes of the Shh concentration associated with a particular boundary resembled the temporal changes in amplitude - as the gradient expanded, the concentration at the boundary increased. Conversely, a constant or retracting Shh amplitude correlated with constant or decreasing concentrations at the boundaries. There were also differences between the two species - for example, at the time of peak amplitude, the concentration at the dorsal Nkx2.2 and ventral Olig2 boundaries were a different fraction of the amplitude in mouse and chick. This dynamics could be at least partially responsible for the scaling of the target gene domain positions between the two species (Figure 4.5 C) and would imply that the mechanism of the Shh transduction and interpretation compensates for the differences in the ligand gradients between mouse and chick to achieve scaling.

An alternative possibility is that the concentration of Shh at the boundaries is not instructive for the positions of the boundaries. A scenario consistent with this idea is the existence of an early pre-pattern which is expanded only by proliferation and differentiation over time at the same relative rates in the two species. The mechanism that would determine similar relative rates of proliferation and differentiation in mouse and chick remains an open question. Finally, it could be that scaling could be achieved by a combination of the two mechanisms: regulating proliferation and differentiation in the same relative way in the two species, and compensating for the difference in gradient dynamics by tuning the morphogen response.

In summary, these results suggest an association between the temporal accumulation of Shh and the progressive ventralization of the neural tube. However, the interpretation of Shh levels is not linear, as the position of the target gene boundaries was not associated with a fixed Shh level over time. Thus, the dynamics of target gene expression may depend also on the temporal changes in the response of cells to Shh and the dynamics of intracellular signalling.

In the following chapter I examine how the temporal changes in the Shh gradient are translated into temporal changes in the levels and spatial distribution of signalling activity. In addition, I investigate how signalling activity correlates with the dynamics of gene expression.

CHAPTER 5 - DYNAMICS OF SHH SIGNALLING ACTIVITY

The characterisation of the dynamics of Shh distribution revealed the gradual increase in the levels and spread of the gradient, which correlated with the progressive induction of Nkx2.2 and Olig2 expression at increasingly more dorsal positions. However, the data showed that the levels of Shh at a particular boundary changed over time. This result is consistent with a non-linear relationship between morphogen levels and levels of intracellular signalling, and subsequently, patterns of target gene expression, a model proposed by several studies (Ahn and Joyner, 2004; Dessaud et al., 2007; Gregor et al., 2007; Harfe et al., 2004; Houchmandzadeh et al., 2002; Jaeger et al., 2004; Liberman et al., 2009; Nahmad and Stathopolous, 2009).

In the neural tube, in vitro assays have shown that the differential expression of Nkx2.2 and Olig2 in response to changes in Shh concentration depends on different durations of intracellular signalling (Dessaud et al., 2007). Exposure to high or low Shh concentrations for short periods of time initially results in similarly high levels of Gli activity. However, cells gradually adapt their response to Shh, becoming desensitised to ongoing Shh signalling. Thus, with increasing times the level of Gli activity gradually declines, and the rate of this decline is inversely proportional to Shh levels. The temporal adaptation of cells to Shh appears to be controlled by the gradual up-regulation of pathway inhibitors such as Ptch1. As Ptch1 accumulates, increasingly higher concentrations of Shh are required to bind and inactivate the receptor and, therefore, to sustain intracellular signalling for longer periods. Increased durations of intracellular signalling specify more ventral identities: Nkx2.2 induction requires longer periods of signalling than Olig2. Thus, this study presented a dynamic morphogen interpretation mechanism that converts levels of Shh into proportional durations of intracellular signalling. To investigate whether a similar process is observed in vivo we used a mouse reporter of Gli transcriptional activity, the transgenic *Tg(GBS-GFP)* mouse line. Here, we characterise the activity of the transgene *Tg(GBS-GFP)* and assess its reliability as a reporter of Shh signalling. In addition, we examine the temporal profiles of Gli activity that result from a continuously evolving Shh gradient. Finally, we determine whether levels and/or durations of signalling explain the dynamic patterning of the Shh target genes Nkx2.2 and Olig2.

5.1 Characterization of *Tg(GBS-GFP)* activity

To visualize Gli-dependent transcriptional activation we made use of a recently generated mouse transgenic line, *Tg(GBS-GFP)*, containing eight concatemerized Gli Binding Sites (GBS) (Sasaki et al., 1997) upstream of the *hsp68* minimal promoter and the *eGFP* sequence (generated by Vanessa Ribes). The activity of *Tg(GBS-GFP)* was detected throughout development in tissues responding to Shh signalling, including the limb, ventral somites and the gut endoderm (V. Ribes, personal communication). Importantly, the expression of *Tg(GBS-GFP)* was observed in the ventral neural tube, consistent with a Shh-dependent regulation (Figure 5.1 A,E).

A more detailed analysis of *Tg(GBS-GFP)* activity showed a graded DV distribution in early stages (24hps), with higher levels of expression in more ventral positions (Figure 5.1A). The initial distribution of GFP was comparable to that of the Shh target and pathway inhibitor *Ptch1* (Figure 5.1 A,B). However, in later times *Tg (GBS-GFP)* expression was more ventrally restricted than *Ptch1* mRNA expression, which expanded dorsally (Figure 5.1 E,F). Strikingly, the *Tg(GBS-GFP)* profile correlated well with the distribution of Ptch1 protein (Figure 5.1 C,G,I-L). The detection of Ptch1 protein showed a distinctive localization in the neural tube: a strong punctate apical distribution along the lumen of the neural tube, and a lower density punctate localization in basal lateral portions of neuroepithelium cells (Figure 5.1 C,G). While the apical pool was detected along most of the DV extent of the neural tube, the basal-lateral pool was located more ventrally. The distribution of the basal-lateral pool was similar to that of *Tg(GBS-GFP)* expression (quantified in Figure 5.7), suggesting that the subcellular localization of Ptch1 protein was associated with the activation of the pathway. Consistently, in these early stages the *Tg(GBS-GFP)*-active region, and the Ptch1 basal-lateral pool region, encompassed the Nkx2.2 domain of expression (Figure 5.1 D,H). Thus, the distribution of *Tg(GBS-GFP)* in the neural tube had the expected pattern of a Shh-responding gene.

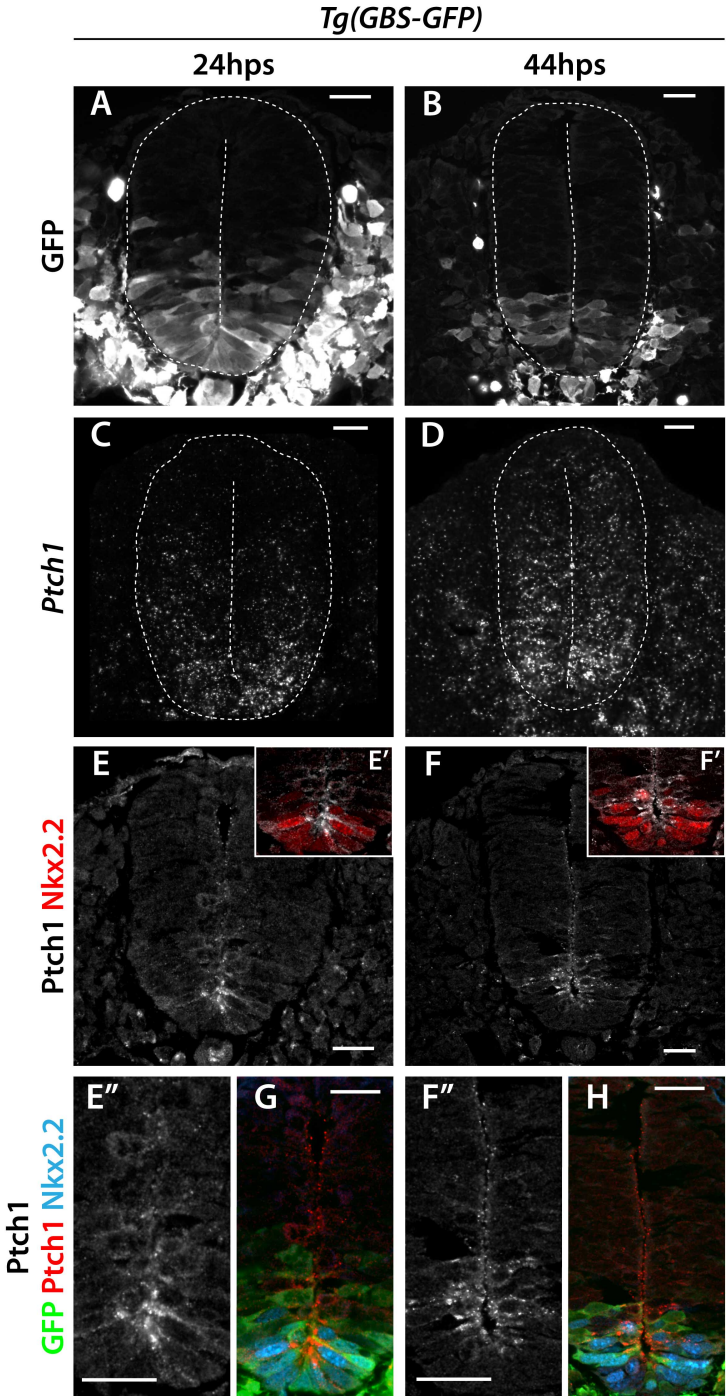

Figure 5.1 The expression of *Tg(GBS-GFP)* reports Shh signalling activity.

(**A-H**) Immunohistochemistry against GFP, expressed from *Tg(GBS-GFP)*, reveals GFP expression in the neural tube in a similar pattern to other Shh targets. Expression of GFP (white - A,B - or green - G,H), *Ptch1* mRNA (white - C,D), Ptch1 protein (white - E,E″,F,F″- or red - E′,G,F′H) and Nkx2.2 (red - E′,F′ - or blue - G,H) in *Tg(GBS-GFP)* mouse embryos at the indicated developmental stages (in hours post initiation of somitogenesis - hps). (E″,F″) Higher magnification images of the ventral region of the neural tubes in (E,F). The graded

distribution of GFP in early stages (A) resembles the expression pattern of *Ptch1* mRNA (C) and Ptch1 protein (E″,G). In this stage the Nkx2.2 domain is associated with the highest levels of Ptch1 protein and *Tg(GBS-GFP)* activity (E′,G). At a later stage the pattern of GFP expression (B) is more restricted than the spatial distribution of the *Ptch1* transcripts (D). By contrast, the GFP expression correlates well with the spatial extent of the basal-lateral distribution of Ptch1 protein (F″,H) and the expression domain of Nkx2.2 (F′,H). Scale bars: 20 µm.

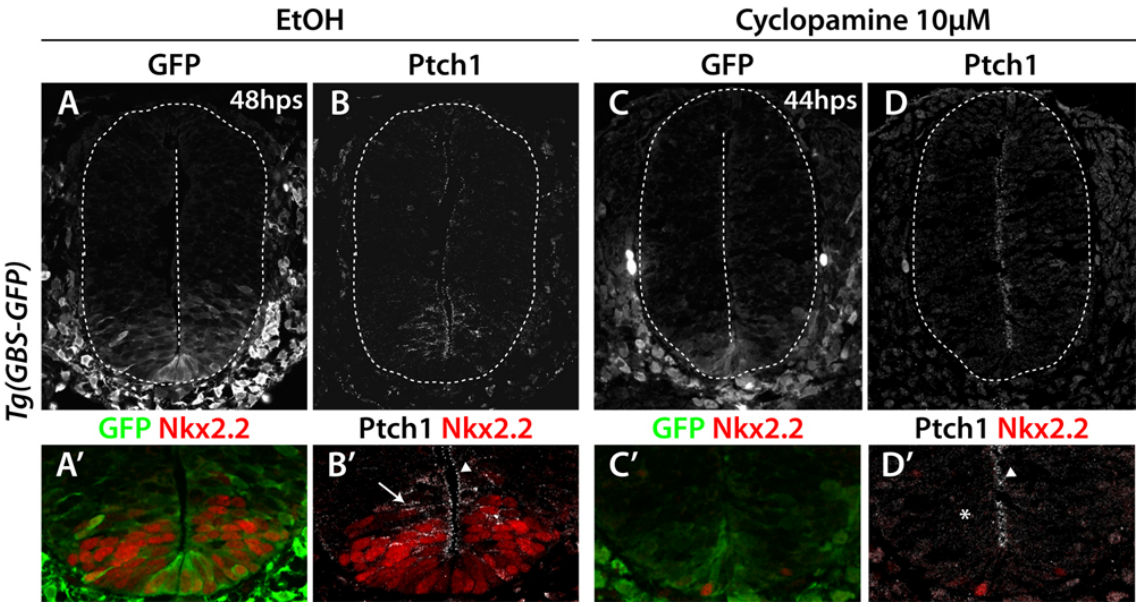

Figure 5.2 Inhibition of Shh signalling decreases the *Tg(GBS-GFP)* activity.
(**A-D′**) *Tg(GBS-GFP)* activity decreases in embryos exposed to cyclopamine. Expression of GFP (white or green), Ptch1 (white) and Nkx2.2 (red) in *Tg(GBS-GFP)* mouse embryos cultured for 24h in control media (A-B′) or with the Smo inhibitor cyclopamine (C,D′). Embryos cultured in presence of 10µM cyclopamine have reduced levels of GFP in the neural tube (C) compared to controls (A). Consistent with a decrease in Shh signalling, Nkx2.2 expression in these embryos is reduced (C′,D′). Likewise, Ptch1 protein expression is affected in embryos exposed to cyclopamine (B,D). In control embryos (B′) Ptch1 protein is detected both in puncta along the lumen (arrow heads) and in more basal-lateral positions (arrow). In cyclopamine treated embryos (D′) the lumen-associated Ptch1 expression is observed (arrow head), but the basal-lateral distribution is lost (*).

To confirm that *Tg(GBS-GFP)* expression depended on Shh signalling, the activation of the pathway was inhibited using the Smo antagonist cyclopamine (Taipale et al., 2000). Mouse embryos, at approximately 12hps, were cultured ex vivo with 10μM cyclopamine for 24h. The inhibition of Smo activity resulted in a pronounced decrease in the levels and range of *Tg(GBS-GFP)* in the neural tube (Figure 5.2 A,C). Importantly, the decrease in the activity of *Tg(GBS-GFP)* following cyclopamine exposure correlated with the down-regulation of the Shh target genes Ptch1 and Nkx2.2 (Figure 5.2 B,D,A'-D'). The effect of cyclopamine on Ptch1 protein was limited to the medially located pool, further supporting the idea that Shh signalling regulates the subcellular localization of this pool (Figure 5.2 B',D'). These results suggested that *Tg(GBS-GFP)* activity in the neural tube required the activation of Shh signalling through Smo.

We next assessed the response of the reporter to different concentrations of the Smo agonist purmorphamine (Sinha and Chen, 2005). *Tg(GBS-GFP)* embryos (8-12hps) were cultured with 0, 5 or 10μM of Purmorphamine for 12 or 24h. Embryos exposed to 5μM of purmorphamine for 12h showed an increase in the levels and dorsal extent of *Tg(GBS-GFP)* expression when compared to control embryos (Figure 5.3 A,B,F,G). Exposure to increasing levels of purmorphamine for 12h resulted in increasingly stronger and more expanded *Tg(GBS-GFP)* expression. This result suggested that the activity of the reporter was sensitive to the level of Shh signalling. However, after 24h of exposure to purmorphamine, GFP intensity was considerably decreased, even in the presence of the highest concentration of purmorphamine. Nevertheless, the DV range of *Tg(GBS-GFP)* expression remained expanded in Purmorphamine-treated embryos, consistent with the observed dorsal expansion of Nkx2.2 and Olig2 expression and increased levels of Ptch1 (Figure 5.3 C-E, H-J). The decline in *Tg(GBS-GFP)* expression levels after longer periods of Smo activation points to the presence of feedback mechanisms downstream of Smo, which regulate the levels of Gli activity.

These results demonstrate that the *Tg(GBS-GFP)* transgene reliably reports Shh signal transduction and is a useful tool to examine the dynamics of Shh intracellular signalling in vivo.

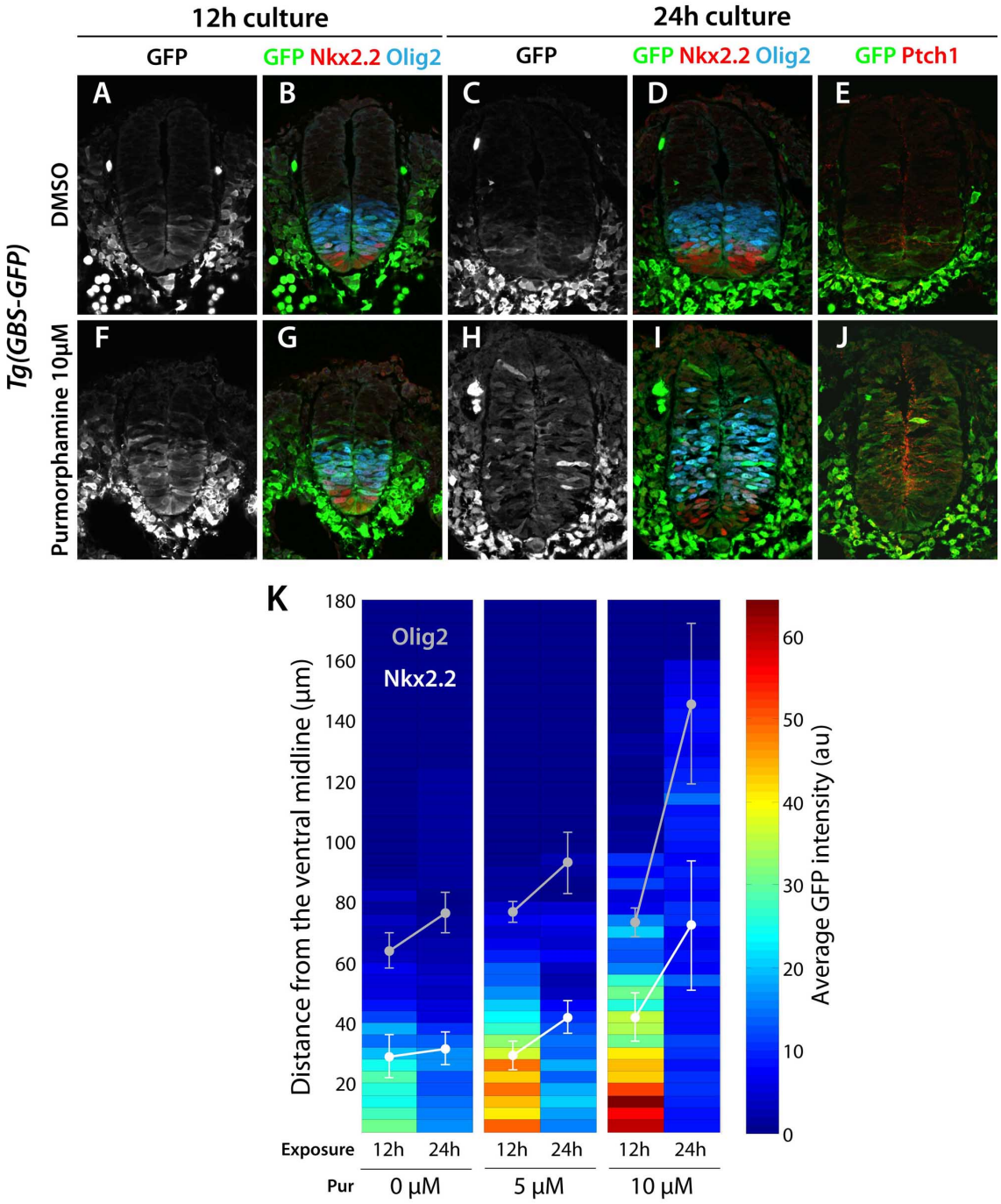

Figure 5.3 *Tg(GBS-GFP)* activity responds to increases in Shh signalling.

(**A-J**) *Tg(GBS-GFP)* activity increases in purmorphamine treated embryos. Expression of GFP (white or green), Ptch1 (white), Nkx2.2 (red), Olig2 (blue) and Ptch1 (red) in *Tg(GBS-GFP)* mouse embryos cultured for 12h or 24h in control media (A-E) or with the Smo agonist purmorphamine (F,J). Exposure to 10μM purmorphamine for 12h results in the increased levels and dorsal expansion of *Tg(GBS-GFP)* expression (A,F), whereas Nkx2.2 and Olig2 expression remains unaffected (B,G). More prolonged periods of culture with purmorphamine (24h) result in the ectopic induction of Nkx2.2 and Olig2 expression at more dorsal positions (D,I). By contrast, after 24h of exposure to purmorphamine the levels of *Tg*

(GBS-GFP) expression decline, although the dorsal expansion is maintained (C,H). Furthermore, the levels of Ptch1 protein along the dorsoventral axis were elevated in the presence of purmorphamine (E,J). (**K**) Quantification of *Tg(GBS-GFP)* activity in embryos cultured ex vivo with 0, 5 or 10μM purmorphamine for 12h or 24h. Heat maps illustrate GFP intensity (mean in arbitrary units (au)) along the dorsoventral axis (distance from the ventral midline in μm) and the positions of the dorsal boundary of Nkx2.2 (white line) and Olig2 (grey line) domains (mean ± s.d.) in embryos at the indicated conditions (n≥2 embryos/condition). Exposure for 12h to progressively higher concentrations of purmorphamine results in enhanced and dorsally expanded *Tg(GBS-GFP)* activity. After more prolonged exposure times (24h), the GFP intensity decreases, suggesting that mechanisms downstream of Smo are involved in the negative feedback.

5.2 Dynamics of *Tg(GBS-GFP)* expression

The visualization of *Tg(GBS-GFP)* expression in vivo revealed the changing pattern both in space and in time (Figure 5.4 A-F). The qualitative analysis of the Gli activity reporter showed an initial increase in the levels of GFP along the DV axis, accompanied by a progressive dorsal expansion. After reaching a peak at ~30hps, the levels of signalling gradually declined and GFP was undetectable by 80hps. These observed dynamics of the signalling reporter differed from those of the Shh ligand, the amplitude of which continuously increased until 60 to 70hps (Figure 5.4 A'-F').

To more accurately examine the signalling dynamics we quantified the fluorescence intensity distribution of *Tg(GBS-GFP)* during development, from 12hps to 90hps (Figure 5.5 A,C). Similarly to the Shh gradient, the levels of *Tg(GBS-GFP)* at early stages decayed approximately exponentially as a function the distance from the source (12hps to 16hps). However, at later times the intensity level in the first 15-20μm from the source were constant, forming a "shoulder" in the profile. Nevertheless, it was clear that, as observed qualitatively, the levels and range of Gli activity progressively increased from 12 to 32hps. The initial increase in GFP levels, which reached a peak at 32hps, was followed by a decrease. The decline in GFP intensity was very pronounced from 36 to 40hps and the levels remained low as development proceeded. By 80hps the levels of expression of *Tg(GBS-GFP)* in the ventral neural tube were indistinguishable from background levels.

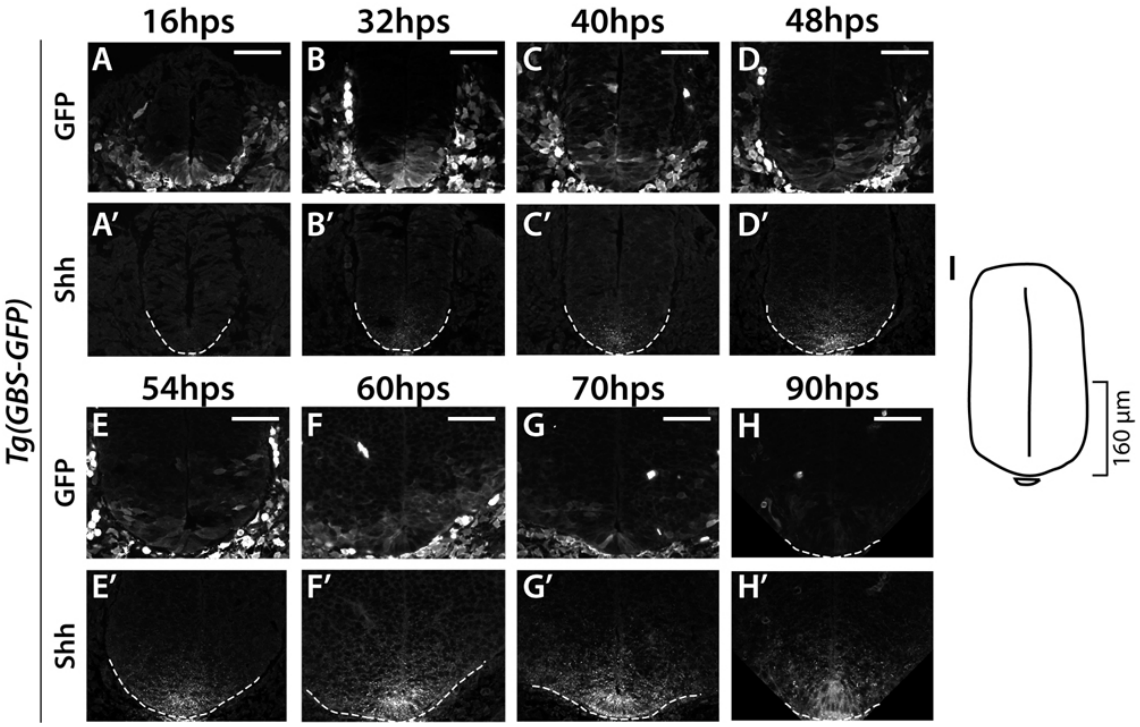

Figure 5.4 Spatial and temporal changes in the expression of *Tg(GBS-GFP)* and Shh in the mouse neural tube.

(**A-H'**) Expression of GFP (A-H) or Shh (A'-H) in neural tube sections of *Tg(GBS-GFP)* mouse embryos at the indicated stages in hours post initiation of somitogenesis (hps). The images depict a region of 160µm from the ventral midline (I). The dynamics of *Tg(GBS-GFP)* expression do not correlate with spatial and temporal changes of the Shh gradient. The level and range of Shh gradually increase over time (A'-G'), and only decline at the last stage analyzed (H'). Conversely, the levels of GFP peak early (A,B) and progressively decline afterwards (C-H). Scale bars: 50 µm.

In order to understand how the ligand gradient of Shh was converted into Gli activity in vivo, we directly compared the dynamics of the Shh and *Tg(GBS-GFP)* profiles in the same set of embryos (Figure 5.5). The levels of Shh gradually increased until 60hps, and started to decline between 70hps and 90hps (Figure 5.5 B). Gli activity similarly showed a progressive increase in levels in initial stages, but started to decline at an earlier time point, at 36hps (Figure 5.5 A). Thus, one of the most obvious differences between the two is that the most dynamic changes in Gli activity are observed early in development (up to 40hps), in contrast to the amplitude of the Shh gradient, which continues to increase at late stages (after 40hps). This is

consistent with the previous quantifications of Gli activity in explants, where Gli activity reached saturating levels in less than 6 hours after exposure to a range of Shh concentrations and subsequently declined at a rate that was inversely proportional to the Shh concentrations (Dessaud et al., 2010). Thus, the dynamics of the *Tg(GBS-GFP)* reporter suggests that cells also respond nonlinearly to ligand levels in vivo and confirms that even low Shh concentrations are sufficient to elicit high levels of signalling.

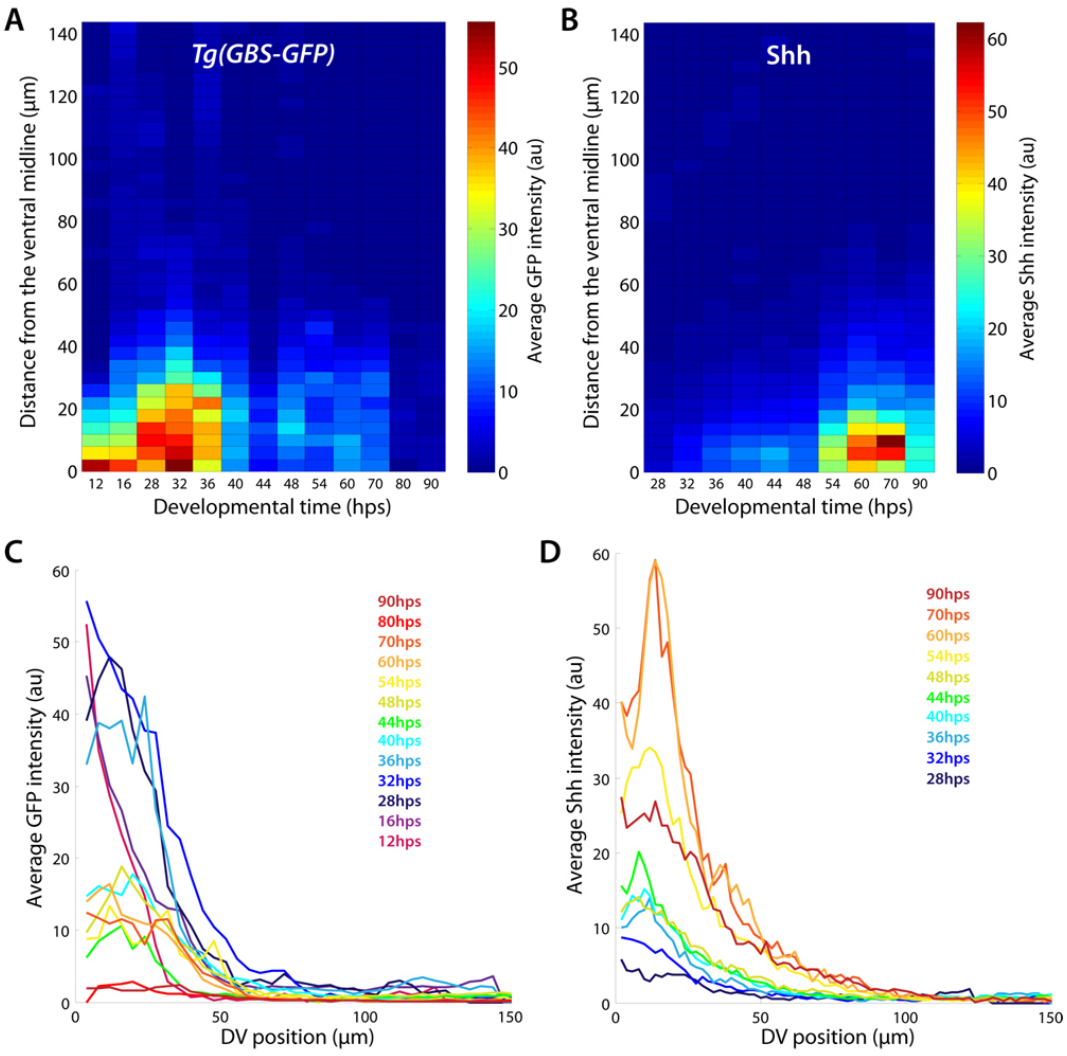

Figure 5.5 Shh protein and the Shh signalling reporter *Tg(GBS-GFP)* have different dynamics in the mouse neural tube.

(**A-D**) Quantification of GFP and Shh intensity levels in the neural tube *Tg(GBS-GFP)* mouse embryos, plotted as a function of the distance from the ventral midline (µm) at the indicated developmental stages in hours post initiation of somitogenesis (hps). (**A,B**) Heat maps

illustrate the average GFP (A) and Shh (B) fluorescence intensity (arbitrary units (au)) in 4µm bins along the dorsoventral axis of the neural tube of mouse embryos at the indicated stages (n≥3 embryos/stage). (**C,D**) Average GFP (C) and Shh (D) fluorescence intensity profiles (arbitrary units (au)) as a function of the distance from the ventral midline (µm) at the indicated stages. Like Shh (D), *Tg(GBS-GFP)* expression shows an exponential decay as function of the distance from the source (C). However, the expression of the ligand and the signalling reporter follow different dynamics over time. The intensity and dorsal expansion of GFP gradually increase until 32hps, and rapidly decline afterwards (A,C), whereas Shh intensity levels and range continue to increase until 60hps (B,D).

To be able to compare the temporal dynamics of Shh and Gli activity in vivo to previous data from explants, we plotted the average intensity levels at defined relative distances from the source as a function of time (Figure 5.6 A-D). Using distances relative to the total size of the neural tube instead of absolute distances in microns allowed us to take into account the tissue growth: since proliferation is uniform along the DV axis and differentiation is minimal until 54hps, then the relative position of each cell during this period can be considered constant. Hence, Shh and *Tg(GBS-GFP)* levels at a specific relative position at different time points represent the history of Shh concentration and Gli activity experienced by a cell and its progeny. Figure 5.6 (A,B) shows that Shh concentration experienced by a cell increases continuously until 60hps. The rate of the increase in Shh levels appears to be higher from 46hps, which could be due to the transition to a definite floor plate identity occurring at this stage (Ribes et al., 2010). Another possibility is that the steeper increase in Shh levels at ventral positions reflects the slower effective increase in size of the ventral domains relative to the dorsal domains during the intermediate phase (see Chapter 4). In fact, this sharp increase coincides with the onset of MN differentiation (approximately 54hps). As a result, during this phase of increased differentiation the gradient would appear to expand faster than the domains. Therefore, to confirm this marked increase it would be necessary to measure the differentiation rate in these stages and rescale the Shh profiles accordingly.

Before 28hps, a period during which Shh levels were too low to be measured, the *Tg(GBS-GFP)* profiles showed a rapid increase (Figure 5.6 D). *Tg(GBS-GFP)* activity maintained high levels until around 36hps and subsequently decreased at different

rates depending on the distance to the source. The peak of Gli activity coincided with a period of increase in the amplitude of the Shh gradient, even though at this time ligand levels were still low. Thus, the initial increased signalling activity was consistent with the gradual accumulation of Shh (Figure 5.6 A,B).

It is interesting to note that the in vivo data shows that it takes at least 20 hours (from 12 to 32hps) for Gli activity to reach maximum levels. This is in contrast to explant data where the maximum Gli activity is observed within 6 hours after the onset of the experiment (Dessaud et al., 2010). The difference between the in vivo and ex vivo results could reflect species differences in the transcriptional response to increasing Shh levels (the explants used ex vivo were obtained from chick embryos). Alternatively, the gradual increase of Shh in vivo delays the time of peak Gli activity. The initial expansion of the Shh gradient and the consequent delay of the onset of adaptation are likely to be functionally significant in vivo for expanding the range of Gli activity to more dorsal positions (i.e. an earlier peak of Gli activity could result in more ventrally compressed patterns). Consistent with this, the initial transduction of the early Shh gradient into Gli activity appears to be proportional (Figure 5.6 E). This suggests that the increase in amplitude of the Shh gradient before 36hps leads to a proportional expansion of the signalling activity gradient.

After 36hps, although Shh intensity increased, Gli activity declined. The rate of the decline of Gli activity in vivo was broadly comparable to the data from ex vivo assays: exposure to two different Shh concentrations in explants resulted in a 2 to 4 fold decline in Gli activity over a period of 24h (Dessaud et al., 2007), and in vivo the decrease in *Tg(GBS-GFP)* intensity was 4 to 5 times over the same period of time (Figure 5.6 C,D). The increased rate of decline in vivo could be due to differences between the degradation rates of the GBS-luc reporter used in explants and GBS-GFP, even though one might expect to see a faster decay ex vivo rather than slower, given the shorter half-life of luciferase. Another possibility is that mouse and chick tissues cannot be directly compared - if, for example, the proliferation rates or the molecular mechanisms involved in temporal adaptation are different between the two species. Finally, it could be that there are additional signalling molecules involved in Shh response - for instance, BMP or Wnt signalling in vivo in the neural tube could contribute to enhancing the levels of Gli receptor, which would then decrease the net Gli activity measured by the *Tg(GBS-GFP)* reporter. It would be interesting to address these possibilities in the future by comparing ex vivo and in vivo assays using the

same species or in explant assays where the BMP and Wnt concentrations are also exogenously controlled.

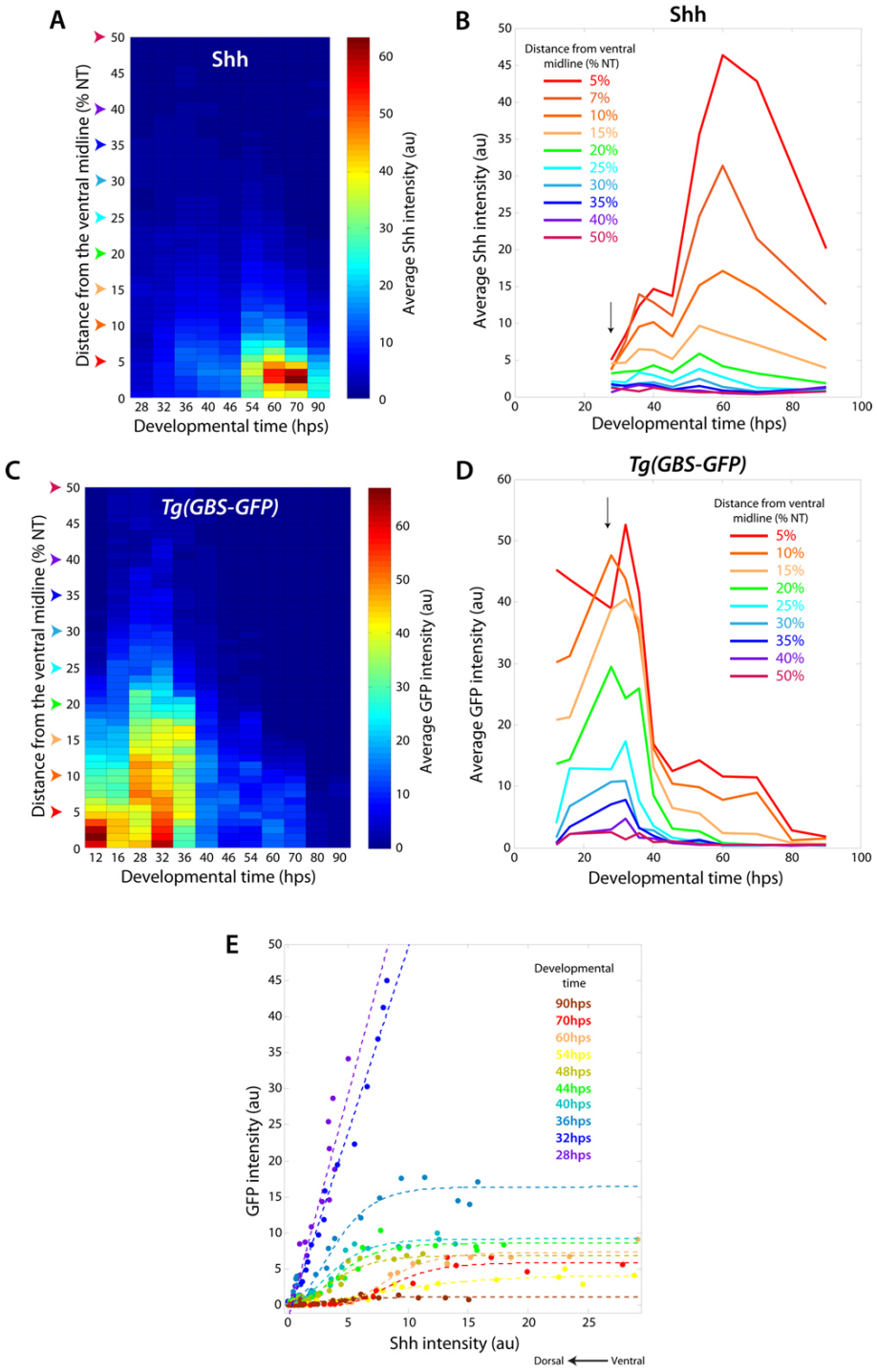

Figure 5.6 Conversion of Shh concentration into intracellular signalling activity.

(**A-D**) Quantification of GFP and Shh intensity levels at different relative positions of the neural tube of *Tg(GBS-GFP)* mouse embryos. (**A,C**) Heat maps illustrate the average Shh (A)

and GFP (C) fluorescence intensity (arbitrary units (au)) plotted as a function of the relative distance from the ventral midline (percentage of the neural tube size (%NT)) at the indicated developmental stages in hours post initiation of somitogenesis (hps) (n≥3 embryos/stage). (**B,D**) Temporal profiles of the average Shh (B) and GFP (D) fluorescence intensity levels (au) at the indicated relative positions, which correspond to the relative positions marked by arrow heads in (A,C). Arrows in (B,D) indicate the first stage in which Shh fluorescence intensity was measured. The temporal profiles of Shh and GFP expression show that Shh levels are not directly converted into levels of signal transduction, consistent with the temporal adaptation of cells to ongoing signalling. However, in cells exposed to higher levels of Shh, in more ventral positions (B), display a slower rate of decline in *Tg(GBS-GFP)* activity (D) than cells at more dorsal positions. (**E**) Relationship between Shh and *Tg(GBS-GFP)* expression over time. Average GFP fluorescence intensity (au) in bins of cells placed along the dorsoventral axis of the neural tube plotted as a function of the average Shh fluorescence intensity (au) measured in the same bins at the indicated stages (n≥3 embryos/stage). Each point corresponds to the average fluorescence intensity in a bin of 1%NT at a specific relative distance from the ventral midline. In each stage, bins with higher Shh intensity levels correspond to bins located at more ventral positions. In early stages (28hps to 32hps) the levels of intracellular signalling in a cell are proportional to the level of Shh it is exposed to. From 36hps, below-maximum levels of Shh are saturating, and over time the levels of *Tg(GBS-GFP)* activity elicited by Shh gradually decline.

The temporal adaptation of cells to increasing levels of Shh has been proposed to involve Shh induced negative feedback mechanisms, such as the up-regulation of Ptch1 (Dessaud et al., 2007). To determine whether the changing response of cells to Shh correlated with an increase in the levels of the receptor we measured the expression of Ptch1 protein in the developing neural tube (Figure 5.7). The distribution of Ptch1 displayed similar dynamics to the activity of the signalling reporter: Ptch1 levels increased during the first stages analyzed and subsequently declined (Figure 5.7 J, K). However, the peak intensity of Ptch1 was reached at 16hps (Figure 5.7 A', K), whereas *Tg(GBS-GFP)* expression reached its maximum levels later, at 32hps (Figure 5.7 B, B', J). This difference between Ptch1 and *Tg(GBS-GFP)* expression could result from differences in the half-life of the two proteins. The half-life of GFP in the neural tube was estimated to be approximately 13-19h (Vanessa Ribes, personal communication). The half-life of Ptch1 in the neural tube is unknown, but Ptch1 could have a more rapid turn-over in response to Shh (Incardona et al., 2002).

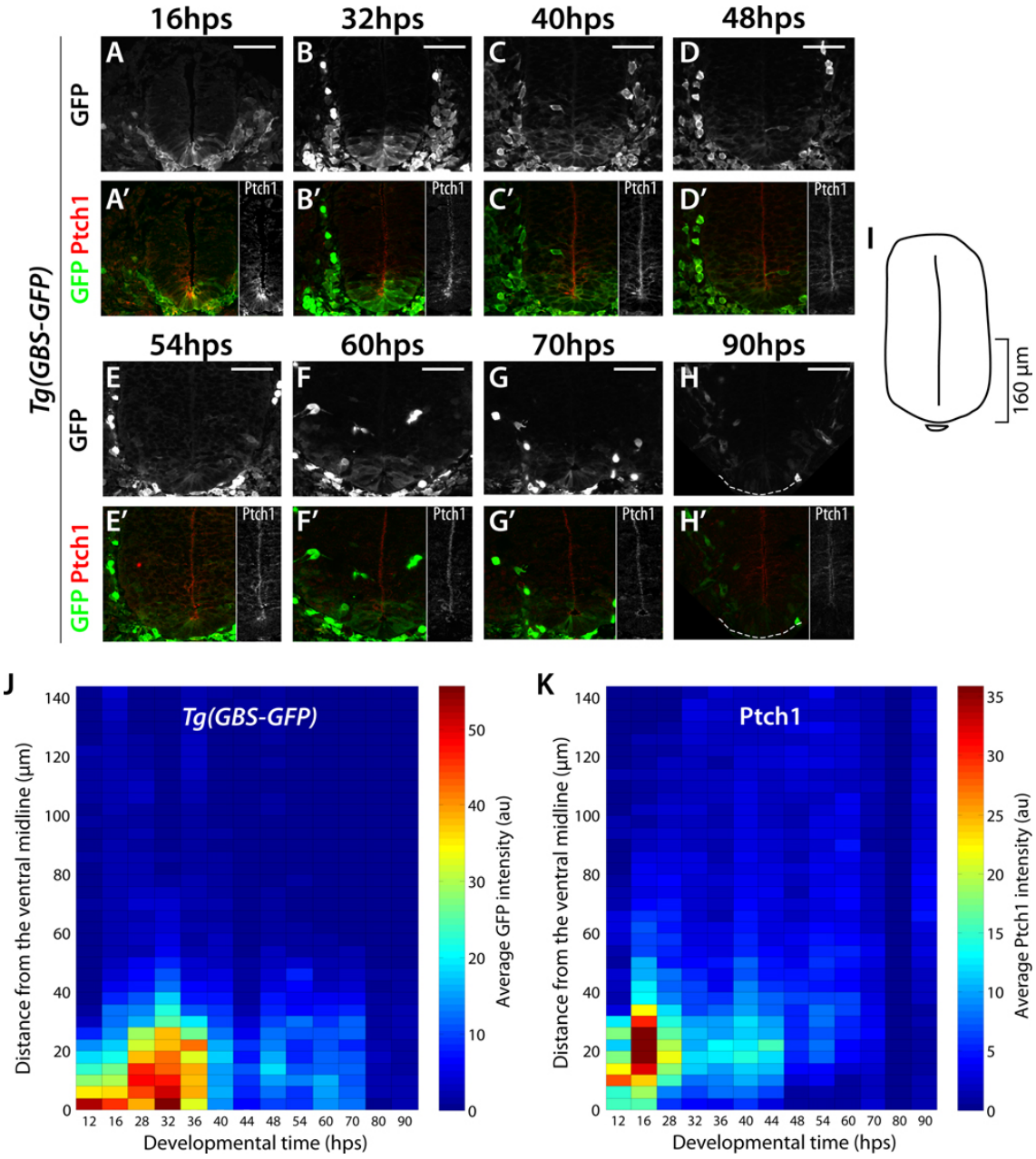

Figure 5.7 Ptch1 expression has similar dynamics to *Tg(GBS-GFP)* in the mouse neural tube.

(**A-H'**) Patterns of of *Tg(GBS-GFP)* and Ptch1 in the mouse neural tube over time. Expression of GFP (white (A-H) or green (A'-H')) and Ptch1 protein (red or white (insets) in A'-H) in neural tube sections of *Tg(GBS-GFP)* mouse embryos at the indicated stages in hours post initiation of somitogenesis (hps). The images correspond to a region of 160µm from the ventral midline (I). The spatial and temporal changes in Ptch1 distribution resemble that of *Tg(GBS-GFP)* expression (A,H'). The dynamic changes in Ptch1 protein distribution are more noticeable in the basal-lateral pool (A'-H', insets). (**J,K**) Quantification of GFP (J) and Ptch1 protein (K) intensity levels in the neural tube *Tg(GBS-GFP)* mouse embryos, plotted as a function of the distance from the ventral midline (µm) at the indicated developmental stages

in hours post initiation of somitogenesis (hps) (n≥3 embryos/stage). The average GFP (J) and Ptch1 (K) fluorescence intensity (arbitrary units (au)) measured in bins located along the dorsoventral axis are illustrated as heat maps. Although Ptch1 expression reaches peak levels at an earlier stage (16hps, A',K) than GFP expression (32hps, B,B',J), after reaching peak levels both proteins show a decline in intensity over time. This result suggests that Ptch1 up-regulation alone cannot explain the down-regulation of Gli activity over time and other factors must be involved in negative feedback mechanisms. Scale bars: 50 µm.

Regardless of the difference in the timing of the peak levels of expression, Ptch1 protein showed a similar response to *Tg(GBS-GFP)*, with decreasing levels over time, suggesting that Ptch1 is not the sole mediator of the negative feedback. This finding is consistent with the result obtained with Purmorphamine-treated embryos. The activation of Smo using Purmorphamine, which bypasses the negative feedback mediated by Ptch1, still resulted in decreased levels of signalling after longer exposure times, suggesting that other factors downstream of Smo are involved in the negative feedback (Figure 5.3 C,D). Nevertheless, low levels of Ptch1 protein are maintained in the ventral region of the neural tube, which could contribute to the decrease in Gli activity over time.

The temporal characterization of the *Tg(GBS-GFP)* reporter showed that the dynamics of Shh signalling differed from the dynamics of the Shh gradient. During a period of continuous increase in Shh levels, an initial increase in signalling activity was followed by a sharp decline. This suggests that a temporal adaptation mechanism is operating in vivo in the neural tube.

5.3 Correlation between the expression of *Tg(GBS-GFP)* and Shh target genes

To examine how the changes in Shh signalling correlated with the expression of Shh target genes we compared the dynamics of the *Tg(GBS-GFP)* reporter and the neural expressed transcription factors Nkx2.2 and Olig2 (Figure 5.8 A-K). In early stages (12 to 32hps) the increase in the levels and range of Gli activity paralleled the

positional shifts of the boundaries of the Nkx2.2 and Olig2 domains (Figure 5.8 J). Moreover, at each stage the highest levels of signalling were found in more ventral regions, where Nkx2.2 was expressed, whereas lower levels were detected in the region expressing Olig2. However, the level of Shh signalling associated with each gene changed over time. For example, higher levels of *Tg(GBS-GFP)* were present in the Olig2 domain in early stages (12 to 32hps) than in the Nkx2.2 domain in later stages (40 to 90hps) (Figure 5.8 J). In addition, cells in the region of the p3/pMN boundary, which expressed either Nkx2.2 or Olig2, exhibited similar levels of Gli activity. The quantification of the intensity of *Tg(GBS-GFP)* at the position of the boundaries confirmed that the expression of Nkx2.2 and Olig2 is not associated with fixed levels of Gli activity over time (Figure 5.8 K). Thus, in vivo the level of Gli activity is not sufficient to predict the positional identity of a cell. This is consistent with ex vivo data, in which similar levels of Gli activity are able to induce the expression of either Olig2 or Nkx2.2 depending on the duration of the signalling activity (Dessaud et al., 2007).

To examine if the differential expression of Nkx2.2 and Olig2 in vivo could also be explained by different durations of Gli activity we estimated the cumulative levels and duration of signalling - the time integral of Gli activity (Dessaud et al., 2010). The time integral of Gli activity is equivalent to the area under the temporal profile of Gli activity at a particular DV position (Figure 5.9 A,B). This measurement was determined by interpolating curves (5^{th} order polynomials) to the temporal profiles of GFP intensity at the specified relative positions, which were subsequently integrated to obtain the cumulative GFP intensity (Figure 5.9 C).

The quantification of the cumulative amount of GFP at different relative positions shows that cells located ventrally experience more cumulative Gli activity than more dorsally positioned cells (Figure 5.9 C). Thus, the history of Gli activity appears to be a better indicator of positional identity in vivo. This finding raises the question of how cells integrate level and duration of signalling to generate the appropriate patterns of gene expression. The transcriptional network downstream of Shh signalling might be important for the differential regulation of gene expression. In the neural tube, cross-repressive interaction between Shh target genes help define the DV extent of the progenitor domains (Briscoe et al., 2000). These regulatory interactions could also be involved in the dynamics of gene expression, together

with the changing levels of Gli activity. In this model, termed "sequential cell context model" (Pages and Kerridge, 2000), prior levels of signalling determine the current transcriptional profile of a cell, which is thus equivalent to the history of Gli activity. The transcriptional profile will in turn influence the response of the cell to the current levels of signalling. The study of the role of the gene regulatory network in the interpretation of Shh signalling in the neural tube will help test this model.

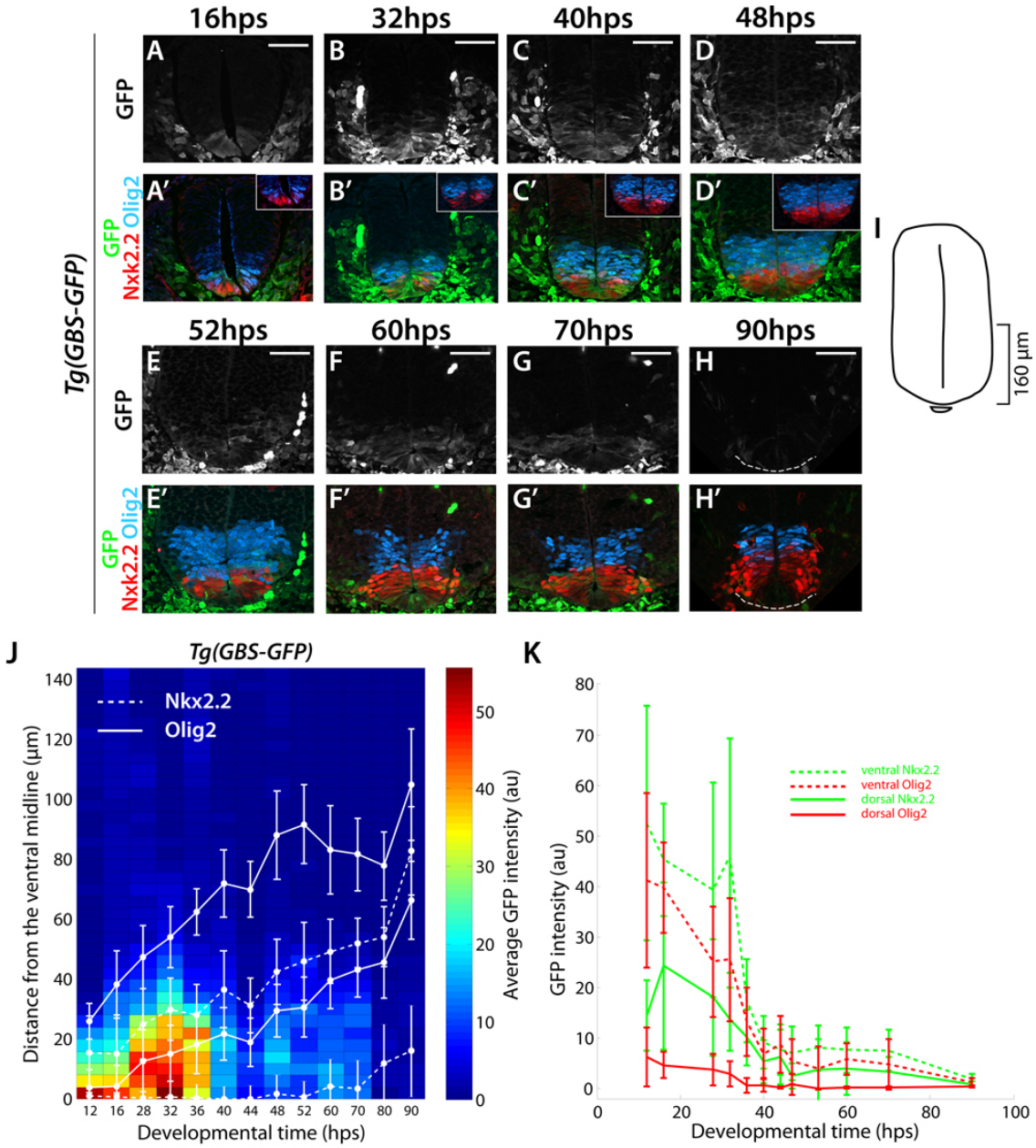

Figure 5.8 Level of Shh intracellular signalling is not predictive of progenitor identity.

(**A-H'**) Expression patterns of *Tg(GBS-GFP)* and the Shh-dependent progenitor markers Nkx2.2 and Olig2 in the mouse neural tube. Expression of GFP (white (A-H) or green (A'-H')), Nkx2.2

(red; A'-H) and Olig2 (blue, A'-H') in neural tube sections of *Tg(GBS-GFP)* mouse embryos at the indicated stages in hours post initiation of somitogenesis (hps). The images capture the region within 160µm of the ventral midline (I). (**J,K**) Comparison between the level of Tg(GBS-GFP) activity and the position of target gene boundaries. (J) Heat map depicts the average GFP fluorescence intensity (arbitrary units (au)) along the dorsoventral axis of the neural tube at the indicated stages, and the positions of the boundaries of the target genes Nkx2.2 (dashed white line) and Olig2 (full white line) are also shown, expressed as the distance from the ventral midline in µm (mean ± s.d; n≥3 embryos/stage). (K) Quantification of the GFP fluorescence intensity at the position of the boundaries of the Nkx2.2 and Olig2 domains (mean ± s.d in arbitrary units (au); n≥3 embryos/stage), plotted as a function of developmental time (hps). Although GFP intensity is always higher in the domain of expression of Nkx2.2 than in the Olig2 domain, the level of *Tg(GBS-GFP)* activity in a cell is not sufficient to identify its neuronal fate (J). Moreover, the levels of GPF at the position of the target gene boundaries changed over time (K). These results suggest that the identity of a cell is not specified simply by the level of Gli activity.

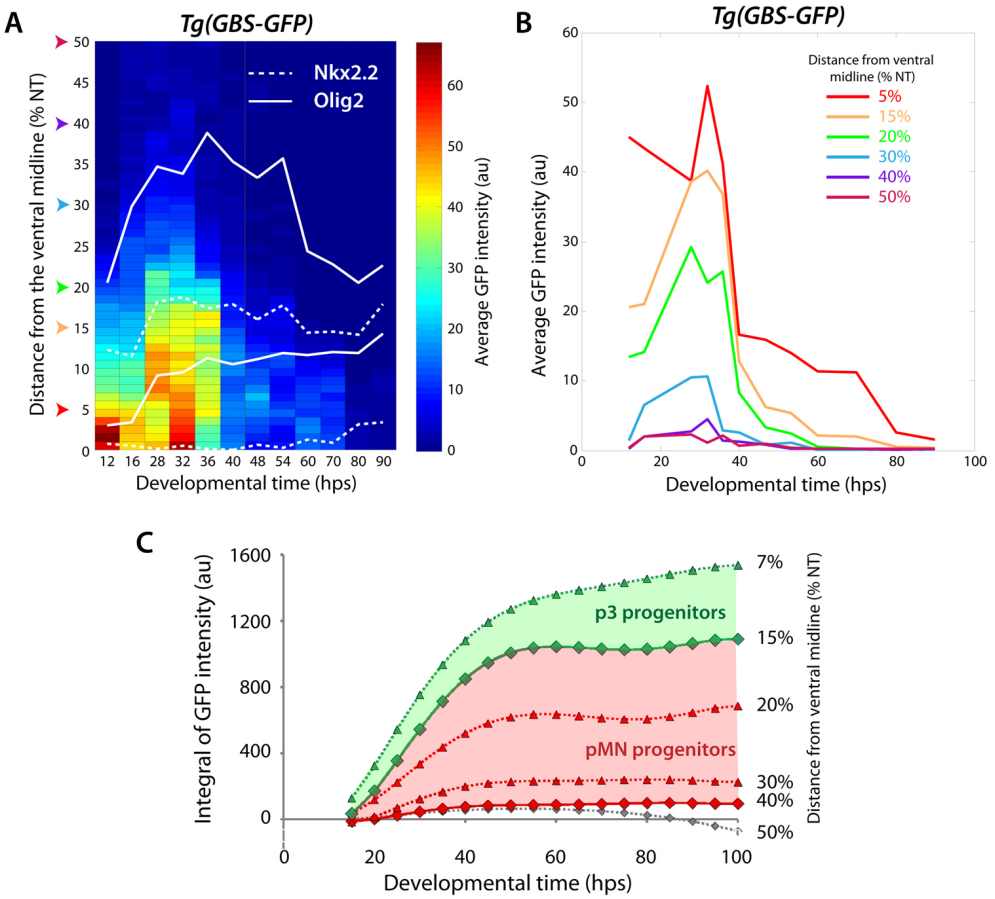

Figure 5.9 The cumulative amount of Gli activity defines progenitor identity.

Figure 5.9 The cumulative amount of Gli activity defines progenitor identity.
(**A,B**) History of Gli activity experienced by cells at different relative positions in the neural tube. (A) Heat map presents the average GFP fluorescence intensity (arbitrary units (au)) along the normalized dorsoventral axis (percentage of the neural tube size (%NT)) of the neural tube of *Tg(GBS-GFP)* mouse embryos at the indicated stages. The average relative position of the boundaries of the target genes Nkx2.2 (dashed white line) and Olig2 (full white line) are also shown (%NT). (**B**) Temporal profiles of the average GFP fluorescence intensity levels (au) at the indicated relative positions, which correspond to the relative positions marked by arrow heads in (A,C). (**C**) Cumulative amount of *Tg(GBS-GFP)* activity in cells at the indicated relative positions from the ventral midline (%NT). The time integrals of GFP were obtained from curves fit to the data in (B), and these correspond to the area underneath the temporal profiles of Gli activity. These data confirm that p3 progenitors experience higher cumulative levels of *Tg(GBS-GFP)* activity than pMN progenitors.

In summary, these data indicate that the levels of Shh signalling are not sufficient to explain the induction of target genes in vivo and suggests that both the level and duration of Gli activity are required to specify gene positional identity.

CHAPTER 6 - DISCUSSION I

Sonic Hedgehog (Shh) signalling plays a key role in the development of the vertebrate central nervous system. Shh signalling is required for the specification of several neuronal subtypes in the spinal cord. Moreover, the graded activity of Shh ensures that the different neuronal subtypes are generated at the appropriate positions within the spinal cord, a process that is crucial for the correct wiring of spinal neural networks. The spatial organization of neuronal cell types in the spinal cord reflects the arrayed distribution of the groups of progenitor cells that give rise to these neuronal subtypes. The identity of each neural progenitor domain is governed by a distinctive set of transcription factors, whose expression in the ventral half of the neural tube is regulated by a temporally changing Shh gradient (Briscoe et al., 2000; Chamberlain et al., 2008; Ericson et al., 1997). The expression patterns of the Shh-dependent transcription factors are established in a progressive manner, both temporally and spatially, as observed for the p3 (Nkx2.2) and pMN (Olig2) markers (Chamberlain et al., 2008; Jeong and McMahon, 2005; Stamataki et al., 2005). Crucially, both the level and the duration of Shh signalling are important to induce the differential expression of target genes in responding cells ex vivo (Dessaud et al., 2007; Ericson et al., 1997).

To gain insight into the mechanisms underlying the dynamic patterning of the neural tube in vivo it is important to understand how a changing morphogen gradient is interpreted by responding cells to progressively specify progenitor identity. Here we investigated the relationship between the Shh gradient, the intracellular response and the elaboration of pattern in vivo. First, we quantitatively characterized the temporal changes in the expression patterns of the transcription factors that delineate the neural progenitors domains, to determine how patterning and growth are coordinated during development. We also confirmed that the Shh gradient is dynamic, displaying an increasing amplitude in early stages that correlates with the progressive ventralization of the neural tube. In this study we have also addressed the conservation of the patterning process between chick and mouse. The quantitative comparison of chick and mouse data revealed similar dynamics in pattern formation and in Shh gradient formation. Moreover, these data suggested a non-linear relationship between the levels of morphogen and the

transcriptional response of cell in both species. Finally, we used an in vivo reporter of Shh intracellular signalling to examine how the temporal changes in the Shh gradient were translated into temporal profiles of Gli transcriptional activity. This analysis confirmed the temporal adaptation of cells to ongoing morphogen exposure, with a rate of decline in Gli activity that is inversely proportional to the level of Shh. Together, these data are consistent with the idea that the specification of Shh target gene expression depends not on the direct response to the levels of Gli activity, but rather on the history of Gli activity experienced by a cell.

6.1 Quantitative analysis of neural tube patterning in chick embryos

During the formation of the vertebrate neural tube several mechanisms contribute to the elaboration of patterning over time, such as proliferation, differentiation and morphogen-induced cell fate changes. To assess the role of these mechanisms in the dynamic patterning of the neural tube we systematically quantified the expression patterns of a set of transcription factors that identify different neural progenitor domains along the dorsoventral (DV) axis over a range of developmental stages. This characterization revealed that as the neural tube grows, the position of the expression boundaries of the progenitor markers also changes along the DV axis. However, the changes in boundary position were not proportional to the changes in the total size of the neural tube, that is, the sizes of the different domains were not changing at the same rate. This result indicated that different mechanisms regulate the size of the different neural progenitor domains. Moreover, the contributions of proliferation, differentiation and cell fate switches to the changes in the size of the domains appear to change over time.

In the early patterning phase the boundaries of the Nkx2.2 and Olig2 domains, Shh targets, exhibit increasingly more dorsal relative positions. This increased proportion of the p3-pMN region was not the result of a domain-specific increase in proliferation, as the fraction of dividing progenitors was similar in all domains along the DV axis. In addition, differentiation was minimal during these stages (Briscoe, et al., 1999; Ericson et al., 1992; Anna Kicheva, personal communication). These findings suggested that, during this phase, the changes in the sizes of the Nkx2.2 and Olig2 domains result from cell fate changes. Thus, the

dorsal expansion of the Olig2 domain is partially due to the down-regulation of p2 markers in the intermediate part of the neural tube and the up-regulation of Olig2 in these progenitors. Similarly, Olig2 progenitors could adopt a Nkx2.2 state at this phase. Consistent with this, we and others observed that a gradual increase in the level and range of the Shh gradient (Chamberlain et al., 2008; this study). As a result of the increasing Shh concentration, cells located at a particular relative position experience higher levels of Shh with time. This suggests a model whereby the dynamics of the target genes during this early patterning phase results directly from the concurrent expansion of the Shh gradient. This model is in accordance with ex vivo data showing that the induction by Shh of more ventral markers is delayed in relation to more dorsal markers, and increasing levels and/or durations of signal induce increasingly more ventral cell fates (Dessaud et al., 2007; Dessaud et al., 2010). Importantly, cell lineage studies have also demonstrated that cell fate changes contribute to the dynamic patterning of the neural tube, as p3 cells have previously expressed Olig2 and pMN cells have previously expressed Dbx1 (Dessaud et al., 2007; Dessaud et al., 2010).

As in the early patterning phase, during the intermediate phase the sizes of the different progenitor domains also change at different rates. However, unlike in the early phase, in the intermediate phase the ventral-most domains displayed a lower than average increase in size. The decreasing proportions of the p3 and pMN domains appear to result mainly from domain-specific differences in the differentiation rate. Because the fraction of differentiating cells is higher in the pMN domains than in other domains (Jeong and McMahon, 2005; Anna Kicheva, personal communication), and the proliferation rate remains similar between domains, during the second phase the proportion of the Olig2 domain decreases. Similarly, the p3 domain shows a decrease in relative size, which correlates with a period of higher differentiation. By contrast, the Pax7 domain, which appears to have a lower fraction of differentiating cells, becomes proportionally larger. Hence, domain-specific differentiation rates play an important role in the neural patterning dynamics during the intermediate phase.

The higher ventral differentiation rate was also evident when the apico-basal size of the domains was measured. The width of the p3, pMN and p2-p0 domains progressively decreased during phase II, as opposed to the dorsal region, which

remained constant. These differences are consistent with the idea that the fraction of post-mitotic cells that exit the ventricular zone is larger in the ventral than in the dorsal region.

The mechanisms underlying the varying differentiation rates along the DV axis of the neural tube are not entirely understood. The cell cycle exit of neural progenitor cells is promoted by proneural bHLH proteins, including Neurogenin1 (Ngn1), Neurogenin2 (Ngn2) and Mash1 (also known as Ascl1) (reviewed in Briscoe and Novitch, 2008). The nested expression of proneural bHLH proteins along the DV axis of the spinal cord (Sommer et al., 1996; Ma et al., 1997) raises the possibility that the differential expression of proneural genes is associated with the domain-specific differences in differentiation rates. Moreover, the ability to confer different rates of differentiation to distinct progenitor domains suggests a logic for the spatially controlled expression of different bHLH factors. However, the role of proneural bHLH proteins in neural patterning is not restricted to the control of neuronal differentiation. Proneural factors are also involved in the specification of progenitor identity (Parras et al., 2002; Scardigli et al., 2001), and it is not clear how these two activities are coordinated. In addition, the expression of individual proneural bHLH proteins is not always restricted to a specific progenitor domain. Together, these data suggest that, although proneural bHLH proteins are possibly involved in the regulation of differentiation rates, additional factors might also be required. In particular, the interaction between neural progenitor transcription factors and proneural factors could determine the timing and rate of differentiation within a domain. This has been proposed to occur in the pMN domain (Briscoe and Novitch, 2008). The pMN marker Olig2 induces the expression of Ngn2 and the downstream bHLH protein NeuroM, thus promoting cell cycle exit and differentiation (Novitch et al., 2001; Zhou and Anderson, 2002). The elevated levels of proneural factors induced by Olig2 might account for the early onset of differentiation within the pMN domain and promote the differentiation of a larger fraction of cells than in other domains. Hence, the domain-specific differentiation rates may be dependent on the relationship between specific neural progenitor transcription factors and pan-neuronal differentiation factors.

The patterning dynamics during the intermediate period are influenced not only by the increased differentiation, but also by cell fate changes. From 64hpf (HH

stage 16), the time point that we defined as the transition from early to intermediate phases, Nkx2.2 expression started to be down-regulated in the ventral midline, and Arx expression was induced. The exclusion of Nkx2.2 from the floor plate contributed to the decreased proportion of the p3 domain during the intermediate phase. By contrast, the floor plate displayed a gradual increase in size, comparable to the average growth of the neural tube. The expansion of the floor plate likely results from the combination of proliferation and induction of floor plate identity in more dorsal cells. However, the direct contribution of Shh signalling to this cell fate change is likely to be limited, as the requirement for Shh for Arx induction is temporally restricted to much earlier in development (Ribes et al., 2010). It is also important to note that floor plate cells exhibit a characteristic pyramidal shape, which may influence the measurement of the size of the domain. Therefore, to accurately assess the changes in the floor plate a direct measurement of the number of cells, rather than the physical distance, would be required.

Cell fate switches could also contribute to changes in the relative size of domains at more dorsal positions. The increased proportions of the dorsal domains, marked by Pax7, could result not only from lower differentiation rates, but also from ventral-to-dorsal changes in identity in the intermediate region of the neural tube. Further studies using cell lineage tracing will be useful to assess the contribution of these two mechanisms.

In the later developmental stages analysed, the proportions of the domains remained uniform over time, which suggests that the ratio between proliferation and differentiation might be similar in all neural progenitor domains. The exception to the uniform increase in the size of the domains was the increase above average of the Nkx2.2 domain. The late expansion of the Nkx2.2 domain could be explained by the induction of Nkx2.2 expression in Olig2-positive cells. Accordingly, the co-expression of Nkx2.2 and Olig2 at these late stages has been proposed to promote oligodendrocyte differentiation in the chick embryo (Zhou et al., 2001). The presence of cells co-expressing Nkx2.2 and Olig2 in later time points is intriguing considering the expression patterns of these transcriptions factors at earlier stages. Although at very early stages the boundary between the Nkx2.2 and Olig2 domains is not well delineated, this boundary becomes progressively more defined, resulting in adjacent but exclusive domains of expression. The gradual resolution of the boundary is likely

associated with the cross-repressive activity of these factors (Novitch et al., 2001; Balaskas et al., personal communication). The late emergence of Nkx2.2/Olig2 co-expressing cells suggests that the relationship between the two transcription factors changes over time. The dorsal expansion of the Nkx2.2 domain of expression prior to oligodendrocyte generation has been shown to result from the re-patterning of the neural tissue at these later stages, and Shh is required for this process (Agius et al., 2004).

The quantitative characterization of neural tube patterning revealed the dynamic inputs of proliferation, differentiation and cell fate changes. The spatial and temporal regulation of these processes dictates the dynamic elaboration of neural progenitor domains and differential generation of neuronal subtypes. At early time points the temporal changes in the size of the domains result mainly from proliferation and morphogen-induced changes in progenitor identity. At later time points the size of progenitor domains change in response to proliferation and due to differences in the timing and rate of differentiation.

Among the signals involved in the early patterning of the neural tube is the morphogen Shh. The key role of Shh on the specification of ventral progenitor identities is well established (Briscoe et al., 2000; Dessaud et al., 2007; Ericson et al., 1997). The sequential induction of ventral cells fates in vivo has been proposed to result from the gradual increase in the level and range of the Shh gradient (Chamberlain et al., 2008; Kutejova et al., 2009). Accordingly, increasing levels and durations of Shh signalling generate progressively more ventral cell fates ex vivo (Dessaud et al., 2007; Ericson et al., 1997). Our characterization of the temporal changes of Shh distribution confirmed that the gradual accumulation of Shh in the early patterning phase is paralleled by the progressive induction of Nkx2.2 and Olig2 expression at increasingly more dorsal positions. Moreover, the Nkx2.2 domain was associated with higher levels of Shh than the Olig2 domain, consistent with in vitro data (Ericson et al., 1997). However, the quantification of the Shh intensity at the domain boundaries showed that the limits of expression of Nkx2.2 and Olig2 were not associated with specific Shh thresholds over time. Thus, the concentration of Shh needed to induce the expression of Nkx2.2 or Olig2 changes as development proceeds. This result is consistent with the temporal adaptation of responding cells

to ongoing Shh exposure (Dessaud et al., 2007). In this model, the activation of the pathway by Shh induces the expression of negative pathway regulators, such as Ptch1. As a result, higher levels of Shh are required subsequently to elicit equivalent levels of intracellular signalling and activate gene expression. The continuous increase in the amplitude of the Shh gradient in the early time points, accompanied by the progressive induction of the Shh target genes, is consistent with this model.

At later time points the amplitude of the gradient stabilised. Similarly, the decay length of the gradient remained constant over time. Therefore, at these later stages the changes the Shh gradient did not scale with the growth of the neural tube and consequently the range of the gradient decreased. As a result, cells at a distance from the source (for example, cells in the Nkx2.2/Olig2 boundary), which occupied progressively more dorsal positions, were exposed to decreasing levels of Shh. This decrease in the level of signal target cells are exposed to raises the possibility that lower levels of Shh are required for the maintenance than for the induction of target gene expression. Previous work has shown that ongoing Shh signalling is required for the expression of Nkx2.2 and Olig2 even at later stages (Dessaud et al., 2010). However, further work is needed to assess whether different levels of Shh are required for induction and maintenance of target genes.

The temporal changes of the Shh gradient also raise the question of what are the mechanisms involved in the regulation of the amplitude and spread of the Shh protein. The increase in the size of the floor plate and the notochord, the sites of Shh production, is consistent with the gradual accumulation of Shh at early stages. However, although the number of Shh producing cells continues to increase at later time points, the Shh concentration at the source boundary remained stable. The limited accumulation of Shh at these stages could result from the increased expression of factors that bind to Shh and promote its internalization and degradation, such as Ptch1 and Hhip1 (Briscoe et al., 2001; Incardona et al., 2002; Jeong and McMahon, 2005). The sequestration of Shh by these factors also restricts the spread of the morphogen (Chamberlain et al., 2008; Chuang et al., 2003; Chuang and McMahon, 1999; Goodrich et al., 1997; Jeong and McMahon, 2005), which could explain the decrease in the range of the gradient in neural tissue exposed to ongoing Shh levels. A better understanding of the processes that shape the distribution of the morphogen will provide insight into the mechanisms underlying the dynamics of the Shh gradient. For this it will be important to quantitatively characterize the dynamics

of Shh production, diffusion and degradation and assess their contribution to the temporal changes of the gradient. In addition, it is fundamental to complement these data with modeling studies, to help predict the mechanisms of gradient formation that best fit the measured dynamics. This type of modeling has started to be applied to different signals and systems, including Shh in the neural tube and Hh in the Drosophila wing disc (Nahmad and Stathopolous, 2009; Saha and Schaffer, 2006). The inclusion of quantitative data to these models will undoubtedly improve their accuracy and predictive ability.

6.2 Comparative analysis of neural tube patterning in mouse and chick

The process of neural tube patterning has been extensively studied in multiple organisms. In particular, chick and mouse models have been invaluable for the understanding of the mechanisms involved in the specification neuronal cell fates. In these species the patterning events, and the role of Shh, appear to be highly conserved, and knowledge obtained in one species is usually extrapolated to the other. However, a comparative characterization of the molecular patterning process between chick and mouse had not been carried out prior to this study. Moreover, the observed similarity in patterning between the two species raised additional questions: whether the proportions of the progenitor domains are maintained in the two differently sized organisms, and whether the elaboration of the progenitor domains follows similar dynamics in chick and mouse.

The quantitative characterization of the expression patterns of the progenitor markers Nkx2.2, Olig2 and Pax7 over time revealed a striking similarity in the dynamics of neural tube patterning between chick and mouse. The comparative analysis of neural tube patterning showed that in both organisms an early phase, in which there was a dorsal expansion in the induction of ventral cell fates, was followed by a period of increased differentiation in ventral domains. The mouse data set was limited to these two phases and, therefore, we were unable to compare the following period of development (characterised by stable proportions of the progenitor domains). These data confirmed the conservation of the patterning process between chick and mouse. However, this study also revealed important differences between the two species, in particular differences in the size of the neural tube and differences in the timing of certain patterning events.

In order to accurately extract the similarities and differences in the patterning process between chick and mouse we had to find a way of comparing equivalent developmental stages between the two data sets. The time registration of the chick and mouse data sets was based on the number of somites of the embryos (either converted to developmental time or not), with additional adjustments to achieve a better juxtaposition of the data sets. These adjustments included the use of the time of Nkx2.2 induction as the starting point and the exclusion of the floor plate region. Nevertheless, we cannot exclude the possibility that alternative modes of registration may allow a more accurate comparison of the data sets.

Using this method of registration we observed that the neural tube was bigger in mouse than in chick at later developmental stages. The increased size of the mouse neural tube at later time points could result from a higher division rate in mouse or differences in cell size, differentiation rate or anisotropy. The quantification of these parameters in mouse will allow us to discriminate between these possibilities. This analysis also revealed that, although the size of the neural tube differed between the two species, the proportions of the progenitor domains were similar, i.e., the patterns scaled between species. One possible explanation for this is that changes in the signals that pattern the spinal cord compensate for the differences in size. In the case of Shh our quantification revealed that the Shh amplitude reached similar values in chick and mouse, arguing against the idea that the patterning differences result from different absolute levels of Shh. However, we cannot exclude the possibility that the levels of fluorescence intensity detected in the two species are influenced by differences in antibody recognition. Alternatively, changes in the response of cells to the patterning signals could compensate for the differences in size.

Another possibility is that progenitor domains are specified by morphogens early in development, during a period in which the dimensions of the neural tube are similar between mouse and chick. At later time points, when the size of the neural tube diverges between the two species, the proportions of the domains would be maintained by the uniform growth of the tissue and differentiation rates that scale with tissue size. However, the previously shown requirement of Shh activity for the maintenance of the ventral domains even at later stages argues against this model (Dessaud et al., 2010).

The scaling of pattern between species could also be achieved if the same signals are used to coordinate pattern and proliferation (reviewed in Schwank and Basler, 2010; Ulloa and Briscoe, 2007). For example, Shh has been proposed to act both as morphogen and a mitogen (Cayuso et al., 2006; Jeong and McMahon, 2005), although it is not clear how Shh is differentially interpreted to regulate both uniform growth and graded cell fate specification in the vertebrate neural tube. In this model Shh would be responsible for both the increased growth rate of the mouse neural tube and the complementing increase in the size of the ventral progenitor domains. Interestingly, the developmental period in which the mouse neural tube starts to grow at a faster rate than the chick neural tube coincides with the period in which the amplitude of the Shh gradient sharply increases. It is tempting to hypothesize that the rate of increase of Shh (rather than absolute levels) enhances proliferation, and at the same time the gradient ensures the scaling of pattern. Future work addressing the role of Shh in the regulation of proliferation at later time points will help understand how patterning is coordinated with growth and whether there are differences between species. In addition, it will be important to assess the relationship between the Shh gradient and dorsal morphogens, such as Wnts and BMPs, to determine whether these opposing gradients cooperate to regulate uniform proliferation along the neural tube.

To understand the mechanisms underlying the scaling between species it is also important to take into account neuronal differentiation. In later stages of development the differentiation of progenitor cells plays an important role in shaping the size of progenitor domains over time. Although the rate of differentiation has not been measured in mouse, the similar dynamics of patterning between chick and mouse at later stages suggest that domain-specific differences in the timing and rate of differentiation could also occur in mouse. In particular, we observed a marked decrease in the proportions of the pMN domain during the second patterning phase, which is consistent with an increased generation of post-mitotic motor neurons when compared to other neuronal identities. The scaling of the patterns at these later stages is consistent with a model in which the balance between proliferation and differentiation is similar between chick and mouse, even though their specific rates may differ. This possibility could be addressed by

quantifying and comparing the proliferation and differentiation parameters in chick and mouse

Nevertheless, despite the overall similarity in the patterning dynamics, some differences between species were detected in particular progenitor domains. Moreover, the degree of this divergence depended on the method used to register the two data sets: the conversion of the number of somites to hours based on the periodicity of somite formation in chick and mouse resulted in a better juxtaposition of the two data sets than the use of somite number alone. In the case of the Olig2 domain, using the first method resulted in the scaling of the domain in the final stages analyzed, but the timing of the peak motor neuron generation diverged. Conversely, using the number of somites, the timing of motor neuron generation coincided between chick and mouse, but the final size of the Olig2 domain was proportionally smaller in mouse. A slightly better scaling was obtained using developmental time, however, the noise of the data does not allow to unambiguously conclude which is the best method to compare the two species. However, to assess whether the mouse and chick data sets are accurately registered it will be essential to extend the mouse data to later developmental stages. In addition, the quantification of the number of post-mitotic cells that are generated from each progenitor domain will allow us to determine whether the number of neurons also scales between species. Alternatively, it might be more functionally important to maintain a specific ratio between the number of sensory (dorsal) neurons and motor (ventral) neurons, even if the number of neurons varies in different organisms.

The comparison of the dynamics of patterning in chick and mouse also revealed a difference in the timing of induction of definite floor plate identity, marked by the expression of Arx (this study and Ribes et al., 2010). The different timing of Arx induction correlated well with the different dynamics of the Shh gradient in chick and mouse. In particular, the time of Arx induction coincided with the time of the peak amplitude of the gradient. One possibility is that the transition to a definite floor plate identity in ventral midline cells results in an increased production of Shh. Alternatively, the induction of Arx expression could occur only when the levels of Shh surpass a high threshold. However, recent work showing that the competence of cells to respond to Shh and induce floor plate identity is restricted to very early developmental stages argues against this hypothesis (Ribes et al., 2010).

In addition, the acquisition of floor plate identity requires not only exposure to high levels of Shh at early stages, but also the subsequent decrease in intracellular Shh signalling, otherwise cells acquire a p3 identity (Ribes et al., 2010). The decrease in Shh signalling in the floor plate has been proposed to be associated with the down-regulation of the positive pathway regulators Gas1 and Cdo (Allen et al., 2007; Tenzen et al., 2006; Ribes et al., 2010). The expression of Gas1 and Cdo is inhibited by Shh signalling (Allen et al., 2007; Tenzen et al., 2006), suggesting that the gradual increase in Shh levels could result in the progressive down-regulation of Gas1 and Cdo expression and consequently in the reduction of intracellular pathway activation. The shut-down of intracellular Shh signalling would ultimately allow the specification of floor plate identity. This model raises the question of whether differences in the timing of the down-regulation of Shh signalling in the floor plate could account for the differences in the timing of Arx induction. It is possible that the more rapid accumulation of Shh in chick results in the enhanced repression of Gas1 and Cdo expression and earlier down-regulation of Shh signalling in the ventral midline and Arx induction. However, the mechanisms underlying the dynamics of Shh accumulation in chick and mouse are not well understood. The earlier peak of Shh amplitude in chick than in mouse could result from an increased Shh production rate in chick. The noticeable difference in the size of the notochord between chick and mouse could also have a significant influence in the amount of Shh produced in the two species. Alternatively, the rates of diffusion and/or degradation could be different between mouse and chick, resulting in differences in the level of Shh at the source boundary and in the spread of the gradient at a distance from the source.

Although the characterization of the Shh distribution revealed temporal differences in the dynamics of the Shh gradient between chick and mouse, in each case there was a similar correlation between the dynamics of the morphogen and the dynamics of patterning in both organisms. The gradual accumulation of Shh in early stages was mirrored by the induction of the ventral cell markers Nkx2.2 and Olig2 at progressively more dorsal positions. At later stages the Shh amplitude stopped increasing. Moreover, this comparison also showed that in both species the concentration of Shh at the boundaries of target genes changes over time. In early stages the Shh levels at the position of the boundaries gradually increased, whereas in later stages the Shh concentration decreased at the boundaries. These results are

consistent with an unconventional model of morphogen interpretation, in which the transcriptional response of a cell to the gradient does not reflect a direct transduction of the levels of ligand. In this model, cells adapt their response to an ongoing Shh gradient, and consequently require increasing amounts of signal in order to sustain the level of intracellular signalling and transcriptional activity (Dessaud et al., 2007). As a result, the level of intracellular signalling gradually declines as development proceeds, and the rate of this decline is inversely proportional to the Shh concentration cells are exposed to. The non-linear Shh signal transduction has been demonstrated in chick, using in vitro assays (Dessaud et al., 2007; Dessaud et al., 2010) and in mouse, in vivo (this study, see below). These data suggest that the mechanism of Shh interpretation in the neural tube is similar between chick and mouse. Nevertheless, the comparison of in vitro chick studies and in vivo mouse studies revealed noticeable differences in the transcriptional response of cells to changing levels of Shh, namely in the rate of decline of Gli activity (Dessaud et al., 2007; this study). These differences could reflect real species differences, or could result from experimental differences between in vitro and in vivo assays. To better understand whether the mechanisms involved in morphogen interpretation are conserved between chick and mouse it will be useful to study this process using the same assay for both species.

6.3 Dynamics of Shh signalling activity

In the conventional model of morphogen interpretation a signal gradient specifies the positional identity of cells in a tissue by activating the expression of target genes in a concentration dependent manner (Wolpert, 1969). In this model, the concentration-dependent response of target cells implies that the levels of signal received by a cell are linearly transduced and generate equivalent levels of transcriptional activity. However, this model has been subsequently challenged, as alternative models of morphogen interpretation are used by various morphogens in different tissues and organisms (reviewed in Ibañez and Belmonte, 2008; Kutejova et al., 2009). This is the case for the Shh gradient in the specification of ventral cell fates in the neural tube. In vitro studies have shown Shh interpretation is not linear and

the levels of morphogen are integrated over time to activate target gene expression (Dessaud et al., 2007; Dessaud et al., 2010).

In this study we used a mouse reporter of Shh signalling activity (*Tg(GBS-GFP)*) to investigate the mechanism of Shh interpretation in vivo. The expression of the *Tg (GBS-GFP)* transgene was detected in tissues that respond to Shh signalling, including the neural tube. In addition *Tg(GBS-GFP)* expression was sensitive to changes in the level of Shh, both with gain-of-function (purmorphamine) and loss-of-function (cyclopamine) assays. Moreover, *Tg(GBS-GFP)* activity correlated well with the expression of the receptor Ptch1, which is also positively regulated by Shh (Goodrich et al., 1996; Goodrich et al., 1997; Jeong and McMahon, 2005; Marigo and Tabin, 1996). These data demonstrate that *Tg(GBS-GFP)* transgenic mice can be used as reporters of Shh intracellular signalling activity.

The characterization of the expression of the *Tg(GBS-GFP)* transgene revealed different dynamics between the Shh gradient and the downstream Gli activity. The quantification of Gli activity in vivo showed a gradual increase in levels and range in early stages. However, the amplitude of Gli activity peaked early and subsequently declined and was undetectable in the last stages analyzed. By contrast, the amplitude of Shh continued to increase until later stages, when the gradient stabilized and finally declined. These data are consistent with the temporal adaptation model and correlate well with ex vivo data previously published (Dessaud et al., 2007; Dessaud et al., 2010). In these assays, cells exposed to Shh for short periods of time quickly up-regulate Gli activity (Dessaud et al., 2007; Dessaud et al., 2010). In these conditions, even moderate concentrations of Shh are able to fully activate the pathway and peak levels of Gli activity are quickly reached (~6h; Dessaud et al., 2010). Similarly, in vivo the peak amplitude of Gli activity is reached at very early stages, when the levels of Shh are still low. Importantly, both ex vivo and in vivo, the levels of signalling are proportional to the levels of ligand during the initial response of cells. As development proceeds, cells become desensitized to the morphogen, and the level of Gli activity declines and ultimately reaches basal levels. The time it takes for the level of Gli activity in a cell to return to basal levels - the duration of Gli activity - depends on the amount of Shh received by the cell. This duration-based mechanism of Shh interpretation was observed ex vivo and in vivo. Explants exposed to a higher concentration of Shh will sustain Gli activity above a

particular threshold for a longer period of time than lower levels (Dessaud et al., 2010). Likewise, in vivo, cells located at more ventral positions in the neural tube, which are exposed to higher levels of Shh, experience longer durations of Gli activity than cells positioned more dorsally. Hence, different concentrations of Shh generate different temporal profiles of Gli activity and accordingly specify different cell fates.

Even though ex vivo (Dessaud et al., 2010) and in vivo data (this study) showed similar signalling dynamics in response to a morphogen gradient, there are nevertheless differences between assays. The time it takes for Gli activity to reach its maximal level is considerably shorter ex vivo than in vivo. In addition, the rate of the decline of Gli activity after reaching peak levels was higher in vivo than in explants. These differences could be explained by differences in the response of chick and mouse cells, or by differences introduced by the type of assay used (see above). In particular, differences in the dynamics of the signal received by the cells could influence the temporal profile of Gli activity. In ex vivo assays cells are exposed to constant concentration of Shh, whereas cells in the neural tube experience changing levels of Shh. It is possible that the gradual accumulation of Shh results in the delayed saturation of Gli activity. The differential response of cells in explants or in the neural tube could also be explained by differences in the expression of the positive regulators of the pathway Gas1, Cdo and Boc. The gradual increase in Shh levels could progressively down-regulate Gas1, Cdo and Boc expression and thereby limit the full activation of the pathway. Further studies will be required to address these hypotheses.

The desensitization of cells to ongoing Shh signalling has been proposed to result from the induction of negative feedback mechanisms that restrict the activation of the pathway (Dessaud et al., 2007). The factors involved in the negative feedback likely include the negative regulator Ptch1. To address the role of Ptch1 up-regulation in the temporal adaptation to Shh in vivo we quantified the expression of Ptch1 protein in the neural tube. The distribution of Ptch1 protein showed similar dynamics to the *Tg(GBS-GFP)* transgene: initial increase in levels and range followed by a gradual decline. Although the similar dynamics between Ptch1 and *Tg(GBS-GFP)* indicates that both markers are reporting Gli activity, the low levels of Ptch1 at later stages implies that the gradual decrease in Gli activity over time cannot be explained solely by Ptch1 up-regulation. These data suggest that other factors contribute to the

desensitization to Shh. Mouse embryo culture assays using purmorphamine to activate the pathway also argue for the role of other negative feedback mediators. Purmorphamine activates the pathway downstream of Ptch1, and therefore the response of cells is insensitive to Ptch1-mediated negative feedback. However, cells exposed to purmorphamine for prolonged periods show a decline in Gli activity, which must occur independently of Ptch1. Other factors that might be involved in the diminished response to Shh over time include the co-receptor of Ptch1 Hhip1 and the transcriptional effector Gli2. In particular, the down-regulation of Gli2 expression in the floor plate and p3 domain at later time points could limit the response of cells to the level of Shh available (Bai et al., 2002; Ribes et al., 2010).

To investigate the contribution of duration and levels of intracellular Shh signalling to the specification of progenitor identity in the neural tube we examined how the expression of Shh target genes correlated with the levels of Gli activity. Consistent with a duration model, the level of Gli activity in a cell was not predictive of its identity. The measurement of the Gli activity at the borders of expression of the Nkx2.2 and Olig2 domains showed that the position of the boundaries was not defined by a fixed threshold of signalling activity. These data indicate that the level of Gli activity is not sufficient to assign positional identity and supported the hypothesis that the duration of signalling is also important.

Although it was not possible to directly quantify the duration of signalling activity experienced by a cell in vivo, we obtained an approximate value by estimating the cumulative level and duration of signalling. For this, the temporal profiles of Gli activity at different relative distances from the ventral midline were integrated to obtain the cumulative GFP intensity. This analysis revealed that the cumulative amount of Gli activity correlates well with the relative position of a cell in the neural tube. This result supports a model in which the level of morphogen received by a cell is integrated over time to generate a specific profile of signalling activity. The positional identity of a cell is then defined by the level and duration of Gli activity it experiences over time.

Although the history of Gli activity appears to be a good indicator of positional identity it is not clear how level and duration of intracellular signalling are integrated to generate differential transcriptional responses. The temporal integration of the signal is consistent with the “sequential cell context” model

proposed by Pages and Kerridge (Pages and Kerridge, 2000). According to this model the induction of a gene by a morphogen depends not only on the level of signalling activity downstream of the morphogen but also on the transcriptional state of the cell. In turn, the transcriptional state of a cell depends on the level of signalling activity previously experienced by the cell. In the context of the neural tube, the transcriptional state of a cell could correspond to the combination of GRN transcription factors that are expressed in the cell. The cross-repressive interactions between pairs of transcription factors downstream of Shh-Gli signalling could explain the delayed response of some target genes to the signal. In early stages the presence of a particular Class I gene (for example, Pax6) would block the induction of the reciprocal Class II gene (for example, Nkx2.2) by Shh signalling. However, this initial exposure to Shh signalling would result in the down-regulation of the Class I gene. The removal of the Class I factor would allow the Class II gene to respond to later periods of Gli activity. Hence in this model the architecture of the Gene Regulatory Network plays a role in the response of cells to Shh signalling and, in conjunction with the changing levels of Gli activity, contributes to the dynamic elaboration of neural tube patterning.

6.4 Conclusions and future work

This study has contributed to the understanding of the processes involved in the dynamic patterning of the vertebrate neural tube. These data showed that the early patterning events, which result in the progressive ventralization of the neural tube, are regulated mainly by proliferation and Shh-induced cell fate changes. At later stages proliferation and differential differentiation play a determinant role in the shape of the progenitor domains. This characterization provided initial evidence of the coordination between proliferation, differentiation and patterning in the developing neural tube. In addition, this study highlighted the importance of quantitative analysis to describe and extract useful information from experimentally and biologically variable data.

This characterization also provides an important basis for future work aiming to understand the mechanisms that regulate proliferation, differentiation and morphogen response and how these processes interact during pattern formation. In

particular, it is fundamental to address the role of Shh in the regulation of proliferation and whether a dual role for Shh signalling could explain the coordination between patterning and growth during neural tube development. Furthermore, it will be important to investigate the interaction between signalling pathways, namely between the opposing gradients Shh and BMPs/Wnts, and whether communication between gradients contributes to the uniform growth of the neural tube.

Further work addressing the relationship between transcription factors that define progenitor identity and pan-neuronal differentiation factors will provide insight into the mechanisms that govern the varying rates and timing of differentiation in the different progenitor domains. The regulation of timing of differentiation is likely to be particularly relevant in progenitor domains that generate different neuronal subtypes at different periods of development, such as the Olig2 domain. In addition, it will be of interest to examine the role of other signalling in the regulation of neuronal specification and differentiation, such as RA and Notch signalling.

One important limitation of this analysis is that it is restricted to a single anteroposterior (AP) level. Although our data provide a detailed description of the dorsoventral patterning process over time, this process is also dynamic along the AP axis. These AP differences in patterning are not only a result of the progressive elaboration of pattern from rostral to caudal regions, but also reflect specific AP differences in the size of progenitor domains that may be functionally relevant. For example, AP differences in the size of the Olig2 domain could indicate that a higher ratio of motor neurons to sensory neurons are formed at limb level than at trunk level. Therefore, it will be interesting to extend this analysis to other AP levels of the neural tube.

The quantitative characterization of neural tube patterning also demonstrated the conservation of the patterning process between chick and mouse. The comparison of the mouse and chick data sets showed remarkable similarity in the dynamics of pattern elaboration. Moreover, this analysis revealed that the proportions of the progenitor domains are maintained between species even when the total size of the neural tube diverges. These findings suggest that the two

organisms use similar mechanisms to regulate patterning and these mechanisms are coordinated with growth to ensure scalability.

To better understand how pattern scales between different species additional data are needed, quantifying and comparing the proliferation and differentiation rates between chick and mouse. These data will allow us to determine whether patterns scale by maintaining a conserved ratio between proliferation and differentiation, even if the specific rates of differentiation vary between species. The scaling of the morphogen gradients that pattern the neural tube also needs to be addressed. In the case of Shh, it appears that the Shh gradient does not scale between species, but it is possible that the response of cells to the morphogen is adjusted depending on the species. Differences in morphogen interpretation between species could be assessed in ex vivo assays using chick and mouse tissues in parallel and examining their transcriptional response to defined levels and durations of Shh.

The comparative characterization of the dynamics of the Shh gradient in chick and mouse also showed differences between species, with the chick gradient reaching peak amplitude at an earlier time point than the mouse gradient. The time of the peak Shh amplitude coincides with the timing of Arx induction in both species, raising the possibility that the two events are associated. Further work is needed to determine whether the transition to definite floor plate identity, marked by Arx expression, results in the increased production of Shh.

The differences in Shh dynamics also highlight the importance of understanding the processes that determine gradient formation. The characterization of the dynamics of Shh production, diffusion and degradation will provide insight into the dynamics of Shh gradient formation. This analysis must include not only the experimental measurements of the production, diffusion and degradation parameters, but also mathematical models to predict and subsequently test the mechanisms of Shh gradient formation that operate in the neural tube. Such studies will also help understand what differentiates the dynamics of Shh between chick and mouse.

Finally, this study addressed the mechanisms of Shh interpretation in vivo. The quantification of the dynamics of the Shh gradient, the intracellular signalling activity and the transcriptional response of target genes in mouse confirmed the non-linear

transduction of the Shh pathway in the neural tube. These data show that after a brief period in which the level of Shh is directly converted into intracellular signalling activity, the continuous exposure to Shh desensitizes cells to the available levels of morphogen and Gli activity gradually declines. This analysis confirmed that a temporal adaptation mechanism of Shh interpretation is in action in vivo. The desensitization of cells to Shh could be, at least in early stages, explained by the up-regulation of the receptor Ptch1. However, other negative feedback mechanisms must also be involved in the gradual decline of Gli activity. Further work is needed to address the role of other Shh-binding proteins, such as Hhip1, Gas1, Cdo and Boc, in the dynamic response of cell of the morphogen. In addition, Gli2, which shows a dynamic expression on the neural tube, could also play a role in the negative feedback mechanisms that regulate Gli activity.

The comparative analysis of Gli activity and the expression of the Shh target genes Nkx2.2 and Olig2 showed that the levels of intracellular signalling are not sufficient to define progenitor identity. Instead, the cumulative amount of Gli activity appears to provide a better proxy for positional information. These data are in agreement with a model in which the duration of signalling activity is also important for cell fate specification (Dessaud et al., 2007; Dessaud et al. 2010). The mechanisms underlying the integration of levels and durations of signalling are not well understood, but might involve the combined action of transcription factors in the Gene Regulatory Network (GRN) and Shh signalling. The cross-repressive interactions between GRN factors, together changing levels of Shh signalling, may explain the sequential induction of Shh target genes in the neural tube (reviewed in Dessaud et al., 2008). Studies in the lab are currently addressing the role of the GRN in the temporal interpretation of Shh signalling. In particular, whether the removal of specific members of the GRN affects the response of cells to Shh signalling and the timing of the induction of the reciprocal factors. These studies will help to further dissect the complexities of neural tube patterning dynamics and elucidate the mechanisms of morphogen

SECTION II

CHAPTER 7 - KINESIN MOTOR PROTEIN KIF7 IS A COSTAL2 HOMOLOG IN VERTEBRATE HEDGEHOG SIGNALLING

The Hedgehog signalling cascade is largely conserved from Drosophila to vertebrates. However, the structure and function of some of the core components have diverged during evolution (reviewed in Wilson and Chuang, 2010). At the time this study was initiated Costal2 function was thought to have been lost in higher vertebrates. In Drosophila, Costal2 acts as a scaffolding protein, binding multiple components of the cytoplasmic signalling complex, including Smo, Ci, and the kinases Fu, PKA, CKI and GSK3β. The interaction of Cos2 with these different components is dynamic, depending on the Hh state of the cell. Moreover, Cos2 function is required for both the positive and negative response to Hh levels. Even though Cos2 has a key role in Hh signalling in Drosophila, the Cos2 homologs Kif7 and Kif27 failed to show any Hh-related functions in in vitro studies using mammalian cell lines (Varjosalo et al., 2006). The absence of Cos2-like function in higher vertebrates was thought to be associated with the coincident divergence of mouse Smo structure. Compared to Drosophila Smo, vertebrate Smo lacks the putative Cos2 binding site, as well as phosphorylation sites. However, the analysis of Varjosalo et al. was based only on cell line assays, a system that may not be sensitive enough to detect small changes in the activity of the pathway. In addition, the dual function of Cos2 in the regulation of Hh signalling might complicate the interpretation of the levels of signalling activity in cells.

The uncertainty surrounding the role of the Cos2 homologs in the vertebrate Hh pathway led us to readdress this question using the chick neural tube. The in ovo electroporation of the chick neural tube is commonly used in gain and loss of function studies, for its quick and straightforward results. Importantly, this model organism has significantly contributed to the understanding of the function of Shh in the induction of ventral neuronal cell types in the vertebrate neural tube (reviewed in Jessell, 2000). Using chick electroporation we can ectopically express specific genes and analyze their effect in Hh signalling by assaying for alterations in the expression of Shh target genes. This assay allowed us to start characterizing vertebrate Cos2-like function in a functionally relevant system.

7.1 Kif7 is a negative regulator of the Hedgehog pathway

To reexamine whether a Cos2-like function was preserved in higher vertebrates we set out to determine whether the putative vertebrate Cos2 ortholog Kif7 participates in the transduction of the Shh pathway. In Drosophila the overexpression of Cos2 results in the cell-autonomous repression of Hh target gene transcription in the wing imaginal disk (Ho et al., 2005). If functionally conserved, the vertebrate orthologs would be expected to similarly disrupt the expression of Shh target genes. To test this, we first assessed whether the overexpression of Kif7 affected the Shh-dependent ventral patterning of the chick neural tube. The full-length cDNA of mouse Kif7 (provided by C.-c. Hui), inserted into the expression vector pCAGGS, was introduced into the neural tube of stage HH10-12 chick embryos using in ovo electroporation. The embryos were collected after a 48h period of incubation and the effects of the transfection on the expression patterns of several progenitor domain markers assayed. As the pCAGGS vector allows the bicistronic expression of both the inserted cDNA and nuclear-targeted GFP, the expression of GFP was used to identify the transfected cells. The electroporation of an empty pCAGGS vector, which expresses only GFP, did not affect the patterning of the neural tube (Figure 7.1). By contrast, the ectopic expression of Kif7 resulted in the cell-autonomous inhibition of a high-Shh response gene, the p3 marker Nkx2.2 (Figure 7.2A-A″). However, the negative effect of Kif7 overexpression did not extend to other Shh target genes. The floor plate markers Foxa2 and Arx remained unaffected when exposed to high levels of Kif7 (Figure 7.2C-D″). Moreover, the pMN domain marker Olig2 was not repressed by Kif7 expression and appeared extended in some of the transfected embryos, compared to the control side (Figure 7.2B-B″). Although it is possible that Kif7 also has a positive role and directly promotes Olig2 expression, this expansion is more likely to be a consequence of the loss of $Nkx2.2^{+}$ cells and the repressive effect of Nkx2.2 on Olig2. Consistent with this, in some Kif7-electroporated embryos Pax6 also expanded ventrally (Figure 7.3A-A″). The expression pattern of the more dorsal gene Pax7 remained unaltered following transfection with Kif7 (Figure 7.3A-A″).

Together these data suggest that Kif7 inhibits the response of the cells to the highest levels of Shh. The observed inhibitory phenotype suggests some conservation of Cos2-like function in the vertebrate Hh pathway.

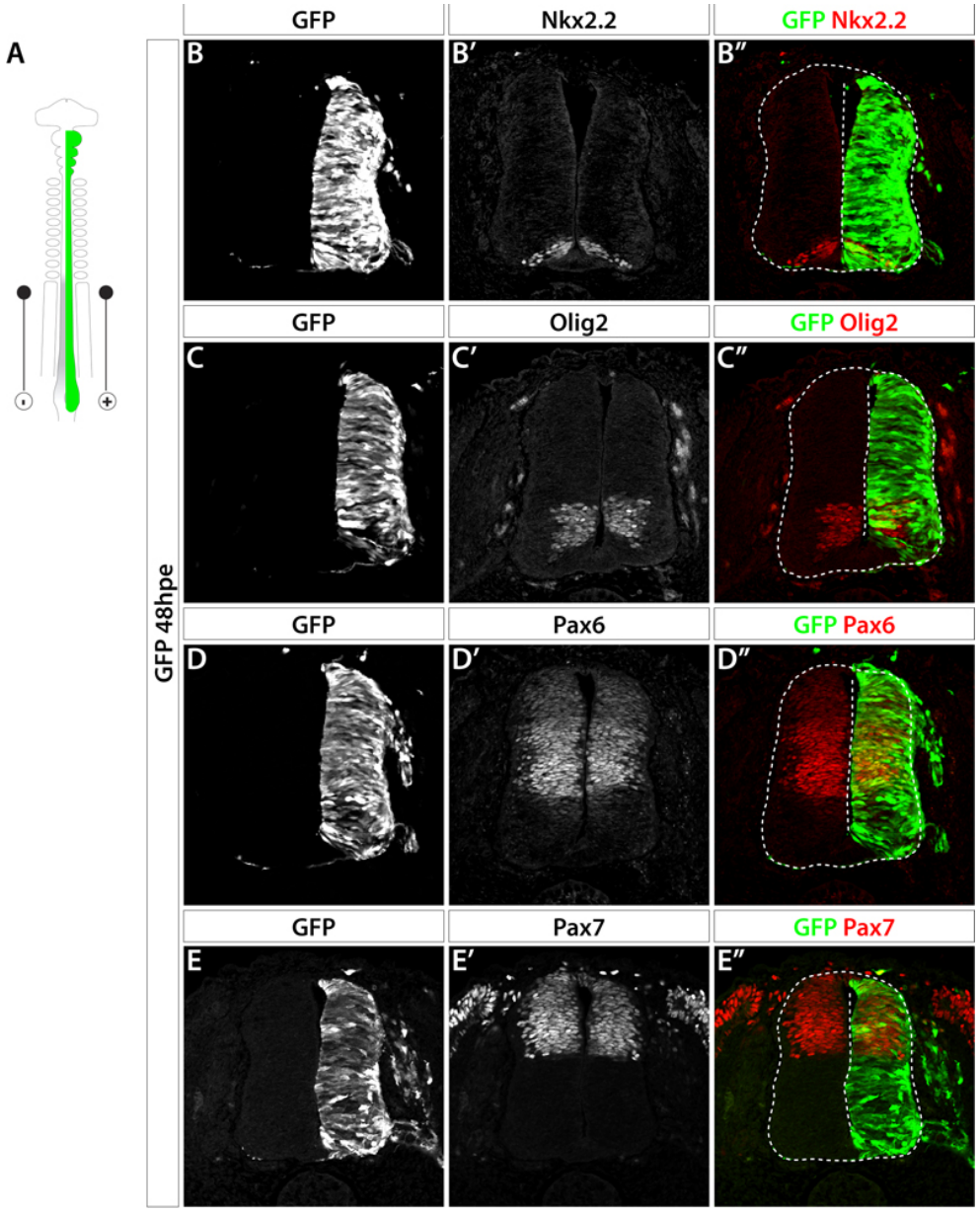

Figure 7.1 In ovo electroporation of a control vector does not alter the patterning of the neural tube.

HH10 to HH12 chick embryo neural tube transfected with pCAGGS-IRES-GFP (green) (**A**) and assayed for the expression of neural progenitor markers Nkx2.2, Olig2, Pax6 and Pax7, as indicated (red), at 48hpe, at brachial level (**B-E″**). The electroporated side of the neural tube shows a pattern of expression of the ventral markers Nkx2.2 (**B-B″**) and Olig2 (**C-C″**) identical to the non-electroporated. Similarly, the expression of the dorsal markers Pax6 (**D-D″**) and Pax7 (**E-E″**) remained unaffected after transfection with pCAGGS-IRES-GFP.

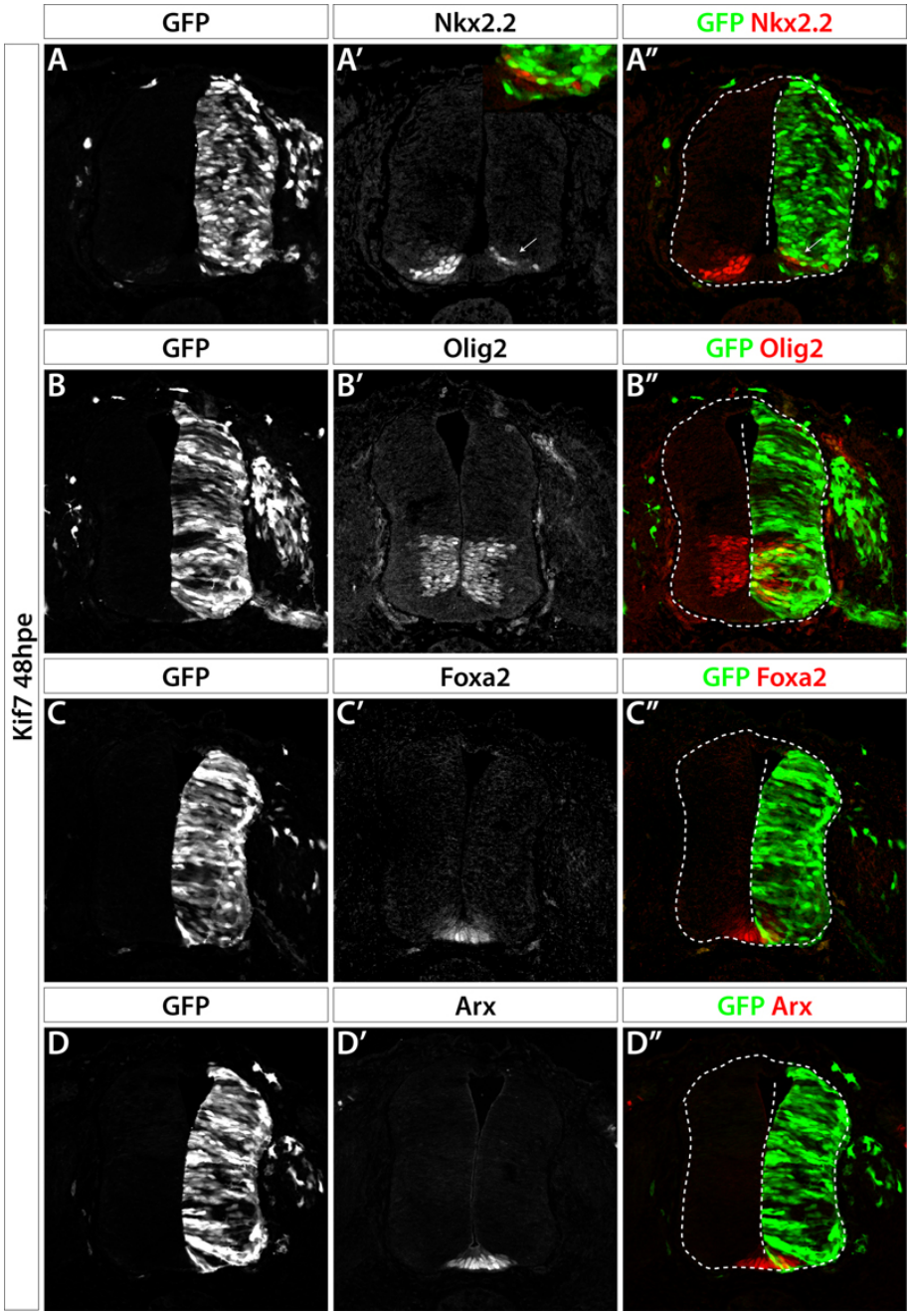

Figure 7.2 Ectopic expression of Kif7 represses Nkx2.2 expression.

Expression of progenitor markers Nkx2.2, Olig2, Foxa2 and Arx (red) at the brachial level of the chick neural tube 48h after in ovo transfection with pCAGGS-Kif7-IRES-GFP (transfected cells identified by GFP expression in green) (**A-D″**). The ectopic expression of Kif7 cell-autonomously repressed the expression of the p3 marker Nkx2.2 (arrow; **A-A″**). By contrast, Kif7 overexpression did not inhibit the expression of the pMN marker Olig2 (**B-B″**) or the floor plate markers Foxa2 (**C-C″**) and Arx (**D-D″**).

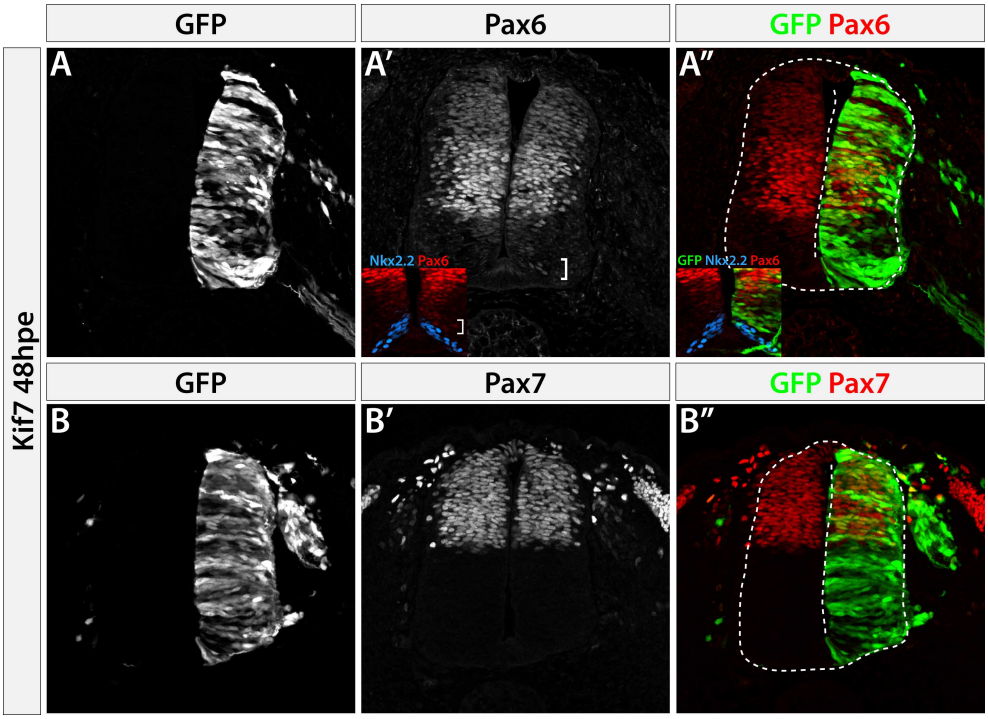

Figure 7.3 Expression of dorsal markers Pax6 and Pax7 is unaffected by ectopic expression of Kif7.

Expression of progenitor markers Pax6 and Pax7 (red) at the brachial level of the chick neural tube 48h after transfection with pCAGGS-Kif7-IRES-GFP (GFP in green) (**A-B''**). The ectopic expression of Kif7 does not significantly alter the pattern of expression of the neural transcription factors Pax6 (**A-A''**) or Pax7 (**B-B''**). A few cells ectopically expressing Pax6 are detected in ventral regions of transfected neural tubes (white bracket in **A''** and inset). These may result from the down-regulation of Nkx2.2 expression (inset in **A', A''**).

We next assessed whether Kif7 acts at a similar level of the pathway as Cos2. In Drosophila Cos2 establishes a bridge between Smo and Ci and, in the response to the Hh signal, mediates the transition between repression and activation of target genes (Lum et al., 2003b). To determine if Kif7 also acts downstream of Smo we tested the ability of Kif7 to interfere with Smo activity. For this we made use of SmoM2, a constitutively active form of Smo that stimulates the Shh pathway independently of ligand (Hynes et al., 2000). The introduction of SmoM2 into the spinal cord resulted in the ectopic induction of the p3 domain marker Nkx2.2 (Figure 7.4 A-A''). In addition, SmoM2 promoted the dorsal expansion of Olig2^{+} pMN domain

(Figure 7.4 C-C″). The SmoM2-induced ventralization of the neural tube was accompanied by the repression of the dorsal markers Pax6 and Pax7, confirming the elevated levels of Shh signalling (Figure 7.5 A-A″, C-C″).

The simultaneous transfection of Kif7 and SmoM2 was able to partially inhibit the SmoM2 phenotype. An expansion in the p3 domain was apparent in these embryos but was more ventrally restricted than in embryos transfected with SmoM2 alone. Importantly, Kif7 blocked the dorsal induction of the ectopic Nkx2.2 cells (Figure 7.4 B-B″). This result reinforced the repressive activity of Kif7 and places Kif7 downstream of Smo. However, the dorsal expansion of the Olig2 domain remained unchanged after co-expression of SmoM2 and Kif7 (Figure 7.4 D-D″), as did the repression of Pax6 and Pax7 (Figure 7.5 B-B″, D-D″). This suggests that Kif7 did not completely block ectopic Shh signalling and, therefore, was only able to restrict the induction of the high-response target genes.

The epistatic effect of Kif7 on Smo was also confirmed by the measurement of Gli transcriptional activity. To determine the levels of Gli activity we took advantage of a well established assay based on a Gli binding site (GBS)-luciferase reporter (Sasaki et al., 1997) (Figure 7.6). The Gli reporter construct was electroporated into the neural tube of chick embryos together with a normalization plasmid and the constructs being tested. The levels of Gli activity were assayed after appropriate periods of incubation and the results were normalized to the control levels. In accordance with the patterning results, the levels of Gli activity also reflected the negative role of Kif7. The electroporation of SmoM2 resulted in a 15-fold increase in Gli activity compared to control levels, correlating well with the observed induction of Shh positive targets in the neural tube. The transfection of Kif7 together with SmoM2 lowered the levels of Gli activity when compared to SmoM2 alone. This is consistent with the decrease in the Nkx2.2 ectopic expression. However, Gli-activity was not reduced to control levels, in agreement with the unaltered ectopic induction of Olig2.

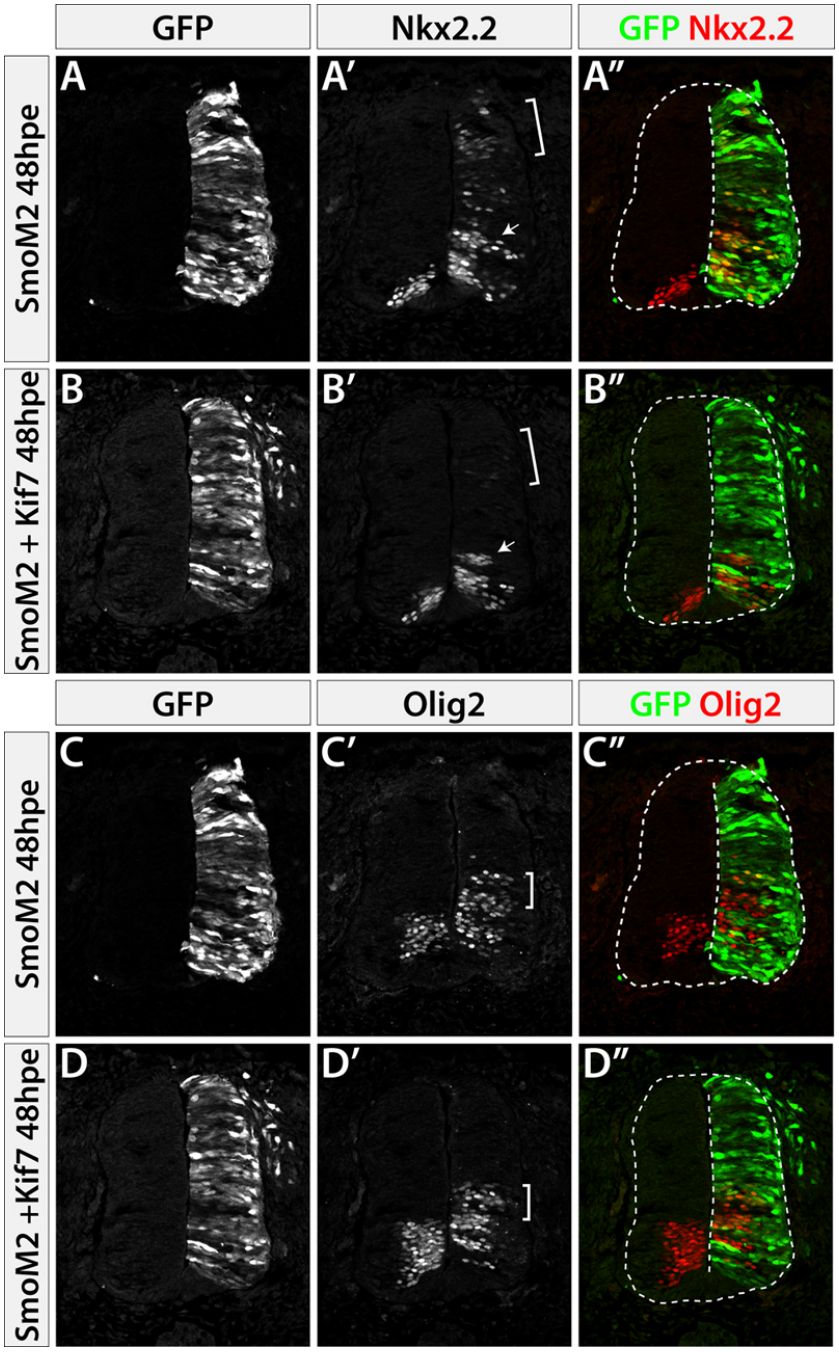

Figure 7.4 Kif7 inhibits SmoM2-induced Nkx2.2 expression.

Chick neural tube co-transfected with pCAGGS-SmoM2 and pCAGGS-GFP (GFP in green; **A-A″, C-C″**) or pCAGGS-SmoM2 and pCAGGS-Kif7-IRES-GFP (GFP in green; **B-B″, D-D″**) and assayed for the expression of neural progenitor markers Nkx2.2 and Olig2 (red) at 48hpe, at brachial level (**A-D″**). The ectopic induction of Nkx2.2 expression following SmoM2 transfection (**A-A″**) is partially inhibited by Kif7 (white bracket in **B-B″**). However, a few ectopic Nkx2.2 cell are still detected dorsally to the endogenous Nkx2.2 domain (white arrow in **B-B″**). The dorsal expansion of the Olig2 domain induced by SmoM2 (white bracket in **C-C″**) is not affected by Kif7 (white bracket in **D-D″**).

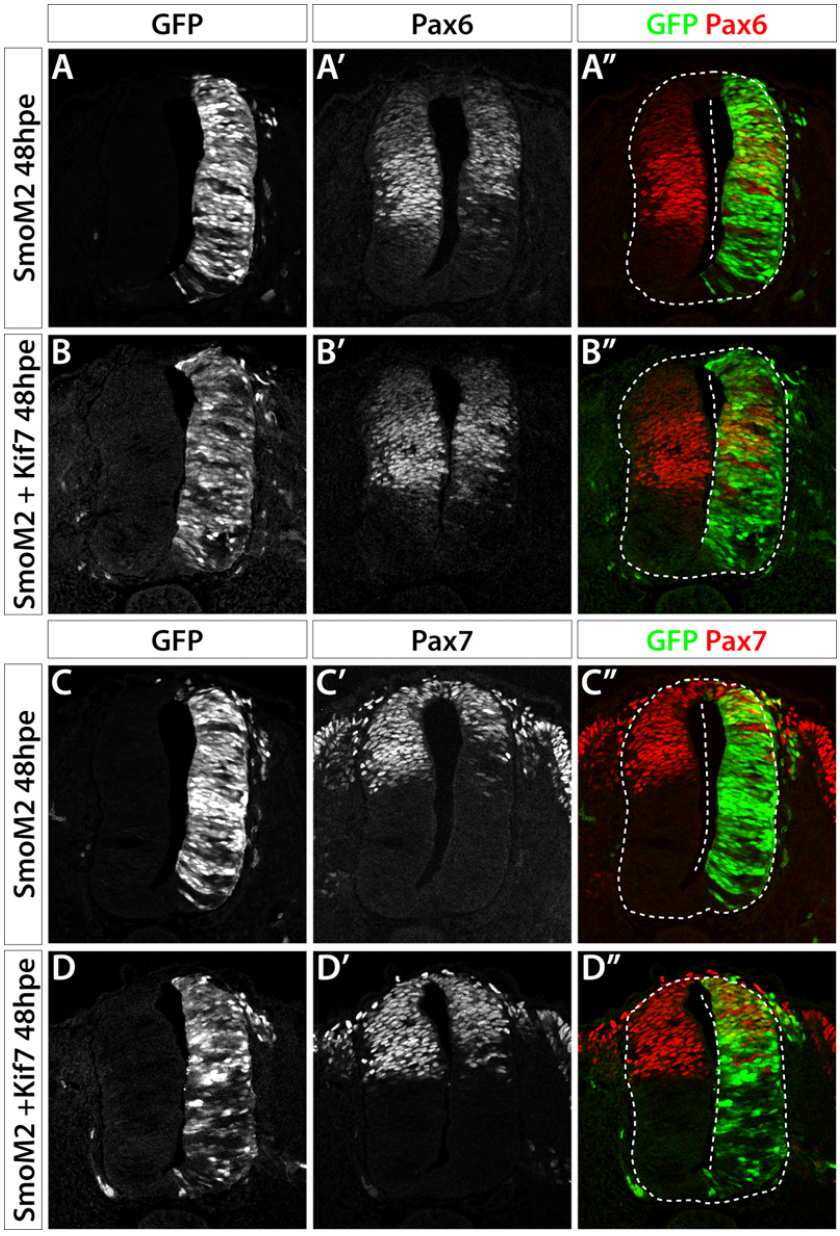

Figure 7.5 SmoM2-mediated repression of Pax6 and Pax7 is not affected by Kif7.

Chick neural tube co-transfected with pCAGGS-SmoM2 and pCAGGS-GFP (GFP in green; **A-A″, C-C″**) or pCAGGS-SmoM2 and pCAGGS-Kif7-IRES-GFP (GFP in green; **B-B″, D-D″**) and assayed for the expression of neural progenitor markers Pax6 and Pax7 (red) at 48hpe, at brachial level (**A-D″**). SmoM2 cell-autonomously down-regulated Pax6 and Pax7 expression in ventral regions of the domains (**A-A″, C-C″**). SmoM2 and Kif7 transfected embryos show a similar degree of repression of the Pax6 and Pax7 domains to single SmoM2 transfection (**B-B″, D-D″**).

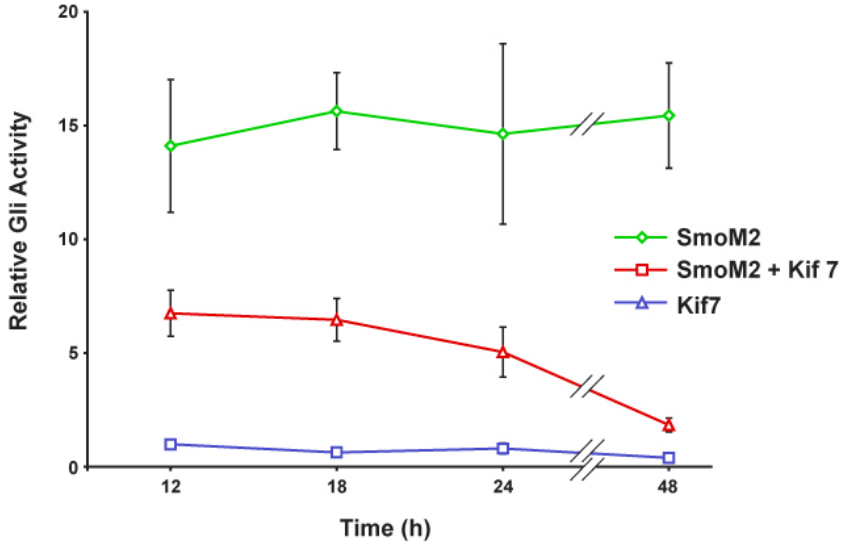

Figure 7.6 Kif7 decreases SmoM2-induced Gli transcriptional activity.

HH10 to HH12 chick neural tubes were transfected in ovo with a GBS-luciferase reporter and pCAGGS-SmoM2, pCAGGS-Kif7-IRES-GFP or pCAGGS-SmoM2 and pCAGGS-Kif7-IRES-GFP constructs. Luciferase assays from transfected embryos were performed to measure Gli activity at the indicated times post electroporation(relative Gli activity ±s.e.m.). SmoM2 electroporation yields a 15-fold increase in Gli activity. Co-transfection with Kif7 decreases the SmoM2-induced level of Gli activity 2-3 fold.

Taken together these results support the idea that Kif7 acts as a negative regulator of the Hh pathway, retaining at least some of the functions played by its Drosophila counterpart. In Drosophila Cos2 has also been ascribed a positive role in Hh signalling, where it appears necessary for the highest responses to signalling. In maximally stimulated cells, expressing high levels of Smo and in the presence of Hh, the introduction of intermediate levels of Cos2 increased the levels of pathway activity (Lum et al., 2003b). While it is possible that Kif7 also participates in the positive regulation of the pathway in vertebrates, we were unable to probe the positive role of Kif7 due to limitations of the chick overexpression system. A feature of the electroporation of the chick neural tube is the capacity to control the number of transfected cells, but not the levels of expression within a cell, precluding the use of this system to test the requirement of Kif7 for the maximal activation of the Shh pathway. The analysis of Kif7 function in the stimulation of the pathway was facilitated by use of loss-of-function assays, conducted by our collaborators (described below).

7.2 Kif7 localizes to cilia

We next explored the mode of action of Kif7. The activity of proteins is often associated with the subcellular locations and this has been shown to be the case for Cos2. The subcellular distribution of Cos2 is linked to the Hh state of the cells: in the absence of Hh Cos2 is cytoplasmic and binds to microtubules; when cells are stimulated Cos2 translocates to the plasma membrane in association with Smo (Ruel et al., 2003). As the distribution of Kif7 might also prove to be insightful we examined the subcellular localization of Kif7 in neural tube cells. To achieve this we made use of the Flag-tag attached to the protein. While GFP, the transfection marker, presented cytoplasmic and nuclear distribution, Kif7-Flag was detected in discrete puncta in the cytoplasm of electroporated cells (Figure 7.7 A-B′). The observed distribution is consistent with a vesicular accumulation, although we have been unable to determine the identity of the vesicles.

In addition Kif7 also localized to cilia. We were able to label the primary cilia distributed along the lumen walls of the neural tube using an antibody against acetylated-α-tubulin, a marker of stable microtubules found in cilia (Muresan et al., 1993). Kif7-Flag was detected at the tip of cilia marked by acetylated-α-tubulin (Figure 7.7 D-D″). By contrast, GFP was not present in cilia. These data suggest that the ability to translocate into cilia is specific to Kif7 (Figure 7.7 C-C″). Kif7-Flag was also found at the basal body of cilia, colocalized with the centrosomal protein γ-tubulin (Oakley, 1992) (Figure 7.7 E-E″).

Although the relevance of the ciliary localization of Kif7 is uncertain, these results place Kif7 in the same structure where several other Shh components are detected, including Smo and Gli proteins (Corbit et al., 2005; Haycraft et al., 2005; Rohatgi et al., 2007; Chen et al., 2009). The limited volume of cilia might bring together these components, thereby facilitating the regulatory interactions between Kif7 and other elements of the pathway. Alternatively, the putative kinesin activity of Kif7 might be the mediator of the movement of other components into the cilium. This possibility would indicate that Kif7, like Cos2, exhibits a dynamic distribution in response to Shh. Our analysis of Kif7-Flag expression along the dorsoventral axis of the neural tube did not reveal a correlation between levels of Shh and subcellular localization of Kif7. However, the elevated levels of Kif7-Flag in these experiments might limit the detection of subtle distribution differences in the transfected cells.

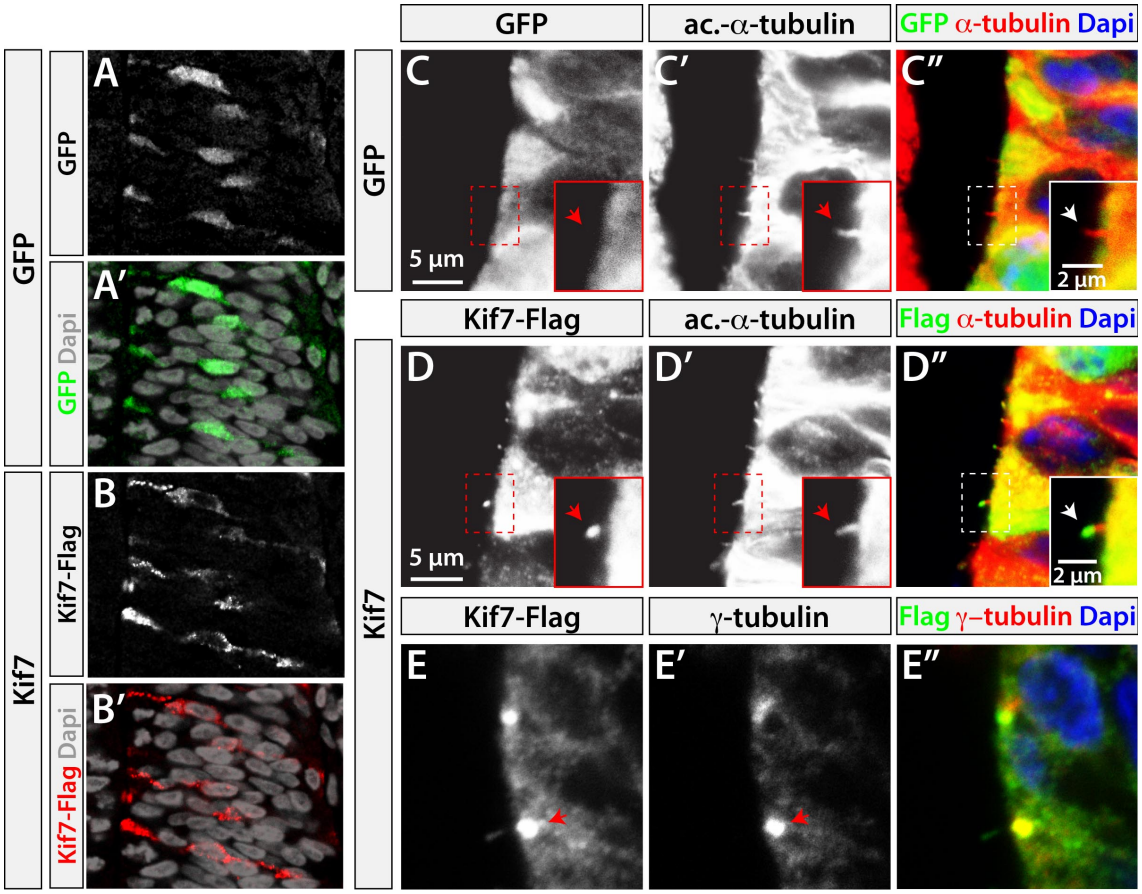

Figure 7.7 Kif7 localizes to cilia.

Subcellular localization of Kif7-Flag in the neural tube of chick embryos electroporated with pCAGGS-Kif7-IRES-GFP, 48hpe (**A-E″**). Kif7-Flag (red) displays a punctate cytoplasmic distribution (**B-B′**), whereas GFP (green) is located both in the cytoplasm and in the nucleus (**A-A′**). High power images indicate that Kif7-Flag is present in primary cilia located along the lumen of the neural tube (**D-E′**). Kif7 (green) colocalizes with the microtubule marker acetylated α-tubulin (red) at the tip of cilia (**D-D″**). GFP is not detected at the tip of cilia (**C-C″**). Insets in images C-D″ show high magnifications of the regions delineated by the dashed rectangles. Arrows point to the tip of cilia (insets in C-D″), showing that Kif7 is localized at the tip (D″), but not GFP (C″). Kif7-Flag is also detected in the same location as the centrosomal marker γ-tubulin (red) at the base of cilia (**E-E″**, red arrows).

7.3 Kif7 is unable to oppose the ectopic activity of Gli proteins

The coincident localization of Kif7, Smo and Gli proteins in cilia raised the question of whether Kif7 activity depends on the interaction with either Smo or Gli proteins. While the ability of Kif7 to rescue the SmoM2 phenotype points to a mode of action downstream of Smo, it is not clear whether it involves a direct interaction. Indeed, vertebrate Smo is predicted to have lost the Cos2 binding region (Varjosalo et al., 2006). Furthermore, in Drosophila the C-tail of Cos2, which binds to Smo, is dispensable for the repressive action of Cos2 (Lum et al., 2003b; Ho et al., 2005). As for the association between Cos2 and Ci in flies, Cos2 overexpression is able to block the transcriptional activation of Hh target genes induced by Ci overexpression (Wang et al., 2000). These observations directed our attention to the relation between Kif7 and Gli proteins. In addition, data from our collaborators showed binding between Kif7 and both Gli2 and Gli3, in mammalian cell lines and in embryo lysates (Cheung et al., 2009). Therefore we decided to focus on the interaction between Kif7 and Gli proteins and test whether Kif7 is able to interfere with Gli activity in the context of the chick neural tube.

We tested the effect of Kif7 on Gli2. The forced expression of Gli2 in the neural tube resulted in the weak induction of ectopic Nkx2.2^{+} and Olig2^{+} cells (Figure 7.8 A-B″) and in the repression of dorsal marker Pax6 (Figure 7.8 C-C″). These data are indicative of stimulated Shh pathway. However, the strongest effect of Gli2 overexpression was proliferative, with the electroporated side greatly increased in size compared to the control side (Figure 7.8 A-C″). Since at 48hpe the proliferative effects were very strong we decided to analyze the patterning defects at 24hpe. Even after the shorter period of incubation the electroporation of Gli2 caused a strong proliferative effect (Figure 7.9 A-A″, C-C″). However, Gli2 overexpression had only a restricted effect on ventral patterning after 24h, with the cell-autonomous inhibition of Olig2 expression in the pMN domain but no effect on Nkx2.2 expression. Nonetheless, the activating effect of Gli2 was reflected in the dorsal induction of a few ectopic Olig2^{+} cells and in the consistent repression of dorsal markers Pax6 and Pax7 (Figure 7.10 A-A″, C-C″).

Surprisingly, the introduction of Kif7 was unable to reverse the defects caused by Gli2 both in patterning and proliferation, despite the described in vitro interaction between the two proteins. The simultaneous transfection of Gli2 and Kif7 resulted in

the enlargement of the electroporated side of the neural tube and in the repression of Pax6 and Pax7, to an extent comparable to the transfection of Gli2 alone (Figure 7.10 B-B″, D-D″). Similarly, Nkx2.2 expression remained unaffected, while the Olig2 expression was inhibited in the endogenous domain and ectopically induced in dorsal regions, albeit in lower levels (Figure 7.9 B-B″, D-D″).

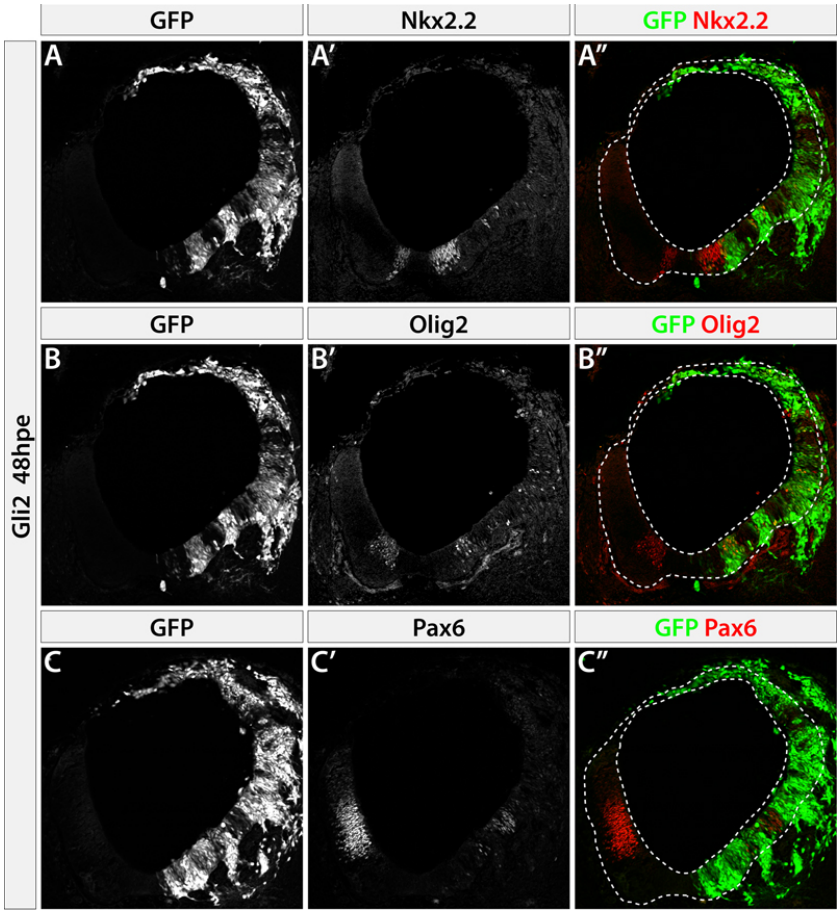

Figure 7.8 Gli2 increases progenitor proliferation in the neural tube.

Chick neural tube transfected with pCAGGS-Gli2-IRES-GFP (transfected cells identified by GFP expression in green) and assayed for the expression of neural progenitor markers Nkx2.2, Olig2 and Pax6 (red) at 48hpe, at brachial level (**A-C″**). The transfection with Gli2 resulted in the increased growth of the electroporated side of the neural tube. Gli2 induced the ectopic expression of Nkx2.2 (**A-A″**) and Olig2 (**B-B″**) and repressed Pax6 expression (**C-C″**).

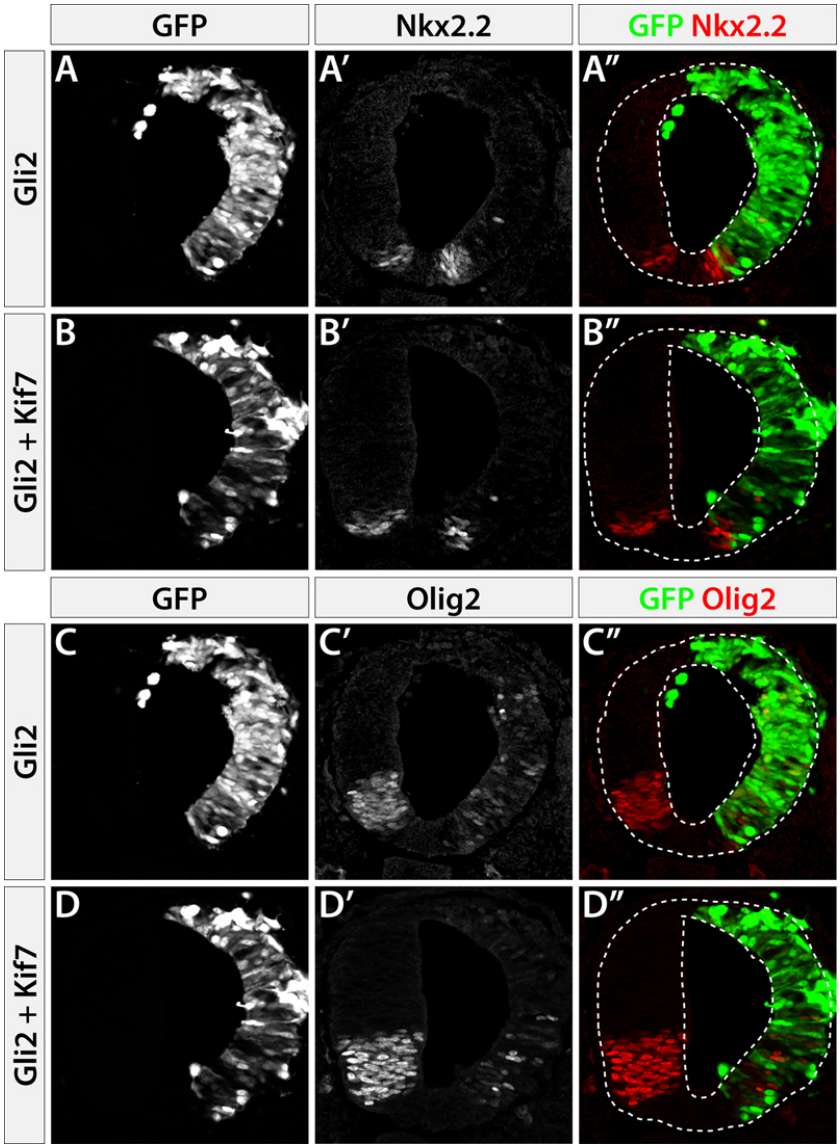

Figure 7.9 Kif7 does not affect Gli2-induced proliferation and patterning changes in the neural tube.

Chick neural tube transfected with pCAGGS-Gli2-IRES-GFP (GFP in green; **A-A″, C-C″**) or pCAGGS-Gli2-IRES-GFP and pCAGGS-Kif7-IRES-GFP (GFP in green; **B-B″, D-D″**) and assayed for the expression of neural progenitor markers Nkx2.2 and Olig2 (red) at 24hpe, at brachial level (**A-D″**). Gli2 overexpression had no significant effect on Nkx2.2 expression after 24h of incubation (**A-A″**). By contrast, transfection with Gli2 caused the down-regulation of Olig2 expression in the endogenous domain and induced ectopic Olig2^{+} cells at more dorsal positions (**C-C″**). The Gli2-electroporated side of the neural tube showed increased growth compared to control side (**A-A″, C-C″**). Co-transfection with Kif7 did not influence the effect of Gli2 on proliferation (**B-B″, D-D″**) or on the expression of Nkx2.2 (**B-B″**) and Olig2 (**D-D″**).

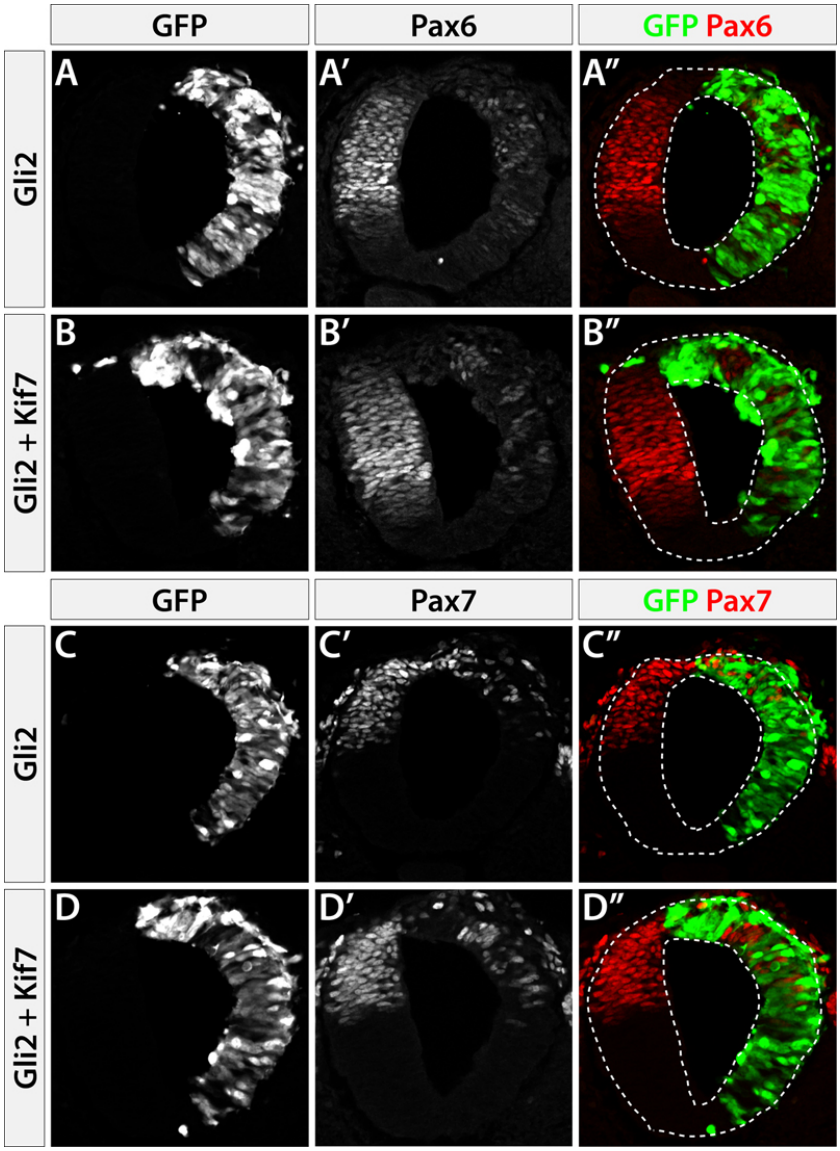

Figure 7.10 Kif7 does not affect Gli2-mediated repression of Pax6 and Pax7 expression. Chick neural tube transfected with pCAGGS-Gli2-IRES-GFP (GFP in green; **A-A″, C-C″**) or pCAGGS-Gli2-IRES-GFP and pCAGGS-Kif7-IRES-GFP (GFP in green; **B-B″, D-D″**) and assayed for the expression of neural progenitor markers Pax6 and Pax7 (red) at 24hpe, at brachial level (**A-D″**). Gli2 overexpression cell-autonomously represses Pax6 (**A-A″**) and Pax7 expression (**C-C″**). Co-transfection of Gli2 and Kif7 results in a similar degree of repression of Pax6 (**B-B″**) and Pax7 (**D-D″**) as the transfection with Gli2 alone.

These results suggested that in these experiments Kif7 was unable to inhibit Gli2. This prompted us to determine if the failure to block the activation of the pathway was associated with a failure to block the translocation of Gli2 into the nucleus. In Drosophila the repressive action of Cos2 has been proposed to involve the tethering of Ci to the cytoplasm, thereby abrogating its transcriptional function in the nucleus (Wang et al., 2000). Similarly, in mammalian cell lines Kif7 was able to prevent the entry of Gli1 into the nucleus (C-c Hui, personal communication). To test if Kif7 has lost the ability to maintain Gli2 in the cytoplasm in vivo we made use of the tags that were attached to the cDNA sequences of Gli2 (Myc) and Kif7 (Flag). The presence of these tags allowed us to follow the subcellular localization of these proteins and to determine how this localization is affected by their interactions. In accordance with the observed Shh-pathway activating effect, ectopic Gli2-Myc was present in the nucleus (Figure 7.11 A, A'). As described earlier, Kif7-Flag is excluded from the nucleus and is detected in puncta in the cytoplasm (Figure 7.11 B, B'). The simultaneous expression of Kif7 and Gli2 did not alter the nuclear localization of Gli2 and Kif7 remained cytoplasmic (Figure 7.11 D-D'''). The almost mutually exclusive localization of the two proteins is consistent with the inability of Kif7 to interfere with Gli2 transcriptional activity.

The unchanging nuclear distribution of Gli2 raised the question of whether this was a feature of the specific Gli2 construct used in these experiments. To assess if this is the case, we examined the ability of Sufu to interfere with Gli2 distribution. Sufu is a known regulator of Hh signalling and its inhibitory effect on the pathway has been suggested to involve the maintenance of Ci/Gli proteins in the cytoplasm (Svärd et al., 2006; Chen et al., 2009; Humke et al., 2010). Upon introduction into the chick neural tube Sufu-Flag localized predominantly in the cytoplasm (Figure 7.11 C, C'). When transfected together with Gli2, Sufu-Flag colocalized with Gli2-Myc and, importantly, both remained excluded from the nucleus (Figure 7.11 E-E'''). Therefore, this result suggested that in our system Gli2 distribution is susceptible to regulation by Sufu but is resistant to Kif7. We next asked whether the observed association between Gli2 and Sufu was reflected in a change in the transcriptional activity of Gli2. As Gli2 is blocked from entering the nucleus in the presence of Sufu it is expected that this effect is accompanied by the corresponding effect on proliferation and patterning. To test if this was true we examined whether the co-electroporation of Gli2 and Sufu impacted on the formation of Shh-dependent cell types in the chick

neural tube. As predicted by its effect on subcellular localization, Sufu was able to rescue the Gli2-dependent proliferation, and partially rescue the neural progenitor patterning (Figure 7.12). In embryos transfected with both constructs the Nkx2.2-positive domain was slightly extended in the electroporated side, while the pMN domain was comparable to the control side. Consistent with the decreased Gli activity, Pax6 expression appeared relatively normal and the Pax7 domain was repressed to a lesser extent. These findings indicate that Sufu and Kif7 exhibit different potentials to retain Gli2 in the cytoplasm, which might explain their different capacities to rescue the Gli2 phenotype. This suggests that Sufu and Kif7 operate at different levels of the Shh signalling pathway.

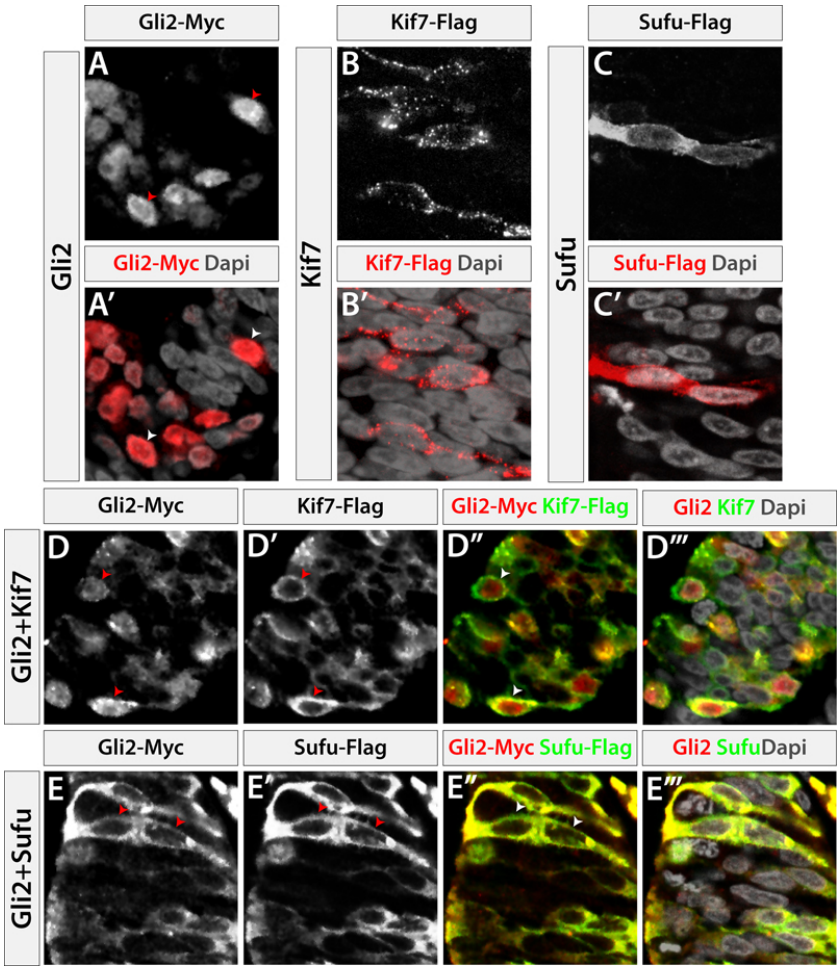

Figure 7.11 Kif7 does not block nuclear translocation of Gli2.

Subcellular localization of transfected Gli2-Myc (**A-A'**), Kif7-Flag (**B-B'**) and Sufu-Flag (**C-C'**) in the chick neural tube at 24hpe. Gli2 predominantly localizes to the nucleus (red/white arrow heads in **A-A'**), whereas Kif7 distribution is mostly cytoplasmic (**B-B'**). Sufu is detected at low

levels in the nucleus and strongly in the cytoplasm (**C-C'**). The nuclear localization of ectopic Gli2 is not altered by the co-transfection with Kif7 (red/white arrow heads in **D,D",D'"**), which remained cytoplasmic (**D'-D'"**). Sufu overexpression results in the exclusion of ectopic Gli2 from the nucleus and colocalization of both proteins in the cytoplasm (red/white arrow heads in **E-E'"**).

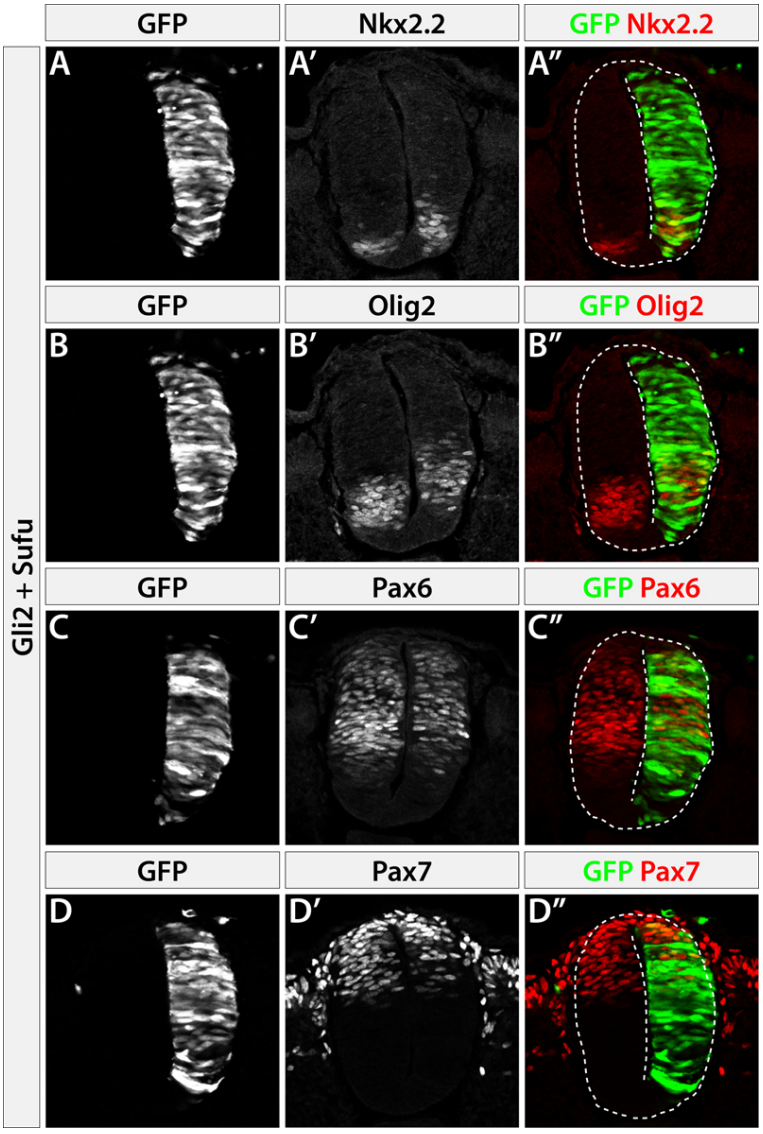

Figure 7.12 Sufu blocks Gli2-induced proliferation and patterning changes in the neural tube.

Chick neural tube transfected with pCAGGS-Gli2-IRES-GFP and pCAGGS-Sufu-IRES-GFP (GFP in green) and assayed for the expression of neural progenitor markers Nkx2.2, Olig2, Pax6 and Pax7 (red) at 24hpe, at brachial level (**A-D"**). Co-transfection of Gli2 and Sufu results in a mild expansion of the Nkx2.2 domain (**A-A"**), whereas the size of the Olig2 domain in the

electroporated side is comparable to the control side (**B-B"**). Sufu also blocked the Gli2-mediated repression of Pax6 (**C-C"**). Pax7 expression is decreased cell-autonomously in embryos co-electroporated with Gli2 and Sufu (**D-D"**), but to a lesser extent than in embryos transfected with Gli alone (Figure 7.10 C-C"). In the presence of Sufu Gli2 is unable to promote increased proliferation, as the electroporated side has a similar size to the control side (**A-D"**).

To test if the lack of interaction with Kif7 was specific to Gli2 we assayed the effect of Kif7 on Gli1. Similar to Gli2, the overexpression of Gli1 in the neural tube resulted in increased proliferation (Figure 7.13 A-A", C-C", Figure 7.14 A-A"). Moreover, Gli1 was able to induce ectopic Nkx2.2^{+} and Olig2^{+} cells dorsally and to repress Pax6 expression. Similar to Gli2, Gli1 activity was not inhibited by co-transfection with Kif7. Even in the presence of Kif7, Gli1 was able to ectopically induce Nkx2.2 and Olig2 and repress Pax6 (Figure 7.13 B-B", D-D", Figure 7.14 B-B"). Thus, the similar effect on Gli1 and Gli2 suggests that, in these conditions, Kif7 is generally unable to counteract the pathway activation induced by Gli proteins. Conversely, Sufu was able to inhibit the positive activity of Gli1 to a similar extent to its effect on Gli2. Sufu overexpression promoted a clear rescue of the proliferation effect of Gli1 (Figure 7.15). Furthermore, the co-expression of Sufu resulted in reduced Gli-dependent ectopic induction of Nkx2.2 and Olig2 (Figure 7.15 A-B"), as well as reduced repression of the dorsal marker Pax6 (Figure 7.15 C-C"). These results confirm the inhibitory role of Sufu at the level of Gli proteins.

Together, these data place Kif7 in the negative branch of the Shh transduction pathway, revealing Cos2-like activity in a vertebrate system. However, these experiments showed only a partial conservation of Cos2 function, as Kif7 was able to interact with Smo but not with Gli proteins. Moreover, our overexpression assay failed to uncover a positive role for Kif7 on Shh signalling. Therefore, these results needed to be confirmed and extended with loss of function studies. This analysis was conducted by our collaborators and others and a summary of these results is presented in the next section.

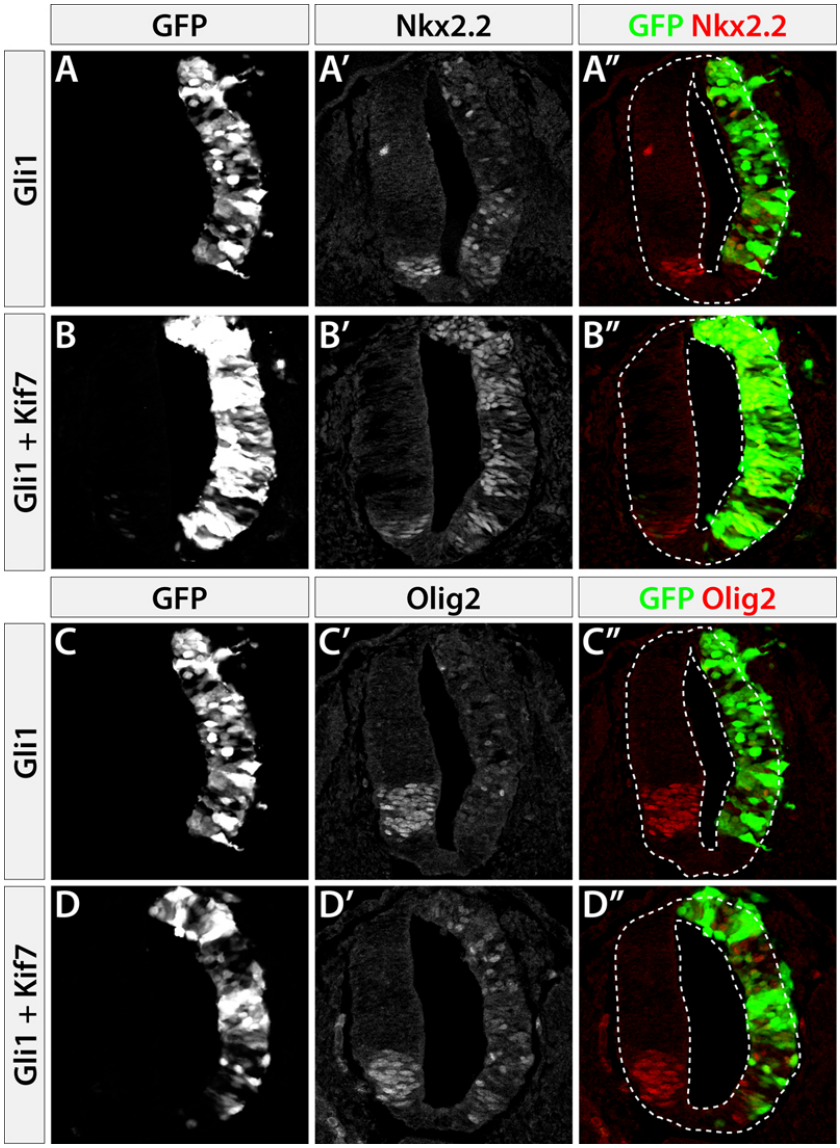

Figure 7.13 Kif7 does not block Gli1 activity in neural tube.

Chick neural tube transfected with pCAGGS-Gli1-IRES-GFP (GFP in green; **A-A″, C-C″**) or pCAGGS-Gli1-IRES-GFP and pCAGGS-Kif7-IRES-GFP (GFP in green; **B-B″, D-D″**) and assayed for the expression of neural progenitor markers Nkx2.2 and Olig2 (red) at 24hpe, at brachial level (**A-D″**). Ectopic Gli1 caused the increased growth of the electroporated side (**A-A″**). Kif7 overexpression failed to block the proliferation phenotype induced by Gli1 (**B-B″**). Gli1 transfection induced ectopic Nkx2.2 and Olig2 cells (**A-A″, C-C″**). Kif7 is not able to inhibit Gli1-induced ectopic Nkx2.2 and Olig2 expression (**B-B″, D-D″**).

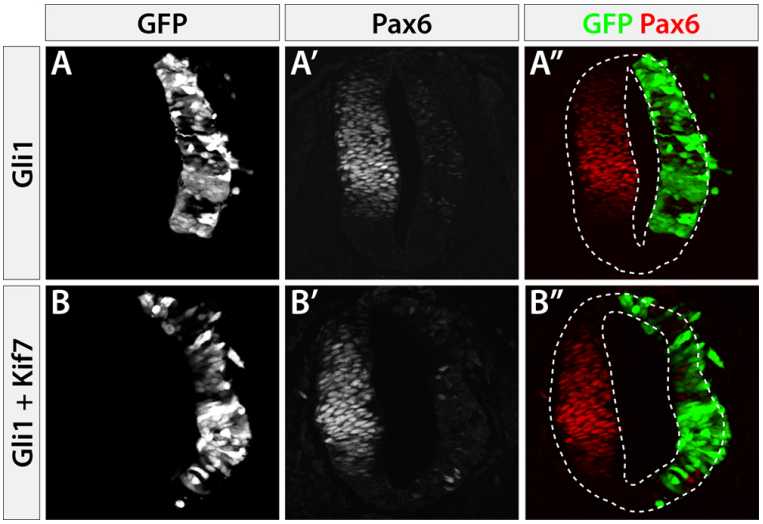

Figure 7.14 Kif7 is unable to block Gli1-mediated repression of Pax6 expression.

Chick neural tube transfected with pCAGGS-Gli1-IRES-GFP (GFP in green; **A-A″**) or pCAGGS-Gli1-IRES-GFP and pCAGGS-Kif7-IRES-GFP (GFP in green; **B-B″**) and assayed for the expression of neural progenitor marker Pax6 (red) at 24hpe, at brachial level (**A-B″**). Ectopic Gli1 down-regulates Pax6 expression (**A-A″**). Kif7 overexpression fails to block Pax6 repression by Gli1 (**B-B″**).

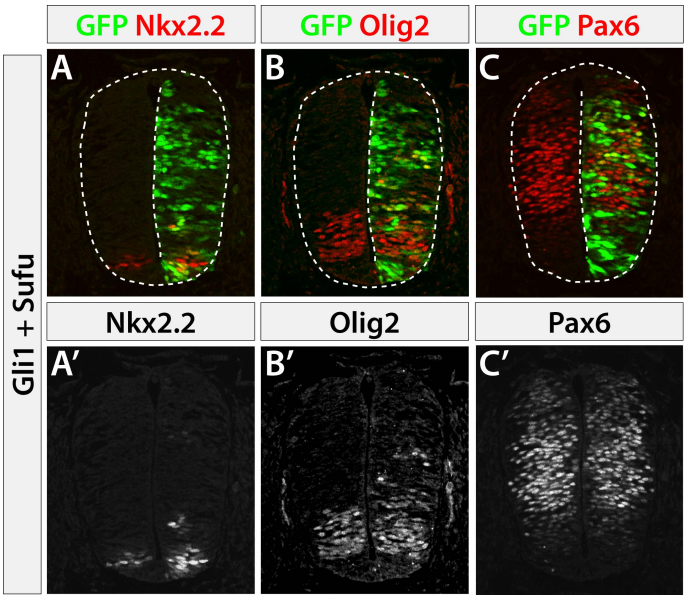

Figure 7.15 Sufu inhibits Gli1 activity in the neural tube.

Chick neural tube transfected with pCAGGS-Gli1-IRES-GFP and pCAGGS-Sufu-IRES-GFP (GFP in green) and assayed for the expression of neural progenitor markers Nkx2.2, Olig2 and Pax6 (red) at 24hpe, at brachial level (**A-C′**). Sufu inhibits the overgrowth of the neural tube

induced by ectopic Gli1 (**A-C'**). In addition, Sufu partially blocks the induction of ectopic Nkx2.2 (**A-A'**) and Olig2 (**B-B'**) expression by Gli1. The Gli1-mediated repression of Pax6 expression is also blocked by Sufu (**C-C'**).

7.4 Kif7-null mice display significant Hh-related phenotypes (Cheung et al., 2009)

Our collaborators generated a null allele of Kif7, which was shown to be lethal in homozygous mutant mice. Kif7$^{-/-}$ mice died at birth with malformations such as exencephaly and polydactyly. This resembled the Gli3 mutant phenotype. Unlike Gli3$^{-/-}$ embryos, however, Kif7 mutant mice also displayed neural tube patterning defects characteristic of enhanced Hh pathway activation, with the expansion of Nkx2.2 and Olig2 progenitor domains. Together with the in ovo results, these findings support a role for Kif7 as an inhibitor of the Hh pathway in vertebrates and suggest a possible involvement in the control of Gli3 repressor function or abundance. Indeed, the biochemical analysis of the Gli2 and Gli3 proteins in total embryo lysates revealed an increase in the amount of full-length Gli2 (185 KD) and a reduction in the truncated form of Gli3 (83 KD) in Kif7 mutants. The altered levels of Gli activator and repressor forms could explain the Shh-related patterning phenotype observed in the absence of Kif7.

To help define at which level of the pathway Kif7 acts, Kif7$^{-/-}$;Smo$^{-/-}$ embryos were examined. The double mutants showed a partial rescue of the Smo single mutants defects, with longer survival and larger size. The removal of Kif7 in a Smo-null background also allowed the generation of Shh-dependent neural cell types, including Olig2 and some scattered Nkx2.2 cells. The activation the pathway even in the absence of Smo suggests a mode of action for Kif7 at a step downstream of Smo. Similar to what was shown for Kif7 single mutants, the activation of Shh signalling in Kif7$^{-/-}$Smo$^{-/-}$ embryos was accompanied by the increase of full-length Gli2 and reduction of truncated Gli3, further supporting the role of Kif7 in the regulation of Gli proteins stability or processing.

The possible involvement of Gli2 activator function in the enhanced activation of the pathway following removal of Kif7, and consequent effect in ventral cell types specification, was corroborated by the analysis of Kif7;Gli3 mutant embryos. $Gli3^{-/-}$ embryos showed no defects in ventral neural tube patterning, and the additional loss of one copy of Kif7 in these embryos also had no effect. Conversely, the loss of Gli3 exacerbated the $Kif7^{-/-}$ patterning phenotype in a dose dependent manner. The dorsal expansion of the Olig2 domain was enhanced in $Kif7^{-/-};Gli3^{+/-}$ embryos, whereas the complete loss of Gli3 in Kif7 mutants resulted in the increase of both Olig2 and Nkx2.2 cells. The ectopic induction of these ventral cell types was likely to depend on the elevated Gli2 activity associated with the loss of Kif7, since the removal of Gli3 alone had no phenotype.

While the negative function of Cos2 appeared to be conserved in its vertebrate homolog, it remained to be determined whether Kif7 also has a Cos2-like positive role in Hh signalling. This was shown to be true in the ventral-most cell type in the neural tube, the floor plate cells. Floor plate formation, a process mediated by Gli2 activator function in response to high levels of Shh, was unaffected in Kif7-null mice. The additional removal of one copy of Gli2 interfered with floor plate differentiation, causing the disruption of Shh expression in the midline at e10.5 and loss of the characteristic floor plate epithelial structure at e14.5. Nkx2.2 expression was also shifted ventrally to the midline, consistent with the absence of floor plate. The decreased Hh signalling in $Kif7^{-/-}Gli2^{+/-}$ mice was also reflected in the decreased number of Olig2+ and Nkx2.2+ progenitor cells when compared with Kif7 mutants. Together, these findings revealed the positive function of Kif7 in the formation of high Shh-dependent cell types. Furthermore, this experiment confirmed the requirement of Gli2 for the ectopic pathway activation observed in the absence of Kif7, since this ectopic activation was restricted when Gli2 levels were reduced.

This study established Kif7 as a key regulator of the Hh pathway in vertebrates, confirming the conserved function of this core component from Drosophila to mammals.

CHAPTER 8 - FUNCTIONAL DOMAINS OF KIF7 IN HEDGEHOG SIGNALLING

The transduction of the Shh pathway in higher vertebrates requires the kinesin-like protein Kif7. Gain and loss-of-function assays provided evidence that Kif7 coordinates the response of the pathway to both positive and negative inputs (Cheung et al., 2009; Endoh-Yamagami et al., 2009; Liem et al., 2009). While Kif7 appears to have maintained the core functions of Costal2 on Hh signalling, it is not clear whether the underlying mechanisms are conserved. Drosophila Cos2 has been proposed to act as a cytosolic scaffold, mediating the Hh-induced interactions between components of the pathway and thereby influencing Ci processing and localization (for review see Wilson and Chuang, 2010). Thus, Cos2 appears to function as a sensor to the Hh signal, being required for both the activation and the repression of the pathway. In addition to its scaffolding role Cos2 also displays motor activity, a property that is important for the regulation of Ci proteolysis, although the mechanism is still unclear (Farzan et al., 2008). The analysis of Kif7 mouse mutants points to a conserved mode of regulation of the pathway, as it implicates Kif7 in the control of the levels of Gli activator to Gli repressor. However, Kif7 activity in vivo depends on the presence of a functional cilium, as double mutants for Kif7 and the ciliogenesis-associated protein IFT172 are identical to ITF172 single mutants (Liem et al., 2009). Furthermore, in mammalian cell lines Kif7 displays a dynamic localization within cilia in response to Shh and promotes an equivalent distribution of Gli proteins (Endoh-Yamagami et al., 2009; Liem et al., 2009). The observed association between Kif7 and cilia, a structure that is dispensable for fly Hh signalling, suggests a mechanistic divergence between Cos2 and Kif7, prompting us to investigate the distinctive features of Kif7.

To gain insight into the degree of conservation between the two lineages we explore the functionality of Cos2 in a vertebrate system and ask whether it mimicked the mode of action of Kif7. Moreover, to try to identify the essential elements in the Kif7 protein we assess the role of specific protein domains in the regulation of Shh target genes in the neural tube.

8.1 Costal2 has a strong inhibitory effect on Shh signalling in the chick neural tube

To assess the similarities between Kif7 and Cos2 we tested the activity of Cos2 in a vertebrate system. If Kif7 function depends on vertebrate specific structures the Drosophila protein would not to be predicted to influence the vertebrate pathway. To test the ability of Cos2 to interfere with vertebrate Shh signalling Cos2 was ectopically expressed in the chick neural tube and its effect on the formation of Shh-dependent progenitor markers was inspected. Unexpectedly, Cos2 proved to have a stronger effect than Kif7 on ventral neural tube patterning. Cos2 overexpression consistently caused the cell-autonomous repression of Nkx2.2 and Olig2 expression (Figure 8.1 A-B″), while the introduction of Kif7 resulted only in the partial repression of the high Shh-response marker Nkx2.2 while leaving other ventral markers unaffected. The reduction of the ventral progenitor domains following Cos2 electroporation was accompanied by the complementing expansion of the $Pax6^{+}$ domain, a negative target of Shh (Figure 8.1 C-C″). This effect had also been observed in Kif7-electroporated embryos (Figure 6.3) but the Cos2-induced expression of Pax6 was much more pronounced both in number of cells and in levels of expression. Strikingly, Cos2 was also able to induce ectopic $Pax7^{+}$ cells in ventral regions of the neural tube, unequivocally confirming the stronger inhibitory activity on the pathway than its vertebrate homolog (Figure 8.1 D-D″). The ability of Cos2 to efficiently impair ventral patterning indicates that at least some of the mechanisms used in fly to regulate the pathway are conserved in higher vertebrates. Cos2 overexpression also resulted in the reduced size of the transfected side of the neural tube, an effect that has been associated with reduced Shh signalling (Cayuso et al., 2006).

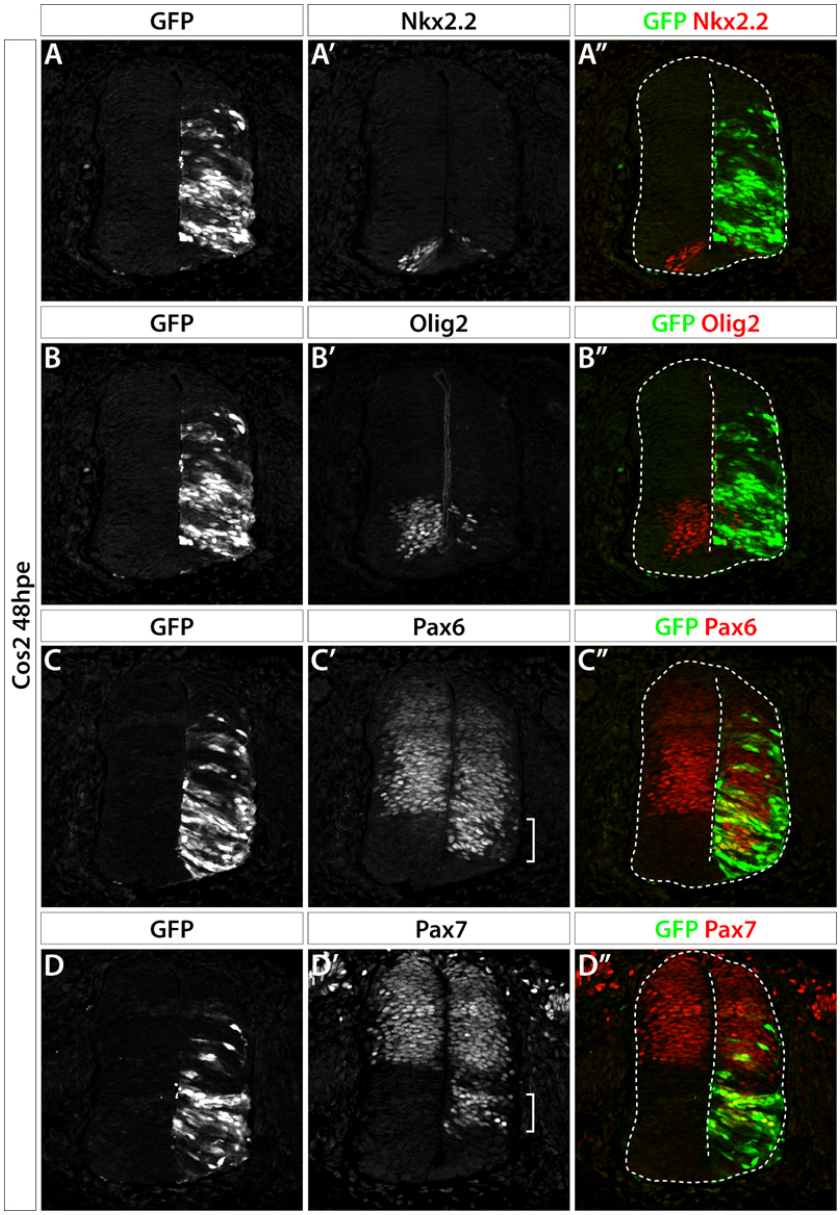

Figure 8.1 Cos2 inhibits Shh signalling in the chick neural tube.

Expression of progenitor markers Nkx2.2, Olig2, Pax6 and Pax7 (red) at the brachial level of the chick neural tube 48h after transfection with pCAGGS-Cos2-IRES-GFP (transfected cells identified by GFP expression in green) (**A-D″**). The ectopic expression of Cos2 cell-autonomously represses the expression of the Shh-induced target genes Nkx2.2 (**A-A″**) and Olig2 (**B-B″**). In addition, Cos2 overexpression cell-autonomously induces the Shh-repressed dorsal markers Pax6 (**C-C″**; white bar in **C′** highlights ectopic Pax6 cells) and Pax7 (**D-D″**; white bar in **D′** highlights ectopic Pax7 cells).

The marked repressive action of Cos2 on Shh signalling prompted us to determine if, like Kif7, Cos2 is able to oppose the stimulating effect of SmoM2. In cultured mammalian cells Cos2 is unable to interfere with the activity of mouse Smo, suggesting that mSmo is insensitive to Cos2 (Varjosalo et al., 2006). To further explore the association between Cos2 and the vertebrate pathway we tested the ability of Cos2 to restrict Smo-induced ventralization of the neural tube, using in ovo electroporation. The transfection with SmoM2, a constitutively active form of Smo, resulted in the generation of ectopic Nkx2.2^{+} cells in dorsal regions of the neural tube and caused the dorsal expansion of the Olig2 domain (Figure 8.2 A-A″, C-C″). The positive input of SmoM2 was also reflected in the repression of dorsal markers Pax6 and Pax7 (Figure 8.3 A-A″, C-C″). The co-electroporation of SmoM2 and Cos2 resulted in a significant reduction of the length of the neural tube in transfected embryos. As the independent electroporation of either of these proteins has an inhibitory effect on neural tube size, it is possible that this effect is additive upon joint expression of SmoM2 and Cos2. Therefore we analyzed the patterning phenotype in embryos with lower rates of transfection. Remarkably, even in the presence of SmoM2, Cos2 was able not only to restrict the dorsal induction of Nkx2.2, but also to cell-autonomously repress Olig2 (Figure 8.2 B-B″, D-D″). Moreover, Cos2 blocked the SmoM2-driven repression of the endogenous Pax6 and Pax7 domains and additionally induced ectopic Pax6^{+} and Pax7^{+} cells in more ventral regions (Figure 8.3 B-B″, D-D″). These results suggest that, similar to Kif7, Cos2 acts downstream of Smo to inhibit Shh signalling. This assay also confirmed that Cos2 has a more potent negative impact on the pathway than Kif7, which only partially blocked Smo-induced ectopic Nkx2.2 and did not affect the other patterning phenotypes. The differences between Cos2 and Kif7 activity may result from differences in the interaction with Smo. Mouse Smo structure has diverged from the Drosophila counterpart, particularly the C-terminal region containing Cos2-binding sites (Jia et al., 2003; Lum et al., 2003b). Cos2 binds to different regions of Smo depending on the Hh-state of the cell, and this alternative binding is important for the subsequent transduction of the signal (Liu et al., 2007). Kif7 also binds to different regions of Smo, but the functional relevance of this binding is still unclear (Endoh-Yamagami et al., 2009). Therefore, it is possible that the two homologs regulate Smo activity through different mechanisms. Another possibility is that the function of Cos2 has been partitioned between the two vertebrate homologs, Kif7 and Kif27, and consequently the activity of the individual

proteins is less significant. To test this possibility we examined the function of Kif27 in Hh signalling in the vertebrate neural tube.

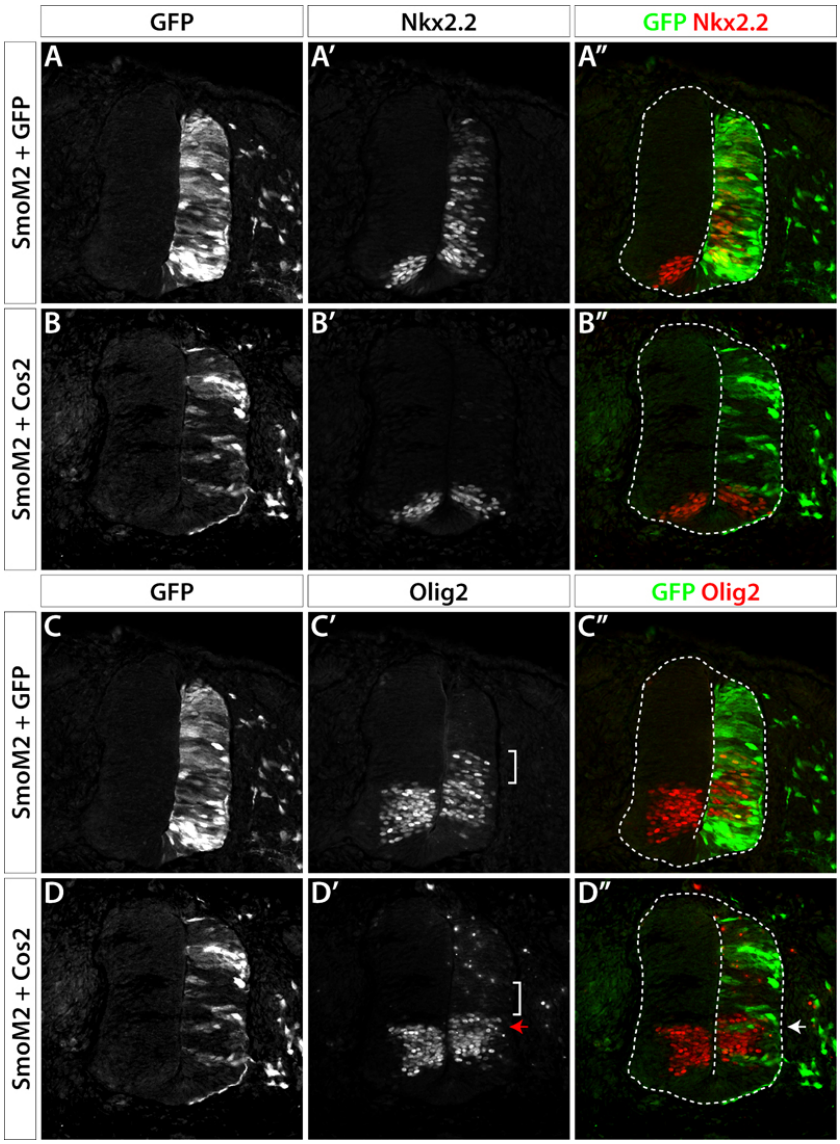

Figure 8.2 Cos2 inhibits Smo-induced Nkx2.2 and Olig2 expression.

Chick neural tube transfected with pCAGGS-SmoM2 and pCAGGS-IRES-GFP (GFP in green; **A-A″, C-C″**) or SmoM2 and pCAGGS-Cos2-IRES-GFP (GFP in green; **B-B″, D-D″**) and assayed for the expression of neural progenitor markers Nkx2.2 and Olig2 (red) at 48hpe, at brachial level (**A-D″**). The ectopic induction of Nkx2.2 expression following SmoM2 transfection (**A-A″**) is inhibited by co-transfection with Cos2 (**B-B″**). Similarly, the ectopic expression of Olig2 dorsally to the endogenous domain induced by SmoM2 (white bar in **C-C″**) is blocked by Cos2 (white bar in **D-D″**). Cos2 overexpression results in the down-regulation of Olig2 expression within the endogenous domain (red arrow in **D′** and white arrow in **D″**).

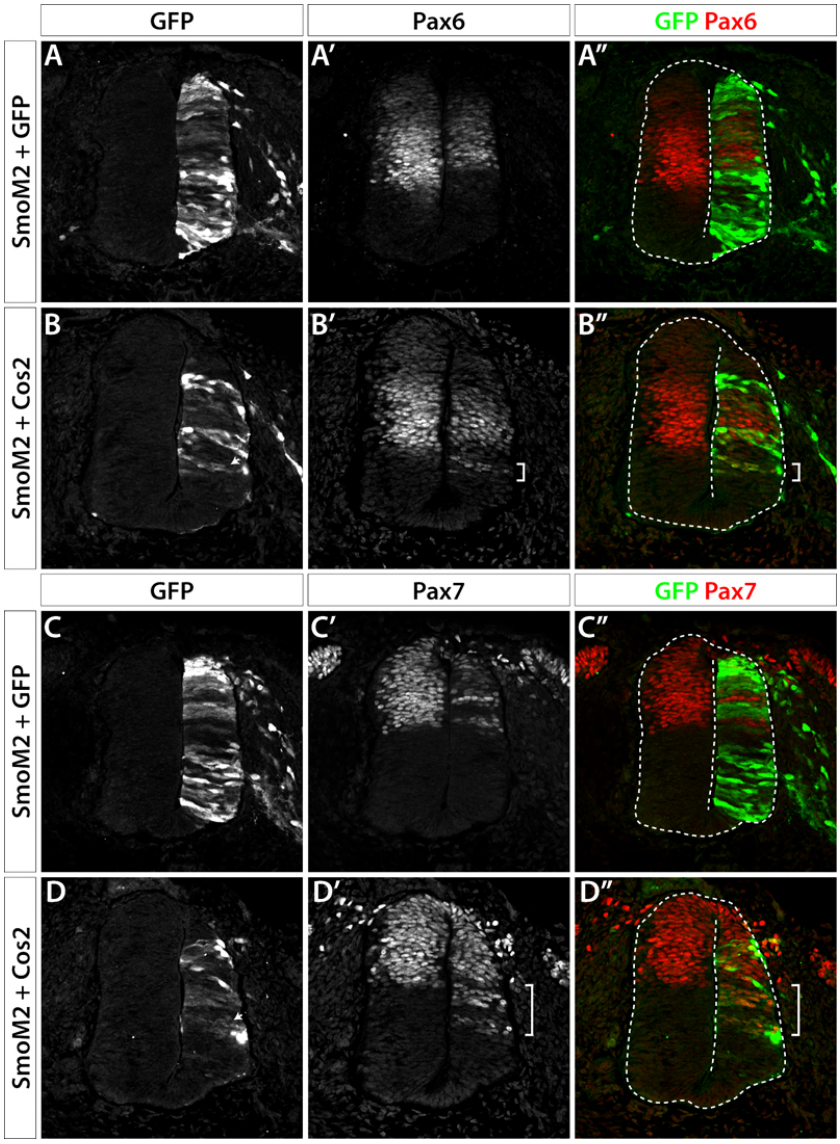

Figure 8.3 Cos2 blocks Smo-mediated repression of Pax6 and Pax7 expression.

Chick neural tube transfected with pCAGGS-SmoM2 and pCAGGS-IRES-GFP (GFP in green; **A-A″, C-C″**) or SmoM2 and pCAGGS-Cos2-IRES-GFP (GFP in green; **B-B″, D-D″**) and assayed for the expression of neural progenitor markers Pax6 and Pax7 (red) at 48hpe, at brachial level (**A-D″**). The cell-autonomous repression of Pax6 expression following SmoM2 transfection (**A-A″**) is blocked by Cos2 (**B-B″**). In addition, Cos2 cell-autonomously induces Pax6 expression in positions ventral to the endogenous domain (white bar in **B′-B″**). Similarly, cell-autonomous repression of Pax7 expression caused by SmoM2 (**C-C″**) is blocked by Cos2 (**D-D″**), and Pax7 ectopic cells are induced at more ventral positions (white bar in **D′-D″**).

8.2 Kif27 is not involved in Hh signalling in the neural tube

To assess the function of Kif27 in Hh signalling we introduced a pCAGGS-Kif27 construct into the chick neural tube. Unlike Kif7 and Cos2, the electroporation of Kif27 had no effect in the patterning of the neural tube (Figure 8.4). The expression of the Shh target genes Nkx2.2 and Olig2 following Kif27 overexpression was unchanged compared to the contralateral untransfected side of the neural tube and to embryos electroporated with the control vector (Figure 8.4 A-B″, E,F). Likewise, the expression of dorsal markers Pax6 and Pax7 remained unaffected upon transfection with Kif27 (Figure 8.4 A-B″, G,H). This result suggests that Kif27 has either a very mild or no effect on Shh signalling when compared with Kif7.

To further explore the role of Kif27 we tested its inhibitory effect on Smo activity. This sensitized assay could help reveal the repressive action of Kif27. However, overexpression of Kif27 was unable to reverse the SmoM2-induced patterning phenotype. After Kif27/SmoM2 double electroporation the progenitor marker Nkx2.2 was expanded to a similar extent to the SmoM2 single electroporation (Figure 8.5; experiment performed by James Briscoe). These findings strongly suggest that Kif27 is not critically involved in the regulation of the Shh pathway. The distinct impact that Kif7 and Kif27 have on Shh signalling favors a model where the two Cos2 orthologs evolved different functions. Nevertheless, Kif27 might maintain a minor role on the Shh pathway undetectable in our overexpression assay. Alternatively, Kif27 might act in partnership with Kif7 and in association these proteins might exert a more efficient inhibition of the pathway. This hypothesis could also explain why Kif7 has only a limited effect on Gli activity and is unable to rescue the Gli overexpression phenotype.

To test if Kif27 is able to influence the ability of Kif7 to block Gli-mediated activation of the Shh pathway Kif7 and Kif27 were co-expressed with Gli1 and the effect on neural tube patterning was analyzed. If the two related proteins cooperate, the co-electroporation of Kif7 and Kif27 might have an stronger repressive effect on Gli activity. As described earlier, the overexpression of Gli1 results in the induction of ectopic Nkx2.2^{+} and Olig2^{+} cells and in the repression of Pax6 (Figure 6.13, Chapter 6). Kif7 alone was unable to restrict the ectopic activation of the pathway promoted by Gli1 (Figure 8.6 A-C′). The introduction of Kif27 alongside Kif7 did not change the outcome of Gli1 electroporation (Figure 8.6 D-F′). These results therefore failed to

disclose an interaction between Kif7 and Kif27, further supporting the idea that Kif27 does not play a significant role in Shh signalling.

Together, these data suggest that Kif27 functionally diverged from Cos2 and Kif7 and is no longer involved in Hh signalling in the neural tube. Interestingly, a recent study showed that mouse Fused interacts with Kif27, but not Kif7, leading the authors to propose the divergence of the two Cos orthologs (Wilson et al., 2009). This study presented the possibility that Kif27 had lost Hh-related functions and was involved in ciliogenesis in partnership with Fused. However, it remains to be determined whether Kif27 is involved in Shh signalling in other organs and to confirm these results with loss of function studies.

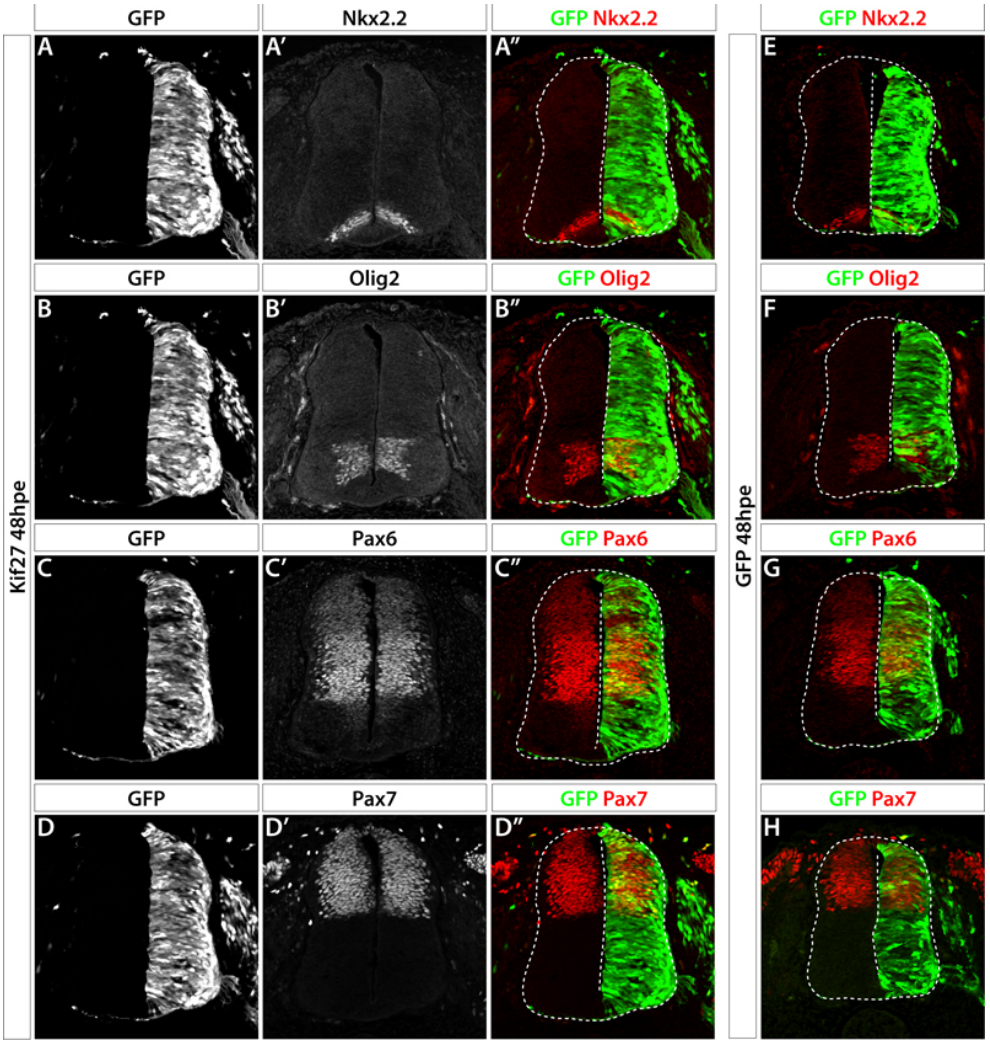

Figure 8.4 Ectopic expression of Kif27 does not alter the patterning of the neural tube. Expression of progenitor markers Nkx2.2, Olig2, Pax6 and Pax7 (red) at the brachial level of the chick neural tube 48h after transfection with pCAGGS-Kif27-IRES-GFP (GFP in green; **A-**

D") or pCAGGS-IRES-GFP (green; **E-H**). The ectopic expression of Kif27 does not affect the expression pattern of Nkx2.2 (**A-A"**), Olig2 (**B-B"**), Pax6 (**C-C"**) or Pax7 (**D-D"**), when compared to the non-electroporated side of the neural tube, or compared to embryos electroporated with GFP (**E-H"**).

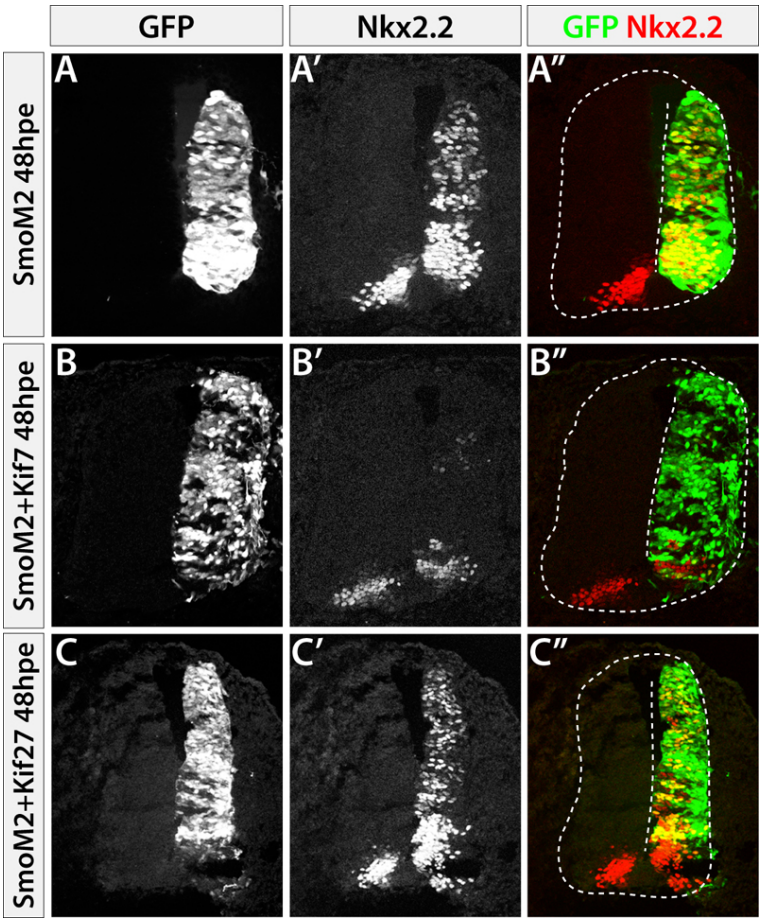

Figure 8.5 Kif27 does not block SmoM2-induced Nkx2.2 expression.

Chick neural tube transfected with pCAGGS-SmoM2 and pCAGGS-IRES-GFP (green; **A-A"**), pCAGGS-SmoM2 and pCAGGS-Kif7-IRES-GFP (green; **B-B"**) or pCAGGS-SmoM2 and pCAGGS-Kif27-IRES-GFP (green; **D-D"**) and assayed for the expression of Nkx2.2 (red) at 48hpe, at brachial level (**A-C"**). The dorsal expansion of Nkx2.2 expression following SmoM2 transfection (**A-A"**) is partially inhibited by Kif7 (**B-B"**). By contrast, Kif27 overexpression has no effect on the ectopic induction of Nkx2.2 expression by SmoM2 (**C-C"**). Experiments performed by James Briscoe.

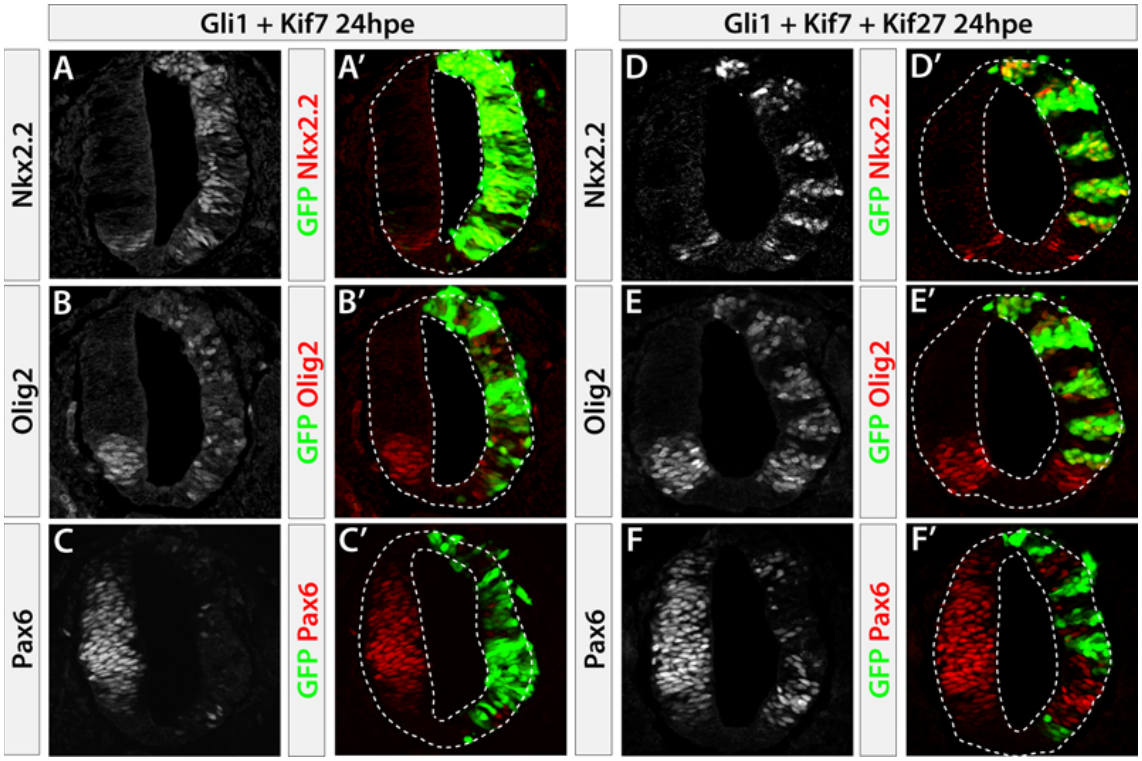

Figure 8.6 Kif7 and Kif27 do not cooperate to inhibit Gli1 overexpression.

Chick neural tube transfected with pCAGGS-Gli1-IRES-GFP and pCAGGS-Gli1-IRES-GFP (GFP in green; **A-C'**) or pCAGGS-Gli1-IRES-GFP, pCAGGS-Kif7-IRES-GFP and pCAGGS-Kif27-IRES-GFP (GFP in green; **D-F'**) and assayed for the expression of neural progenitor markers Pax6 and Pax7 (red) at 24hpe, at brachial level (**A-D"**). Kif7 overexpression is unable to block Gli1-induced ectopic Nkx2.2 (**A-A'**) and Olig2 (**B-B'**) expression. In addition Kif7 fails to inhibit Gli1-repressed Pax6 expression (**C-C'**). The inclusion of Kif27 in the transfection does alter the effect of Gli1 and Kif7 co-transfection on Nkx2.2 (**D-D'**), Olig2 (**E-E'**) and Pax6 (**F-F'**) expression.

8.3 Kif7 N-terminal domain, but not the C-terminal domain, is required for its negative role in Hedgehog signalling

The apparent divergence of Kif27 in the regulation of Shh signalling indicated that Kif7 is the functional Cos2 homolog in vertebrates. In addition, the functionality of Cos2 in a vertebrate tissue indicates that the core elements of the protein required for the regulation of the Hh pathway are conserved between the two lineages. Therefore, to gain insight into the mechanisms underlying Kif7 function it is important to establish which protein domains are essential for its activity. In Cos2 the N-terminal region has been shown to contain the motor domain (Robbins et al., 1997; Sisson et al., 1997) and the Ci binding region (Monnier et al., 2002), whereas the C-terminal domain is involved in the interaction with Smo (Ruel et al., 2003) (Figure 8.7). Mutational analysis have revealed that only the motor domain and the neck region (adjacent to the motor domain) are required for the repressive action of Cos2 on Hh targets (Ho et la., 2005). To investigate whether these regions are also necessary for Kif7 function we undertook a structure/function analysis, in which either the N-terminal region (Kif7ΔN: 674-1349 aa) or the C-terminal region (Kif7ΔC: 1-724 aa) were removed from the Kif7 sequence (engineered by C.-c. Hui and collaborators). In the event of one of these domains being dispensable, its deletion is predicted to leave Kif7 activity intact. The deletion constructs were tested in the chick neural tube. As the electroporation of wild type Kif7 by itself only affected Shh-dependent patterning in the most ventral region of the neural tube, we elected to use the SmoM2-sensitized assay. As previously described, full-length Kif7 was able to restrict the activity of SmoM2, inhibiting the induction of ectopic Nkx2.2^{+} cells in the dorsal region of the neural tube. Likewise, the Kif7ΔC construct was able to limit the activation of the pathway downstream of SmoM2, blocking the dorsal expression of Nkx2.2 (Figure 8.8 B-B″). By contrast, the deletion of the N-terminal region impaired the ability of Kif7 to counteract SmoM2, as the co-transfection of Kif7ΔN and SmoM2 resulted in a phenotype identical to the transfection of SmoM2 alone (Figure 8.8 C-C″). The expansion of the Olig2 domain following electroporation with SmoM2 was not affected by the co-transfection with either Kif7ΔC or Kif7ΔN (Figure 8.9 A-C″). The distinct results obtained with Kif7ΔC and Kif7ΔN on Smo-induced Nkx2.2 expression imply that the C-terminal domain of Kif7 is not required for its negative role whereas the N-terminal region appears to be essential.

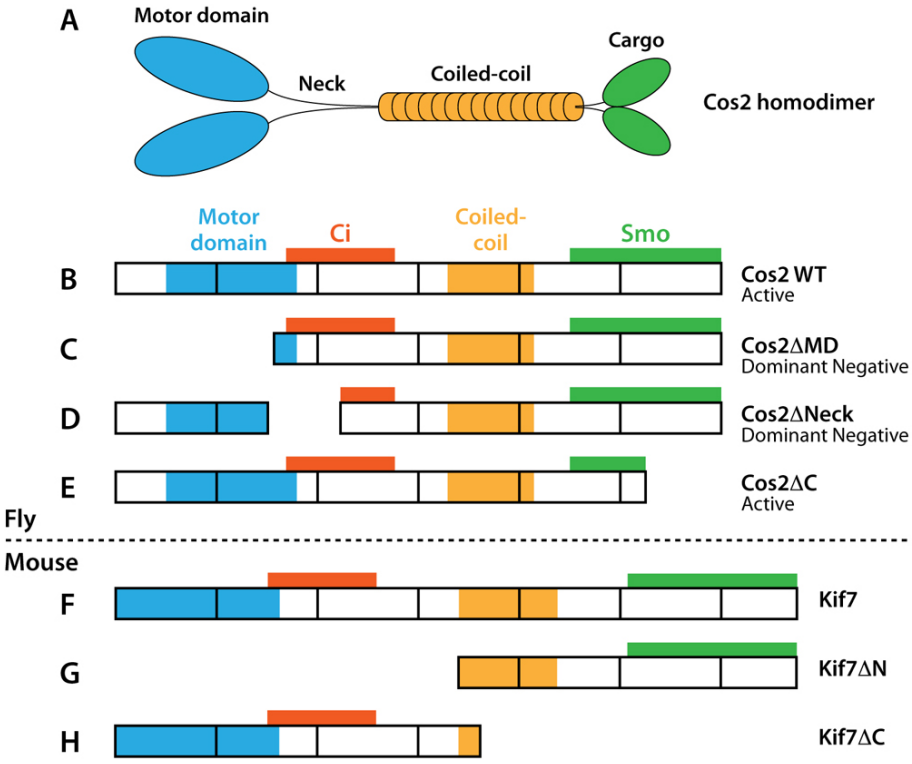

Figure 8.7 Deletion constructs of Costal2 and Kif7.

(A) Diagramatic representation of the predicted structure of a Kif7 or Cos2 homodimer (based on diagrams in Robbins et al., 1997 and Sisson et al., 1997). **(B)** Diagram of the functional domains identified in Cos2: the N-terminal motor domain (blue), the Ci binding region (red), the coiled-coil region (yellow) and the C-terminal Smo binding region (green). **(C)** The deletion of the N-terminal domain generates a dominant negative form of Cos2 (Ho et al., 2005). **(D)** The deletion of the neck region generates a dominant negative form of Cos2 (Ho et al., 2005). **(E)** The removal of the C-terminal domain does not impair the repressive activity of Cos2 (Ho et al., 2005). **(F)** Diagram of the presumptive functional domains of the mouse homolog of Cos2, Kif7. **(G)** Diagram of the Kif7ΔN construct, in which the presumptive motor domain and Gli binding region were deleted. **(H)** Diagram of the Kif7ΔC construct, in which the coiled-coil region and the cargo domain were deleted.

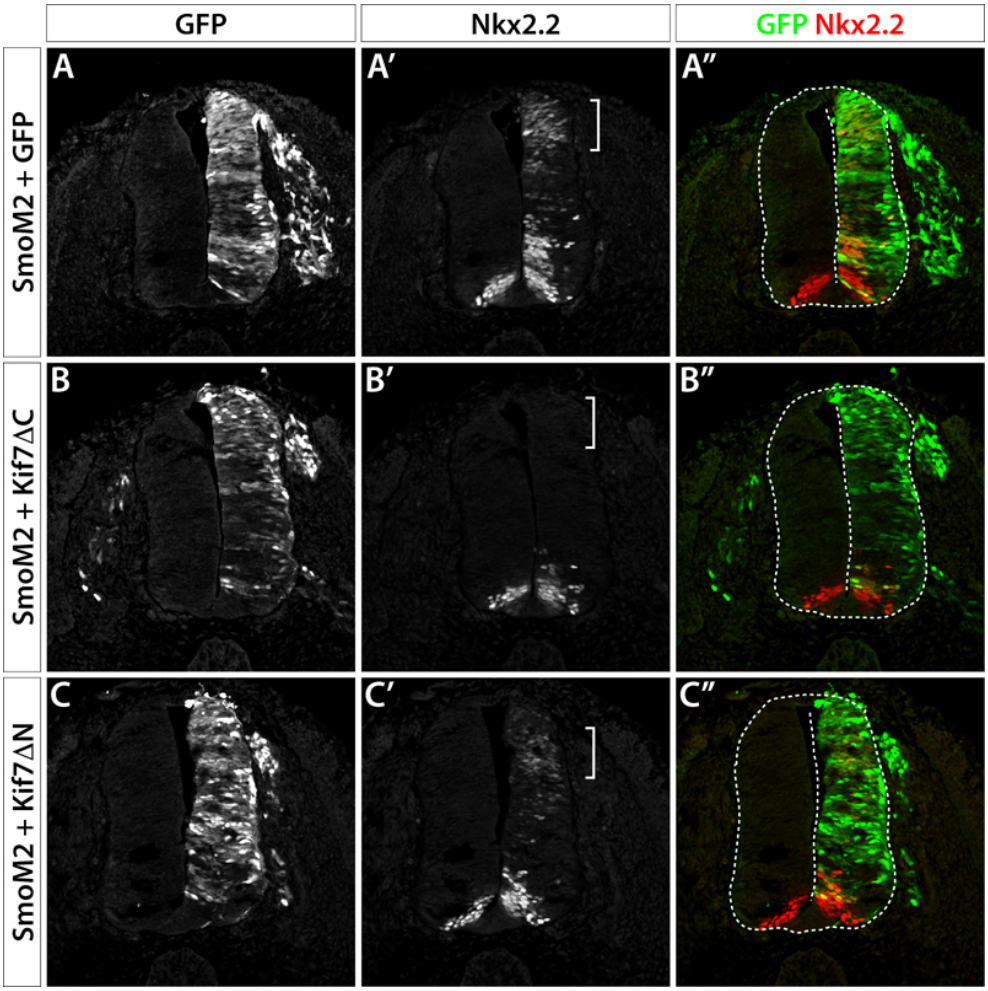

Figure 8.8 The N-terminal domain, but not the C-terminal domain, is required for the repressive activity of Kif7.

Chick neural tube transfected with pCAGGS-SmoM2 and pCAGGS-IRES-GFP (GFP in green; **A-A″**), pCAGGS-SmoM2 and pCAGGS-Kif7ΔC-IRES-GFP (GFP in green; **B-B″**) or pCAGGS-SmoM2 and pCAGGS-Kif7ΔN-IRES-GFP (GFP in green; **C-C″**) and assayed for the expression of p3 marker Nkx2.2 (red) at 48hpe, at brachial level (**A-C″**). SmoM2 transfection induces ectopic Nkx2.2 expression (white bar in **A-A″**). The deletion of the C-terminal region of Kif7 (Kif7ΔC) does not impair the ability of the protein to inhibit the ectopic expression of Nkx2.2 induced by SmoM2 (white bar in **B-B″**). By contrast, the loss of the N-terminal region disrupts the repressive activity of Kif7, as Kif7ΔN is unable to inhibit SmoM2-induced Nkx2.2 expression at dorsal positions (white bar in **C-C″**).

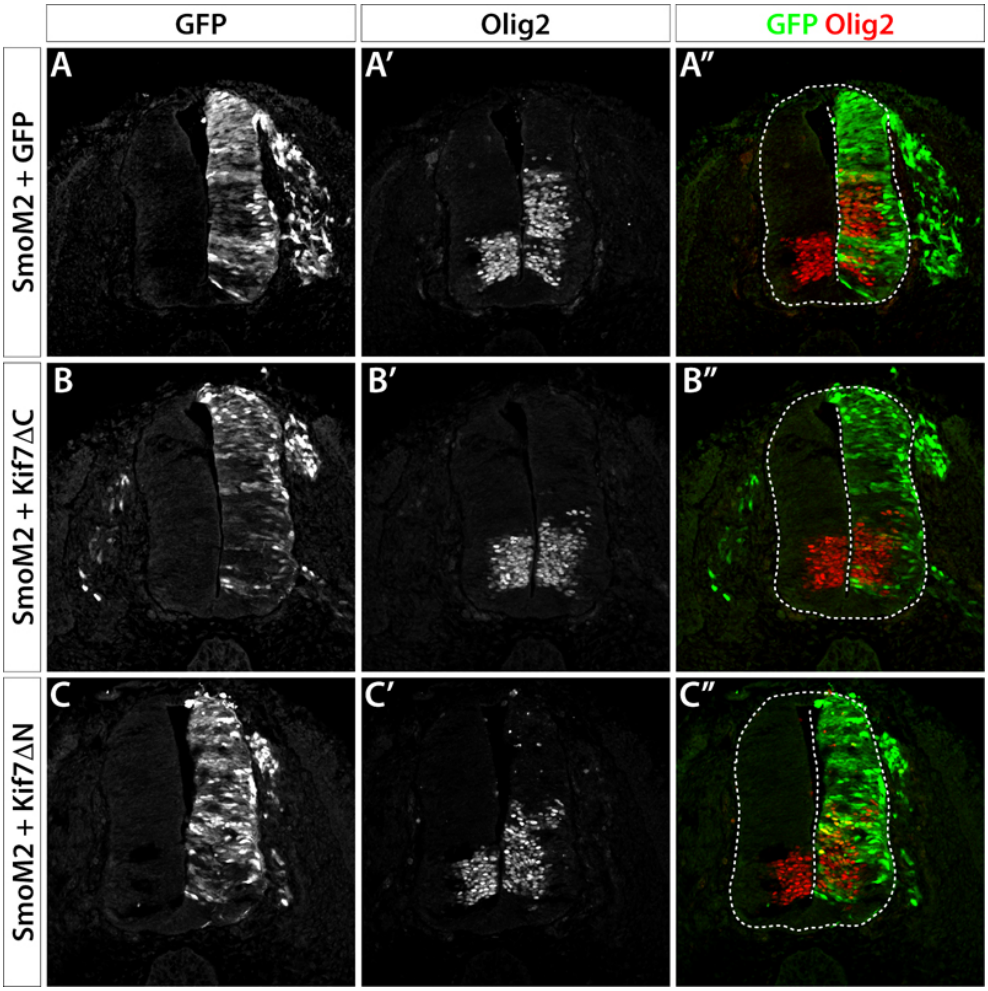

Figure 8.9 Removal of either the C-terminal or the N-terminal region of Kif7 does not affect the SmoM2-mediated induction of Olig2.

Chick neural tube transfected with pCAGGS-SmoM2 and pCAGGS-IRES-GFP (GFP in green; **A-A″**), pCAGGS-SmoM2 and pCAGGS-Kif7ΔC-IRES-GFP (GFP in green; **B-B″**) or pCAGGS-SmoM2 and pCAGGS-Kif7ΔN-IRES-GFP (GFP in green; **C-C″**) and assayed for the expression of pMN marker Olig2 (red) at 48hpe, at brachial level (**A-C″**). The induction of induced by SmoM2 (**A-A″**) is not affected by the deletion of either the C-terminal region of Kif7 (Kif7ΔC; **B-B″**) or the N-terminal region of Kif7 (Kif7ΔN; **C-C″**).

To try to determine if the motor domain structure or motor function is an essential element within the N-terminal region we tested the activity of a form of Kif7 in which motor activity is disabled (MDKif7). In this form of Kif7 the positions 99-101, GKT, were mutated to AAA. This is predicted to disrupt the "P-loop" motif involved in binding to ATP. This mutation is analogous to the S182N mutation in Drosophila, which renders Cos2 unable to repress Hh target genes and impairs its microtubule-dependent motility (Ho et al., 2005; Farzan et al., 2008). The motor domain has also been proposed to be critical for Kif7 function, as mice with a single point mutation within the motor domain of Kif7 displayed Shh phenotypes identical to Kif7-null mutant mice (Liem et al., 2009). These observations raised the possibility that inactivation of motor activity would also compromise the activity of Kif7 in our system. Surprisingly, the ability of MDKif7 to restrict Shh pathway activation in SmoM2-transfected embryos was identical to that of wild-type Kif7. In the presence of MDKif7, as with wild-type Kif7, SmoM2 was unable to promote the generation of ectopic Nkx2.2^{+} cells in the dorsal neural tube (Figure 8.10 A-B"), although the dorsal expansion of the Olig2 domain remained unaffected (Figure 8.10 C-D"). These results indicate that the motor domain of Kif7 is not essential for the inhibition of Shh signalling in the context of the chick neural tube. Consistent with this, in vitro assays also show that the motor dead form of Kif7 is still able to bind to Gli2 and to reduce Gli transcriptional activity (C.-c. Hui, personal communication).

In summary, these data confirm the conservation of Cos2 function in the vertebrate Hh signalling. This function appears to have been lost in one of the Cos2 orthologs, Kif27, suggesting that only Kif7 is involved in the regulation of Hh signalling in the neural tube. The negative role of Kif7 depends on the N-terminal domain of the protein, containing the Gli-binding site, whereas the C-terminal region and the motor domain appear to be dispensable.

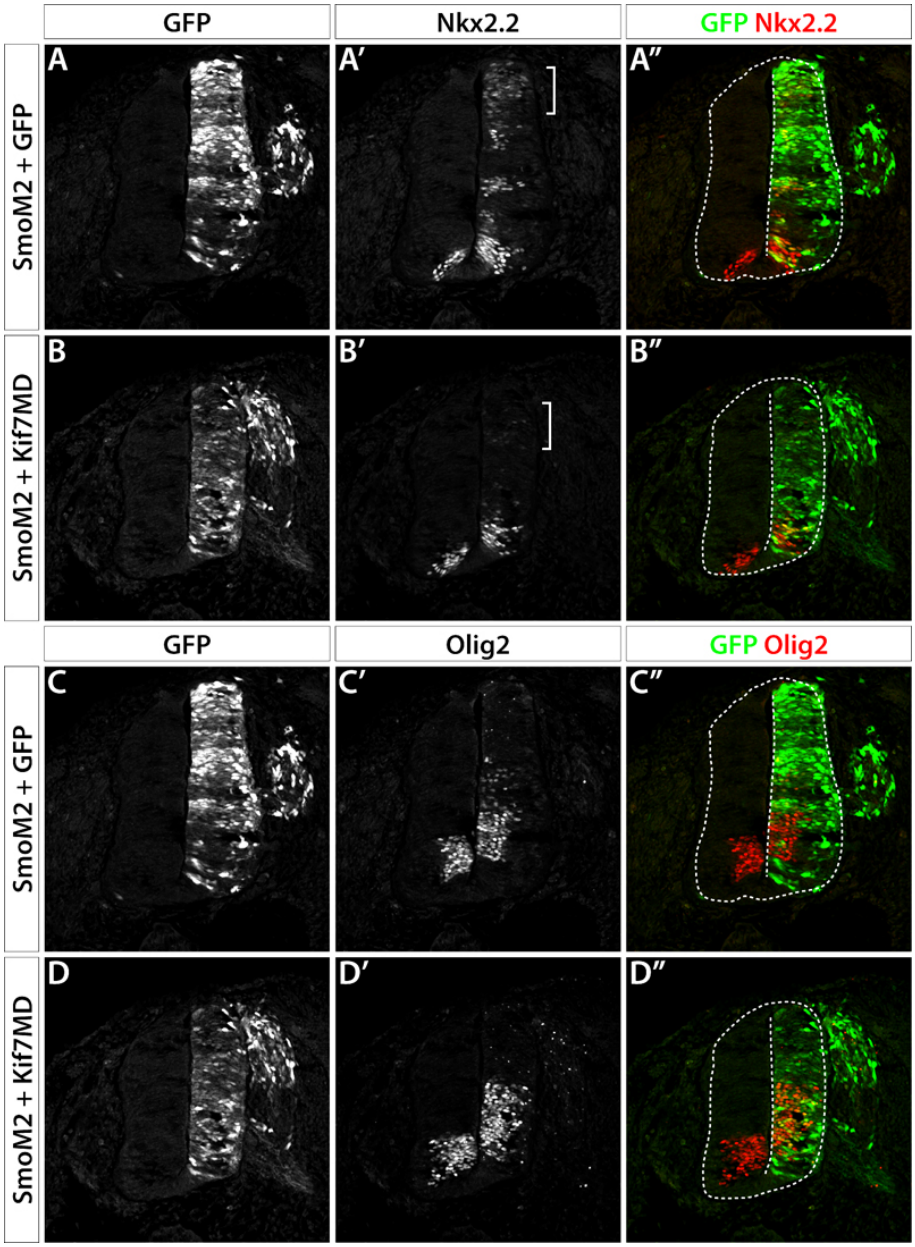

Figure 8.10 A functional motor domain is not required for the repressive activity of Kif7. Chick neural tube transfected with pCAGGS-SmoM2 and pCAGGS-IRES-GFP (GFP in green; **A-A″, C-C″**) or pCAGGS-SmoM2 and pCAGGS-Kif7MD-IRES-GFP (GFP in green; **B-B″, D-D″**) and assayed for the expression of ventral progenitor markers Nkx2.2 and Olig2 (red) at 48hpe, at brachial level (**A-D″**). The ectopic induction of Nkx2.2 domain induced by SmoM2 (**A-A″**) is blocked by the overexpression of the Kif7MD construct, in which the ATP binding site in the motor domain is disrupted (**B-B″**). By contrast, the SmoM2-induced expansion of the Olig2 domain (**C-C″**) is not affected by the ectopic expression of Kif7MD (**D-D″**).

CHAPTER 9 - DISCUSSION II

9.1 Kinesin motor protein Kif7 is a Costal2 homolog in Vertebrate Hedgehog signalling

The regulation of Hh target genes relies on the ability of the pathway to sense the levels of ligand and to trigger the appropriate transcriptional response (reviewed in Wilson and Chuang, 2010). In Drosophila the kinesin-like protein Costal2 (Cos2) has been suggested to act as a switch within the signalling complex, coordinating both the positive and the negative responses of the pathway. Cos2 differentially regulates Ci processing in a Hh dependent manner, thereby adjusting the ratio of activator to repressor Ci and subsequently the induction or repression of target genes. Until recently Costal2, like several components of the Hh pathway such as Fused and Suppressor of Fused, was thought to have functionally diverged between Drosophila and mammals (Varjosalo et al., 2006). Using in ovo electroporation of the chick neural tube to manipulate the expression of the vertebrate Cos2 orthologs we were able to demonstrate that Kif7 has functional homology to Cos2. Kif7 overexpression represses Shh-dependent Nkx2.2 expression, indicating that the inhibitory function of Cos2 is preserved in Kif7. Furthermore, Kif7 is able to counteract Smo-induced ectopic Nkx2.2 expression and elevated Gli transcriptional activity, suggesting that it acts downstream of Smo. These results have been corroborated by work done by our collaborators and others examining the effects of loss of Kif7 in mouse embryos (Cheung et al., 2009; Endoh-Yamagami et al., 2009; Liem et al., 2009).

The genetic disruption of Kif7 function in mice resulted in embryonic defects, such as polydactyly, suggestive of altered Gli3 repressor activity (Cheung et al., 2009; Endoh-Yamagami et al., 2009; Liem et al., 2009). However, Kif7 mutants were not exact phenocopies of Gli3 mutants. In particular, Kif7 mutants, unlike Gli3 mutants, displayed an expansion of Shh-dependent cell fates in the ventral neural tube. The inhibitory function of Kif7 was further demonstrated by the analysis of Smo;Kif7 double mutants. The removal of Kif7 in Smo-null embryos partially restored the formation of ventral cell types in the neural tube, suggesting that in the absence of Kif7 there is ligand-independent activation of the pathway downstream of Smo (Cheung et al., 2009; Liem et al., 2009). Moreover, Kif7 activity might require direct interaction with Smo, as Kif7 was shown to physically bind to Smo in vitro,

contradicting previous observations (Endoh-Yamagami et al., 2009; Varjosalo et al., 2006).

Although Kif7 appears to have retained Cos2 inhibitory function it is not clear if it employs similar mechanisms to regulate the pathway. The mechanism of Cos2 function involves the regulation of Ci localization/processing/degradation (Smelkinson et al., 2007; Wang et al., 2000; Wang and Jiang, 2004; Zhang et al., 2005), prompting us to investigate the effect of Kif7 on Gli proteins. In our experiments Kif7 was unable to block the proliferation and patterning defects caused by overexpression of Gli1 or Gli2 proteins. Kif7 also failed to block Gli2 entry into the nucleus. By contrast, Sufu, another negative regulator of the pathway, was able to retain Gli2 in the cytoplasm and accordingly rescue the proliferation and patterning defects caused by forced expression of Gli2.

The inability of Kif7 to counteract Gli activity in the chick neural tube was in contrast to in vitro and in vivo data obtained by others. Cell-based assays showed the direct interaction between Kif7 and Gli proteins (Cheung et al., 2009; Endoh-Yamagami et al., 2009). Moreover, the disruption of Kif7 function in mice confirmed that Kif7 is involved the regulation of Gli2 abundance and Gli3 proteolysis (Cheung et al., 2009; Liem et al., 2009). These data suggested that the mode of action of Cos2 is at least partially conserved in Kif7, in that both proteins mediate the processing and degradation of the Hh pathway transcriptional effectors Ci/Gli.

The reason for the discrepancy between the loss-of-function results in mouse and the gain-of-function results in chick is unclear. Although loss of Kif7 affected the levels and activity of Gli proteins, an excess of Kif7 had no effect on the activity of ectopic Gli proteins. The inability of Kif7 to promote the exclusion of Gli proteins from the nucleus could indicate that Kif7 function, in contrast to Cos2, does not involve regulation of the localization of Gli proteins. However, this result could reflect an inefficient interaction or imbalance in the ratio between the Kif7 and Gli constructs when overexpressed in the neural tube. It is also possible that the forms of Gli proteins used in this study are refractory to processing and degradation and therefore resistant to Kif7 activity. This hypothesis could be tested by assaying the effect of Kif7 on other Gli constructs. Alternatively, the activity of Kif7 might rely on other, limiting, components and Kif7 is unable to counteract the excess of Gli proteins when overexpressed on its own. To test if Kif7 is able to inhibit lower levels

of Gli proteins other expression vectors that generate lower levels of the encoded protein could be used.

The analysis of the Kif7 mutants demonstrated that Kif7 also has a positive role in Shh signalling. This reinforces the functional homology between Kif7 and Cos2 (Cheung et al., 2009; Liem et al., 2009). Kif7 is required for the maximal activation of the pathway observed in Ptch1$^{-/-}$ mice, as the ectopic expression of Foxa2 and Nkx2.2 was reduced in Ptch1;Kif7 double mutants (Liem et al., 2009). Furthermore, floor plate induction, a process reliant on high Gli activity, was impaired in Kif7 mutants when one copy of Gli2 was removed (Cheung et al., 2009). These data confirm that Kif7 is involved in the transduction of both positive and negative inputs. In addition, these data might offer an explanation for the limited effect of Kif7 on ectopically expressed Gli proteins. High levels of Kif7 might be insufficient to inhibit ectopic Gli proteins, as additional changes in the pathway are involved in regulating Kif7 activity.

The dual role of Kif7 in Shh pathway regulation raises the question of how Kif7 activity changes in response to Shh levels and how it contributes to opposing outcomes. In Drosophila, the transition of Cos2 function from repressive to activating is associated with the Hh-dependent modulation of other components of the intracellular signalling complex, such as Smo, Fu, PKA, CKI and GSK3 (Liu et al., 2007; Smelkinson et al., 2007; Zhang et al., 2005). Changing levels of Hh result in the dynamic interaction between components of the complex and, subsequently, in the differential regulation of Ci activity. A similar mechanism might be in action in vertebrates, although the composition of the signalling complex might differ. The modulation of Kif7 activity might also be associated with its ciliary distribution, where other components of the pathway are also detected (Chen et al., 2009; Corbit et al., 2005; Endoh-Yamagami et al., 2009; Haycraft et al., 2005; Liem et al., 2009); Rohatgi et al., 2007). Our analysis of the distribution of a Flag-tagged form of Kif7 showed that Kif7 is present in cilia in the neural tube. Other studies confirmed the ciliary localization of Kif7-GFP in cultured cells, and further showed that the distribution of Kif7 in response to Shh is dynamic within the cilium (Endoh-Yamagami et al., 2009; Liem et al., 2009). The ciliary position of Kif7-GFP, predominantly basal in control conditions, shifted towards the tip in the presence of Shh or Smoothened agonist (SAG). The apical enrichment of Kif7 in cilia depended on Smo and, in turn,

Kif7 was required for the Shh-induced accumulation of Gli2 and Gli3 in the tip of cilia, in accordance with the role of Kif7 downstream of Smo and upstream of Gli proteins (Endoh-Yamagami et al., 2009). The distinct subcellular localization triggered by changing levels of Shh could enable Kif7 to modulate distinct processes. In the absence of Shh Kif7 might promote Gli proteolysis at the base of cilia. Upon Hh stimulation, the trafficking of the Kif7 and Gli complex towards the tip of cilia might allow the binding to Smo and activation of full-length Gli factors.

Consistent with this model, PKA is found at the base of cilia in the absence of Shh (Barzi et al., 2010), where it has been proposed to promote the removal of Gli2 and Gli3 from cilia (Tukachinsky et al., 2010; Wen et al., 2010; Zeng et al., 2010) and possibly target them to the proteasome. PKA activity also antagonizes SUMOylaton of full-length Gli2 and Gli3, a post-translational modification proposed to increase Gli transcriptional activity (Cox et al., 2010). In the presence of Hh PKA activity is inhibited, allowing Gli proteins to accumulate in cilia. Whether Gli SUMOylation occurs before or after Gli translocation to the tip of cilia is currently unknown. One possibility is that when Shh is absent Kif7 is associated with PKA at the base of the cilium and facilitates the PKA-mediated phosphorylation of full-length Gli proteins, which are subsequently targeted to the proteasome. However, a recent study suggested that the role of PKA in the regulation of Gli proteins in vertebrates might be independent of phosphorylation (Zeng et al., 2010). In cells exposed to Shh, Smo accumulates at the tip of cilia and drives the equivalent movement of Kif7 (Endoh-Yamagami et al., 2009), a process proposed to disrupt the interaction between Kif7 and PKA, resulting in diminished PKA-mediated Gli processing and degradation and enhanced Gli SUMOylation. However, further studies are required to investigate the relation between Kif7 and PKA (and other kinases that might be involved in Gli regulation), and how the ciliary localization of these proteins influences their activity. Intriguingly, in our analysis of Kif7 distribution, Kif7-Flag was found both at the base and at the tip of cilia. Whether this observation is related with the ability of Kif7 to transduce both positive and negative inputs is unclear. The dual ciliary localization of ectopic Kif7 could contribute to its neutral effect on Gli proteins in the chick neural tube.

Although Kif7 appears to be required for the maximal response of cells to Shh by establishing a bridge between activated Smo and Gli proteins, Kif7 is not required for the activation of the pathway in the presence of sub-maximal levels of Shh.

Therefore, other mechanisms must be involved in the positive regulation of Gli transcriptional activity. It is possible that the anterograde movement of Gli proteins within cilia occurs even in the absence of Kif7, allowing the formation of Gli activator forms. However, studies that address the role of other kinesins, such as Kif3A/3B and KAP3, in the anterograde transport of Gli proteins have been complicated by the fact that in the absence of these proteins cilia do not form (Huangfu et al., 2006; Marszalek et al., 1999). Thus, further studies are required to understand the mechanisms underlying the formation of Gli activator within cilia.

In summary, the data obtained by ours and other groups uncovered both conserved and divergent aspects of Cos2 function in its vertebrate homolog Kif7. Like Cos2, Kif7 has a strong influence on the inhibitory branch of the pathway and appears to regulate the levels of Gli activator to Gli repressor. Kif7 is also required for the formation of cell types that depend on the maximal activation of the pathway, reflecting the conservation of a positive function. However, Kif7 has diverged, at least in part, in the mode of action, as Kif7 requires cilia function to regulate Hh signal transduction, unlike its Drosophila counterpart.

9.2 Functional domains of Kif7 in Hedgehog signalling

Although Cos2 and Kif7 show clear functional similarities, the distinct subcellular distribution and association with cilia suggest mechanistic differences. This prompted us to explore the mechanisms underlying Kif7 negative function. We demonstrated the ability of Cos2 to interfere with the transduction of the vertebrate Shh pathway, implying that key domains in Kif7 are conserved in the fly homolog. Remarkably, Cos2 overexpression had a stronger impact on Shh signalling than Kif7. Cos2 repressed the expression of Shh-induced markers Nkx2.2 and Olig2 in the ventral neural tube, while Kif7 only blocked Nkx2.2 expression. Furthermore, Cos2 promoted the ectopic expression of Shh-repressed dorsal markers Pax6 and Pax7. Likewise, Cos2 was able to block the SmoM2 patterning phenotype in the neural tube more efficiently than Kif7. These results offer an interesting perspective on the homology between Cos2 and Kif7.

First, the functionality of Cos2 in a vertebrate system provides a starting point for the dissection of the inhibitory function of Kif7. In Drosophila the repressive activity of Cos2 is thought to involve the assembly of a complex containing the kinases PKA, CKI, GSK3 and Ci. Within this complex, the proteolysis of Ci into its repressor form is thought to be promoted. As these kinases are conserved in mammals and have been shown to mediate Gli processing through phosphorylation (Pan et al., 2006), it is possible that Kif7 also promotes the interaction between kinases and Gli proteins. Cos2 additionally prevents Ci accumulation in the nucleus by tethering the transcription factor in the cytoplasm (Wang et al., 2000; Wang and Jiang, 2004). While it is possible that this property also applies to Gli proteins in a vertebrate context, our analysis of Gli2 distribution following Kif7 overexpression failed to show the nuclear exclusion of Gli2 (see above). However, this result might be inconclusive, since we were only able to test Kif7 activity on ectopic Gli2, which was expressed in abnormally high levels. In addition, it is possible that the Gli constructs used in this assay are insensitive to Kif7-mediated regulation.

Second, the ability of Cos2 to impair Shh signalling raises questions about the role of cilia and ciliary localization. We were unable to assess the distribution of Cos2 in the chick neural tube and therefore cannot exclude the possibility that Cos2 is able to localize to cilia. But, plausibly Cos2 remains cytoplasmic and it is here that it performs its inhibitory role. This result raises the possibility that the ciliary localization is not required for Kif7 negative activity. However, in physiological conditions the association with cilia might facilitate the regulatory interactions between the different components of the Shh pathway.

Finally, the enhanced impact of Cos2 overexpression has on vertebrate Shh signalling when compared with Kif7 points to some degree of mechanistic divergence between the two lineages. Although at present the specific differences between the two proteins are still unclear, we can speculate on what might cause the strengthened activity of Cos2. One possibility is that Kif7 is under the control of a regulatory mechanism to which Cos2 is insensitive. Conceivably, such difference could derive from the vertebrate-specific role of cilia. Alternatively, Kif7 might have lost some of the mechanisms used by Cos2. For example, if Cos2 proves to be able to retain Gli proteins in the cytoplasm while Kif7 is not, this could confer an additional level of regulation to Cos2 and explain its stronger impact on the repression of Shh target genes.

To further investigate the similarities between Cos2 and Kif7 and to begin to identify the key elements in Kif7 we deleted presumptive functional domains within the vertebrate protein. This approach disclosed a parallel between the two proteins regarding the domains required for the inhibition of the pathway. The removal of the N-terminal region in Kif7 rendered it incapable of restricting the ectopic activation of the pathway downstream of Smo. This result mirrors the equivalent deletion in Cos2, where the loss of either the motor domain or the neck within the N-region disrupted the ability of the protein to repress Hh target genes (Jia et al., 2003; Ho et al., 2005). The comparable findings support the hypothesis that the N-terminal region of Kif7 contains essential Cos2-like domains, such as the motor domain and the binding sites for Gli proteins and kinases PKA, CKI and GSK3. Thus, these results provide a starting point for the investigation of the mechanistic properties of Kif7.

Importantly, the functional conservation of the N-terminal domain does not mean that motor function is required for Kif7 activity. Indeed, mutation of the ATP binding site within the motor domain of Kif7, which is predicted to inactivate motor function, did not affect the inhibitory activity of Kif7 downstream of Smo. One possibility is that the functionality of the motor dead form of Kif7 might result from overexpression and excess availability of the protein. Nevertheless, this result suggests that other elements of Kif7 might be more relevant, and that ciliary localization is not essential for function. Supporting this hypothesis, work by our collaborators (C.-c. Hui) showed that the loss of function of Kif7ΔN was accompanied by the inability to bind to Gli, whereas motor dead Kif7 retained the binding to Gli. However, these findings contradict the analysis of a Kif7 mouse mutant, containing a point mutation (L130P) within the motor domain, which appears to lose all Kif7 function (Liem et al., 2009). Although presently we cannot explain this discrepancy, one possibility is that the L130P mutation causes a disruption in the conformation of the protein, thereby affecting its binding to other proteins. Consistent with this hypothesis, a preliminary model of the protein structure of Kif7 predicted that the L130P mutation would disrupt the helix α2 of the protein (J. Saldanha, personal communication). However, it is unclear whether the disruption of this region would affect the overall conformation of the protein. The L130P mutation was also shown to block the ability of Kif7 to translocate to the tip of cilia (Liem et al., 2009). Therefore it is also possible that the motor activity of Kif7 is involved in cilia-dependent regulatory mechanisms.

The role of the C-terminal cargo domain of Kif7 was also investigated. In Cos2 the cargo domain is dispensable for its repressive activity, but is involved in the interaction with Smo during the maximal activation of the pathway (Ho et al., 2005; Jia et al., 2003; Lum et al., 2003b). Likewise, our analysis showed that the loss of the C-terminal region of Kif7 did not impair its inhibitory effect on Smo-induced ventralization of the chick neural tube. This result indicates that in vertebrates, as in Drosophila, the binding between Smo and the cargo domain of Kif7 is not required for the repressive activity of Kif7. However, it is possible that other regions of Kif7 are involved in Smo binding in the absence of Shh and further studies are required to assess this possibility.

Although this work suggests that some domains are not required for Kif7 activity, it is important to note that these assays only assess the role of the distinct Kif7 domains in the negative response of the pathway. Therefore, it is plausible that the domains shown to be dispensable for the inhibition of the pathway, namely the cargo domain and the ATP-binding site, might be required for the positive regulation of the Shh target genes. Consistent with this hypothesis, immunoprecipitation studies showed that Kif7 is able to bind to the different regions of Smo (Endoh-Yamagami et al., 2009). Kif7 binds not only to full-length Smo, but also to isolated C-terminal tail of Smo, as well as a form of Smo without the C-tail (Endoh-Yamagami et al., 2009, supplementary data). The multiple Kif7 binding sites are reminiscent of the binding of Cos2 to different regions of Smo depending on the Hh-state of the cell (Lum et al., 2003b; Jia et al., 2003). These findings raise the possibility that that Kif7, like Cos2, mediates the transition between the repressed and the activated state of the pathway by binding to alternative regions of Smo and possibly allowing Smo to interact with different proteins depending on the level of Hh. However, whether distinct regions of Kif7 are involved in the dynamic binding to Smo in response to Shh remains to be determined. In addition, further studies using loss of function assays are required to identify more accurately the positive elements within the protein structure of Kif7.

These data support a switch-like function for Kif7, in which the differential activity of Kif7 coordinates the positive and negative response of the pathway. However, it is still unclear how the differential activity of Kif7 is regulated. In Drosophila, Cos2 is phosphorylated by Fused (Fu) in the presence of Hh, an event

that promotes Cos2 dissociation from the membrane proximal region of Smo and allows Smo phosphorylation (Liu et al., 2007). Smo phosphorylation results in conformational changes that allow the subsequent re-association of Cos2 to the C-terminal domain of Smo and downstream activation of the pathway via formation of CiA. Although it is possible that phosphorylation of Kif7 also drives its dynamic binding to Smo, it is unlikely that this process depends on Fu. The targeted disruption of mouse Fused does not yield any Hh-related phenotype, thus excluding Fu as the kinase involved in the regulation of Kif7 (Chen et al., 2005; Merchant et al., 2005; Wilson et al., 2009a). If Kif7 activity is indeed mediated through phosphorylation, it might depend on other kinases shown to influence Gli activity, such as Cdc2l1, DYRK2 and Ulk3, (Evangelista et al., 2008; Varjosalo et al., 2008; Maloverjan et al., 2010). However, additional work is needed to address the presumptive role of phosphorylation in Kif7 activity and to identify the kinases involved. Alternatively (or additionally), the differential activity of Kif7 might be a consequence of its dynamic localization within primary cilia (see above; Endoh-Yamagami et al., 2009; Liem et al., 2009). It is also possible that Kif7 activity is associated with the regulation of Sufu activity. In the absence of Shh Sufu retains full-length Gli proteins in the cytoplasm (Humke et al., 2010; Svard et al., 2006) and Kif7 might cooperate with Sufu in this process. In Shh-exposed cells Gli-Sufu complexes are detected in cilia (Tukachinsky et al., 2010; Zeng et al., 2010), where the two proteins are proposed to dissociate, allowing Gli proteins to translocate to the nucleus. Kif7, which is suggested to be required for the ciliary accumulation of Gli proteins (Endoh-Yamagami et al., 2009), might also incorporate the Gli-Sufu complex that moves into cilia. A better understanding of the relationship between Kif7 and Sufu will help clarify the mechanism of action of these Shh pathway regulators.

Consistent with the dispensability of Fu for mammalian Hh pathway, a recent study described the absence of physical interaction between Fu and Kif7 (Wilson et al., 2009b). Remarkably, Fu was able to bind to the other Cos2 ortholog, Kif27. Moreover, Kif27 associated to the basal body of motile cilia, prompting the authors to propose a model in which Kif27 cooperates with Fu to regulate the assembly of motile cilia (Wilson et al., 2009b). Consistent with this model, our analysis of Kif27 function in the chick neural tube suggests that Kif27 is not involved in Shh signalling.

The analysis of Fu in the fly and vertebrate lineages has revealed a progressive functional divergence, with an Hh-related role in Drosophila, a dual role in Hh signalling and motile ciliogenesis in zebrafish, and a role in ciliogenesis only in higher vertebrates (Alves et al., 1998; Chen et al., 2005; Merchant et al., 2005; Therond et al., 1999; Wilson et al., 2009b; Wolff et al., 2003). The Kif7/Kif27 data argue for a complementing process during Cos2 evolution, culminating in a duplication event in higher vertebrates. Cos2 associates with Fu to regulate Hh signalling in Drosophila. The single Cos2 homolog in zebrafish, zKif7, is required for both Fu-regulated processes, Hh signalling and motile cilia assembly. In higher vertebrate lineages the two Cos2 orthologs, presumably arising through gene duplication, exhibit distinct functions. Kif7, like Sufu, is dedicated to the regulation of the Shh pathway, whereas Kif27 retains its association with Fu and is conceivably involved in motile ciliogenesis. A better understanding of the mechanisms of action of Kif7 and Kif27 will provide insight into how they acquired their exclusive functions and what are their distinguishing features.

9.3 Conclusions and future work

The data presented in this study demonstrate the conservation of a Cos2-like function in higher vertebrates, in the form of the Cos2 homolog Kif7. Moreover, an increasing body of work dedicated to the study of Kif7 function is starting to provide insight into the mechanism of action of Kif7. This and other studies propose a model for vertebrate Hh signal transduction that relies on Kif7 activity to coordinate the response of the pathway to both negative and positive inputs (Figure 9.1).

In this model, in the absence of Shh Kif7 inhibits Gli activity downstream of Smo, likely by promoting the proteolytic processing and degradation of full-length Gli proteins (Figure 9.1 A). At present it is still unclear how Kif7 mediates Gli processing and degradation, but it is tempting to hypothesize that Kif7, in a Cos2-like fashion, facilitates the interaction of full-length Gli proteins with particular kinases, such as PKA, CKI and GSK3, resulting in their phosphorylation. Phosphorylated Gli proteins would then be recognized by β-TrCP and subsequently targeted to the proteasome. Once in the proteasome, full-length Gli proteins might be completely

degraded (Gli2) or partially processed to generate a Gli repressor form (Gli3). Gli repressor forms might then translocate to the nucleus and repress the transcription of Shh target genes.

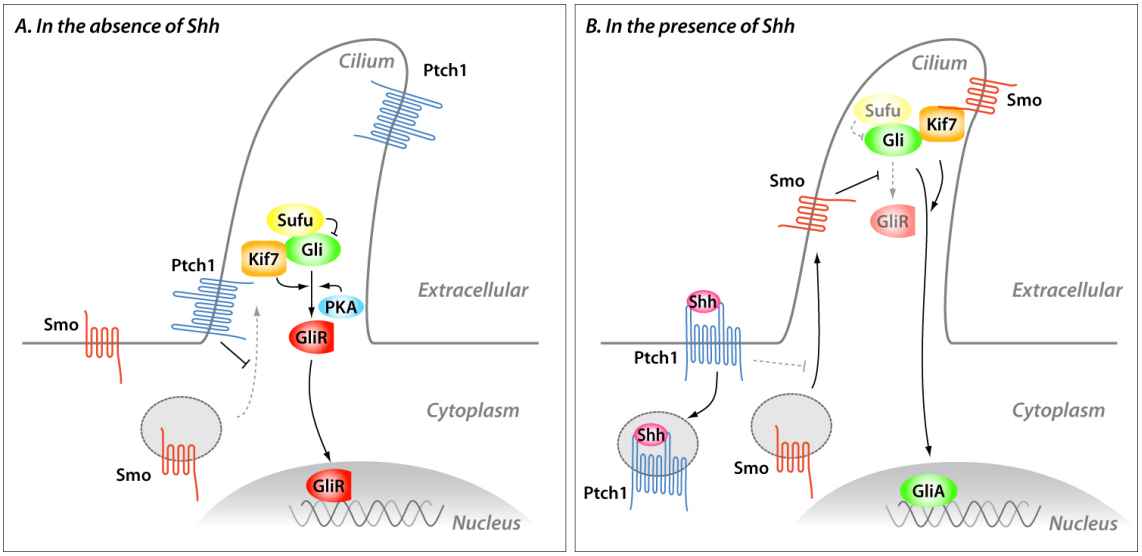

Figure 9.1 A model for vertebrate Shh signal transduction.

Scheme of the Shh signal transduction in vertebrates in the absence (**A**) and presence (**B**) of Shh. In the absence of the ligand Patched1 (Ptch1) represses the activity of Smo (A). In cells exposed to the ligand, Ptch1 is bound by Shh and the inhibition of Smo is relieved (B). The repressive activity of Ptch1 has been proposed to be associated with the transport of small molecules that modulate Smo activity (Bijlsma et al., 2006; Corcoran and Scott, 2006; Dwyer et al., 2007). The activity of Ptch1 and Smo is also possibly regulated by their dynamic subcellular localization. In the absence of Shh Ptch1 is enriched in cilia (Rohatgi et al., 2007) (A). Upon Shh binding Ptch1 exits the cilium and is internalized, allowing Smo to translocate from lateral membranes and internal pools and enter the cilium (Milenkovic et al., 2009; Rohatgi et al., 2007; Wang et al., 2009) (B). In Smo-inactive cells full-length Gli proteins are either degraded or processed into Gli repressor forms. Several factors have been proposed to contribute for Gli regulation in the absence of Shh: phosphorylation- and ubiquitinylation-mediated processing and degradation and cytoplasmic tethering of Gli proteins (A). PKA-dependent phosphorylation primes full-length Gli proteins for CKI and GSK3 phosphorylation and subsequent β-TrCP-mediated ubiquitination and targeting to the proteasome (Pan et al., 2006). PKA also inhibits SUMOylation of full-length Gli proteins, a process that enhances Gli transcriptional activity (Cox et al., 2010). In addition, Gli proteins are recognized by SPOP, which promotes ubiquitinylation by Cul3-E3, followed by complete degradation of Gli proteins (Zhang et al., 2006b; Zhang et al., 2009). Sufu has been proposed

to inhibit the translocation of full-length Gli proteins into the nucleus (Chen et al., 2009; Humke et al., 2010; Svard et al., 2006). Furthermore, Sufu appears to antagonize SPOP, preventing the degradation of Gli proteins (Chen et al., 2009). The mechanism of action of Kif7 in the absence of Shh is still unclear, but possibly Kif7 promotes the interaction between Gli proteins and PKA and/or cooperates with Sufu to retain Gli proteins in the cytoplasm. Proteolytically processed Gli proteins (mostly Gli3) traffic to the nucleus, where they act as transcriptional repressors of Shh target genes (Persson et al., 2002) (A). In Smo-active cells, the accumulation of Smo in cilia is paralleled by the movement of Kif7, Sufu and full-length Gli proteins to the tip of cilia (Endoh-Yamagami et al., 2009; Haycraft et al., 2005; Liem et al., 2009; Tukachinsky et al., 2010) (B). The translocation of Gli proteins from the base to the tip of cilia possibly inhibits PKA-mediated processing and/or degradation and enables Gli SUMOylation. In addition, the transport of Gli-Sufu complexes to the tip of cilia is proposed to result in the dissociation of the complex, allowing full-length Gli proteins to translocate to the nucleus (Tukachinsky et al., 2010). Kif7 might play a role in these processes by transporting Gli proteins (and other pathway components) towards the tip of the cilium. Kif7 might also establish a bridge between active Smo and other components of the signalling complex, promoting the formation of Gli activator forms. Fully active Gli proteins translocate to the nucleus and activate the expression of Shh target genes (Barnfield et al., 2005; Merchant et al., 2004; Pan et al., 2006).

Upon Shh exposure, Kif7 activity is required for the full activation of the pathway (Cheung et al., 2009; Liem et al., 2009) (Figure 9.1 B). This function might involve the inhibition of full-length Gli processing and degradation, for example by preventing Gli phosphorylation and targeting to the proteasome. Kif7 might also promote the full activation of full-length Gli proteins, a process not well understood that likely involves post-translational modifications. The role of Kif7 in the activation of the pathway appears to be closely related with its ciliary localization (Endoh-Yamagami et al., 2009; Liem et al., 2009). In the presence of Shh, the repressive activity of Ptch1 on Smo is removed, allowing Smo to enter the primary cilium (Milenkovic et al., 2009; Rohatgi et al., 2007; Wang et al., 2009). Smo promotes the translocation of Kif7 to the tip of cilia, which then drives the accumulation of Gli proteins at the ciliary tip (Endoh-Yamagami et al., 2009). The motor activity of Kif7 appears to be necessary for its movement to the cilium tip (Liem et al., 2009), raising the possibility that Kif7 acts as a kinesin to carry Gli proteins within the cilium.

Although the dynamic ciliary localization of Kif7 in response to Shh suggests that the kinesin-like activity of Kif7 might be important for its positive role in Shh signal transduction (Endoh-Yamagami et al., 2009; Liem et al., 2009), further work is needed to determine whether motor activity is required for the inhibitory function of Kif7. The efficient inhibition of the pathway by a motor dead form of Kif7, as well as by the cilia-independent Drosophila homolog Cos2, raise the possibility that the movement of Kif7 within cilia is not required to drive Gli processing and degradation in the absence of Shh. This possibility is consistent with a model in which Kif7 coordinates the negative response of the pathway at the base of cilia. However, the phenotype of the L130P mutation in the mouse Kif7 motor domain argues against this model (Liem et al., 2009). It will be interesting to examine whether the motor dead form of Kif7 is excluded from the tip of cilia, but retains the basal localization. In addition, the visualization of the endogenous Kif7 protein using antibody staining might also reveal differences in the ciliary distribution of the protein along the dorsoventral axis of the neural tube, in which the position of a cell reflects the level of exposure to Shh. A bias in the basal-to-tip localization of Kif7 in cells exposed to lower versus higher levels of Shh would indicate that the localization of Kif7 within the cilium is associated with the activation state of the cell in a functionally relevant system. To address the functional relevance of the ciliary localization of Kif7 for its repressive role it will also be useful to examine whether ectopically expressed Cos2, which has repressive activity in the chick neural tube, fails to localize in cilia.

To understand the inhibitory function of Kif7 it will also be important to address the mechanisms underlying Gli proteolytic processing and/or degradation, and namely, to determine whether Kif7 cooperates with the kinases PKA, CKI and GSK3 in this process. For this, we propose to investigate whether Kif7 enhances the inhibitory activity of constitutively active PKA ectopically expressed in the chick neural tube. It will also be interesting to assess whether Kif7 inhibitory function in vivo requires PKA activity, either by making use of a dominant negative form of PKA or by using PKA inhibitor compounds.

Kif7 might also be involved in the tethering of full-length Gli proteins to the cytoplasm, even though our data failed to show the cytoplasmic retention of Gli proteins by Kif7. One possibility is that Kif7 cooperates with Sufu to prevent the translocation of full-length Gli proteins to the nucleus. Future experiments will aim to address the synergy between Kif7 and Sufu by analyzing the inhibitory effect of Kif7/

Sufu co-expression on the ectopic Gli phenotype. Although Sufu overexpression resulted in the near complete rescue of ectopic Gli1 and Gli2 phenotype, it is possible that the additional expression of Kif7 would further inhibit Gli activity.

It will also be of value to investigate the association between Kif7 and the SUMO E3 ligase Pias1 and whether Kif7 is involved in blocking or enhancing Pias1-mediated SUMOylation of full-length Gli proteins. Pias1 overexpression in the chick neural tube induces ectopic Nkx2.2 expression and it will interesting to determine whether this phenotype is affected by co-expression of Kif7.

This work has also uncovered the functional divergence of Kif27 in Shh signalling. This finding suggests that the two Cos2 homologs Kif7 and Kif27 have acquired distinct functions in vertebrate development. In vitro studies by Wilson et al., have additionally proposed that Kif27 cooperates with Fused to regulate motile cilia assembly in higher vertebrates (Wilson et al., 2009b). The possibility that Kif27 is not involved in Shh signalling in the neural tube and other organs is currently being examined by our collaborator C.-c. Hui, using genetically engineered Kif27 mutant mice. The presumptive divergence of Kif7 and Kif27 raises the question of what accounts for their role in distinct processes, given their sequence similarity. The inability of ectopic Kif27 to counteract SmoM2 activity in the neural tube suggests that the differential activity of the two homologs is not simply dependent on the expression in different cell types. It is possible that specific functional domains have diverged in Kif27, impairing its interaction with other components of the Shh signalling pathway. Future experiments using recombinant constructs combining domains of Kif7 and Kif27 will allow us to assess the differences between the two proteins and the role of the different domains. Similar experiments combining Cos2 domains will also be useful to understand what determines the similarities and the differences between these related proteins. These experiments will help gain insight into the mechanisms underlying Kif7 function and further our understanding of the evolutionary conservation of Hh signalling pathway.

References

Agius, E., Soukkarieh, C., Danesin, C., Kan, P., Takebayashi, H., Soula, C. and Cocharda, P. (2004). Converse control of oligodendrocyte and astrocyte lineage development by Sonic hedgehog in the chick spinal cord. Developmental Biology 270, 308–321.

Ahn, S., and Joyner, A.L. (2004). Dynamic changes in the response of cells to positive hedgehog signaling during mouse limb patterning. Cell 118, 505-516.

Akiyama, H., Shigeno, C., Hiraki, Y., Shukunami, C., Kohno, H., Akagi, M., Konishi, J., and Nakamura, T. (1997). Cloning of a mouse smoothened cDNA and expression patterns of hedgehog signalling molecules during chondrogenesis and cartilage differentiation in clonal mouse EC cells, ATDC5. Biochem Biophys Res Commun. 235, 142-147.

Albright, T. D., Jessell, T. M., Kandell, E. R. and Posner, M. I. (2001). Progress in the neural sciences in the the century after Cajal (and the mysteries that remain). Ann N Y Acad Sci. 929, 11-40.

Allen, B. L., Tenzen, T. and McMahon, A. P. (2007). The Hedgehog-binding proteins Gas1 and Cdo cooperate to positively regulate Shh signaling during mouse development. Genes Dev. 21, 1244-1257.

Alves, G., Limbourg-Bouchon, B., Tricoire, H., Brissard-Zahraoui, J., Lamour-Isnard, C., and Busson, D.. (1998). Modulation of Hedgehog target gene expression by the Fused serine-threonine kinase in wing imaginal discs. Mech. Dev. 78, 17–31.

Amanai, K. and Jiang, J. (2001). Distinct roles of Central missing and Dispatched in sending the Hedgehog signal. Development 128, 5119-27.

Arber, S., Han, B., Mendelsohn, M., Smith, J., Jessell, T. M. and Sockanathan, S. (1999). Requirement for the homeobox gene Hb9 in the consolidation of motor neuron identity. Neuron 23, 659-74.

Ashe, H. L. and Briscoe, J. (2006). The interpretation of morphogen gradients. Development 133, 385-394.

Avidor-Reiss, T., Maer, A.M., Koundakjian, E., Polyanovsky, A., Keil, T., Subramaniam, S., and Zuker, C.S. (2004). Decoding Cilia Function: Defining Specialized Genes Required for Compartmentalized Cilia Biogenesis. Cell 117, 527-539.

Aza-Blanc, P., Ramírez-Weber, F. A., Laget, M. P., Schwartz, C. and Kornberg, T. B. (1997). Proteolysis that is inhibited by hedgehog targets Cubitus interruptus protein to the nucleus and converts it to a repressor. Cell 89, 1043- 1053.

Aza-Blanc, P., Lin, H. Y., Ruiz i Altaba, A. and Kornberg, T. B. (2000). Expression of the vertebrate Gli proteins in Drosophila reveals a distribution of activator and repressor activities. Development 127, 4293–4301.

Bai, C. B., and Joyner, A. L. (2001). Gli1 can rescue the in vivo function of Gli2. Development 128, 5161-5172.

Bai, C.B., Auerbach, W., Lee, J.S., Stephen, D., and Joyner, A.L. (2002). Gli2, but not Gli1, is required for initial Shh signaling and ectopic activation of the Shh pathway. Development 129, 4753-4761.

Bai, C. B., Stephen, D. and Joyner, A. L. (2004). All mouse ventral spinal cord patterning by hedgehog is Gli dependent and involves an activator function of Gli3. Dev. Cell 6, 103-115.

Bailey, P. J., Klos, J. M., Andersson, E., Karlen, M., Kallstrom, M., Ponjavic, J., Muhr, J., Lenhard, B., Sandelin, A. and Ericson, J. (2006). A global genomic transcriptional code associated with CNS-expressed genes. Exp. Cell Res. 312, 3108-3119.

Barkai, N. and Shilo, B.-Z. (2009). Robust generation and decoding of morphogen gradients. Cold Spring Harbor Perspect. Biol. 1 (5), a001990.

Barnfield, P. C., Zhang, X., Thanabalasingham, V., Yoshida, M. and Hui, C. C.. (2005). Negative regulation of Gli1 and Gli2 activator function by Suppressor of fused through multiple mechanisms. Differentiation 73, 397–405.

Barzi, M., J. Berenguer, A. Menendez, R. Alvarez-Rodriguez, and S. Pons. (2010). Sonic-hedgehog-mediated proliferation requires the localization of PKA to the cilium base. J. Cell Sci. 123, 62–69.

Beadle, G. W., Tatum, E. L. and Clancy, C.W. (1938). Food level in relation to rate of development and eye pigmentation in Drosophila melanogaster. Biol Bull 75, 447–462.

Beddington, R. S. P. and Robertson, E. J. (1999). Axis development and early asymmetry in mammals. Cell 96, 195-209.

Bellaiche, Y., The, I. and Perrimon, N. (1998). Tout-velu is a Drosophila homologue of the putative tumour suppressor EXT-1 and is needed for Hh diffusion. Nature 394, 85-88.

Bergmann, S., Sandler, O., Sberro, H., Shnider, S., Schejter, E., Shilo, B.-Z. and Barkai, N. (2007). Pre-steady-state decoding of the Bicoid morphogen gradient. PLoS Biol 5: e46.

Bergmann, S., Tamari, Z., Schejter, E., Shilo, B.-Z. and Barkai, N. (2008). Re-examining the stability of the Bicoid morphogen gradient. Cell 132, 15–17; author reply 17–18.

Bessho, Y., Sakata, R., Komatsu, S., Shiota, K., Yamada, S. and Kageyama, R. (2001). Dynamic expression and essential functions of Hes7 in somite segmentation. Genes Dev 15, 2642-2647.

Bhatia, N., Thiyagarajan, S., Elcheva, I., Saleem, M., Dlugosz, A., Mukhtar, H. and Spiegelman, V. S. (2006). Gli2 is targeted for ubiquitination and degradation by beta-TrCP ubiquitin ligase. J. Biol. Chem. 281, 19320-19326.

Bijlsma, M. F., Spek, C. A., Zivkovic, D., van de Water, S., Rezaee, F. and Peppelenbosch, M. P. (2006). Repression of smoothened by patched- dependent (pro-)vitamin D3 secretion. PLoS Biol. 4, e232.

Blumberg, B., Bolado, J., Jr., Moreno, T. A., Kintner, C., Evans, R. M. and Papalopulu, N. (1997). An essential role for retinoid signaling in anteroposterior neural patterning. Development 124, 373-379.

Bornemann, D. J., Duncan, J. E., Staatz, W., Selleck, S. and Warrior, R. (2004) Abrogation of heparan sulfate synthesis in Drosophila disrupts the Wingless, Hedgehog and Decapentaplegic signaling pathways. Development 131, 1927-38

Briscoe, J., Sussel, L., Serup, P., Hartigan-O'Connor, D., Jessell, T.M., Rubenstein, J.L., and Ericson, J. (1999). Homeobox gene Nkx2.2 and specification of neuronal identity by graded Sonic hedgehog signalling. Nature 398, 622-627.

Briscoe, J., Pierani, A., Jessell, T.M., and Ericson, J. (2000). A homeodomain protein code specifies progenitor cell identity and neuronal fate in the ventral neural tube. Cell 101, 435-445.

Briscoe, J., Chen, Y., Jessell, T.M., and Struhl, G. (2001). A hedgehog-insensitive form of patched provides evidence for direct long-range morphogen activity of sonic hedgehog in the neural tube. Mol Cell 7, 1279-1291.

Briscoe, J. and Novitch, B. G. (2008). Regulatory pathways linking progenitor patterning, cell fates and neurogenesis in the ventral neural tube. Philos Trans R Soc Lond B Biol Sci 363, 57-70.

Bumcrot, D. A., Takada, R. and McMahon, A. P. (1995). Proteolytic processing yields two secreted forms of sonic hedgehog. Mol. Cell. Biol. 15, 2294-2303.

Burke, R. and Basler, K. (1996). Dpp receptors are autonomously required for cell proliferation in the entire developing Drosophila wing. Development 122, 2261 – 2269.

Burke, R., Nellen, D., Bellotto, M., Hafen, E., Senti, K.-A., Dickson, B.J., and Basler, K. (1999) Dispatched, a Novel Sterol-Sensing Domain Protein Dedicated to the Release of Cholesterol-Modified Hedgehog from Signaling Cells. Cell 99, 803- 815.

Capdevila, J. and Guerrero, I. (1994). Targeted expression of the signaling molecule decapentaplegic induces pattern duplications and growth alterations in Drosophila wings. EMBO J 13, 4459–4468.

Casali, A. and Struhl, G. (2004) Reading the Hedgehog morphogen gradient by measuring the ratio of bound to unbound Patched protein. Nature 431, 76–80

Caspary, T., Garcia-Garcia, M. J., Huangfu, D., Eggenschwiler, J. T., Wyler, M.R., Rakeman, A. S., Alcorn, H. L. and Anderson, K. V. (2002). Mouse Dispatched homolog1 is required for long-range, but not juxtacrine, Hh signaling. Curr. Biol. 12, 1628-1632.

Cayuso, J., Ulloa, F., Cox, B., Briscoe, J., and Marti, E. (2006) The Sonic hedgehog pathway independently controls the patterning, proliferation and survival of neuroepithelial cells by regulating Gli activity. Development 133, 517-528.

Chamberlain, C.E., Jeong, J., Guo, C., Allen, B.L., and McMahon, A.P. (2008). Notochord-derived Shh concentrates in close association with the apically positioned basal body in neural target cells and forms a dynamic gradient during neural patterning. Development 135, 1097-1106.

Chamoun, Z., Mann, R.K., Nellen, D., von Kessler, D.P., Bellotto, M., Beachy, P.A., and Basler, K. (2001) Skinny Hedgehog, an Acyltransferase Required for Palmitoylation and Activity of the Hedgehog Signal. Science 293, 2080-2084.

Chang, D.T., Lopez, A., von Kessler, D.P., Chiang, C., Simandl, B.K., Zhao, R., Seldin, M.F., Fallon, J.F., and Beachy, P.A. (1994). Products, genetic linkage and limb patterning activity of a murine hedgehog gene. Development 120, 3339-3353.

Chen, Y. and Struhl, G. (1996). Dual roles for patched in sequestering and transducing Hedgehog. Cell 87, 553–563.

Chen, W., Burgess, S. and Hopkins, N. (2001). Analysis of the zebrafish smoothened mutant reveals conserved and divergent functions of hedgehog activity. Development 128, 2385–2396.

Chen, J. K., Taipale, J., Cooper, M. K. and Beachy, P. A. (2002). Inhibition of Hedgehog signaling by direct binding of cyclopamine to Smoothened. Genes Dev 16, 2743–2748.

Chen, M.-H., Li, Y.-J., Kawakami, T., Xu, S.-M., and Chuang, P.-T. (2004a) Palmitoylation is required for the production of a soluble multimeric Hedgehog protein complex and long-range signaling in vertebrates. Genes Dev. 18, 641- 659.

Chen, W., Ren, X. R., Nelson, C. D., Barak, L. S., Chen, J. K., Beachy, P. A., de Sauvage, F. and Lefkowitz, R. J. (2004b). Activity-dependent internalization of smoothened mediated by beta-arrestin 2 and GRK2. Science 306, 2257-2260.

Chen, M. H., Gao, N., Kawakami, T. and Chuang, P. T. (2005). Mice deficient in the fused homolog do not exhibit phenotypes indicative of perturbed hedgehog signaling during embryonic development. Mol. Cell. Biol. 25, 7042-7053.

Chen, M. H., Wilson, C. W., Li, Y. J., Law, K. K., Lu, C. S., Gacayan, R., Zhang, X., Hui, C. C. and Chuang, P. T. (2009). Cilium-independent regulation of Gli protein function by Sufu in Hedgehog signaling is evolutionarily conserved. Genes Dev. 23, 1910-1928.

Cheung, H. O., Zhang, X., Ribeiro, A., Mo, R., Makino, S., Puviindran, V., Law, K. K., Briscoe, J. and Hui, C. C. (2009). The kinesin protein Kif7 is a critical regulator of Gli transcription factors in mammalian hedgehog signaling. Sci. Signal. 2, ra29.

Chiang, C., Litingtung, Y., Lee, E., Young, K.E., Corden, J.L., Westphal, H., and Beachy, P.A. (1996). Cyclopia and defective axial patterning in mice lacking Sonic hedgehog gene function. Nature 383, 407-413.

Chuang, P. T. and McMahon, A. P. (1999). Vertebrate Hedgehog signalling modulated by induction of a Hedgehog-binding protein. Nature 397, 617-621.

Chuang, P. T., Kawcak, T. and McMahon, A. P. (2003). Feedback control of mammalian Hedgehog signaling by the Hedgehog-binding protein, Hip1, modulates Fgf signaling during branching morphogenesis of the lung. Genes Dev. 17, 342-347.

Colas, J. F., Schoenwolf, G. C. (2001). Towards a cellular and molecular understanding of neurulation. Dev Dyn. 221, 117-45.

Cooper, A. F., Yu, K. P., Brueckner, M., Brailey, L. L., Johnson, L., McGrath, J. M. and Bale, A. E. (2005). Cardiac and CNS defects in a mouse with targeted disruption of suppressor of fused. Development 132, 4407-4417.

Corbit, K. C., Aanstad, P., Singla, V., Norman, A. R., Stainier, D. Y. and Reiter, J. F. (2005). Vertebrate Smoothened functions at the primary cilium. Nature 437, 1018-1021.

Corcoran, R. B. and Scott, M. P. (2006). Oxysterols stimulate Sonic hedgehog signal transduction and proliferation of medulloblastoma cells. Proc. Natl. Acad. Sci. USA 103, 8408-8413.

Cox, B., Briscoe, J. and Ulloa, F. (2010). SUMOylation by Pias1 Regulates the Activity of the Hedgehog Dependent Gli Transcription Factors. PLoS ONE 5(8), e11996. doi: 10.1371/journal.pone.0011996.

Crick, F. (1970). Diffusion in embryogenesis. Nature 225, 420 – 425.

Dai, P., Akimaru, H., Tanaka, Y., Maekawa, T., Nakafuku, M., and Ishii, S. (1999). Sonic Hedgehog-induced activation of the Gli1 promoter is mediated by GLI3. J Biol Chem 274, 8143-8152.

Dasen, J.S., and Jessell, T.M. (2009). Hox networks and the origins of motor neuron diversity. Curr Top Dev Biol 88, 169-200.

Day, S. J. and Lawrence, P. A. (2000). Measuring dimensions: The regulation of size and shape. Development 127, 2977 – 2987.

Denef, N., Neubuser, D., Perez, L. and Cohen, S. M. (2000). Hedgehog induces opposite changes in turnover and subcellular localization of patched and smoothened. Cell 102, 521– 531.

Dessaud, E., McMahon, A. P. and Briscoe, J. (2008). Pattern formation in the vertebrate neural tube: a sonic hedgehog morphogen-regulated transcriptional network. Development 135, 2489 – 2503.

Dessaud, E., Yang, L. L., Hill, K., Cox, B., Ulloa, F., Ribeiro, A., Mynett, A., Novitch, B. G. and Briscoe, J. (2007). Interpretation of the sonic hedgehog morphogen gradient by a temporal adaptation mechanism. Nature 450, 717–720.

Dessaud, E., Ribes, V., Balaskas, N., Yang, L. L., Pierani, A., Kicheva, A., Novitch, B. G., Briscoe, J. and Sasai, N. (2010) Dynamic Assignment and Maintenance of Positional Identity in the Ventral Neural Tube by the Morphogen Sonic Hedgehog. PLoS Biol 8 (6): e1000382. doi:10.1371/journal.pbio.1000382.

Diez del Corral, R., Breitkreuz, D. N. and Storey, K. G. (2002). Onset of neuronal differentiation is regulated by paraxial mesoderm and requires attenuation of FGF signalling. Development 129, 1681 – 1691.

Diez del Corral, R., Olivera-Martinez, I., Goriely, A., Gale, E., Maden, M. and Storey, K. (2003). Opposing FGF and Retinoid pathways control ventral neural patterning, neuronal differentiation and segmentation during body axis extension. Neuron 40, 65 – 79.

Ding, Q., Motoyama, J., Gasca, S., Mo, R., Sasaki, H., Rossant, J., and Hui, C.C. (1998) Diminished Sonic hedgehog signaling and lack of floor plate differentiation in Gli2 mutant mice. Development 125, 2533-2543.

Driever, W., and Nusslein-Volhard, C. (1988a). A gradient of bicoid protein in Drosophila embryos. Cell 54, 83-93.

Driever, W., and Nusslein-Volhard, C. (1988b). The bicoid protein determines position in the Drosophila embryo in a concentration-dependent manner. Cell 54, 95-104.

Driever, W. and Nüsslein-Volhard, C. (1989). The bicoid protein is a positive regulator of hunchback transcription in the early Drosophila embryo. Nature 337, 138–143.

Driever, W., Ma, J., Nüsslein-Volhard, C. and Ptashne, M. (1989a). Rescue of bicoid mutant Drosophila embryos by Bicoid fusion proteins containing heterologous activating sequences. Nature 342, 149–154.

Driever, W., Thoma, G. and Nusslein-Volhard, C. (1989b). Determination of spatial domains of zygotic gene expression in the Drosophila embryo by the affinity of binding sites for the bicoid morphogen. Nature 340, 363-367.

Dwyer, J. R., Sever, N., Carlson, M., Nelson, S. F., Beachy, P. A. and Parhami, F. (2007). Oxysterols are novel activators of the hedgehog signaling pathway in pluripotent mesenchymal cells. J. Biol. Chem. 282, 8959-8968.

Dyson, S. and Gurdon, J. B. (1998). The interpretation of position in a morphogen gradient as revealed by occupancy of activin receptors. Cell 93, 557–568.

Echelard, Y., Epstein, D.J., St-Jacques, B., Shen, L., Mohler, J., McMahon, J.A., and McMahon, A.P. (1993). Sonic hedgehog, a member of a family of putative signaling molecules, is implicated in the regulation of CNS polarity. Cell 75, 1417-1430.

Eldar, A., Rosin, D., Shilo, B. Z. and Barkai, N. (2003). Self-enhanced ligand degradation underlies robustness of morphogen gradients. Dev. Cell 5, 635-646

Eggenschwiler, J. T. and Anderson, K. V. (2007). Cilia and developmental signaling. Annu. Rev. Cell Dev. Biol. 23, 345-373.

Endoh-Yamagami, S., Evangelista, M., Wilson, D., Wen, X., Theunissen, J. W., Phamluong, K., Davis, M., Scales, S. J., Solloway, M. J., de Sauvage, F. J. et al. (2009). The mammalian Cos2 homolog Kif7 plays an essential role in modulating Hh signal transduction during development. Curr. Biol. 19, 1320- 1326.

Ephrussi, A. and Johnston, D. (2004). Seeing is believing: the bicoid morphogen gradient matures. Cell 116, 143–152.

Ericson, J., Thor, S., Edlund, T., Jessell, T. M. and Yamada, T. (1992). Early stages of motor neuron differentiation revealed by expression of homeobox gene Islet-1. Science 256, 1555-60.

Ericson, J., Morton, S., Kawakami, A., Roelink, H., and Jessell, T.M. (1996). Two critical periods of Sonic Hedgehog signaling required for the specification of motor neuron identity. Cell 87, 661-673.

Ericson, J., Rashbass, P., Schedl, A., Brenner-Morton, S., Kawakami, A., van Heyningen, V., Jessell, T.M., and Briscoe, J. (1997). Pax6 controls progenitor cell identity and neuronal fate in response to graded Shh signaling. Cell 90, 169-180.

Evangelista, M., Lim, T. Y., Lee, J., Parker, L., Ashique, A., Peterson, A. S., Ye, W., Davis, D. P. and de Sauvage, F. J. (2008). Kinome siRNA screen identifies regulators of ciliogenesis and hedgehog signal transduction. Sci. Signal. 1, ra7.

Farzan, S., Ascano, M., Ogden, S. K., Sanial, M., Brigui, A., Plessis, A. and Robbins, D. J. (2008). Costal2 Functions as a Kinesin-like Protein in the Hedgehog Signal Transduction Pathway. Current Biology 18, 1215–1220.

Ferguson, E.L., and Anderson, K.V. (1992). Decapentaplegic acts as a morphogen to organize dorsal-ventral pattern in the Drosophila embryo. Cell 71, 451-461.

Fuse, N., Maiti, T., Wang, B., Porter, J.A., Hall, T.M., Leahy, D.J., and Beachy, P.A. (1999). Sonic hedgehog protein signals not as a hydrolytic enzyme but as an apparent ligand for patched. Proc Natl Acad Sci U S A 96, 10992-10999.

Gallet, A., Ruel, L., Staccini-Lavenant, L., and Therond, P.P. (2006) Cholesterol modification is necessary for controlled planar long-range activity of Hedgehog in Drosophila epithelia. Development 133: 407-418.

Gelbart, W. M. (1989). The decapentaplegic gene: A TGF-beta homologue controlling pattern formation in Drosophila. Development (suppl.) 107: 65–74.

Glise, B., Miller, C. A., Crotazier, M., Halbisen, M. A., Wise, S., Olson, D. J., Vincent, A. and Blair, S.S. (2005). Shifted, the Drosophila ortholog of Wnt inhibitory factor-1, controls the distribution and movement of Hedgehog. Dev Cell 8, 255–266.

Goetz, S. C, Ocbina, P. J. R. and Anderson K.,V. (2009). The Primary Cilium as a Hedgehog Signal Transduction Machine Methods Cell Biol. 94, 199–222.

Goodrich, L.V., Johnson, R.L., Milenkovic, L., McMahon, J.A., and Scott, M.P. (1996). Conservation of the hedgehog/patched signaling pathway from flies to mice: induction of a mouse patched gene by Hedgehog. Genes Dev 10, 301-312.

Goodrich, L.V., Milenkovic, L., Higgins, K.M., and Scott, M.P. (1997). Altered neural cell fates and medulloblastoma in mouse patched mutants. Science 277, 1109-1113.

Gorfinkiel, N., Sierra, J., Callejo, A., Ibanez, C. and Guerrero, I. (2005). The Drosophila ortholog of human Wnt inhibitory factor Shifted controls the diffusion of lipid-modified Hedgehog. Dev Cell 8, 241–253.

Green, J.B., New, H.V., and Smith, J.C. (1992). Responses of embryonic Xenopus cells to activin and FGF are separated by multiple dose thresholds and correspond to distinct axes of the mesoderm. Cell 71, 731-739.

Green, J.B., and Smith, J.C. (1990). Graded changes in dose of a Xenopus activin A homologue elicit stepwise transitions in embryonic cell fate. Nature 347, 391-394.

Gregor, T., Bialek, W., de Ruyter van Steveninck, R. R., Tank, D. W. and Wieschaus, E.F. (2005) Diffusion and scaling during early embryonic pattern formation. Proc Natl Acad Sci USA 102, 18403–18407.

Gregor, T., Wieschaus, E. F., McGregor, A. P., Bialek, W. and Tank, D. W. (2007). Stability and nuclear dynamics of the bicoid morphogen gradient. Cell 130, 141–152.

Gritli-Linde, A., Lewis, P., McMahon, A.P., and Linde, A. (2001) The whereabouts of a morphogen: direct evidence for short- and graded long-range activity of hedgehog signaling peptides. Dev Biol 236, 364-386.

Han, Y. G., Kwok, B. H. and Kernan, M. J. (2003). Intraflagellar transport is required in Drosophila to differentiate sensory cilia but not sperm. Curr. Biol. 13, 1679-1686.

Han, C., Belenkaya, T. Y., Khodoun, M., Tauchi, M. and Lin, X. (2004a). Distinct and collaborative roles of Drosophila EXT family proteins in morphogen signalling and gradient formation. Development 131,1563–1575.

Han, C., Belenkaya, T. Y., Wang, B. and Lin, X. (2004b). Drosophila glypicans control the cell-to-cell movement of Hedgehog by a dynamin-independent process. Development 131, 601–611.

Harfe, B.D., Scherz, P.J., Nissim, S., Tian, H., McMahon, A.P., and Tabin, C.J. (2004). Evidence for an expansion-based temporal Shh gradient in specifying vertebrate digit identities. Cell 118, 517-528.

Haycraft, C. J., Banizs, B., Aydin-Son, Y., Zhang, Q., Michaud, E. J. and Yoder, B. K. (2005). Gli2 and Gli3 localize to cilia and require the intraflagellar transport protein polaris for processing and function. PLoS Genet. 1, e53.

Hirata, H., Yoshiura, S., Ohtsuka, T., Bessho, Y., Harada, T., Yoshikawa, K. and Kageyama, R. (2002). Oscillatory expression of the bHLH factor Hes1 regulated by a negative feedback loop. Science 298, 840.

Hirokawa N., Noda Y., Tanaka Y. and Niwa S. (2009). Kinesin superfamily motor proteins and intracellular transport. Nature Reviews Molecular Cell Biology 10, 682-696.

Ho, K. S., Suyama, K., Fish, M. and Scott, M. P. (2005). Differential regulation of Hedgehog target gene transcription by Costal2 and Suppressor of Fused. Development 132, 1401-12.

Houchmandzadeh, B., Wieschaus, E. and Leibler, S. (2002). Establishment of developmental precision and proportions in the early Drosophila embryo. Nature 415, 798–802

Huang, P. and Schier, A. F. (2009). Dampened Hedgehog signaling but normal Wnt signaling in zebrafish without cilia. Development 136, 3089-3098.

Huangfu, D., Liu, A., Rakeman, A. S., Murcia, N. S., Niswander, L. and Anderson, K. V. (2003). Hedgehog signalling in the mouse requires intraflagellar transport proteins. Nature 426, 83-87.

Huangfu, D. and Anderson, K. V. (2005). Cilia and Hedgehog responsiveness in the mouse. Proc. Natl. Acad. Sci. USA 102, 11325-11330.

Huangfu, D. and Anderson, K. V. (2006). Signaling from Smo to Ci/Gli: conservation and divergence of Hedgehog pathways from Drosophila to vertebrates. Development 133, 3-14.

Hui, C.C., Slusarski, D., Platt, K.A., Holmgren, R., and Joyner, A.L. (1994). Expression of three mouse homologs of the Drosophila segment polarity gene cubitus interruptus, Gli, Gli-2, and Gli-3, in ectoderm- and mesoderm-derived tissues suggests multiple roles during postimplantation development. Dev Biol 162, 402-413.

Humke, E. W., Dorn, K. V., Milenkovic, L., Scott, M. P. and Rohatgi, R. (2010). The output of Hedgehog signaling is controlled by the dynamic association between Suppressor of Fused and the Gli proteins. Genes Dev. 24, 670-682

Hynes, M., Ye, W., Wang, K., Stone, D., Murone, M., Sauvage, F., and Rosenthal, A. (2000). The seven-transmembrane receptor smoothened cell-autonomously induces multiple ventral cell types. Nat Neurosci 3, 41-46.

Ibañes, M., Belmonte, J.C.I., (2008). Theoretical and experimental approaches to understand morphogen gradients. Mol. Syst. Biol. 2008 (4), 176.

Ille, F., Atanasoski, S., Falk, S., Ittner, L. M., Marki, D., Buchmann-Moller, S., Wurdak, H., Suter, U., Taketo, M. M. and Sommer, L. (2007). Wnt/BMP signal integration regulates the balance between proliferation and differentiation of neuroepithelial cells in the dorsal spinal cord. Dev Biol 304, 394-408.

Incardona, J. P., Gruenberg, J. and Roelink, H. (2002). Sonic hedgehog induces the segregation of patched and smoothened in endosomes. Curr. Biol. 12, 983- 995.

Ingham, P.W., and McMahon, A.P. (2001). Hedgehog signaling in animal development: paradigms and principles. Genes Dev 15, 3059-3087.

Jacob, J. and Briscoe, J. (2003). Gli proteins and the control of spinal-cord patterning. EMBO Rep 4, 761-5.

Jaeger, J., Surkova, S., Blagov, M., Janssens, H., Kosman, D., Kozlov, K.N., Manu, Myasnikova, E., Vanario-Alonso, C.E., Samsonova, M., Sharp, D.H. and Reinitz, J., (2004). Dynamic control of positional information in the early Drosophila embryo. Nature 430, 368–371.

Jaeger, J. and Reinitz, J. (2006). On the dynamic nature of positional information. BioEssays 28, 1102-1111.

Jeong, J. and McMahon, A. P. (2005). Growth and pattern of the mammalian neural tube are governed by partially overlapping feedback activities of the hedgehog antagonists patched 1 and Hhip1. Development 132, 143-154.

Jessell, T.M. (2000). Neuronal specification in the spinal cord: inductive signals and transcriptional codes. Nat Rev Genet 1, 20-29.

Jia, J., Amanai, K., Wang, G., Tang, J., Wang, B. and Jiang, J. (2002). Shaggy/GSK3 antagonizes Hedgehog signalling by regulating Cubitus interruptus. Nature 416, 548-552.

Jia, J., Tong, C. and Jiang, J. (2003). Smoothened transduces Hedgehog signal by physically interacting with Costal2/Fused complex through its C-terminal tail. Genes Dev. 17, 2709-2720.

Jia, J., Tong, C., Wang, B., Luo, L. and Jiang, J. (2004). Hedgehog signalling activity of Smoothened requires phosphorylation by protein kinase A and casein kinase I. Nature 432, 1045–1050.

Jia, J., Zhang, L., Zhang, Q., Tong, C., Wang, B., Hou, F., Amanai, K. and Jiang, J. (2005). Phosphorylation by double-time/CKIepsilon and CKIalpha targets cubitus interruptus for Slimb/beta-TRCP-mediated proteolytic processing. Dev. Cell 9, 819-830.

Jia, J. and Jiang, J. (2006). Decoding the Hedgehog signal in animal development. Cell. Mol. Life Sci. 63, 1249–1265

Jia, J., Kolterud, A., Zeng, H., Hoover, A., Teglund, S., Toftgard, R. and Liu, A. (2009). Suppressor of Fused inhibits mammalian Hedgehog signaling in the absence of cilia. Dev. Biol. 330, 452-460.

Katoh, Y. and Katoh, M. (2004a). Characterization of KIF7 gene in silico. Int. J. Oncol. 25, 1881-1886.

Katoh, Y. and Katoh, M. (2004b). KIF27 is one of orthologs for Drosophila Costal-2. Int. J. Oncol. 25, 1875-1880.

Kawakami, T., Kawcak, T., Li, Y. J., Zhang, W., Hu, Y. and Chuang, P. T. (2002). Mouse dispatched mutants fail to distribute hedgehog proteins and are defective in hedgehog signaling. Development 129, 5753-5765.

Kicheva, A., Pantazis, P., Bollenbach, T., Kalaidzidis, Y., Bittig, T., Julicher, F. and Gonzalez-Gaitan, M. (2007). Kinetics of morphogen gradient formation. Science 315, 521-525.

Krauss, S., Concordet, J.P., and Ingham, P.W. (1993). A functionally conserved homolog of the Drosophila segment polarity gene hh is expressed in tissues with polarizing activity in zebrafish embryos. Cell 75, 1431-1444.

Kutejova, E., Briscoe, J. and Kicheva, A. (2009). Temporal dynamics of patterning by morphogen gradients. Curr. Opinion Genet. Dev. 9, 315–322.

Landmesser, L. T. (2001). The acquisition of motoneuron subtype identity and motor circuit formation. Int. J. Dev. Neurosci. 19, 175–182.

Lamb, T. M. and Harland, R. M. (1995). Fibroblast growth factor is a direct neural inducer, which combined with noggin generates anterior-posterior neural pattern. Development 121, 3627–3636.

Lawrence PA, Struhl G. 1996. Morphogens, compartments, and pattern: Lessons from Drosophila? Cell 85: 951–961.

Lee, J.J., Ekker, S.C., von Kessler, D.P., Porter, J.A., Sun, B.I., and Beachy, P.A. (1994) Autoproteolysis in hedgehog protein biogenesis. Science 266, 1528- 1537.

Lee, J., Platt, K.A., Censullo, P., and Ruiz i Altaba, A. (1997). Gli1 is a target of Sonic hedgehog that induces ventral neural tube development. Development 124, 2537-2552.

Lee, J. D. and Treisman, J. E. (2001). Sightless has homology to transmembrane acyltransferases and is required to generate active Hedgehog protein. Curr Biol. 11, 1147-52.

Lei, Q., Zelman, A.K., Kuang, E., Li, S., and Matise, M.P. (2004). Transduction of graded Hedgehog signaling by a combination of Gli2 and Gli3 activator functions in the developing spinal cord. Development 131, 3593-3604.

Liberman, L.M., Reeves, G.T. and Stathopolous, A. (2009). Quantitative imaging of the Dorsal nuclear gradient reveals limitations to threshold-dependent patterning in Drosophila. PNAS 106, 22317-22322.

Liem, K.F., Tremml, G., and Jessell, T.M. (1997) A Role for the Roof Plate and Its Resident TGF[beta]-Related Proteins in Neuronal Patterning in the Dorsal Spinal Cord. Cell 91: 127-138.

Liem, K. F., Jr, He, M., Ocbina, P. J. and Anderson, K. V. (2009). Mouse Kif7/Costal2 is a cilia-associated protein that regulates Sonic hedgehog signaling. Proc. Natl. Acad. Sci. USA 106, 13377-13382.

Litingtung, Y., and Chiang, C. (2000). Specification of ventral neuron types is mediated by an antagonistic interaction between shh and gli3. Nat Neurosci 3, 979-985.

Liu, A., Wang, B. and Niswander, L. A. (2005). Mouse intraflagellar transport proteins regulate both the activator and repressor functions of Gli transcription factors. Development 132, 3103-3111.

Liu, Y., Cao, X., Jiang, J. and Jia, J. (2007). Fused-Costal2 protein complex regulates Hedgehog-induced Smo phosphorylation and cell-surface accumulation. Genes Dev. 21, 1949-1963.

Lum, L., Yao, S., Mozer, B., Rovescalli, A., Von Kessler, D., Nirenberg, M. and Beachy, P. A. (2003a). Identification of Hedgehog pathway components by RNAi in Drosophila cultured cells. Science 299, 2039–2045.

Lum, L., Zhang, C., Oh, S., Mann, R. K., von Kessler, D. P., Taipale, J., Weis- Garcia, F., Gong, R., Wang, B. and Beachy, P. A. (2003b). Hedgehog signal transduction via Smoothened association with a cytoplasmic complex scaffolded by the atypical kinesin, Costal-2. Mol. Cell 12, 1261-1274.

Ma, Q., Sommer, L., Cserjesi, P. and Anderson, D. J. (1997) Mash1 and neurogenin1 expression patterns define complementary domains of neuroepithelium in the developing CNS and are correlated with regions expressing notch ligands. J. Neurosci. 17, 3644–3652.

Ma, Y., Erkner, A., Gong, R., Yao, S., Taipale, J., Basler, K. and Beachy, P. A. (2002). Hedgehog-mediated patterning of the mammalian embryo requires transporter-like function of dispatched. Cell 111, 63-75.

Maloverjan, A., Piirsoo, M., Michelson, P., Kogerman, P. and Osterlund, T. (2010). Identification of a novel serine/threonine kinase ULK3 as a positive regulator of Hedgehog pathway. Exp. Cell Res. 316, 627-637.

Marigo, V. and Tabin, C. J. (1996). Regulation of patched by sonic hedgehog in the developing neural tube. Proc Natl Acad Sci U S A. 93, 9346-51.

Marigo, V., Davey, R.A., Zuo, Y., Cunningham, J.M., and Tabin, C.J. (1996a). Biochemical evidence that patched is the Hedgehog receptor. Nature 384, 176-179.

Marigo, V., Johnson, R.L., Vortkamp, A., and Tabin, C.J. (1996b). Sonic hedgehog differentially regulates expression of GLI and GLI3 during limb development. Dev Biol 180, 273-283.

Marszalek, J. R., Ruiz-Lozano, P., Roberts, E., Chien, K. R. and Goldstein, L. S. (1999). Situs inversus and embryonic ciliary morphogenesis defects in mouse mutants lacking the KIF3A subunit of kinesin-II. Proc. Natl Acad. Sci. USA 96, 5043–5048.

Marti, E., Bumcrot, D.A., Takada, R., and McMahon, A.P. (1995). Requirement of 19K form of Sonic hedgehog for induction of distinct ventral cell types in CNS explants. Nature 375, 322-325.

Martin-Castellanos, C. and Edgar, B. A. (2002). A characterization of the effects of Dpp signaling on cell growth and proiferation in the Drosophila wing. Development 129, 1003 – 1013.

Martinelli, D. C. and Fan, C. M. (2007). The role of Gas1 in embryonic development and its implications for human disease. Cell Cycle 6, 2650-2655.

Matise, M.P., Epstein, D.J., Park, H.L., Platt, K.A., and Joyner, A.L. (1998). Gli2 is required for induction of floor plate and adjacent cells, but not most ventral neurons in the mouse central nervous system. Development 125, 2759-2770.

May, S. R., Ashique, A. M., Karlen, M., Wang, B., Shen, Y., Zarbalis, K., Reiter, J., Ericson, J. and Peterson, A. S. (2005). Loss of the retrograde motor for IFT disrupts localization of Smo to cilia and prevents the expression of both activator and repressor functions of Gli. Dev. Biol. 287, 378-389.

McGrew, L. L., Lai, C. J. and Moon, R. T. (1995). Specification of the anteropos- terior neural axis through synergistic interaction of the Wnt signaling cascade with noggin and follistatin. Developmental Biology 172, 337–342.

Megason, S. G. and McMahon, A. P. (2002). A mitogen gradient of dorsal midline Wnts organizes growth in the CNS. Development 129, 2087-98.

Merchant, M., Evangelista, M., Luoh, S. M., Frantz, G. D., Chalasani, S., Carano, R. A., van Hoy, M., Ramirez, J., Ogasawara, A. K., McFarland, L. M. et al. (2005). Loss of the serine/threonine kinase fused results in postnatal growth defects and lethality due to progressive hydrocephalus. Mol. Cell. Biol. 25, 7054-7068.

Methot, N., and Basler, K.. (2000). Suppressor of fused opposes hedgehog signal transduction by impeding nuclear accumulation of the activator form of Cubitus interruptus. Development 127, 4001–4010.

Micchelli, C. A., The, I., Selva, E., Mogila, V. and Perrimon, N. (2002). Rasp, a putative transmembrane acyltransferase, is required for Hedgehog signaling. Development. 129, 843-51.

Milan, M., Campuzano, S. and Garcia-Bellido, A. (1996). Cell cycling and patterned cell proliferation in the wing primordium of Drosophila. Proc Natl Acad Sci 93, 640 – 645.

Milenkovic, L., Scott, M. P. and Rohatgi, R. (2009). Lateral transport of Smoothened from the plasma membrane to the membrane of the cilium. J. Cell Biol. 187, 365-374.

Monnier, V., Dussillol, F., Alves, G., Lamour-Isnard, C. and Plessis, A. (1998). Suppressor of fused links fused and Cubitus interruptus on the hedgehog signalling pathway. Curr. Biol. 8, 583-586.

Morales, C.R., Fox, A., El-Alfy, M., Ni, X. and Argraves, W.S. (2009). Expression of Patched-1 and Smoothened in testicular meiotic and post-meiotic cells. Microsc. Res. Tech. 72, 809-815.

Motoyama, J., Milenkovic, L., Iwama, M., Shikata, Y., Scott, M. P. and Hui, C.C. (2003). Differential requirement for Gli2 and Gli3 in ventral neural cell fate specification. Dev. Biol. 259, 150-161.

Muhr, J., Graziano, E., Wilson, S., Jessell, T. M. and Edlund, T. (1999). Convergent inductive signals specify midbrain, hindbrain, and spinal cord identity in gastrula stage chick embryos. Neuron 23, 689–702

Muhr, J., Andersson, E., Persson, M., Jessell, T. M. and Ericson, J. (2001). Groucho-mediated transcriptional repression establishes progenitor cell pattern and neuronal fate in the ventral neural tube. Cell 104, 861-873.

Muresan, V., Joshi, H., and Besharse, J. (1993) Gamma-tubulin in differentiated cell types: localization in the vicinity of basal bodies in retinal photoreceptors and ciliated epithelia. J Cell Sci 104: 1229-1237.

Muroyama, Y., Fujihara, M., Ikeya, M., Kondoh, H., and Takada, S. (2002) Wnt signaling plays an essential role in neuronal specification of the dorsal spinal cord. Genes Dev. 16: 548-553.

Nahmad, M. and Stathopoulos, A. (2009). Dynamic Interpretation of Hedgehog Signaling in the Drosophila Wing Disc. PLoS Biol 7(9): e1000202.

Nakano, Y., Nystedt, S., Shivdasani, A. A., Strutt, H., Thomas, C. and Ingham, P. W. (2004). Functional domains and sub-cellular distribution of the Hedgehog transducing protein Smoothened in Drosophila. Mech Dev 121, 507–518.

Niswander, L., Tickle, C., Vogel, A., Booth, I. and Martin, G. R. (1993). FGF-4 replaces the apical ectodermal ridge and directs outgrowth and patterning of the limb. Cell 75, 579-587.

Nordstrom, U., Jessell, T. M. and Edlund, T. (2002). Progressive induction of caudal neural character by graded Wnt signaling. Nat Neurosci 5, 525–352

Nornes, H. O. and Carry, M. (1978). Neurogenesis in spinal cord of mouse: an autoradiographic analysis. Brain Res 159, 1-6.

Novitch, B.G., Chen, A.I., and Jessell, T.M. (2001). Coordinate regulation of motor neuron subtype identity and pan-neuronal properties by the bHLH repressor Olig2. Neuron 31, 773-789.

Nusslein-Volhard, C. and Wieschaus, E. (1980). Mutations affecting segment number and polarity in Drosophila. Nature 287, 795-801.

Oakley, B. (1992) γ-tubulin: the microtubule organizer? Trends Cell Biol 2, 1-5.

Ochoa-Espinosa, A., Yucel, G., Kaplan, L., Pare, A., Pura, N., Oberstein, A., Papatsenko, D. and Small, S. (2005). The role of binding site cluster strength in Bicoid-dependent patterning in Drosophila. Proc. Natl. Acad. Sci. USA 102, 4960-4965.

Pages, F., and Kerridge, S. (2000). Morphogen gradients. A question of time or concentration? Trends Genet 16, 40-44.

Palmeirim, I., Henrique, D., Ish-Horowicz, D. and Pourquié, O. (1997). Avian hairy gene expression identifies a molecular clock linked to vertebrate segmentation and somitogenesis. Cell 91, 639-48.

Pan, Y., Bai, C. B., Joyner, A. L. and Wang, B. (2006). Sonic hedgehog signaling regulates Gli2 transcriptional activity by suppressing its processing and degradation. Mol Cell Biol 26, 3365-3377.

Parras, C. M., Schuurmans, C., Scardigli, R., Kim, J., Anderson, D. J. and Guillemot, F. (2002) Divergent functions of the proneural genes Mash1 and Ngn2 in the specification of neuronal subtype identity. Genes Dev. 16, 324–338.

Park, H.L., Bai, C., Platt, K.A., Matise, M.P., Beeghly, A., Hui, C.C., Nakashima, M., and Joyner, A.L. (2000). Mouse Gli1 mutants are viable but have defects in SHH signaling in combination with a Gli2 mutation. Development 127, 1593-1605.

Persson, M., Stamataki, D., te Welscher, P., Andersson, E., Bose, J., Ruther, U., Ericson, J., and Briscoe, J. (2002). Dorsal-ventral patterning of the spinal cord requires Gli3 transcriptional repressor activity. Genes Dev 16, 2865-2878.

Placzek, M. (1995). The role of the notochord and floor plate in inductive interactions. Curr Opin Genet Dev 5, 499-506.

Pierani, A., Brenner-Morton, S., Chiang, C. and Jessell, T.M. (1999). A sonic hedgehog-independent, retinoid-activated pathway of neurogenesis in the ventral spinal cord. Cell 97, 903-915.

Podos, S.D. and Ferguson, E.L. (1999). Morphogen gradients: new insights from DPP. Trends Genet 15, 396-402.

Porter, J. A., Ekker, S. C., Park, W. J., von Kessler, D. P., Young, K. E., Chen, C. H., Ma, Y., Woods, A. S., Cotter, R. J., Koonin, E. V. et al. (1996). Hedgehog patterning activity: role of a lipophilic modification mediated by the carboxy- terminal autoprocessing domain. Cell 86, 21-34.

Preat, T. (1992). Characterization of Suppressor of fused, a complete suppressor of the fused segment polarity gene of Drosophila melanogaster. Genetics 132, 725-736.

Price, M. A. and Kalderon, D. (2002). Proteolysis of the Hedgehog signaling effector Cubitus interruptus requires phosphorylation by Glycogen Synthase Kinase 3 and Casein Kinase 1. Cell 108, 823-835.

Ramón y Cajal, S. (1906). The structure and connexions of neurons. In Nobel Lectures: Physiology or Medicine (1901–1921). :220–253. Elsevier. Amsterdam (1967).

Ribes, V., Stutzmann, F., Bianchetti, L., Guillemot, F., Dollé, P. and Le Roux, I. (2008). Combinatorial signalling controls Neurogenin2 expression at the onset of spinal neurogenesis. Dev Biol 321, 470-481.

Ribes, V. and Briscoe, J. (2009). Establishing and interpreting graded Sonic hedgehog signaling during vertebrate neural tube patterning: the role of negative feedback. Cold Spring Harb Perspect Biol 1:a002014.

Ribes, V., Balaskas, N., Sasai, N., Cruz, C., Dessaud, E., Cayuso, J., Tozer, S., Yang, L. L., Novitch, B., Marti, E., and Briscoe J. (2010). Distinct Sonic Hedgehog signaling

dynamics specify floor plate and ventral neuronal progenitors in the vertebrate neural tube. Genes Dev 24, 1186-200.

Riddle, R.D., Johnson, R.L., Laufer, E., and Tabin, C. (1993) Sonic hedgehog mediates the polarizing activity of the ZP A. Cell 75: 1401-1416.

Rink, J. C., Gurley, K. A., Elliott, S. A. and Sanchez Alvarado, A. (2009). Planarian Hh signaling regulates regeneration polarity and links Hh pathway evolution to cilia. Science 326, 1406-1410.

Rivera-Pomar, R. and Jäckle, H. (1996). From gradients to stripes in Drosophila embryogenesis: Filling in the gaps. Trends in Gen 12, 478–483.

Robbins, D. J., Nybakken, K. E., Kobayashi, R., Sisson, J. C., Bishop, J. M. and Thérond, P. P. (1997). Hedgehog elicits signal transduction by means of a large complex containing the kinesin-related protein costal2. Cell 90, 225-234.

Roelink, H., Augsburger, A., Heemskerk, J., Korzh, V., Norlin, S., Ruiz i Altaba, A., Tanabe, Y., Placzek, M., Edlund, T., Jessell, T.M., et al. (1994). Floor plate and motor neuron induction by vhh-1, a vertebrate homolog of hedgehog expressed by the notochord. Cell 76, 761-775.

Roelink, H., Porter, J.A., Chiang, C., Tanabe, Y., Chang, D.T., Beachy, P.A., and Jessell, T.M. (1995). Floor plate and motor neuron induction by different concentrations of the amino-terminal cleavage product of sonic hedgehog autoproteolysis. Cell 81, 445-455.

Rogulja, D. and Irvine, K. D. (2005). Regulation of cell proliferation by a morphogen gradient. Cell 123, 449–461

Rohatgi, R., Milenkovic, L. and Scott, M. P. (2007). Patched1 regulates hedgehog signaling at the primary cilium. Science 317, 372-376.

Rohatgi, R., Milenkovic, L., Corcoran, R. B. and Scott, M. P. (2009). Hedgehog signal transduction by Smoothened: Pharmacologic evidence for a 2-step activation process. Proc. Natl. Acad. Sci. USA 106, 3196-3201.

Roth, S., Stein, D., and Nusslein-Volhard, C. (1989). A gradient of nuclear localization of the dorsal protein determines dorsoventral pattern in the Drosophila embryo. Cell 59, 1189-1202.

Rubin, J. B., Choi, Y. and Segal, R. A. (2002). Cerebellar proteoglycans regulate sonic hedgehog responses during development. Development 129, 2223-2232.

Ruel, L., Rodriguez, R., Gallet, A., Lavenant-Staccini, L. and Thérond, P. P. (2003). Stability and association of Smoothened, Costal2 and Fused with Cubitus interruptus are regulated by Hedgehog. Nat. Cell Biol. 5, 907-913.

Ruel, L., Gallet, A., Raisin, S., Truchi, A., Staccini-Lavenant, L., Cervantes, A.and Thérond, P. P. (2007). Phosphorylation of the atypical kinesin Costal2 by the kinase Fused induces the partial disassembly of the Smoothened-Fused- Costal2-Cubitus interruptus complex in Hedgehog signalling. Development 134, 3677-3689.

Ruiz i Altaba, A. (1998). Combinatorial Gli gene function in floor plate and neuronal inductions by Sonic hedgehog. Development 25, 2203-2212.

Ruppert, J.M., Kinzler, K.W., Wong, A.J., Bigner, S.H., Kao, F.T., Law, M.L., Seuanez, H.N., O'Brien, S.J., and Vogelstein, B. (1988). The GLI-Kruppel family of human genes. Mol Cell Biol 8, 3104-3113.

Saha, K. and Schaffer, D. V. (2006). Signal dynamics in Sonic hedgehog tissue patterning. Development 133, 889-900.

Sander, M., Paydar, S., Ericson, J., Briscoe, J., Berber, E., German, M., Jessell, T.M., and Rubenstein, J.L. (2000). Ventral neural patterning by Nkx homeobox genes: Nkx6.1 controls somatic motor neuron and ventral interneuron fates. Genes Dev 14, 2134-2139.

Sarpal, R., Todi, S. V., Sivan-Loukianova, E., Shirolikar, S., Subramanian, N., Raff, E. C., Erickson, J. W., Ray, K. and Eberl, D. F. (2003). Drosophila KAP interacts with the kinesin II motor subunit KLP64D to assemble chordotonal sensory cilia, but not sperm tails. Curr. Biol. 13, 1687-1696.

Sasaki, H., Hui, C., Nakafuku, M., and Kondoh, H. (1997). A binding site for Gli proteins is essential for HNF-3beta floor plate enhancer activity in transgenics and can respond to Shh in vitro. Development 124, 1313-1322.

Sasaki, H., Nishizaki, Y., Hui, C., Nakafuku, M., and Kondoh, H. (1999). Regulation of Gli2 and Gli3 activities by an amino-terminal repression domain: implication of Gli2 and Gli3 as primary mediators of Shh signaling. Development 126, 3915-3924.

Scardigli, R., Schuurmans, C., Gradwohl, G. and Guillemot, F. (2001). Crossregulation between Neurogenin2 and pathways specifying neuronal identity in the spinal cord. Neuron 31, 203–217.

Scherz, P.J., McGlinn, E., Nissim, S., and Tabin, C.J. (2007). Extended exposure to Sonic hedgehog is required for patterning the posterior digits of the vertebrate limb. Dev Biol 308, 343-354.

Schwank, G., Restrepo, S. and Basler, K. (2008). Growth regulation by Dpp: An essential role for Brinker and a non-essential role for graded signaling levels. Development 135, 4003 – 4013.

Schwank, G. and Basler, K. (2010). Regulation of organ growth by morphogen gradients. Cold Spring Harb Perspect Biol 2:a001669

Shimizu, K. and Gurdon, J. B. (1999). A quantitative analysis of signal transduction from activin receptor to nucleus and its relevance to morphogen gradient interpretation. Proc. Natl Acad. Sci. USA WTD 6791- 6796.

Sinha, S. and Chen, J. K. (2006). Purmorphamine activates the Hedgehog pathway by targeting Smoothened. Nat Chem Biol 2, 29-30.

Sisson, J. C., Ho, K. S., Suyama, K. and Scott, M. P. (1997). Costal2, a novel kinesin-related protein in the Hedgehog signaling pathway. Cell 90, 235-245.

Smelkinson, M. G., Zhou, Q. and Kalderon, D. (2007). Regulation of Ci- SCFSlimb binding, Ci proteolysis, and hedgehog pathway activity by Ci phosphorylation. Dev. Cell 13, 481-495.

Sommer, L., Ma, Q. and Anderson, D. J. (1996) neurogenins, a novel family of atonal-related bHLH transcription factors, are putative mammalian neuronal determination genes that reveal progenitor cell heterogeneity in the developing CNS and PNS. Mol. Cell Neurosci. 8, 221–241.

Stathopoulos, A. and Levine, M. (2004). Whole-genome analysis of Drosophila gastrulation. Curr. Opin. Genet. Dev. 14, 477-484.

Stamataki, D., Ulloa, F., Tsoni, S.V., Mynett, A., and Briscoe, J. (2005). A gradient of Gli activity mediates graded Sonic Hedgehog signaling in the neural tube. Genes Dev 19, 626-641.

St Johnston, D. and Nüsslein-Volhard, C. (1992). The origin of pattern and polarity in the Drosophila embryo. Cell 68, 201–219.

Summerbell, D. and Harvey, F. (1983). Vitamin A and the control of pattern in developing limbs. Prog Clin Biol Res 110, 109-18.

Stern, C. D. (2001) Initial patterning of the central nervous system: how many organizers? Nat Rev Neurosci. 2, 92-8.

Stone, D. M., Hynes, M., Armanini, M., Swanson, T. A., Gu, Q., Johnson, R. L., Scott, M. P., Pennica, D., Goddard, A., Phillips, H., Noll, M., Hooper, J. E., de Sauvage, F. and Rosenthal, A. (1996). The tumour-suppressor gene patched encodes a candidate receptor for Sonic hedgehog. Nature 384, 129–134.

Storey, K. G., Goriely, A., Sargent, C. M., Brown, J. M., Burns, H. D., Abud, H. M. and Heath, J. K. (1998). Early posterior neural tissue is induced by FGF in the chick embryo. Development 125, 473–484.

Struhl, G., Struhl, K. and Macdonald, P. M. (1989). The gradient morphogen bicoid is a concentration-dependent tran- scriptional activator. Cell 57, 1259–1273.

Svärd, J., Heby-Henricson, K., Henricson, K. H., Persson-Lek, M., Rozell, B., Lauth, M., Bergström, A., Ericson, J., Toftgård, R. and Teglund, S. (2006). Genetic elimination of Suppressor of fused reveals an essential repressor function in the mammalian Hedgehog signaling pathway. Dev. Cell 10, 187-197.

Tabata, T. and Kornberg, T.B. (1994). Hedgehog is a signaling protein with a key role in patterning Drosophila imaginal discs. Cell 76, 89-102.

Taipale, J., Chen, J. K., Cooper, M. K., Wang, B., Mann, R. K., Milenkovic, L., Scott, M. P. and Beachy, P. A. (2000). Effects of oncogenic mutations in Smoothened and Patched can be reversed by cyclopamine. Nature 406, 1005–1009.

Taipale, J., Cooper, M.K., Maiti, T., and Beachy, P.A. (2002) Patched acts catalytically to suppress the activity of Smoothened. Nature 418, 892-897.

Tanabe, Y., and Jessell, T.M. (1996). Diversity and pattern in the developing spinal cord. Science 274, 1115-1123.

Tay, S. Y., Ingham, P. W. and Roy, S. (2005). A homologue of the Drosophila kinesin-like protein Costal2 regulates Hedgehog signal transduction in the vertebrate embryo. Development 132, 625-634.

Ten Berge, D., Brugmann, S. A., Helms, J. A. and Nusse, R. (2008). Wnt and FGF signals interact to coordinate growth with cell fate specification during limb development. Development 135, 3247–3257.

Tenzen, T., Allen, B.L., Cole, F., Kang, J.S., Krauss, R.S., and McMahon, A.P. (2006). The cell surface membrane proteins Cdo and Boc are components and targets of the Hedgehog signaling pathway and feedback network in mice. Dev Cell 10, 647-656.

Therond, P. P., Limbourg Bouchon, B., Gallet, A., Dussilol, F., Pietri, T., van den Heuvel, M. and Tricoire, H. (1999). Differential requirements of the fused kinase for hedgehog signalling in the Drosophila embryo. Development 126, 4039–4051.

Tickle, C., Alberts, B., Wolpert, L. and Lee, J. (1982). Local application of retinoic acid to the limb bud mimics the action of the polarizing region. Nature 296, 564-566.

Torroja, C., Gorfinkiel, N. and Guerrero, I. (2004). Patched controls the Hedgehog gradient by endocytosis in a dynamin- dependent manner, but this internalization does not play a major role in signal transduction. Development 131, 2395–2408.

Torroja, C., Gorfinkiel, N. and Guerrero, I. (2005). Mechanisms of Hedgehog gradient formation and interpretation. J Neurobiol. 64, 334-56.

Towers, M., Mahood, R., Yin, Y. and Tickle, C. (2008). Integration of growth and specification in chick wing digit-patterning. Nature 452, 882–886.

Tukachinsky, H., Lopez, L. V. and Salic, A. (2010). A mechanism for vertebrate Hedgehog signaling: recruitment to cilia and dissociation of SuFu-Gli protein complexes. J Cell Biol 191, 415–428.

Turing, A. M. (1952). The chemical basis of morphogenesis. Philos Trans R Soc Lond B Biol Sci 237, 37–72.

Ulloa, F. and Briscoe, J. (2007). Morphogens and the control of cell proliferation and patterning in the spinal cord. Cell Cycle 6:21, 2640-2649.

Vallstedt, A., Muhr, J., Pattyn, A., Pierani, A., Mendelsohn, M., Sander, M., Jessell, T.M., and Ericson, J. (2001). Different levels of repressor activity assign redundant and specific roles to Nkx6 genes in motor neuron and interneuron specification. Neuron 31, 743-755.

Varjosalo, M., Li, S. P. and Taipale, J. (2006). Divergence of hedgehog signal transduction mechanism between Drosophila and mammals. Dev. Cell 10, 177- 186.

Varjosalo, M., Bjorklund, M., Cheng, F., Syvanen, H., Kivioja, T., Kilpinen, S., Sun, Z., Kallioniemi, O., Stunnenberg, H.G., He, W.W., Ojala, P. and Taipale, J. (2008). Application of active and kinase-deficient kinome collection for identification of kinases regulating hedgehog signaling. Cell 133, 537-548.

Varjosalo, M., and Taipale, J. (2008). Hedgehog: functions and mechanisms. Genes Dev 22, 2454-2472.

Wang, G., Amanai, K., Wang, B. and Jiang, J. (2000). Interactions with Costal2 and suppressor of fused regulate nuclear translocation and activity of cubitus interruptus. Genes Dev. 14, 2893-2905.

Wang, G. and Jiang, J. (2004). Multiple Cos2/Ci interactions regulate Ci subcellular localization through microtubule dependent and independent mechanisms. Dev. Biol. 268, 493-505.

Wang, B. and Li, Y. (2006). Evidence for the direct involvement of {beta}TrCP in Gli3 protein processing. Proc. Natl. Acad. Sci. USA 103, 33-38.

Wang, Y., Zhou, Z., Walsh, C. T. and McMahon, A. P. (2009). Selective translocation of intracellular Smoothened to the primary cilium in response to Hedgehog pathway modulation. Proc. Natl. Acad. Sci. USA 106, 2623-2628.

Wartlick, O., Kicheva, A. and Gonzalez-Gaitan, M. (2009). Morphogen gradient formation. Cold Spring Harbor Perspect. Biol. 1 (3), a001255.

Wen, X., Lai, C. K., Evangelista, M., Hongo, J.-A., de Sauvage, F. J. and Scales, S. J. (2010). Kinetics of Hedgehog-dependent full-length Gli3 accumulation in primary cilia and subsequent degradation. Mol Cell Biol 30, 1910-22.

White, R. J., Nie, Q., Lander, A. D. and Schilling, T. F. (2007). Complex regulation of cyp26a1 creates a robust retinoic acid gradient in the zebrafish embryo. PLoS Biol 5: e304.

Wijgerde, M., McMahon, J.A., Rule, M., and McMahon, A.P. (2002). A direct requirement for Hedgehog signaling for normal specification of all ventral progenitor domains in the presumptive mammalian spinal cord. Genes Dev 16, 2849-2864.

Wilcock, A. C., Swedlow, J. R and Storey, K. G. (2007). Mitotic spindle orientation distinguishes stem cell and terminal modes of neuron production in the early spinal cord. Development 134, 1943-54.

Wilson, S. I. and Edlund, T. (2001). Neural induction: toward a unifying mechanism. Nat Neurosci 4, 1161-8.

Wilson, L., Gale, E., Chambers, D. and Maden, M. (2004). Retinoic acid and the control of dorsoventral patterning in the avian spinal cord. Dev Biol. 269, 433-46.

Wilson, L. and Maden, M. (2005). The mechanisms of dorsoventral patterning in the vertebrate neural tube. Dev Biol. 282, 1-13.

Wilson, C. W., Chen, M. H. and Chuang, P. T. (2009a). Smoothened adopts multiple active and inactive conformations capable of trafficking to the primary cilium. PLoS ONE 4, e5182.

Wilson, C. W., Nguyen, C. T., Chen, M. H., Yang, J. H., Gacayan, R., Huang, J., Chen, J. N. and Chuang, P. T. (2009b). Fused has evolved divergent roles in vertebrate Hedgehog signalling and motile ciliogenesis. Nature 459, 98-102.

Wilson, C.W. and Chuang, P.-T. (2010). Mechanism and evolution of cytosolic Hedgehog signal transduction Development 137, 2079-2094.

Wolff, C., Roy, S. and Ingham, P. W. (2003). Multiple muscle cell identities induced by distinct levels and timing of hedgehog activity in the zebrafish embryo. Curr. Biol. 13, 1169-1181.

Wolpert L. (1969). Positional information and the spatial pattern of cellular differentiation. J Theor Biol. 25, 1-47.

Wolpert L. (1996). One hundred years of positional information. Trends Genet. 12, 359-64.

Wolpert L. (2011). Positional information and patterning revisited. Journal of Theoretical Biology 269, 359–365.

Yang, Y., Drossopoulou, G., Chuang, P.T., Duprez, D., Marti, E., Bumcrot, D., Vargesson, N., Clarke, J., Niswander, L., McMahon, A., et al. (1997). Relationship between dose, distance and time in Sonic Hedgehog-mediated regulation of anteroposterior polarity in the chick limb. Development 124, 4393-4404.

Yao, S., Lum, S. and Beachy, P. A. (2006). The Ihog Cell-Surface Proteins Bind Hedgehog and Mediate Pathway Activation. Cell 125, 343–357.

Yin, Y., Bangs, F., Paton, R., Prescott, A., James, J., Davey, M. G., Whitley, P., Genikhovich, G., Technau, U.,Burt, D. W. and Tickle, C. (2009). The Talpid3 gene (KIAA0586) encodes a centrosomal protein that is essential for primary cilia formation. Development 136, 655-664.

Zechner, D., Fujita, Y., Hulsken, J., Muller, T., Walther, I., Taketo, M. M., Crenshaw IIIrd, E. B., Birchmeier, W. and Birchmeier, C. (2003). beta-Catenin signals regulate cell growth and the balance between progenitor cell expansion and differentiation in the nervous system. Dev Biol 258, 406-18.

Zeng, X., Goetz, J. A., Suber, L. M., Scott, W. J. Jr, Schreiner, C. M. and Robbins, D. J. (2001). A freely diffusible form of Sonic hedgehog mediates long-range signalling. Nature 411, 716 – 720.

Zeng, H., Jia, J. and Liu, A. (2010). Coordinated Translocation of Mammalian Gli Proteins and Suppressor of Fused to the Primary Cilium. PLoS ONE 5(12): e15900.

Zhang, C., Williams, E. H., Guo, Y., Lum, L. and Beachy, P. A. (2004). Extensive phosphorylation of Smoothened in Hedgehog pathway activation. Proc Natl Acad Sci U S A 101, 17900–17907.

Zhang, W., Zhao, Y., Tong, C., Wang, G., Wang, B., Jia, J. and Jiang, J. (2005). Hedgehog-regulated Costal2-kinase complexes control phosphorylation and proteolytic processing of Cubitus interruptus. Dev. Cell 8, 267-278.

Zhang, W., Kang, J. S., Cole, F., Yi, M. J. and Krauss, R. S. (2006a). Cdo functions at multiple points in the Sonic Hedgehog pathway, and Cdo- deficient mice accurately model human holoprosencephaly. Dev. Cell 10, 657- 665.

Zhang, Q., Zhang, L., Wang, B., Ou, C. Y., Chien, C. T. and Jiang, J. (2006b). A hedgehog-induced BTB protein modulates hedgehog signaling by degrading Ci/Gli transcription factor. Dev. Cell 10, 719-729.

Zhang, Q., Shi, Q., Chen, Y., Yue, T., Li, S., Wang, B., and Jiang, J. (2009). Multiple Ser/Thr-rich degrons mediate the degradation of Ci/Gli by the Cul3-HIB/SPOP E3 ubiquitin ligase. Proc Natl Acad Sci U S A 106, 21191-21196.

Zhao, Y., Tong, C., and Jiang, J. (2007). Hedgehog regulates smoothened activity by inducing a conformational switch. Nature 450, 252-258.

Zheng, X., Mann, R. K., Sever, N., and Beachy, P. A. (2010). Genetic and biochemical definition of the Hedgehog receptor Genes Dev. 24: 57-71.

Zhou, Q., Choi, G. and Anderson, D. J. (2001). The bHLH transcription factor Olig2 promotes oligodendrocyte differentiation in collaboration with Nkx2.2. Neuron 31, 791-807.

Zhou, Q. and Anderson, D. J. (2002). The bHLH transcription factors OLIG2 and OLIG1 couple neuronal and glial subtype specification. Cell 109, 61–73.

Zhu, A. J., Zheng, L., Suyama, K. and Scott, M. P. (2003). Altered localization of Drosophila Smoothened protein activates Hedgehog signal transduction. Genes Dev 17, 1240–1252.

Zhu, J., Nakamura, E., Nguyen, M. T., Bao, X., Akiyama, H. and Mackem, S. (2008). Uncoupling Sonic hedgehog control of pattern and expansion of the developing limb bud. Dev Cell 14, 624-632.